STUDY ON THE STRESS-STRAIN-STRENGTH ANISOTROPY OF SATURATED SAND

March 1984

by

Seiichi Miura

TABLE OF CONTENTS

TABLE OF OFTEN USED SYMBOLS

A, B = value corresponding to $W^p=1$ and slope of line in relationship between $\log h$ and $\log w^p$

A_{max} = maximum sectional area of plastic zone due to cone penetration (Eqs.(6-2) and (6-3))

A.R. = axial ratio of sand particle (Eq.(3-3))

C_d = reciprocal of linear gradient of $(d\varepsilon_v/d\gamma)$ vs. η

C_0, C_1, C_2, C_1', C_2' = empirical volume change constants in cavity expansion theory (Eq.(6-7)

DA = double amplitude axial strain

D_{ij} = parameter introduced in order to consider three-diemensional stress system (Eq.(5-29))

D_p = penetration depth

D_{rc} = relative density after consolidation

$\overline{D_{rc}}$ = mean relative density after consolidation for undisturbed sand

F-sand = Fuji River sand used by Yamada and Ishihara (1979)

F_c, F_q = spherical cavity expansion factors (Eq.(6-4))

I-sand = sand sampled from Ishikari-cho, Hokkaido

J_1, J_2, J_3 = first, second and third effective stress invariants

K-sand = sand sampled from the suburb of Kushiro City, Hokkaido

K_o = coefficient of earth pressure at rest

L_i = longest dimension of a sand particle (i)

MSP = sand sample preparation method by using multiple sieve pluviation apparatus

N_c = number of loading cycles to a double amplitude axial strain

N_l = number of loading cycles to initial liquefaction

$R_A V$ = sand specimen prepared by MSP method

$R_B V$, $R_B 45$, $R_B H$ = sand specimens prepared by MSP method with freezing technique

R_C = sand specimen prepared by rodding method

R_D, $R_D(H)$ = sand specimens prepared by tapping method

S_i = shortest dimension of a sand particle (i)

T-sand = Toyoura standard sand

UH = undisturbed sand specimen whose axial direction is coincidental with in-situ horizontal direction

UV = undisturbed sand specimen whose axial direction is coincidental with in-situ vertical direction

V.M. = vector magnitude (Eq.(3-5))

$b = (\sigma_2 - \sigma_3)/(\sigma_1 - \sigma_3)$

d = nozzle diameter of conical hopper in MSP apparatus or diameter of cone

e = void ratio

e_{max}, e_{min} = maximum and minimum void ratios

f, g, h = yield, plastic potential and hardening functions

f_m, f_n = volumetric strain factors for spherical cavity

h_{ij} = hardening function defined in two-dimensional stress system

m = η at the maximum volume contraction during shear

m, n, n′ = exponents in empirical equation (Eq.(6-7))

p = mean principal stress (this imply the effective stress in drained shear test)

p_c = p at isotropic consolidation

p′ = effective mean principal stress

$\bar{p}$ = unit mean principal stress (Eq.(6-7))

p_u = ultimate cavity expansion pressure

q = shear stress

q_c = cone penetration resistance

$(q_c)_m$ = mean cone penetration resistance between $D_p = 50^{mm}$ and 100^{mm}

$(q_c)_r$ = q_c in radial direction

$(q_c)_V$, $(q_c)_{45}$, $(q_c)_H$ = $(q_c)_m$ for $R_B V$-, $R_B 45$- and $R_B H$-specimens

$(q_c)_x$, $(q_c)_y$, $(q_c)_z$ = q_c in x-, y- and z-directions

dW^p = plastic strain work increment due to shear

dW_I^p = plastic strain work increment done by consolidation

M = η at critical state in Cambridge theory

Δ = average volumetric strain within plastic zone (Eq.(6-7))

ΔV = volumetric change due to cone penetration

α = semi-apex angle of cone tip

β = modification factor to account for envelope curvature (Eq.(6-5))

γ = shear strain

γ_d = dry density

γ_{dmax}, γ_{dmin} = maximum and minimum dry densities

$d\gamma$ = shear strain increment

ε_a, ε_r = axial and radial principal strains

ε_v = volumetric strain

ε_{vmax} = ε_v at the maximum volume contraction during shear

$(\varepsilon_v)_c$ = volumetric strain in plastic zone due to cone penetration (Eq.(6-1))

$(\varepsilon_v)_f$ = volumetric strain at failure of triaxial test

$d\varepsilon_1$, $d\varepsilon_2$, $d\varepsilon_3$ = major, intermediate and minor principal strain increments

$d\varepsilon_i$, $d\varepsilon_j$, $d\varepsilon_k$ = three principal strain increments

$d\varepsilon_x$, $d\varepsilon_y$, $d\varepsilon_z$ = principal strain increments in x-, y- and z-directions

$d\varepsilon_{iij}$, $d\varepsilon_{iji}$ = principal strain increments in two-dimensional stress system of $\sigma_i \geq \sigma_j$ and $\sigma_j > \sigma_i$, respectively

η = effective stress ratio

θ = arc tan $\left\{ 3(\sigma_y - \sigma_x)/(2\sigma_z - \sigma_x - \sigma_y) \right\}$

$\bar{\theta}$ = mean vector magnitude (Eq.(3-4))

σ_a', σ_r' = axial and radial effective principal stresses

σ_c' = effective consolidation stress ($= p_c$)

σ_d = maximum single amplitude cyclic axial stress

$\Delta\sigma_a$ = cyclic axial stress

σ_q = initial isotropic effective stress ($=\sigma_c'$) (Eq.(6-4))

σ_o = arbitrary reference stress (Eq.(6-5))

σ_{vc} = in-situ overburden pressure

σ_1, σ_2, σ_3 = major, intermediate and minor principal stresses

σ_i, σ_j, σ_k = three principal stresses

σ_x, σ_y, σ_z = principal stresses in x-, y- and z-directions

ϕ_d = angle of shearing resistance under the drained condition

ϕ_o = angle of shearing resistance when $\sigma = \sigma_o$

CHAPTER 1 INTRODUCTION

1.1 General Introduction

Recent study on static and dynamic mechanical properties of cohesionless soils raises increasingly its importance in the field of soil engineering. Various boundary value problems such as bearing capacity and liquefaction analyses of sandy grounds have been solved by means of numerical technique represented by finite element method, and a number of excellent findings have been made for the important design and construction. However, the mechanical properties of cohesionless soils are the most complicated ones in the engineering material. For example, soils show the inherent characteristics such as dilatancy and stress system dependency during shear deformation. It should be also noted that the static and cyclic deformation and strength properties of cohesionless soil depend strongly on its fabric characteristics and stress (or strain) history. In order to offer reasonable solutions on various engineering problems concerning cohesionless soils, therefore, it is preferable to promote the research on their deformation and strength behaviors. This thesis will treat in detail the anisotropic stress-strain-strength properties of sand as a typical example of cohesion-

less soils.

In this chapter, brief review of previous investigations concerning these subjects and the scope of this thesis will be outlined.

1.2 Brief Review of Previous Investigations

1.2.1 Fabric anisotropy and its relation to mechanical properties of cohesionless soils

When we treat sand as a material in soil mechanics, there are many properties which must be clarified. Mineralogy of particles, particle size, particle shape, water content and spatial arrangement of solid particles and associated void seem to be the most fundamental properties of cohesionless soil (Mikasa, 1964; Oda, 1978). This means that other derived properties of sand such as shear strength, deformation modulus and liquefaction strength are controlled by these properties. Therefore, each derived property (mechanical property) can be properly discussed only by taking account of the five fundamental properties, their interrelations and stress condition.

A large number of theoretical and experimental investigations on these fundamental properties and their relations to mechanical properties have been done so far. For example, the significance of these fundamental properties in shear strength of sand was studied by Tschebotarioff and Welch (1948), Bishop and Eldin (1953), Nash (1953), Horn and Deere (1962), Rowe (1962), Lee and Seed (1967), Marsal (1967) and Vesic and Clough (1968). These researches showed that the shear strength

(or interparticle friction angle) of sand with a given density can be substantially determined only by taking account of the following factors; (1) mineral composition which is evaluated by the modal analysis of minerals, (2) surface roughness of constituent particles (shape of particle), (3) size of particles, (4) effect of lubrication or antilubrication by water (water content) and (5) stress condition. In these researches, the relation of spatial arrangement of particles and associated void to mechanical properties of sand was not considered.

Oda (1972a, 1972b and 1977) has indicated that the spatial arrangement of solid paricles and associated void which will be called " fabric " in this thesis is an important item of study to treat a sand as an assembly of discrete particles. According to Oda's study, fabric of homogeneous sand without cohesion is sufficiently defined by the following two concepts; (a) orientation fabric and (b) packing (Fig.1-1). His laborious study on the fabric of granular material and its relation to the mechanical properties is summarized as the followings:

(1) It is possible to distinguish two types of fabric anisotropy; (a) anisotropy due to the preferred orientation of non-spherical particles and (b) anisotropy due to the concentration of N_i-direction. These fabric anisotropy is caused by the fact that each particle tends to rest in the most stable position with respect to the gravitational

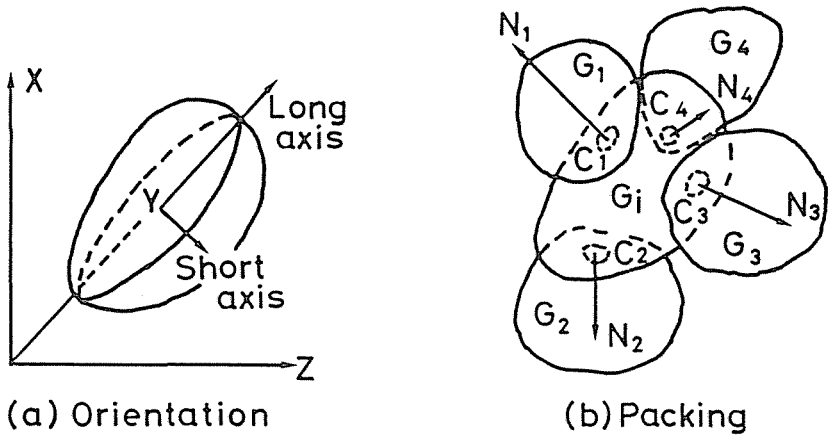

Fig.1-1 Concept of fabric in granular material (After Oda (1977)) ((a) Orientation fabric in sand composed of non-spherical particles must be concretely represented by inclination angles of typical dimensional axes of individual particles to reference directions. The orientation fabric can be sufficiently evaluated from the knowledge concerning parallel alignment of apparent long axes observed in thin sections which are prepared from a sand specimen fixed by polyester resin. (b) Packing means mutual relation of individual particles to other ones. Mutual relation of a particle G_i to other ones can be defined by the directions of normals N_1, N_2, N_3 and N_4 which are perpendicular to the tangents at the contacts C_1, C_2, C_3 and C_4 and number of contacts $n (= 4)$ which is called co-ordination number. The former fabric element can be expressed by a probability density function E of normals N_i. The latter fabric element can be expressed by both of means n and standard deviation ρ_n of co-ordination number.)

force.

(2) When a sand is composed of non-spherical particles, the two types of anisotropy are produced. When a sand is composed of spherical, on the other hand, only the latter type of anisotropy may be possible.

(3) Fabric anisotropy may have a considerable influence on the stress-strain and strength behaviors of sand. The anisotropy of sand in the deformation and strength behaviors depends not only strongly on the fabric anisotropy due to the concentration of N_i-directions but also fairly on the fabric anisotropy due to the parallel alignment of particles.

Arthur and Menzies (1972) have also observed that the anisotropic fabric of Leighton Buzzard Sand deposited in air which is certainly defined by the X-ray method results in a corresponding anisotropy in the peak strength and also in the prefailure stress-strain relationship.

Some other experimental evidences to show anisotropic behavior of sand have been reported by El-Sohby and Andrawes (1972), Tatsuoka and Ishihara (1974a), Green and Reades (1975) and Ishihara and Okada (1978).

On the other hand, Ladd (1974) has shown that the cyclic undrained triaxial strengths of cohesionless soils are remarkably influenced by their fabric characteristics. These findings were also confirmed by Mulilis et al. (1975), Silver et al.

(1980), Tatsuoka et al. (1982) and other researchers. These facts indicate that the static and cyclic mechanical properties of sands are controlled not necessarily only by density, but also by fabric of sand.

The influence of stress (or strain) history on the static and cyclic deformation-strength characteristics has been also clarified by many investigations (e.g., Finn et al., 1970; Tatsuoka and Ishihara, 1974b; Toki and Kitago, 1974; Ishihara and Okada, 1978). Stress (or strain) history effects may be explained by a fabric change of sand due to stress (or strain) undergone previously.

1.2.2 Influence of stress system during shear on stress-strain-strength properties

It is well known in soil mechanics that the stress and strain conditions of soil elements differ from each other by the position they exist in-situ. In general, the mechanical properties of cohesionless soils are significantly influenced by the stress or strain to which they have been or will be subjected before or during shear. Therefore, in order to estimate the in-situ behavior of sands from laboratory test results, it is essential to test them exactly the same conditions as exist in-situ.

Laboratory strength tests are usually performed by using conventional triaxial compression apparatus. However, conventional triaxial compression tests only provide information regarding the soil behavior under stress conditions for which major principal stress σ_1 > intermediate principal stress σ_2 = minor principal stress σ_3. Therefore, it is desirable from the practical point of view that real mechanical properties of cohesionless soils which might be obtained only by the special tests simulating the stress and strain conditions in-situ would be conveniently evaluated from those obtained by the conventional tests.

In the following, the main results of previous studies performed to investigate the influence of the intermediate principal stress on the mechanical properties of cohesionless

soils are described.

The first experimental study in the world in which three principal stresses are controlled independently was performed by Kjellman (1936). He examined the three-dimensional failure criterion for dry sand.

Ko and Scott (1967) designed a soil test box in which a cubical specimen was contained between six membranes. This equipment seems offer the advantage of easy application of normal stresses and ensure that no shear stresses are induced on the faces of the specimen. Their tests performed on Ottawa Sand showed that the angle of shearing resistance increased with increasing intermediate principal stress from the condition of triaxial compression (in which $\sigma_2 = \sigma_3$) to a maximum before a slight decrease at the condition of triaxial extension (in which $\sigma_1 = \sigma_2$).

Green and Bishop (1969) and Green (1971) performed, using a rectangular prismatic specimen, the tests on Ham River Sand with σ_2 values very closely spaced in the range from σ_1 to σ_3. The angle of shearing resistance was reported to increase from triaxial compression to plane strain and to remain constant from plane strain to triaxial extension.

Sutherland and Mesdary (1969) developed a piece of equipment similar to the apparatus described by Bishop (1966). One of the horizontal stresses is applied by the chamber pressure, and the other is applied by two rubber bags filled with

water. Tests performed on Lock Aline Sand showed that the angle of shearing resistance increased from triaxial compression to a maximum in the region of the plane strain condition and then decreased at triaxial extension to a value approximately equal to that obtained in triaxial compression.

Lade and Duncan (1973) designed a new type cubical triaxial apparatus by which three principal stresses can be controlled independently, and performed a series of tests on Monterey No.0 Sand. The testing program included both plane strain tests and tests conducted with constant values of $b = (\sigma_2 - \sigma_3)/(\sigma_1 - \sigma_3)$. Based on the experimental results, they proposed a failure criterion for both dense and loose sands.

Ichihara and Matsuzawa (1970) and Miyamori (1976) examined the deformation and strength behaviors of dry sands under plane strain condition and three-dimensional stress state.

As mentioned in the previous paragraph, sand display significant anisotropy in its mechanical properties. The intermediate principal stress may have a similar influence on the behavior of sand with anisotropic fabric. However, it is expected that the three-dimensional deformation behaviors of anisotropic sand change complicately due to the synthetic effects of stress system and fabric anisotropy.

Oda et al. (1978) showed that strength anisotropy of dense sand was more clearly observed under plane strain condi-

tions than under conditions of symmetrical stress system such as applied in the conventional triaxial compression tests.

The three-dimensional mechanical behavior of anisotropic sand was studied by Yamada and Ishihara (1979 and 1981). Their study indicated that the inherent anisotropic fabric exerted a strong influence on the deformation characteristics at low to medium shear stress level.

The significance of fabric anisotropy in the three-dimensional stress-strain-strength properties of sand was also discussed by Green and Reades (1975), Haruyama (1981) and Ochiai and Lade (1983). However, only a limited number of investigations of the three-dimensional behavior of anisotropic sand have been performed, and the available data are not always consistent.

On the other hand, the influence of stress system on the cyclic undrained strength of saturated sand was investigated by Peacock and Seed (1968), Finn et al. (1971), Ishihara and Li (1972), Yoshimi and Oh-oka (1973), Ishibashi and Scherif (1974), Silver et al. (1980) and Tatsuoka et al. (1982). These experimental results showed that the difference of stress system made the remarkable difference in the liquefaction characteristics and cyclic undrained strength.

Furthermore, in order to evaluate the in-situ mechani-

cal behaviors of sand in a laboratory testing, it seems important to reproduce not only the same density as that of in-situ sand but also the same fabric as that existing in the field. Recently, many attempts have suggested that the undisturbed sand samples could be obtained hopefully by performing the sampling by freezing (e.g., Yoshimi et al., 1978; Ishihara et al., 1978; Walberg, 1978; Singh et al., 1982; Seed et al,. 1982). Therefore, it seems possible to a certain degree to evaluate the feature of in-situ mechanical properties in a laboratory.

1.2.3 Prediction of stress-strain behavior of cohesionless soil

Several theories to describe the stress-strain behavior of soils have been developed. Among them, Roscoe and his colleagues (Roscoe et al., 1963; Roscoe and Burland, 1968; Schofield and Wroth, 1968), who are considered to be pioneers of this subject, developed the Cam Clay Model (or modified Cam Clay Model) for stress-strain behaviors of cohesive soils and the Granta Gravel Model for those of cohesionless soils by inducing the concept of normality rule in the theory of plasticity. These models treat soils as a work-hardening elastoplastic material, and are based on the experimental data of triaxial consolidation-swelling test and triaxial compression test. Although it is considered that these elastoplastic theory is the first consistent constitutive law on the deformation of soils, Drucker et al. (1957) first applied a work-hardening law to the shear deformation of soils. That is, the shape of the yield loci of the Cam Clay and the Granta Gravel Models originates from the theory proposed by Drucker et al. (1957).

Poorooshasb et al. (1966), Poorooshasb (1971) and Lade and Duncan (1975) have proposed another elastoplastic theory to describe the stress-strain characteristics of cohesionless soils by using the non-associated flow rule.

While the shape of the plastic potential curves by Poorooshasb et al. is almost identical to that of the yield surface of the Cam Clay Model and the Granta Gravel Model, the yield loci are straight lines (Poorooshasb et al., 1966) or slightly curved lines (Poorooshasb, 1971).

The fact that the yield loci for sand can be represented by those of Poorooshasb et al. was also confirmed by Cole (1967), Tatsuoka and Ishihara (1974a) and Nishi and Esashi (1978). This means that normality or associated flow rule could not be applied to cohesionless soils.

On the other hand, based on the basic equation concerning the stress-strain relations on the mobilized plane derived from the microscopic considerations of shear mechanism for granular materials, Matsuoka (1974) and Matsuoka and Nakai (1977) proposed a general constitutive equation for cohesionless soil which involved the effect of intermediate principal stress.

Barden and Khayatt (1966) and Barden et al. (1969) gave a concrete plastic potential function for sand under various stress conditions based on the stress dilatancy euqation which was derived from the microscopic viewpoint by Rowe (1962).

In such way, the theories for predicting the stress-strain behaviors of sand have been advanced from various standpoints. However, elastoplastic theories which explain exactly the stress system-dependent behavior and the dilatancy chara-

cteristics that contract initially and expand at prepeak in shear deformation could not be found. Particularly, anisotropic stress-strain behaviors of sand with fabric anisotropy could not be modeled by the above existing theories which assumed cohesionless soil to be isotropic in its mechanical properties.

Recently, the dependency of stress-strain behavior on the fabric anisotropy and stress system has become an important theme of research concerning constitutive law for sand. The studies by Tatsuoka (1980) and Matsuoka et al. (1980) are the representative of this category.

The standard penetration test (SPT) or the cone penetration test (CPT) is an in-situ test which reflects stress (or strain) history, soil fabric, and horizontal effective stress, in addition to the combined effect of the relative density and the vertical stress. Therefore, a number of theoretical and experimental investigations to predict the in-situ mechanical properties of cohesionless soils from the data of the sounding performed in the fields have been done so far by many researchers (e.g., Vesic, 1972; Veismanis, 1974; Durgunoglu and Mitchell, 1975a and b; Schmertmann, 1975; Marcuson and Bieganousky, 1976; Kovacs et al., 1977; Tatsuoka et al., 1978; Seed, 1979; Chapman and Donald, 1981; Baldi et al., 1981 and 1982; Yoshimi and Tokimatsu, 1983). These studies indicated that the SPT N-value

and the CPT q_c-value could be employed as a convenient parameter to express the static and cyclic mechanical properties of cohesionless soils.

The main results of investigations concerning the relations between cone penetration characteristics obtained by the CPT and the static and cyclic mechanical properties of sands will be introduced in some detail in CHAPTER 6.

1.3 Composition of the Present Thesis

As described previously, there are many factors influencing upon the static and cyclic mechanical properties of cohesionless soils. Above all, both static and cyclic stress-strain-strength behaviors of sand at given densities depend strongly on its fabric anisotropy and stress system.

In this study, the fact that anisotropic mechanical properties can be observed clearly not only in artificially deposited sands but also in natural in-situ sand deposits will be introduced. It will be also indicated that anisotropic stress-strain-dilatancy behavior and liquefaction characteristics of natural in-situ sand deposits examined in the present study could be simulated to a certain degree by adopting in a laboratory a sand sample preparation method which is proposed by the present author. Moreover, a method of predicting stress-strain behavior of saturated sand under the in-situ stress conditions will be proposed based on the elasto-plasticity theory, in which effects of fabric anisotropy and stress system are taken into account. The present author will also point out the importance of fabric anisotropy in discussing the correlation between cone penetration resistance and mechanical properties of sand.

The composition of the present thesis is as follows.

In CHAPTER 2, a simple preparation method of sand specimen using multiple sieve pluviation apparatus (MSP method) by which various desired specimen density can be provided exclusively by controlling the rate of sand discharge will be presented. In the granular materials having a relatively small uniformity coefficient, it will be found that the very high density can be achieved by this method without applying vibration or impact.

In CHAPTER 3, test apparatus, in-situ sampling of undisturbed sand, fabric characterization of material used and experimental procedure will be described.

In CHAPTER 4, observed anisotropy in static and cyclic stress-strain-strength behaviors of sand specimen prepared by MSP method will first be outlined. Then, anisotropy in mechanical properties and its laboratory simulation of sand specimen sampled from natural deposits will be presented.

In CHAPTER 5, a new three-dimensional mechanical model for anisotropic sands derived with the help of the concept of non-associated flow rule on the elasto-plasticity and the verification with respect to the measured data of two true triaxial tests which were performed by Yamada and Ishihara (1979) and the present author will be presented. It will be shown

that proposed model is capable of simulating the anisotropic three-dimensional stress-strain behavior of sand with orthotropic fabric.

In CHAPTER 6, the effects of fabric anisotropy on the cone penetration characteristics and the correlation between the static and cyclic stress-strain-strength behaviors and the cone penetration resistance for sand will be shown. Above all, the measured cone penetration resistance will be verified on the basis of the cavity expansion theory which takes account of the fabric anisotropy-dependent compressibility of sand.

In CHAPTER 7, conclusions drawn from this study will be described.

CHAPTER 2 DEVELOPMENT OF SAMPLE PREPARATION METHOD

2.1 Introduction

As mentioned in CHAPTER 1, recent studies on the mechanical properties of cohesionless soils have shown that both static and cyclic deformation-strength characteristics at given densities are profoundly affected by the manner in which the soils are deposited and by the stress or strain histories previously undergone. This means that different methods of reconstitution to a desired density produce in a laboratory sand samples with different fabrics and different mechanical properties. Therefore, the influence of sand sample preparation method on its mechanical properties is an important problem in soil mechanics.

Sample preparation method effects can be considered as a certain kind of stress or strain history. In order to quantitatively evaluate the different mechanical behavior of sand having equal density due to the effect of the sample preparation methods or the stress or strain history, therefore, it is necessary to perform the high-quality laboratory tests on the samples which are formed by a simple preparation method free from human errors and have a uniform and definite characteristic of fabric. Though it has been well known that

non-uniformity may be introduced in the course of sample preparation, no entirely satisfactory method of preparing uniform sand samples has yet been developed. Consequently, it is desired to establish a standard method of sand sample preparation in which homogeneous specimens can be easily formed by a simple procedure in order to obtain reliable results from minimal number of tests.

Presented herein is a simple preparation method of sand sample using the multiple sieve pluviation apparatus.

2.2 Multiple Sieve Pluviation Apparatus and Preparation of Sand Specimen

A multiple sieve pluviation apparatus used in this study consists mainly of a conical hopper to stock a sand, a perspex cylinder equipped with seven layers of sieves and a fixing device to set up both of the hopper and the cylinder vertically. The whole view of apparatus is shown in Fig. 2-1 and Photo.2-1. The reason for adopting the seven layers of sieves is to insure a uniform deposition of sand, so as to produce a homogeneous sample. The rate of sand discharge can be controlled without difficulty by changing the diameter of the nozzle attached at the bottom of the conical hopper. On the other hand, the height of fall that is tentatively in this study defined as the distance between the lowest sieve (7th sieve) and the base of sample mold can be also changed by shifting the position of the fixing device along the three guide rods.

After due consideration of maximum sand particle size used in the tests, square opening sieves which are 1.41 mm for the uppermost sieve and 3.66 mm for the other six sieves are adopted, respectively, and the nozzle diameter sizes of 7.0 mm to 32.0 mm at 0.5 mm intervals are used to produce a desired density. In order to determine the size of nozzle diameters and sieve openings, it should be necessary to take much account

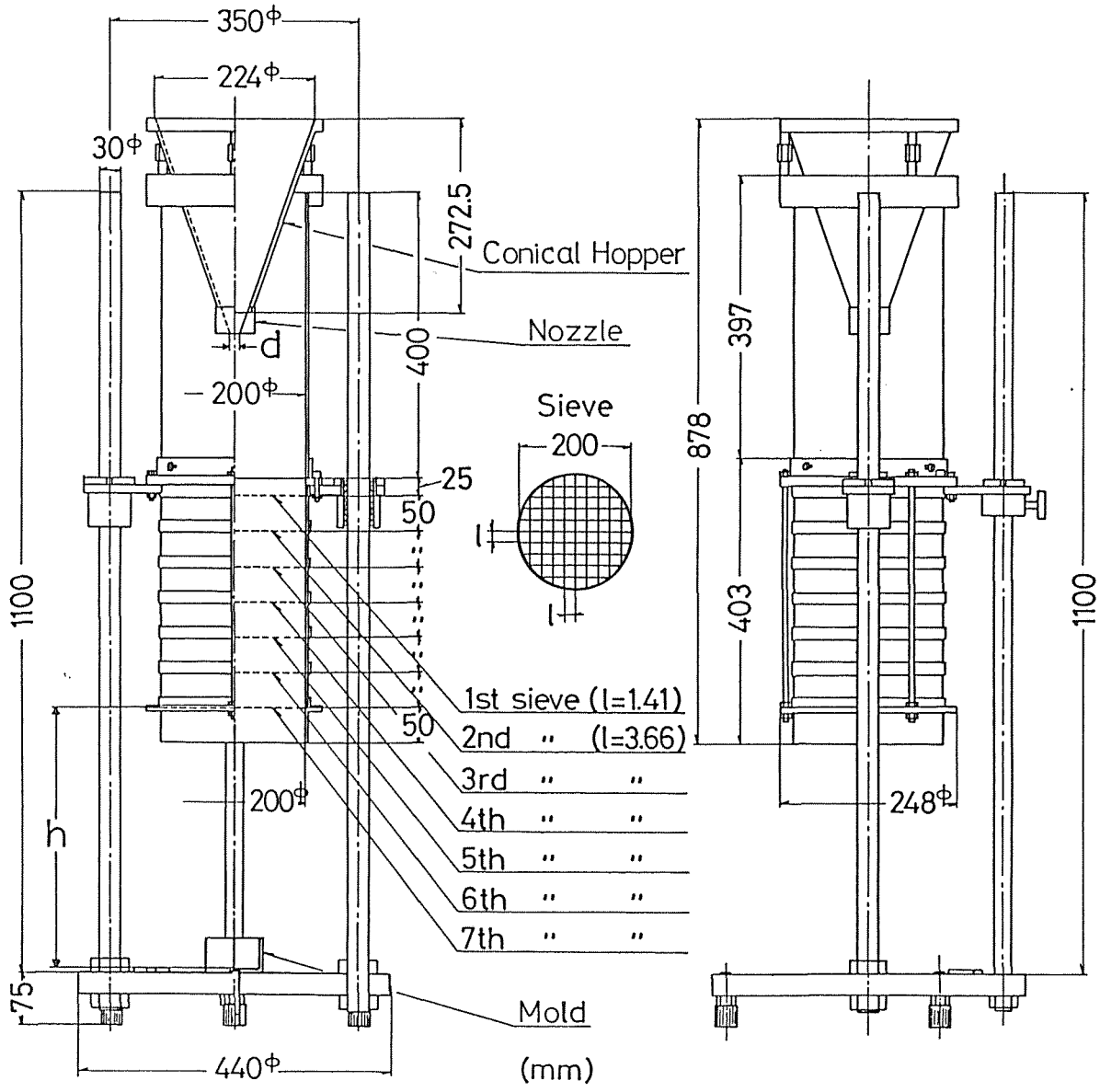

Fig.2-1 General view of multiple sieve pluviation apparatus

Photo.2-1 Typical pluviation manner in preparing Toyoura sand triaxial specimen at the condition of nozzle diameter 25 mm and height of fall 300 mm

of maximum soil particle size and soil gradation of sample which would be used to the test.

For example, the triaxial sand specimen can be prepared by the following manner. A rubber membrane is put on the pedestal of triaxial cell by two O-rings and a split mold as assembled, and then vacuum is applied to the split mold to hold the membrane taut against the inside of the mold. The triaxial cell base arranged as above is set on the base of the multiple sieve apparatus in which both of nozzle diameter and height of fall are preset to produce a desired density, taking care not to disagree their centers each other as much as possible. The oven-dried sand is filled by a necessary weights with a scoop in the hopper, the stopper being in position. As soon as the stopper is quickly removed, sand flows continuously into the mold as if it were a rain fall through sieves. Shown in Photo.2-1 is a typical pluviation manner in Toyoura sand at the condition of nozzle diameter 25 mm and height of fall 300 mm. The stopper is again placed in position when the mold is filled with sand. After the surface is trimmed back to the level of sample height by siphoning off excess sand through a tube connected to a small vacuum source, a loading cap is gently lowered into position, and then membrane is rolled up around the cap and sealed with two O-rings. At the same time a small vacuum of 4 kPa is applied to give the sample rigidity.

2.3 Specimen Density Obtained from Proposed Method

Toyoura standard sand, under 74 μm, washed in water, and oven dried, was used to investigate the density produced by MSP method. The sand, whose physical properties and maximum and minimum dry densities determined by the method proposed to the Japanese Society of Soil Mechanics and Foundation Engineering by the committee for the test method of maximum and minimum densities of sand (1979) are given in Table 2-1, consists of subangular quartz particles. The observations of sand particles by microscope will be shown in CHAPTER 3. All of the dry densities γ_d obtained by MSP method were, for comparison of data, converted to the relative densities D_r which were calculated based on the above maximum and minimum densities (γ_{dmax},γ_{dmin}) from the following expression.

$$D_r = \frac{\gamma_{dmax}(\gamma_d - \gamma_{dmin})}{\gamma_d(\gamma_{dmax} - \gamma_{dmin})} = \frac{e_{max} - e}{e_{max} - e_{min}} \qquad (1\text{-}1)$$

where e_{max} and e_{min} denote the maximum and minimum void ratios, respectively.

The relative densities produced under the various combinations of the nozzle diameter d and the height of fall h are shown in Fig.2-2. The mold used for the examinations was 50 mm diameter and 120 mm high. It can be seen from the figure that this proposed method gives the relative density

Table 2-1 Physical properties and maximum and minimum dry densities of sands determined by JSSMFE method (1979)

Sample name	Specific gravity	Uniformity coefficient	Mean particle size (mm)	Finer fraction ($\leq$74μm) (%)	γ_{dmax}** (kN/m^3)	γ_{dmin}** (kN/m^3)
Toyoura sand	2.65	1.5	0.18	0	16.02	13.07
Sengenyama sand	2.70	3.0	0.40	3	16.61	13.73
Urayasu sand	2.75	9.0	0.31	15	14.39	11.17
Ikebukuro sand	2.73	6.0	0.35	10	15.94	11.11
Glass beads*	2.49	2.5	0.37	3	15.70	14.19

* Glass beads of four diameters are mixed to get the uniformity coefficient of 2.5.

** The average values of ten measurements are adopted for maximum and minimum dry density, respectively.

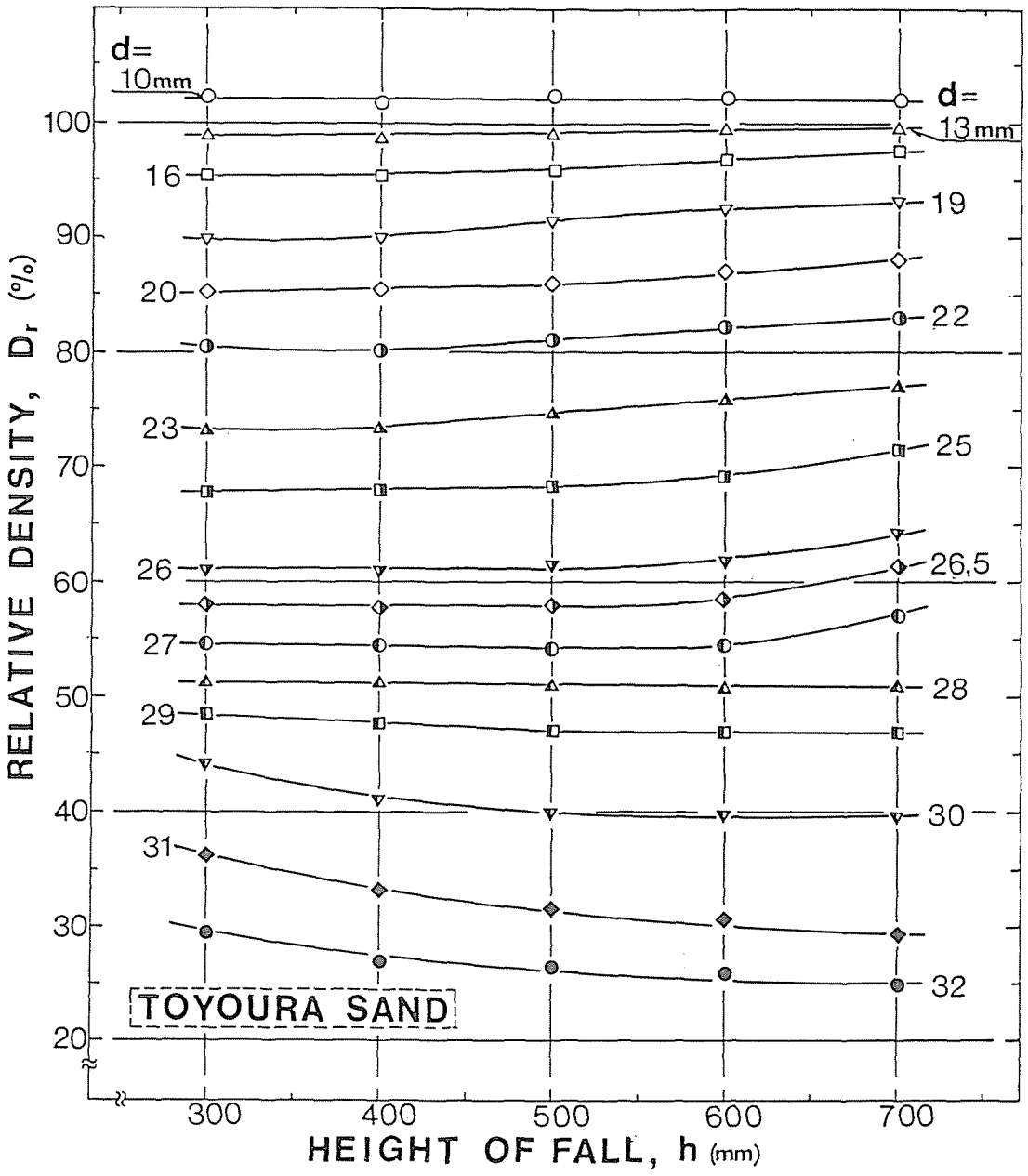

Fig.2-2 Relative densities of Toyoura sand produced under various combinations of nozzle diameter and height of fall

over a fairly wide range from around 25 % to 103 %. Fig. 2-3 shows the relation between the relative density and the nozzle diameter for the various heights of fall. Remarkable change in relative density due to controlling the nozzle diameter is observed. It must be also noted that contribution of the height of fall to the density is very small; for example, relative density produced at d = 20 mm is 85 % for h = 300 mm and 88 % for h = 700 mm respectively.

This tendency in MSP method could not seem to support an intuitive concept popularly accepted in which the larger the height of fall is, the higher the density deposited. Mulilis et al. (1975) have formed a triaxial sand specimen by pluviation through air or water method in which a flask having a cork with a predetermined nozzle size to produce the desired density is used. They have pointed out that the specimen density produced by this method is dependent on the following three factors;

(1) the size of nozzle opening,

(2) the speed of rotation of the flask and

(3) the height of fall.

They have also found that a higher speed of rotation and a smaller nozzle opening resulted in a higher density, but a height of fall within the range of approximately 150 mm to 500 mm had the least effect on the density. Their experimental results on the contribution of height of fall and the

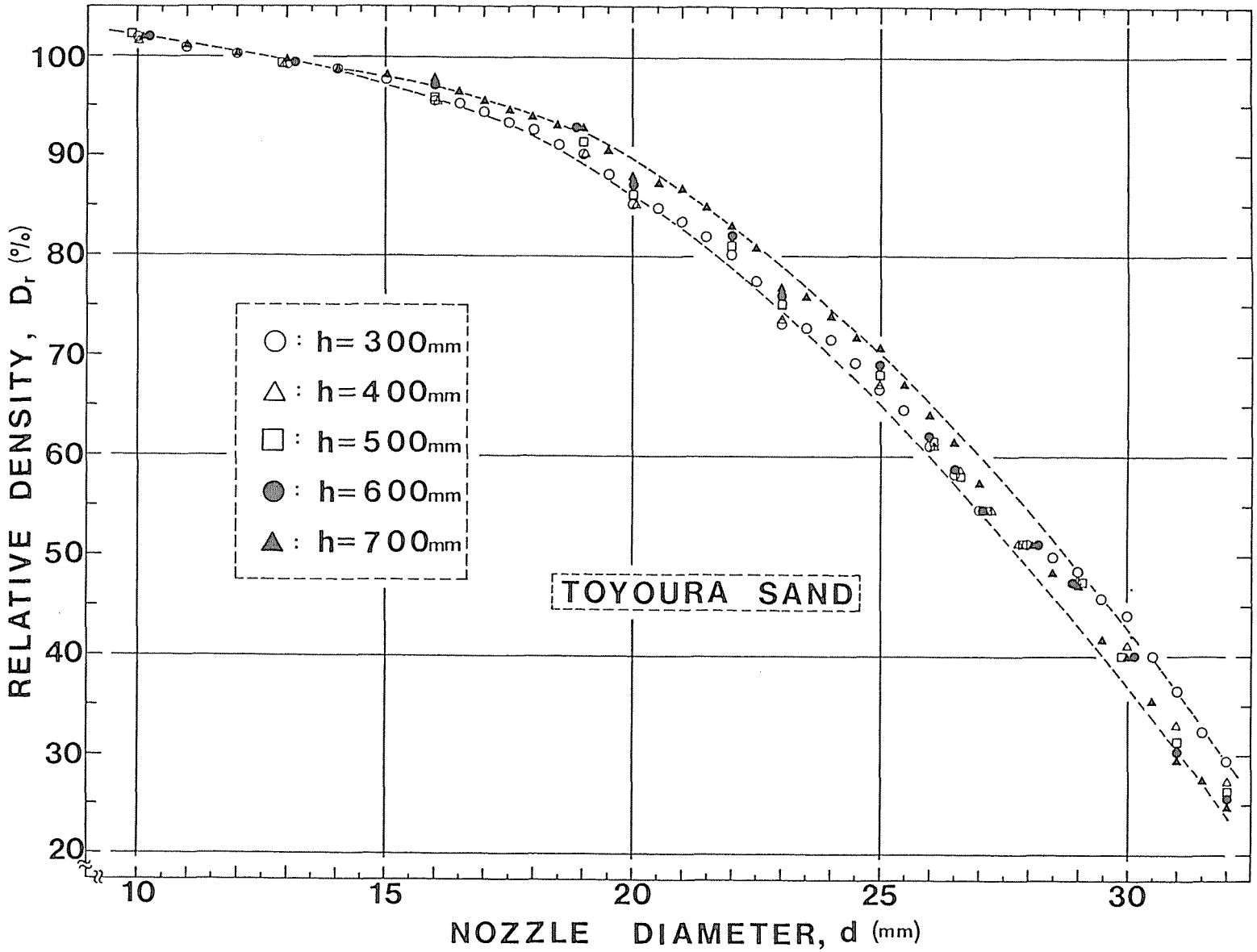

Fig.2-3 Variation of relative density of Toyoura sand with nozzle diameter

nozzle diameter to the density show a similar tendency to those obtained in MSP method.

These facts show that, in the sample preparation methods such as pluviation methods, the desired density can be achieved exclusively by selecting the nozzle diameter. It would be considered that the nozzle diameter is one of the most representative factors controlling the rate of sand discharge per unit depositing area and per unit time. Consequently, it can be said that in MSP method the rate of sand discharge plays the most important role in controlling the specimen density.

It is seen in Fig.2-2 that the relative density decreases slightly with an increase in the height of fall at the larger nozzle diameters ($d \leqq 30$ mm). As described in the previous paper (Toki and Miura, 1979), it has been found that the phenomena of significant convergence of sand nappe occur when large height of fall and large nozzle diameter are used. The phenomena of this convergence result in an increase in the rate of sand discharge per unit depositing area. At the same time, an increase in the rate of sand discharge follows always with an interference action of sand particles such as locking or arching which obstructs the sand particles to settle in a denser state. Accordingly, the reason for which a slight decrease of the density with an increase in the height of fall is induced at the larger nozzle diameter could be explained from the phenomena of convergence of the sand nappe which are

observed when the grains fall into the mold through the sieves. Kolbuszewski (1948) had given already an explanation on the formation of maximum and minimum porosities of sands in a similar fashion to that above mentioned.

In summary, it can be said that MSP method provides easily the specimen density over a wide range from looser state to densest one.

2.4 Maximum Dry Density

It has been generally recognized that vibrations or impacts can be used to densify cohesionless soils, as in vibratory compactions. Similarly, these ways to compact have been often applied in laboratory tests to establish the maximum density of sand. For example, a method to determine the maximum dry density has been recently proposed by the committee for the test method of maximum and minimum densities of sand in the Japanese Society of Soil Mechanics and Foundation Engineering. The detailed procedure to produce the maximum dry density is described in the committee report (1979). In this paper, this test method used to determine the maximum dry density is referred tentatively to as JSSMFE method.

It can be confirmed that a peak dry density is attained when Toyoura sand is pluviated by using the nozzle diameter of 10 mm, as shown in Figs.2-2 and 2-3. It is worthy of note that a peak dry density obtained in MSP method is higher slightly than the maximum dry density obtained from JSSMFE method or almost identical to the one. In order to compare in detail the values of the peak dry density with the maximum dry density achieved by JSSMFE method, the peak dry densities of granular materials whose physical properties and the maximum and minimum densities determined by JSSMFE method are given in Table 2-1

are examined. Sengenyama, Urayasu and Ikebukuro sands sampled from natural deposits were oven-dried and then sieved by a 1.19 mm sieve owing to the limitation of the first sieve size (1.41 mm) in the multiple sieve pluviation apparatus. Tests were performed using a mold for JSSMFE method whose dimensions are 60 mm in inner diameter and 40 mm high, so as to avoid a possible effect of mold size on the measured density. The results of tests are given in Table 2-2. Photo.2-2 shows a typical manner of deposition process of Toyoura sand ($h = 300$ mm, $d = 10$ mm).

These test results are summarized as the followings:

(1) The granular materials having a smaller uniformity coefficient such as Toyoura sand and glass beads indicate that the dry density is slightly higher for MSP method with the nozzle openings less than 10 mm diameters than for JSSMFE method.

(2) The peak dry density obtained in Sengenyama sand whose uniformity coefficient is 3.0 is almost indentical to the maximum dry density produced by JSSMFE method, when the nozzle openings of less than 9 mm diameters are adopted.

(3) The dry densities obtained from MSP method within the range of this test are independent of the height of fall.

(4) However, Urayasu and Ikebukuro sands which contain finer fractions more than 10 % show that the peak dry densities obtained from MSP method are smaller than the maxi-

Table 2-2 High dry densities achieved by MSP method under nozzle diameters of 7 mm to 10 mm and height of fall of 300 mm to 700 mm

Sample name	Nozzle diameter d (mm)	Dry density γ_d (kN/m^3)		
		h=300mm	h=500mm	h=700mm
Toyoura sand	7.0	16.11	16.14	16.13
	8.0	16.13	16.12	16.12
	9.0	16.13	16.12	16.12
	10.0	16.11	16.13	16.14
Sengenyama sand	7.0	16.68	16.63	16.64
	8.0	16.63	16.68	16.69
	9.0	16.63	16.69	16.68
	10.0	16.03	16.04	16.03
Urayasu sand	7.0	13.93	13.88	13.79
	8.0	13.90	13.86	13.90
	9.0	13.68	13.74	13.65
	10.0	13.63	13.75	13.70
Ikebukuro sand	7.0	15.54	15.50	15.60
	8.0	15.50	15.39	15.60
	9.0	14.98	15.10	15.07
	10.0	14.95	14.88	14.93
Glass beads	7.0	15.82	15.82	15.84
	8.0	15.81	15,84	15,83
	9.0	15.83	15.83	15.81
	10.0	15.83	15.80	15.83

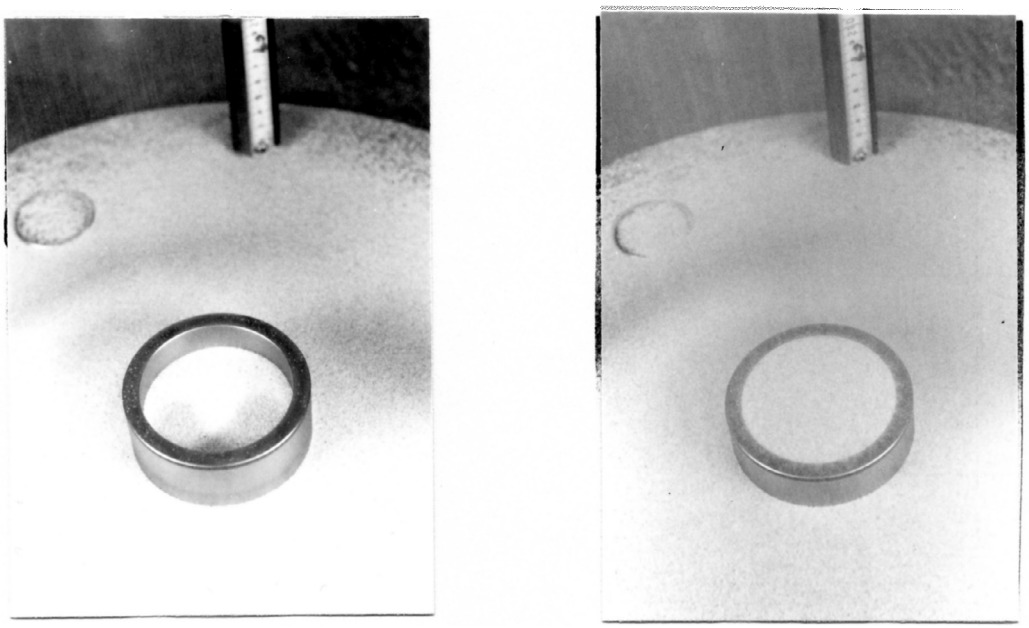

(a) (b)

Photo.2-2 Typical manner of deposition process of Toyoura sand at the condition of nozzle diameter 10 mm and height of fall 300 mm in which the maximum dry density is achieved; (a) at the elapsed time of 30 seconds after allowing pluviation of sand, (b) filling up of sand is completed in about 1 minute

mum dry densities produced by JSSMFE method. This can be attributed to the non-uniform sand flow or the occurrence of particle segregations during pluviation which could not be avoided in sands having relatively high uniformity coefficient.

The reason why in the granular materials with uniformity coefficient of less than 3.0 the dry density corresponding to the maximum dry density determined by JSSMFE method can be produced in MSP method would be explained by the uniform pluviation with less rate of deposition which insures no locking action or arching action. Lambe and Whitman (1969) has mentioned that by sprinkling sand into a container it is possible to achieve a density as high as that which is produced by vibration. Their findings seem to support the present results.

It should be pointed out, however, that there is still room to examine the appropriate selection or combinations of the multiple sieve opening size, so as to apply MSP method to the sands which contain some amount of finer fractions.

CHAPTER 3 TEST APPARATUS, EXPERMENTAL PROCEDURE AND MATERIAL USED

3.1 Test Apparatus and Procedure

All tests in this investigation were performed by employing the following test apparatuses; conventional triaxial compression apparatus, cyclic triaxial apparatus, true triaxial apparatus and cyclic triaxial apparatus improved for cone penetration test. In this paragraph, the conventional triaxial compression, cyclic triaxial and true triaxial apparatuses and their test procedures are explained, and the cyclic triaxial apparatus improved for cone penetration test will be described in CHAPTER 6.

Conventional triaxial compression test apparatus

The conventional triaxial compression test apparatus was used for a series of static triaxial compression and extension tests. Since this apparatus belongs to a conventional type with the specimen dimension of 50 mm in diameter by 120 mm in height, its detailed description will be abbreviated, but a slight modification was done. That is, a rigid load cell is installed inside the triaxial cell to eliminate the possible friction of loading piston, as illustrated in Fig.3-1.

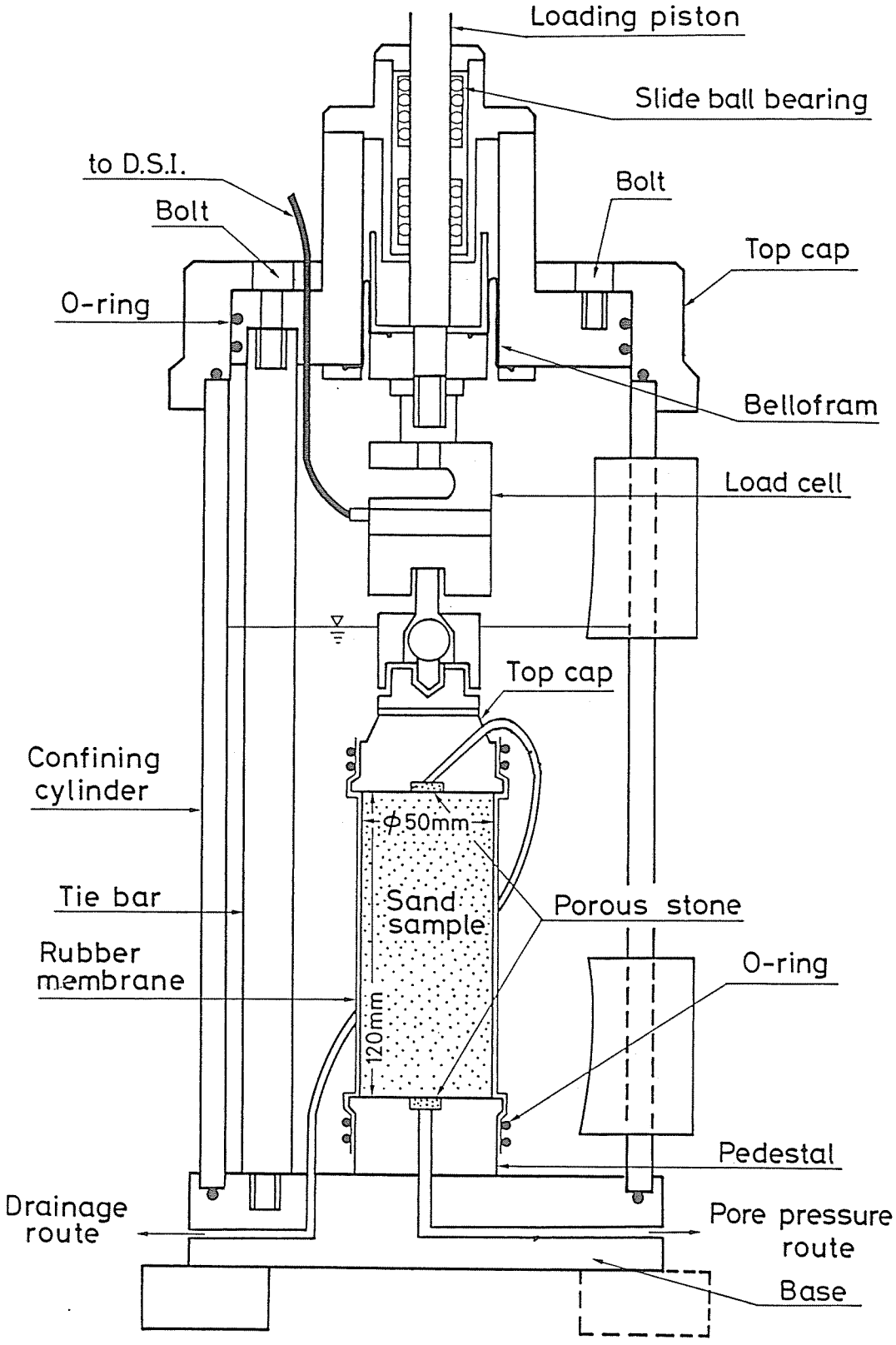

Fig.3-1 Section of triaxial device equipped with inner load cell

Digital strain meter and pressure and displacement transducers were used for the observation and recording of test data. In the conventional drained and undrained triaxial tests, measured variables were axial and radial principal stresses, pore water pressure, axial displacement and volume change. In this study, the change in axial principal stress during consolidation and shear was measured with a rigid load cell (load transducer) placed just above the top cap, and radial principal stress (cell pressure) and pore water pressure were measured by pressure transducer, and axial displacement was measured by displacement transducer. Electrical signals from the pressure and displacement transducers were recorded automatically by the digital strain meter according to time intervals set prior to the start of test. The volume change of specimen was measured in the burette by means of a 4-way valve. Since volume change measured in the burette is generally subjected to errors due to rubber membrane penetration into the interstices between the sand particles when testing sand samples under variable cell pressures, this error was corrected according to membrane penetration calibration test methods whose details are described by Raju and Sadasivan (1974) and Miura et al. (1980).

Procedure for conventional triaxial test

Each sand specimen which was prepared by the various

methods explained in the following paragraph was set up in the triaxial cell and then cell pressure was raised to 19.6 kPa. Since the sand specimens are in dry state or unsaturated state, they must be saturated anyhow. In this study, a saturation system by means of carbon dioxide was employed (Miura, 1983).

This system is schematically shown in Fig.3-2. Carbon dioxide was percolated through the specimen for about 30 minutes at a rate of about 20 specimen volumes per hour to insure that any gas in the specimen voids was carbon dioxide rather than air. Subsequently, the de-aired water was permeated into the voids at a small differential head (4.9 kPa) so as to free from the disturbance of initial fabrics. Since Henry's Constant for carbon dioxide is much larger than that for air, it is considered that a much larger amount of carbon dioxide (as compared to air) can be dissolved into a given amount of water, at much lower pressures. When the water completely filled the specimen voids and no gas bubbles appeared in the bubble chamber, back pressure of 196 kPa was applied for about two hour. By this procedure, Skempton's B-value of greater than 0.98 was obtained in all specimens. Cell pressure was increased up to a desired value to give the isotropic stress condition. After consolidating for two hours, a series of static triaxial compression and extension tests was performed.

The following experiments were carried out under the conditions mentioned below unless otherwise specified. Static

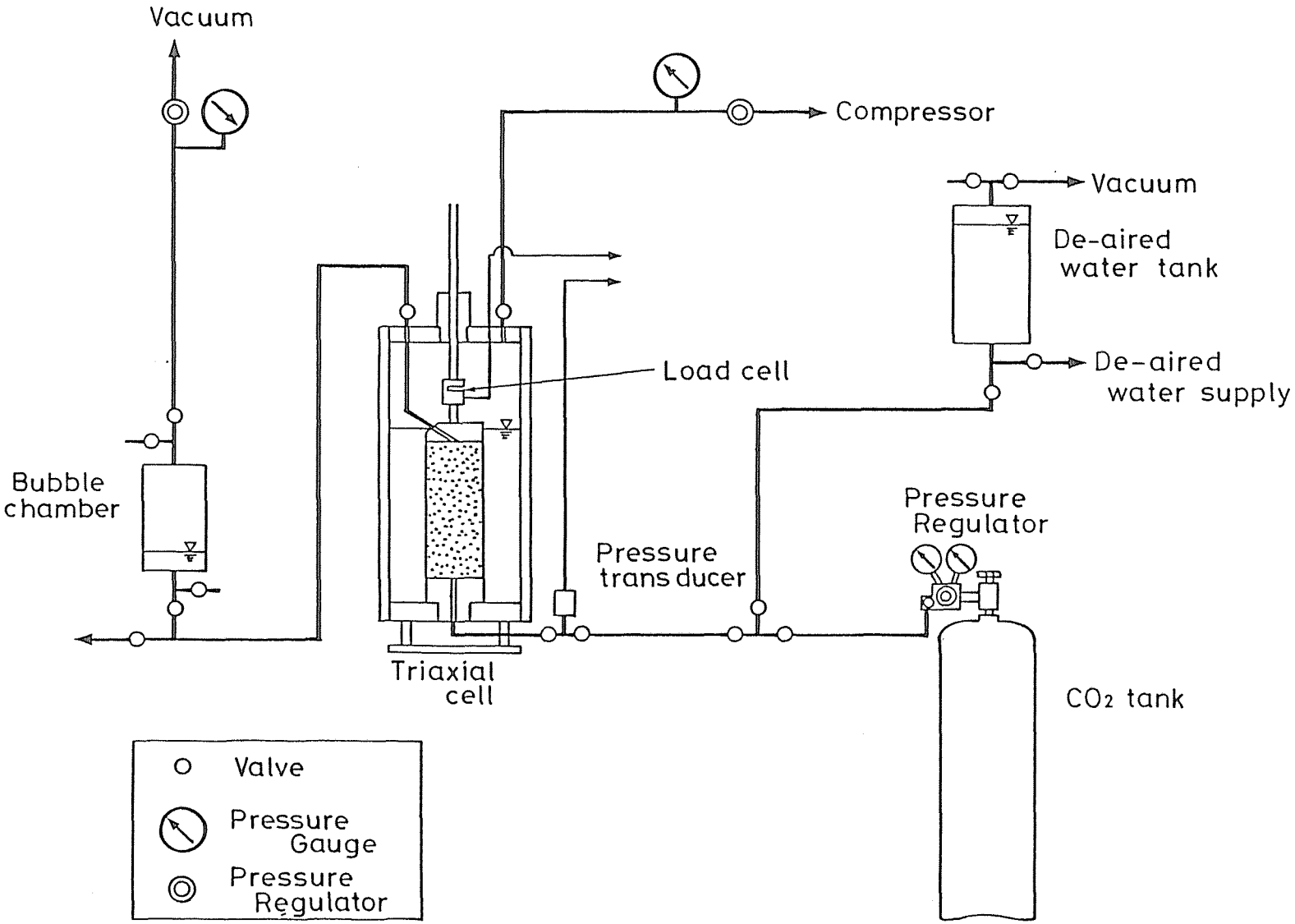

Fig.3-2 Schematic diagram of CO_2 saturation system for triaxial sand specimen

drained and undrained triaxial tests were conducted by increasing axial stress for compression tests or decreasing for extension tests under constant radial stresses. The rate of axial strain was 0.25 % per minute.

These test results were arranged by the following stress and strain parameters:

$$p' = (\sigma'_a + 2\sigma'_r)/3 \ , \ q = |\sigma'_a - \sigma'_r| \ , \ \eta = q/p' \qquad (3\text{-}1)$$

$$\varepsilon_v = (\varepsilon_a + 2\varepsilon_r) \ , \ \gamma = 2|\varepsilon_a - \varepsilon_r|/3 = |\varepsilon_a - \varepsilon_v/3| \qquad (3\text{-}2)$$

where σ'_a and σ'_r imply axial and radial effective principal stresses, p' and q effective mean principal and shear stresses, ε_a and ε_r axial and radial strains, ε_v and γ volumetric and shear strains, respectively. Compressive strains are positive quantities. In this study, the sand specimens were consolidated isotropically to an effective mean principal stress p_c. Therefore, radial effective principal stress after consolidation becomes equal to p_c and will be denoted as σ'_c.

Cyclic triaxial test apparatus

A slightly modified form of the standard cyclic triaxial cell was used for cyclic undrained tests performed in this investigation. Fig.3-3 shows schematically the triaxial cell

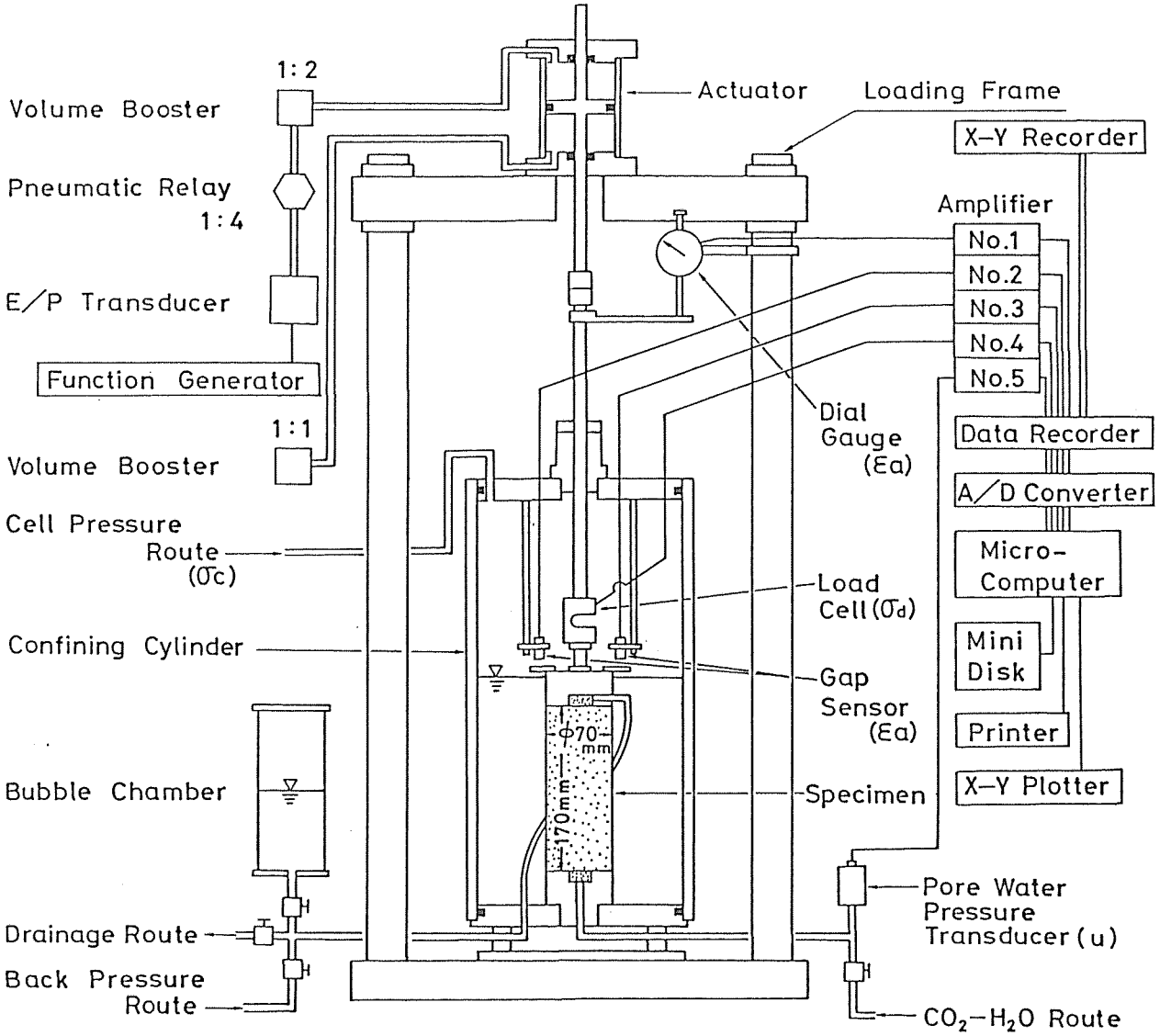

Fig.3-3 Schematic diagram of cyclic triaxial apparatus and data processing system

mounted to the loading system and the data processing system. In order to improve the cyclic triaxial device so that it can measure the cyclic undrained behaviors corresponding to a small strain level (10^{-4} or less), a highly sensitive gap sensor and a load cell were installed in the triaxial cell. Kokusho (1980) and Toki et al. (1983) have shown that such improvements of cyclic triaxial device can give the cyclic stress-strain relationships under a small strain level free from the effects of any friction which is caused by the loading piston and the displacement transducer.

The cyclic loading system used was the pneumatic sinusoidal loading system whose main components are a sine wave generator, a volume booster relay, and a double acting air piston (actuator). The fundamentals of this system were presented by Chan and Mulilis (1976). Initially, the pressures on both sides of the actuator are identical. At the start of the test, when deformations are extremely small, the sine wave generator applies a cyclic load to one side of the actuator while the pressure on the other side of the actuator remains at a static value. As the cyclic undrained test proceeds, the pore water pressure increases and eventually equals the effective confining pressure, which produces relatively large deformations. It is at this point that the volume booster relay boosts the quantity of air flow required to keep the output pressure matching the signal pressure, thus enabling the load on the specimen

to remain constant after liquefaction occurs. It can be seen in CHAPTER 4 that the amplitude of cyclic axial stress is maintained constant during cyclic undrained loading without being affected by the development of large axial strain.

Procedure for cyclic undrained triaxial test

Saturation method of sand specimen for cyclic undrained triaxial tests was the same as that for conventional one. In cyclic undrained triaxial tests, sinusoidal cyclic axial stresses supplied by the pneumatic cyclic loading system mentioned above were applied to the sand specimen with a frequency of 0.1 Hz. The sand specimens were consolidated isotropically to an effective mean principal stress p_c ($= \sigma_c'$). Dimension of specimen was 70 mm in diameter by 170 mm in height. During cyclic loading, the radial principal stress was kept constant. The cyclic axial load, axial deformation and change in pore water pressure were monitored and measured with time. These measured values were recorded automatically by the data recorder and were processed by the microcomputer.

Cyclic triaxial test results were normalized using the conventional stress ratio $\sigma_d / 2\sigma_c'$ where σ_d is the maximum single amplitude of cyclic axial stress $\Delta\sigma_a$ and σ_c' is the radial effective principal stress at consolidation ($= p_c$).

True triaxial test apparatus

True triaxial tests carried out with the apparatus shown schematically in Fig.3-4. This apparatus permitted principal stresses σ_x , σ_y , σ_z to be applied independently through hydraulic pressure (chamber pressure), rubber pressure bag and rigid platen, respectively. Dimension of specimen is 80 × 45 mm in side and 90 mm in height. Construction of base and top of the triaxial cell and measurement method of principal stress σ_z and principal strain ε_z in z-direction were almost the same as those of conventional one. That is, vertical principal stress σ_z was measured by a rigid load cell (load transducer) installed inside the triaxial cell, and vertical principal strain ε_z was measured by a displacement transducer. Principal stress σ_y in y-direction was applied through a set of pressure bags filled with de-aired water. For applying water pressure to the pressure bags, a water reservoir was used. Principal strain ε_y in y-direction was measured by monitoring the amount of water flowing in and out of the pressure bags using a burette with a 4-way valve. In consolidation stage, the pressure bags which were suspended by pulley were pushed against the sand specimen with a small water pressure of 4.9 kPa to insure contact between the sand specimen and the pressure bags before starting shear test. On the other hand, another principal stress σ_x in x-direction (horizontal direction) was controlled easily by the chamber

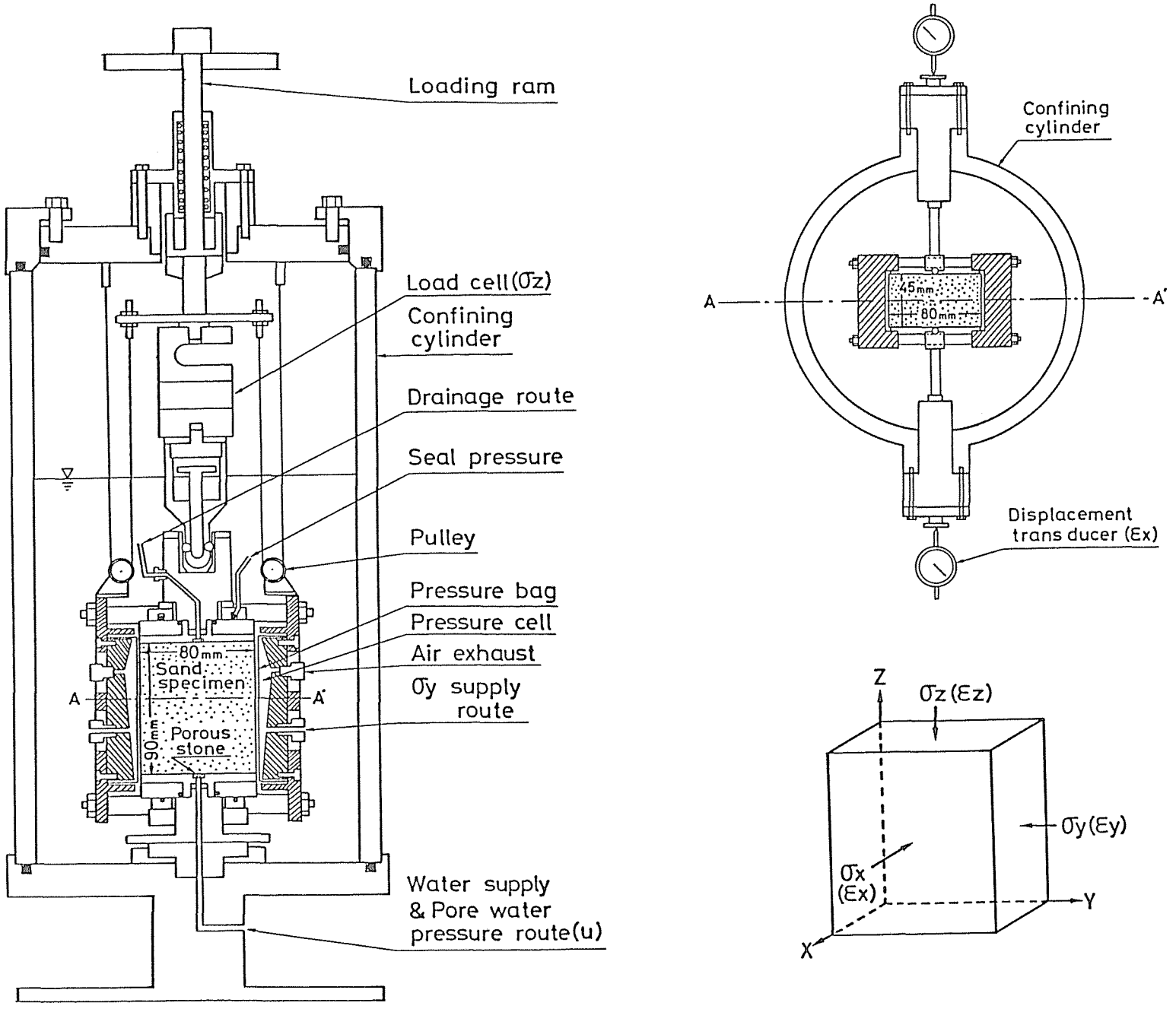

Fig.3-4 Schematic diagram of true triaxial test apparatus

pressure (cell pressure), and corresponding principal strain was measured by means of a measuring system for lateral displacement (Toki et al., 1978) connected to the triaxial cell, as shown in Fig.3-5. Horizontal principal stresses σ_x , σ_y and horizontal principal strain ε_y were measured by pressure and displacement transducers, respectively. Volumetric strain ε_v and another horizontal principal strain ε_x was measured by using two burettes, respectively.

With this arrangement, three principal stresses can be controlled independently.

As explained in CHAPTER 1, various types of true triaxial apparatus have been developed. The true triaxial loading methods for cubical or rectangular prismatic specimens can be grouped into the strain-controlled system with rigid platen boundary-conditions, the stress-controlled system with flexible boundary-conditions and mixed boundary-conditions (Sture and Desai, 1979). According to their grouping method, the true triaxial test apparatus employed by the present author is categorized into the stress-controlled type with mixed boundary-conditions.

Procedure for true triaxial test

Saturation method of sand specimens for true triaxial tests was the same as that for conventional and cyclic ones. In all of the true triaxial tests performed in this study,

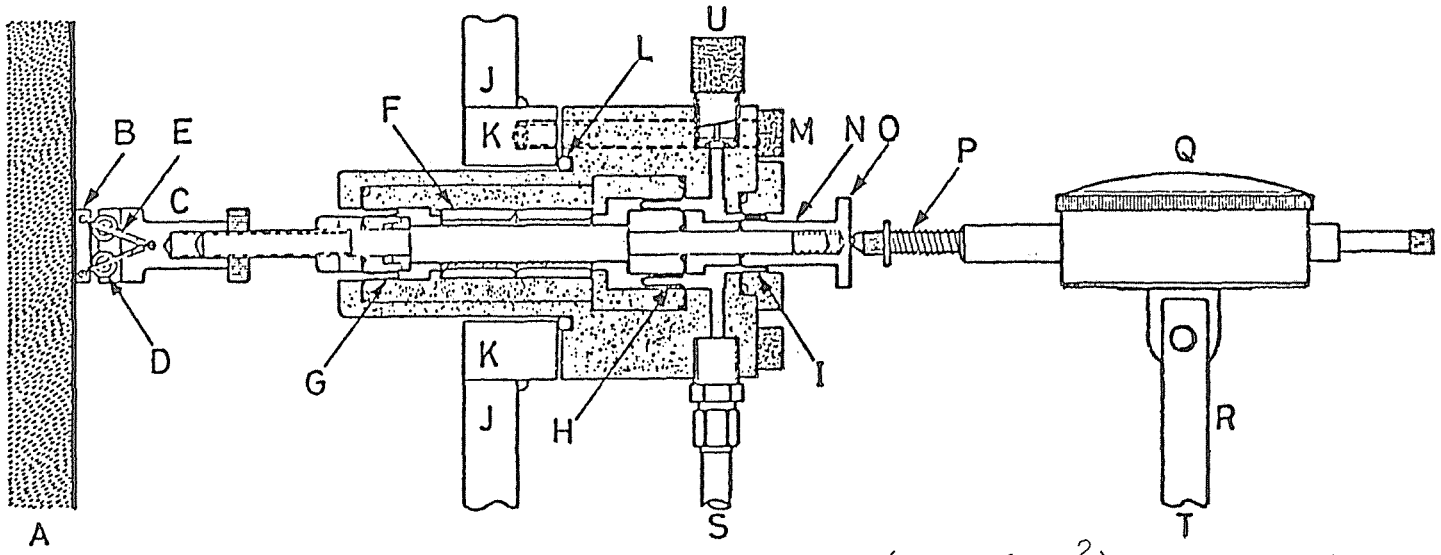

A: Sand Specimen
B: Contact Plate
C: Contact Attachment
D: Roller
E: Spring
F: Slide Ball Bearing
G: Bellofram (A_e=1.65cm^2)
H: Bellofram (A_e=2.60cm^2)
I: Bellofram (A_e=0.95cm^2)
J: Triaxial Cell
K: Boss
L: O-ring
M: Bolt
N: Spindle Piston
O: Dial Gauge Attachment
P: Spring
Q: Displacement Transducer
R: Dial Gauge Stand
S: σ_c Connection
T: to Base Plate (Fixed)
U: Air Release Valve

Fig.3-5 Schematic diagram of measuring system for lateral displacement

sand specimens were first consolidated isotropically to an effective mean principal stress p_c (= σ'_c) of 196 kPa and were then subjected to shear stresses along some stress path extending straight in radial directions on the octahedral plane. These tests were carried out under the drained condition.

These test scheme will be explained in detail later in CHAPTER 5.

All the tests in this study were performed in the temperature controlled laboratory at $20 \pm 0.5^{\circ}C$.

3.2 Preparation of Sample

Because one object of this study is to examine the dependency of static and cyclic deformation-strength behaviors of artificially or naturally deposited sands on their fabric characteristics, the sand specimens prepared by various methods are used in the laboratory. The sand sample preparation methods adopted in the present study were as the followings:

(1) MSP method (R_A method): A desired density was easily controlled by the pertinent combination of the nozzle diameter (d) and the height of fall (h) in the multiple sieve pluviation apparatus. The details of this procedure for preparing the triaxial sand specimen were described in CHAPTER 2.

Because MSP method obliges the sand beforehand oven-dried to be deposited by pluviating vertically through air into the triaxial mold, the specimens prepared by this method seem to possess the fabric characterized by the orthotropic property that the apparent long axis of the sand particles has strongly preferred orientations in the vertical section, but almost completely random orientations in the horizontal section. This will be confirmed in the following paragraph. Therefore, we will refer in this paper the sand specimen prepared by this method to as R_AV-specimen (or MSP specimen).

(2) MSP method (R_B method): The specimens by this method were formed by the preparation procedure shown in Fig.3-6. This preparation method was in principle the same as MSP method (R_A method) mentioned above, whereas the slit whose width could controll the density of sand deposit was equipped in the sand hopper, and the larger size and more layers of sieves than in the previous multiple sieve pluviation apparatus (CHAPTER 2) were utilized in order to deposit uniformly the sand particles in a sand container with the dimension of 220×110 mm in inner side and 200 mm in height (See Fig.3-6). This method can give the relative density D_r over a fairly wide range from 20 % to 100 % by controlling the slit width (Toki et al., 1981).

For facilitation of specimen forming, the sand deposited in the container was frozen in a freezer for about twelve hours at the temperature of about $-25^{\circ}C$. The container was designed to avoid any expansion and/or disturbance of sand fabrics during freezing. The observations indicated that the application of surcharge of 9.8 kPa by weights to the sand deposits in the container which had been permeated by the de-aired water at a small differential head (4.9 kPa) and thereafter unsaturated completely at the suction of 6 kPa induced no measurable volume expansion due to freezing. No measurable expansion observed in this freezing procedure could be also seen in the unidirectional freezing method attempted in the present study in which

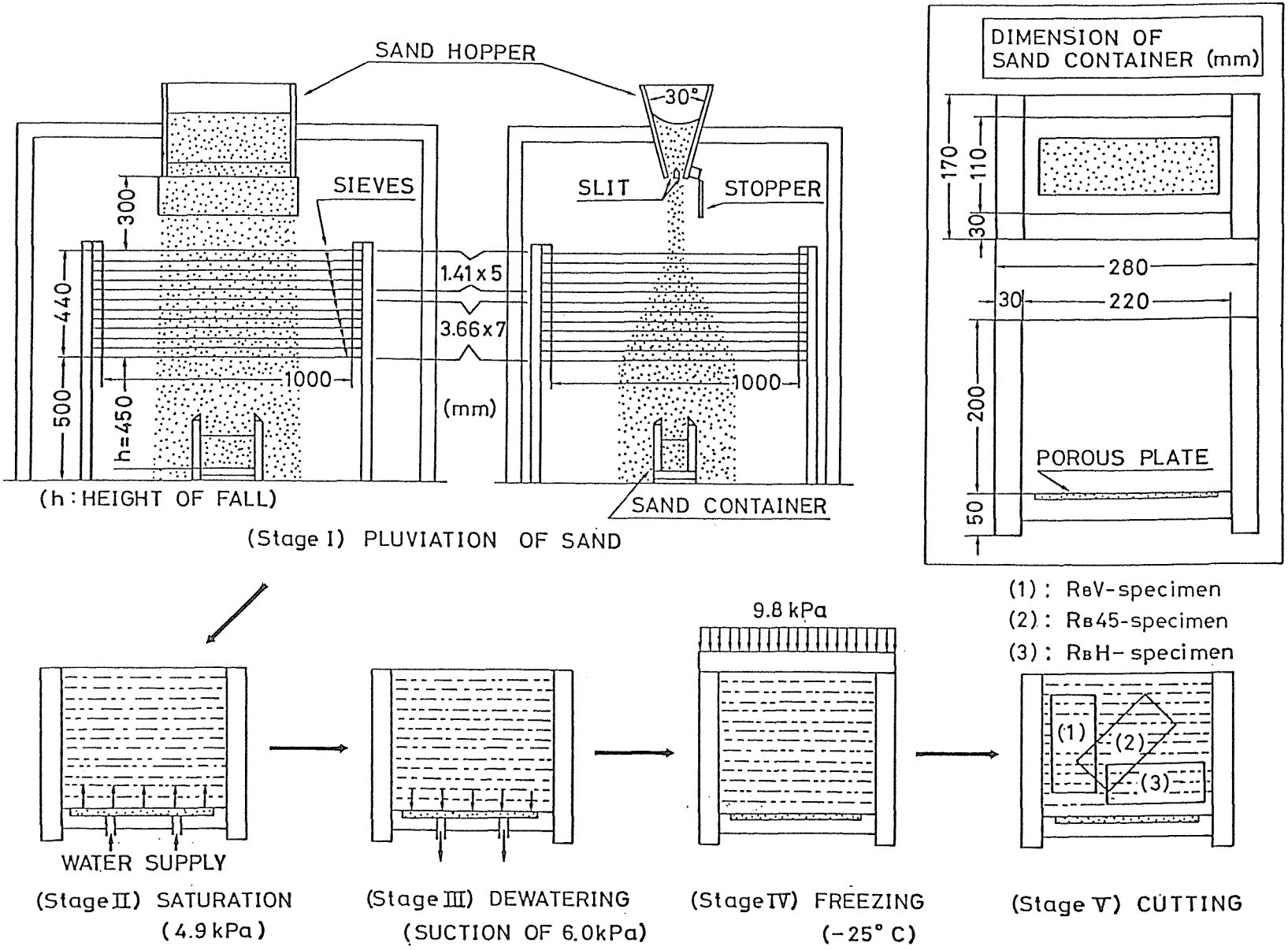

Fig.3-6 Preparation procedure of R_BV-, R_B45- and R_BH-specimens and sand container used in R_B method

freezing of sand deposits proceeded upwards from the bottom plate with perfect drainage of excess water ahead of the freezing front.

Three kinds of cylindrical specimens with the different depositing planes and the various densities were cut by using the saw for slate and the straight edge from the frozen sand blocks made by the procedure mentioned above. That is, the specimens with the angle between the axial direction of the triaxial specimen and the pluviation direction (vertical direction) of 0°, 45° and 90° were prepared in the present study, and they are referred hereafter to as R_BV-, R_B45- and R_BH-specimens, respectively.

Photo.3-1 shows a triaxial test specimen of Toyoura sand (R_BV-specimen) cut from the frozen sand block.

After these frozen specimens were set up in the triaxial cell and then the cell pressure was raised to 19.6 kPa, they were allowed to melt completely in the triaxial cell (for two hours), before percolating the carbon dioxide. Subsequent procedure was the same as that mentioned in the previous paragraph.

R_B45-specimen was used only for the study on the cone penetration characteristic and its correlation to static and cyclic mechanical properties of saturated sand (CHAPTER 6).

As will be explained in the following paragraph, it can be expected that R_BV-specimen has almost the same fabric chara-

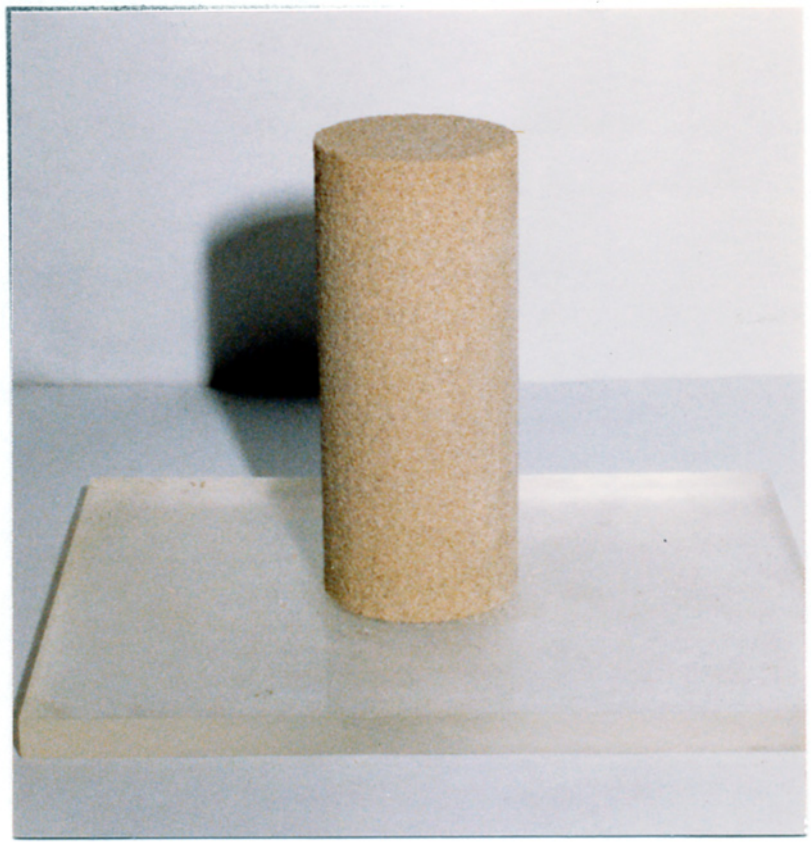

Photo.3-1 Triaxial test specimen of Toyoura sand (R_BV-specimen) cut from frozen sand block

cteristics as those of R_AV-specimen. However, we draw tentatively a distinction between R_AV- and R_BV-specimens, because R_BV-specimen is subjected to the freeze-thaw sequence during the preparation process.

(3) Rodding method (R_C method): Sand of 8 % water content is stuffed in layers with each layer compacted by rodding a hand tamper which is 10 mm in diameter and 250 mm in length into the sand. The rodding depth is about 20 mm. This method produces the relative densities from around 30 % to 95 % by controlling the initial water content of sand and rodding number. The specimen prepared by this method will be called R_C-specimen (or rodded specimen).

(4) Tapping method (R_D method): Oven-dried sand is poured in five or six layers with each layer compacted by tapping the side wall of the triaxial mold by a wooden hammer to a prescribed dry density. Relative densities obtained by this method range from around 40 % to 95 %. The sand specimen formed by this method will be referred to as R_D-specimen (or tapped specimen).

(5) Flask method: Sand oven-dried beforehand is filled in a flask. As schematically shown in Fig.3-7, a flask having a cork with a predetermined nozzle size ($\bar{d}$) to produce the

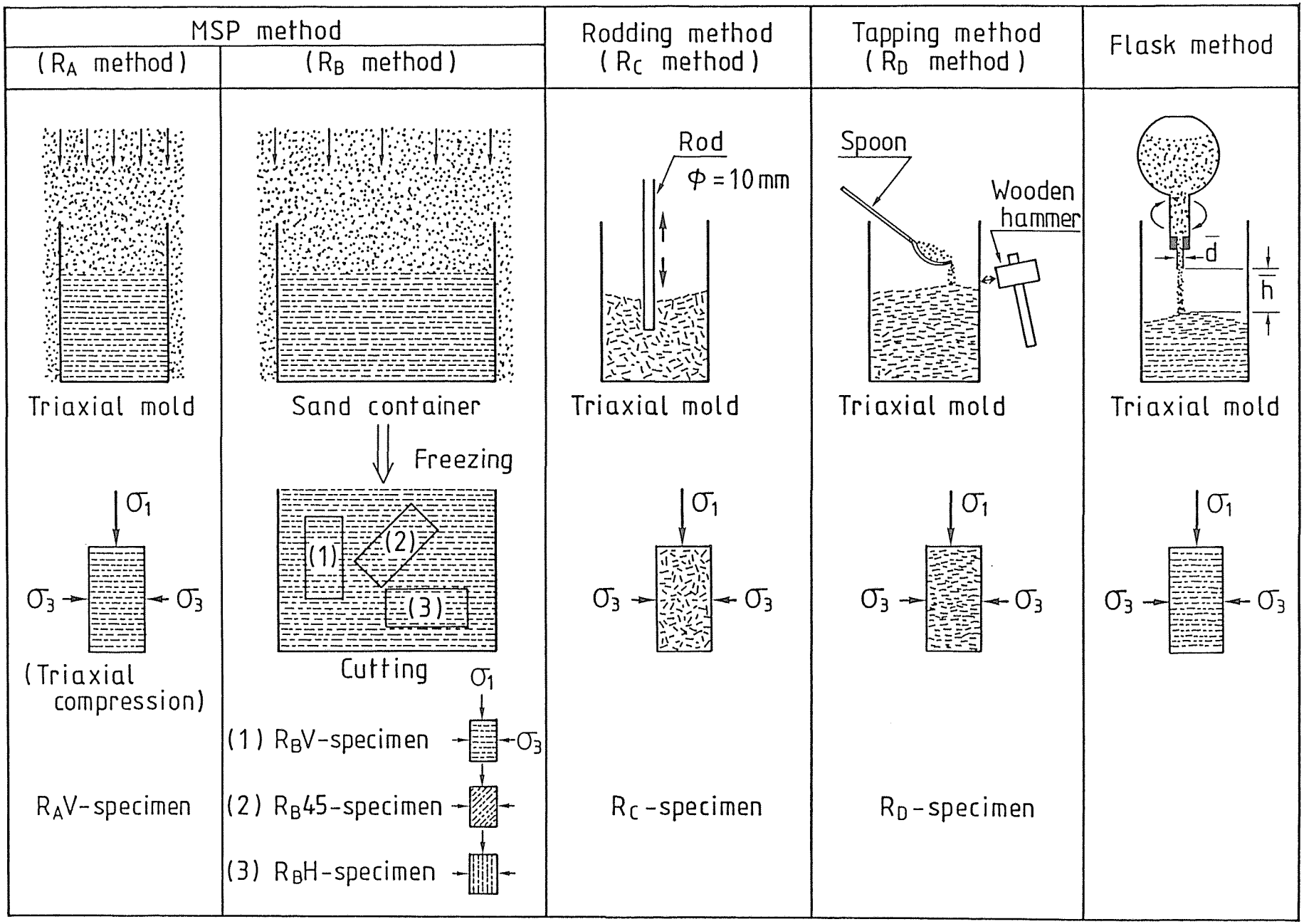

Fig.3-7 Schematic diagram of sand sample preparation methods adopted in this study

desired density is inverted above the triaxial mold and rotated by hand allowing the sand to flow uniformly into the mold, maintaining constant the height of fall ($\bar{h}$). This method whose details have been described by Mulilis et al. (1975) is very similar to MSP method in view of pluviation through air. This method has been widely used in a laboratory testing of sand (e.g., Chaney and Mulilis, 1978; Silver et al., 1980; Tatsuoka et al., 1982), and will be tentatively referred to as flask method in this paper. Relative densities after consolidation D_{rc} at $p_c = 196$ kPa (p_c is the mean principal stress at isotropic consolidation) obtained by this method were, for example, 50 % to 55 % for $\bar{d} = 4.5$ mm and 67 % to 72 % for $\bar{d} = 3.5$ mm at the condition of $\bar{h} = 70$ mm, respectively.

These sand sample preparation methods are summarized in Fig.3-7. The stress condition for the conventional triaxial compression test is also shown in the figure. It should be remembered that different methods of reconstitution to a desired density produce samples with different fabrics and different mechanical properties.

The discussion for artificially deposited sand in this study is mainly based on the test data of the specimens which are specified according to the above sample preparation methods or the fabric characteristics of samples.

3.3 In-Situ Sampling of Undisturbed Sand

In order to make the degree of anisotropy in the static and cyclic deformation-strength properties of naturally deposited sands clear, a series of drained triaxial compression and extension tests and cyclic undrained triaxial tests are performed for the undisturbed sand specimens which are obtained from the in-situ deposits. Although various methods have been proposed for the in-situ sand sampling, a block sampling method with sand freezing process is adopted in this study. It has been indicated by Yoshimi et al. (1978), Ishihara et al. (1978) and Singh et al. (1982) that sand freezing technique is an available means to obtain the undisturbed samples.

The undisturbed sand samples used in the present study were taken by performing the block sampling at two sites of relatively homogeneous natural sand deposits which were located in the suburbs of Kushiro City and Ishikari-cho, Hokkaido. Kushiro and Ishikari sands sampled are referred tentatively to as " K-sand " and " I-sand ", respectively. The sampling depth, depth of water table from ground surface and estimated overburden pressure at both sites were 3.5 ^{m}, 4.5 ^{m} and 61 kPa for K-sand and 2.5 ^{m}, 3.8 ^{m} and 45 kPa for I-sand, respectively.

The in-situ block sampling was performed by using sectional cubical steel boxes with inside lengths of 300 ^{mm} and wall thickness of 5 ^{mm} at open pits exposed by hand (See Figs.

3-8 and 3-9). The evaluation method of quality of sand samples obtained by such block sampling has been examined by Tohno (1977). Block samples which had been cut vertically to a designed size were deliberately enclosed with the cubical steel boxes as shown in Fig.3-9 and Photo.3-2, and then drained for about 24 hr to minimize any disturbance that might be incurred during freezing and specimen handling. After the block samples were hermetically sealed, they were frozen in the insulated boxes packed with dry ice, and transported to the laboratory and stored in a freezer of about -25°C. The speed of freezing were not controlled, whereas the block samples seemed to be frozen completely for about 12 hr.

Although a truly undisturbed sand sample could not be obtained by any sophisticated sampling method because of the release of in-situ stress system and/or any possible mechanical disturbance during sampling process, we will refer temporarily the sands sampled by above mentioned method to as undisturbed sand in this paper.

In order to examine the dependency of static and cyclic deformation-strength behaviors of naturally deposited sands on their fabrics, the following two kinds of triaxial specimen which are specified according to the cutting directions are prepared in the laboratory from the frozen sand blocks sampled by the method mentioned above.

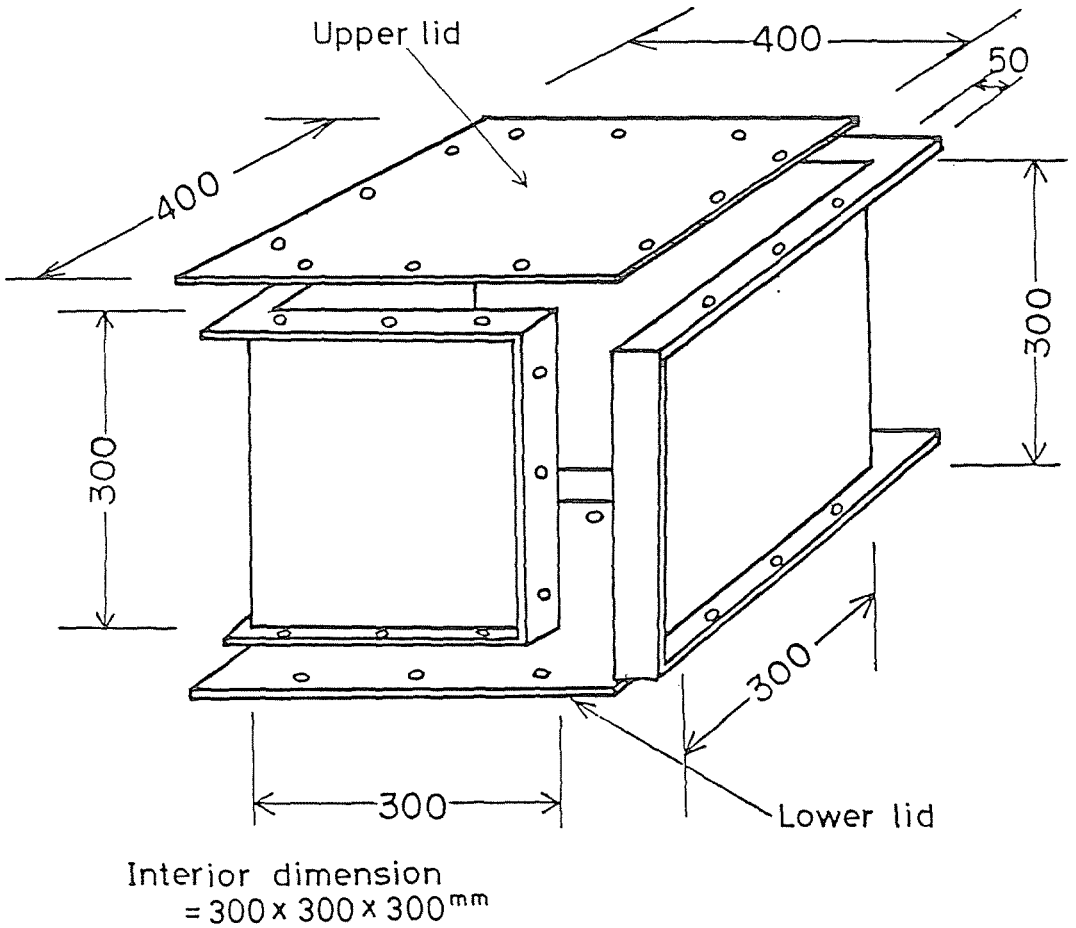

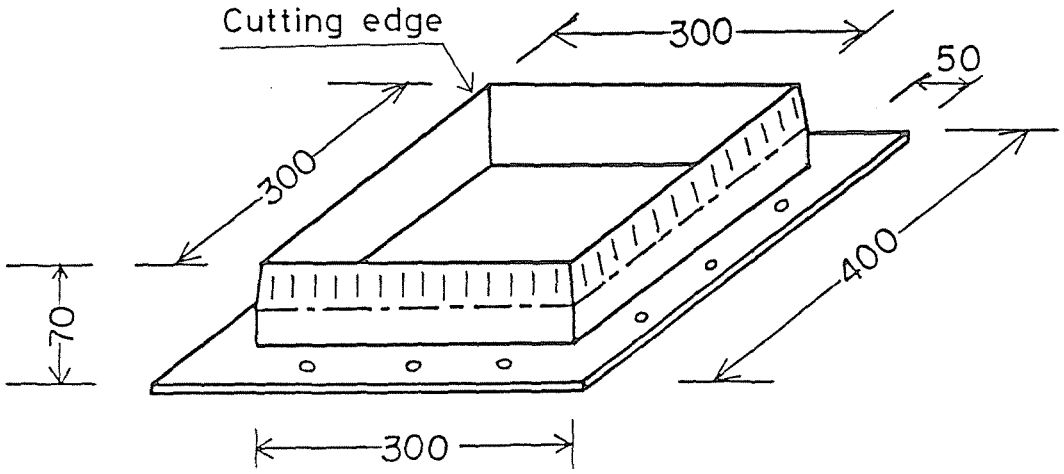

Fig.3-8 Cubical steel box and cutting edge for in-situ block sampling

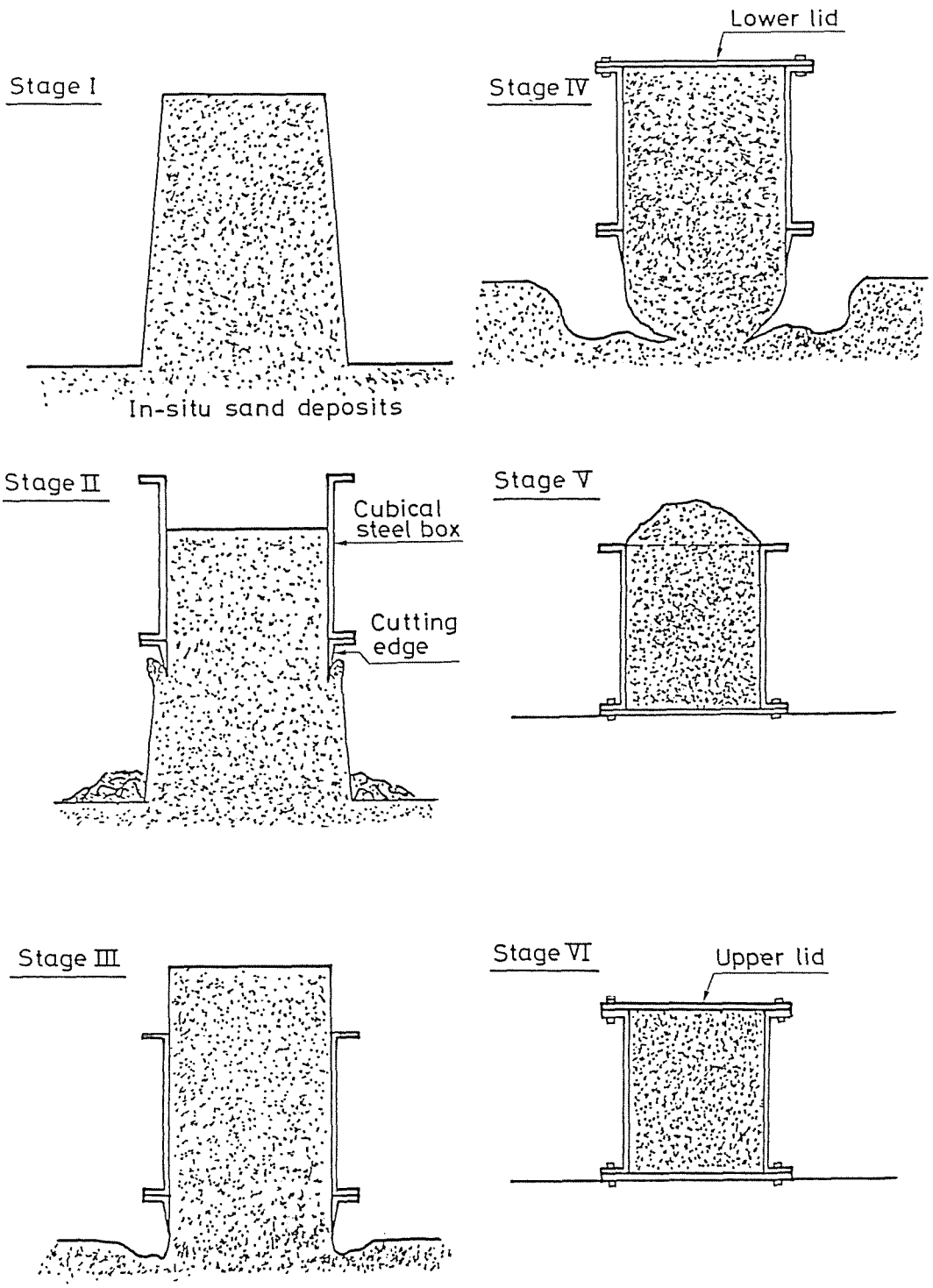

Fig.3-9 Schematic diagram of in-situ block sampling procedure

Stage Ⅰ

Stage Ⅱ

Stage Ⅳ

Stage Ⅵ

Photo.3-2 Procedure of in-situ block sampling for undisturbed I-sand

(1) UV-specimen: As shown in Fig.3-10, this was cut using the saw for slate and the straight edge from the frozen sand blocks so that the axial direction of triaxial test specimen coincided with the in-situ vertical direction.

(2) UH-specimen: By the same procedure as for UV-specimen, this specimen was prepared by cutting in the direction which differed with that of UV-specimen by 90°. Accordingly, it follows that the axial direction of this undisturbed triaxial test specimen was coincidental with the horizontal direction in natural sand deposits as can be seen in Fig.3-10. Photo.3-3 shows a triaxial test specimen of undisturbed I-sand (UV-specimen) cut from the block sample.

Furthermore, whether or not the mechanical properties of these undisturbed triaxial specimens could be simulated in the laboratory testing was examined in the present study. For this purpose, I- and K-sand specimens with the same densities as undisturbed samples were reconstituted by R_A, R_B, R_C and R_D methods whose details were explained in the previous paragraph. As mentioned in the following paragraph, K-sand contains finer fractions of around 3 %. For the granular materials containing finer fractions such as K-sand, MSP method can not produce the uniform sand specimen with very high density because of the non-uniform sand flow or the ocurrence

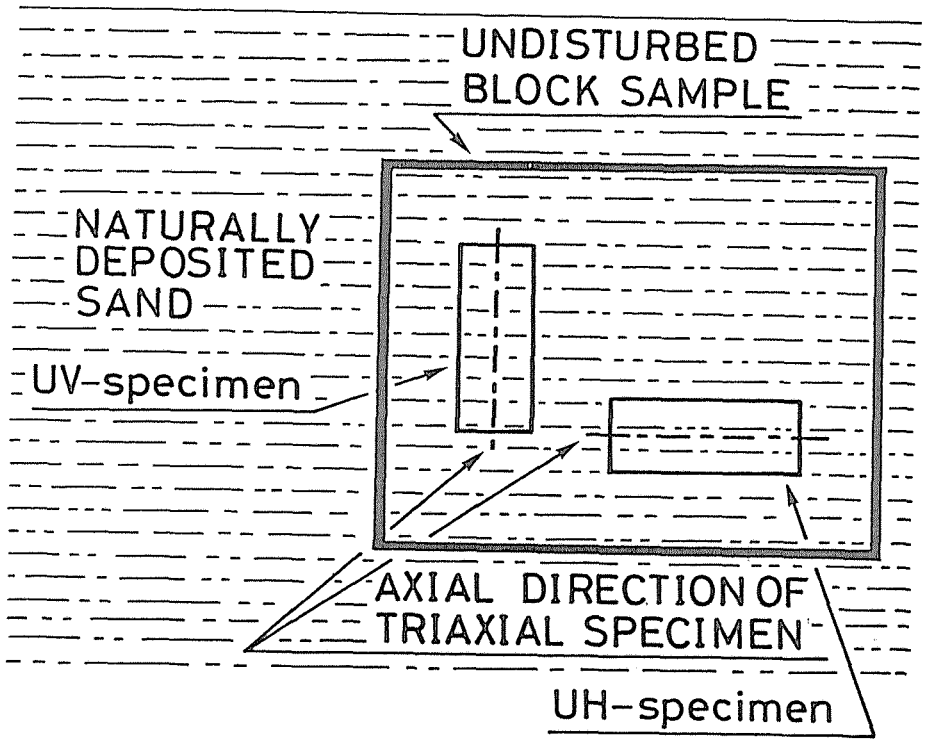

Fig.3-10 Method for preparing UV- and UH-specimens from one undisturbed block sample

Photo.3-3 Undisturbed triaxial test specimen of I-sand (UV-specimen) cut from block sample

of particle segregation during pluviation (See CHAPTER 2). Accordingly, R_A and R_B methods were not adopted for the reconstitutions of K-sand.

The discussion on the undisturbed sands are based on the results of a series of static triaxial compression and extension tests and cyclic undrained triaxial tests performed within around three months after sampling. These test procedures for the undisturbed triaxial specimens are the same as those for the specimens artificially prepared. It may be important to note that the undisturbed triaxial specimens sampled ideally from naturally deposited sands are possessed of the stress system as shown schematically in Fig.3-11, if they were normally consolidated. However, for the simplification of discussion on the anisotropy in mechanical properties of sand, the undisturbed triaxial specimens were consolidated isotropically to an effective mean principal stress p_c ($= \sigma_c'$) of 98 kPa. Consolidation under $\sigma_c' = 98$ kPa which corresponds to about twice the in-situ overburden pressure σ_{vc} of sampled sands would be expected to avoid the possible effects of stress release and/or overconsolidation due to sampling (Tatsuoka et al., 1981).

The relative densities after consolidation (D_{rc}) at $\sigma_c' = 98$ kPa of the undisturbed sand specimens varied between 82 % and 91 % for I-sand and between 93 % and 107 % for K-sand. Since the mean relative densities $\overline{D_{rc}}$ of these undisturbed

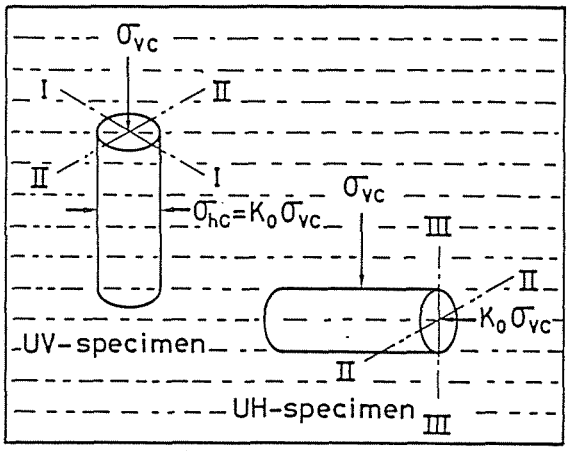

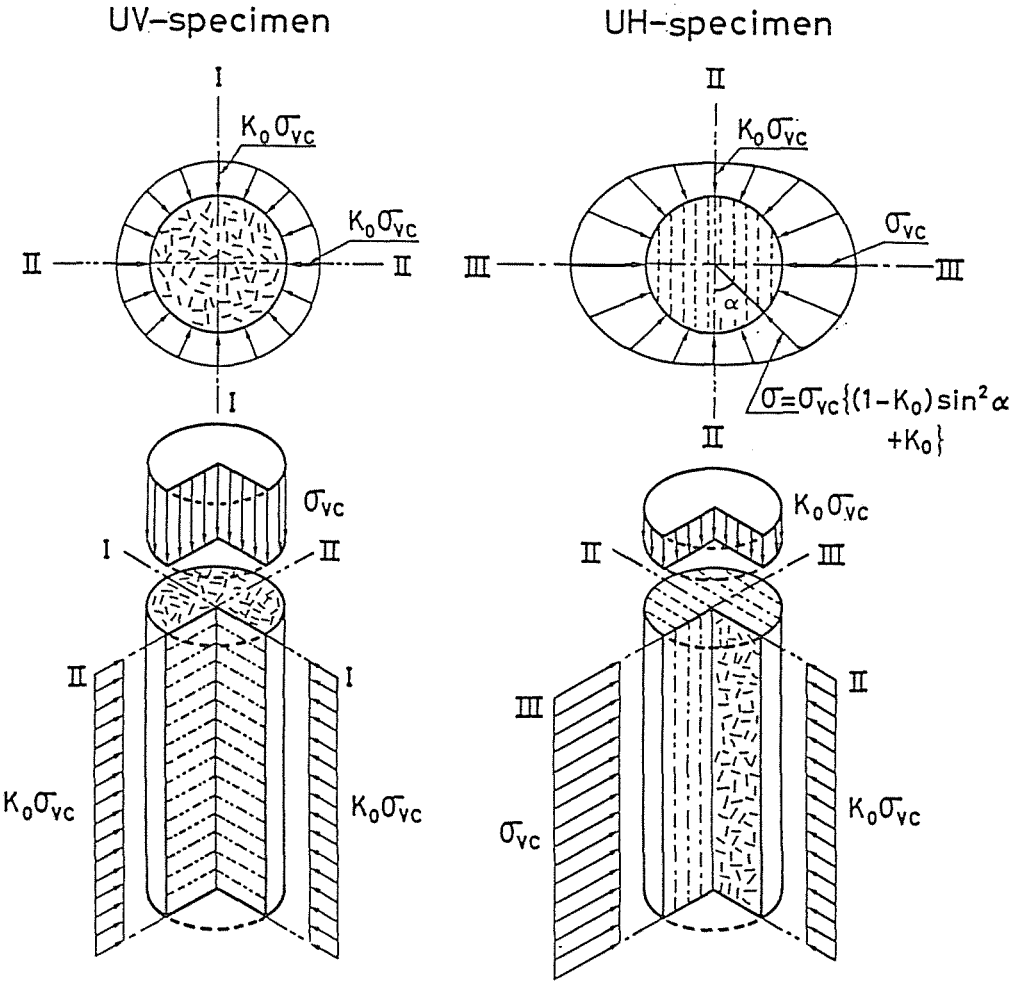

Fig.3-11 Initial stress condition of undisturbed triaxial sand specimens obtained from block sample, where in-situ sands are assumed to have been normally consolidated under K_o condition

specimens were obtained as 85 % for I-sand and 98 % for K-sand, these values were defined in this study as representative relative density for each undisturbed specimen. Accordingly, when I- and K-sands were reconstituted to each $\overline{D_{rc}}$ by the methods in the preceding paragraph, the variations in D_{rc} of reconstituted specimens were limited to the extent within ± 3 % for each $\overline{D_{rc}}$.

3.4 Physical Properties of Sand Used

The physical properties of I- and K-sands sampled are shown in Table 3-1 and Fig.3-12, comparing with those of Toyoura standard sand (referred hereafter to as " T-sand "). The maximum and minimum void ratios were measured according to the JSSMFE method (1979) which was described in the preceding paragraph, and determined from the average values of ten measurements.

K-sand contains finer fractions of around 3 %, whereas its grain size distribution curve is similar to that of T-sand. I- and K-sands were deposited with higher relative density and to some extent cemented due to geological aging.

The particle shape of these sands are shown in Photo. 3-4 which are obtained through a scanning electromicroscope. These sands seem to have a similar particle shape. If they were assumed to be remotely comparable, the feature of these sands is as follows. T-sand consists mainly of flat or rod-like shape particles with relatively smooth surface. I-sand is composed chiefly of elongated or flat particles with irregular surface. K-sand has the similar characteristics to those of T- and I-sands in its mineralogy and particle shape, if the existence of finer fractions is excluded.

The particle shape and orientation fabric of these sands will be quantitatively evaluated in the following paragraph.

Table 3-1 Physical properties and maximum and minimum void ratios of K-, I- and T-sands determined by JSSMFE method (1979)

Sample name	K-sand	I-sand	T-sand
Specific gravity	2.69	2.73	2.65
Uniformity coefficient	1.6	1.5	1.5
Mean particle size (mm)	0.17	0.26	0.18
Finer fraction ($\leq$ 74μm) (%)	3.0	0.5	0
e_{max}	1.294	1.235	0.992
e_{min}	0.774	0.808	0.625
Mean in-situ relative density (%)	98	85	–
Water content at sampling (%)	15	8	–

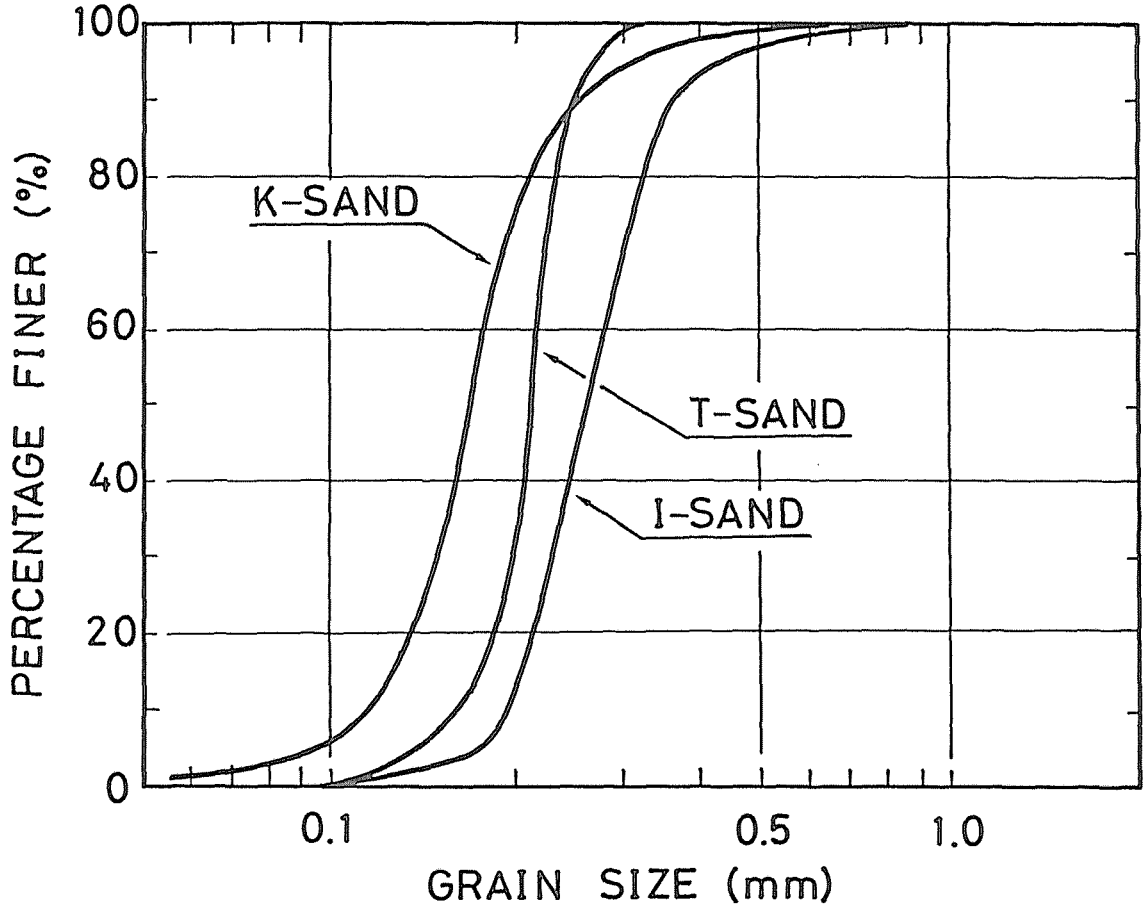

Fig. 3-12 Grain size distribution curves

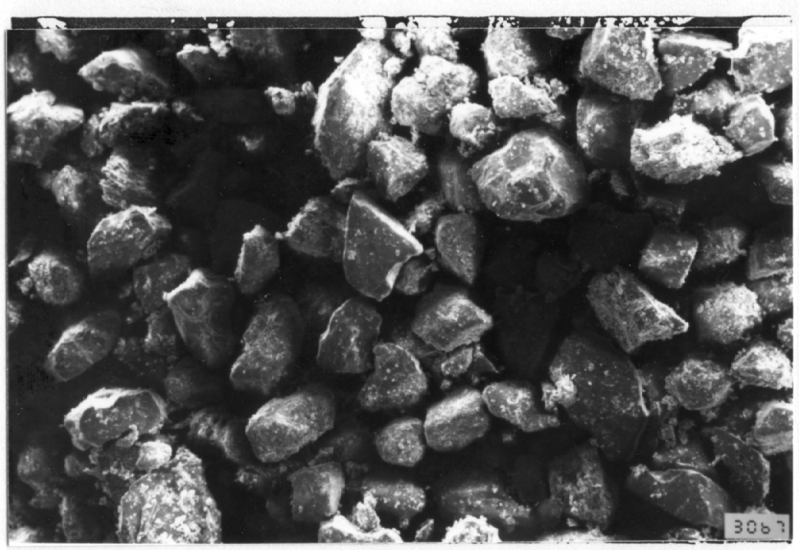

(a) K-sand

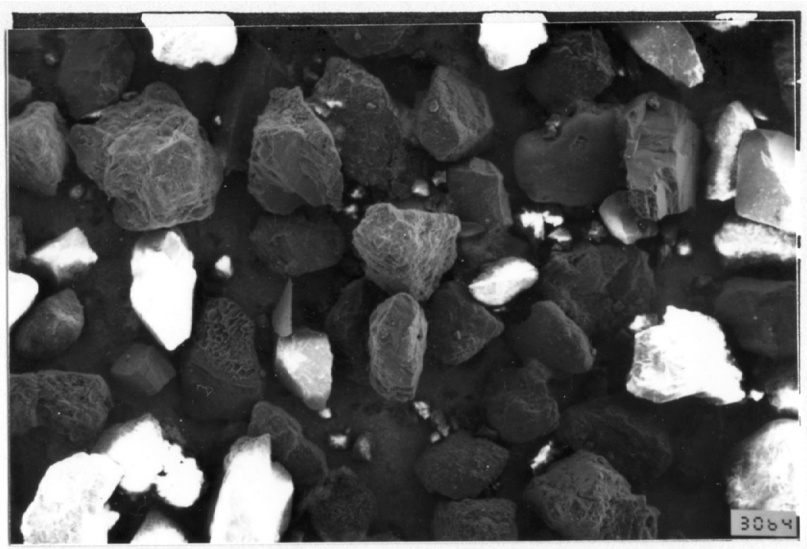

(b) I-sand

0 0.5 1.0mm

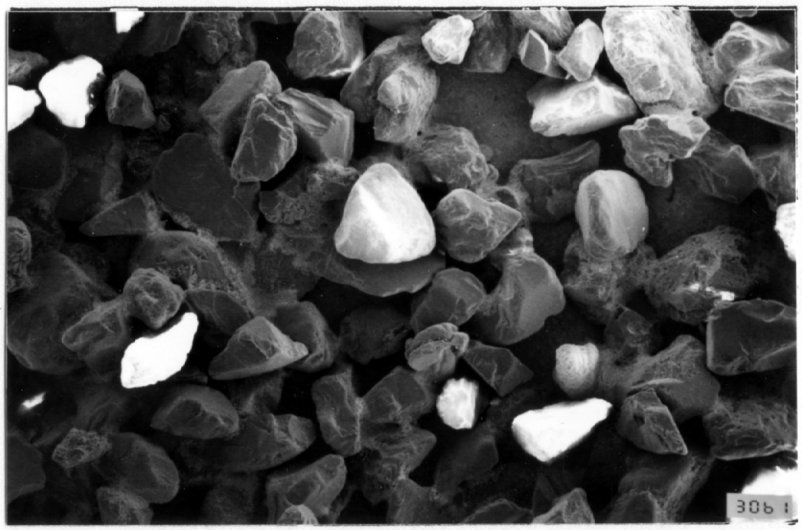

(c) T-sand

Photo.3-4 Particle shape of K-, I- and T-sands

3.5 Characterization of Fabric

The orientation fabric of a particle must be represented by the inclination of its long and short axes with respect to the fixed reference axes. Oda (1972a) and Arthur (1971) have observed the orientation fabric of sand particle by thin section method and X-rays method, respectively.

In this study, the orientation fabric of undisturbed and reconstituted sands was measured by a relatively simple method by means of a scanning electromicroscope. Measurement procedure is as follows. Using a small steel holder with the dimension of 20 ^{mm} in inner diameter by 7 ^{mm} in height, a sand sample for microscopic photograph was cut from the central regions of frozen triaxial test specimens along two planes as shown in Fig.3-13. In this study, these two planes are referred to as V- and H-sections. The reference axis z denotes the vertical direction (axial direction of triaxial specimen), the axes x and y denote the horizontal direction. The central region was used to avoid effects of the side walls which may locally have influenced the fabric.

The sand samples thus made were oven-dried, and then an instantaneous adhesive with low viscosity was slowly permeated into the fine voids so as to free from the disturbance of initial fabric. After about 30 minutes, the sand sample was sufficiently fixed by the bonding agent.

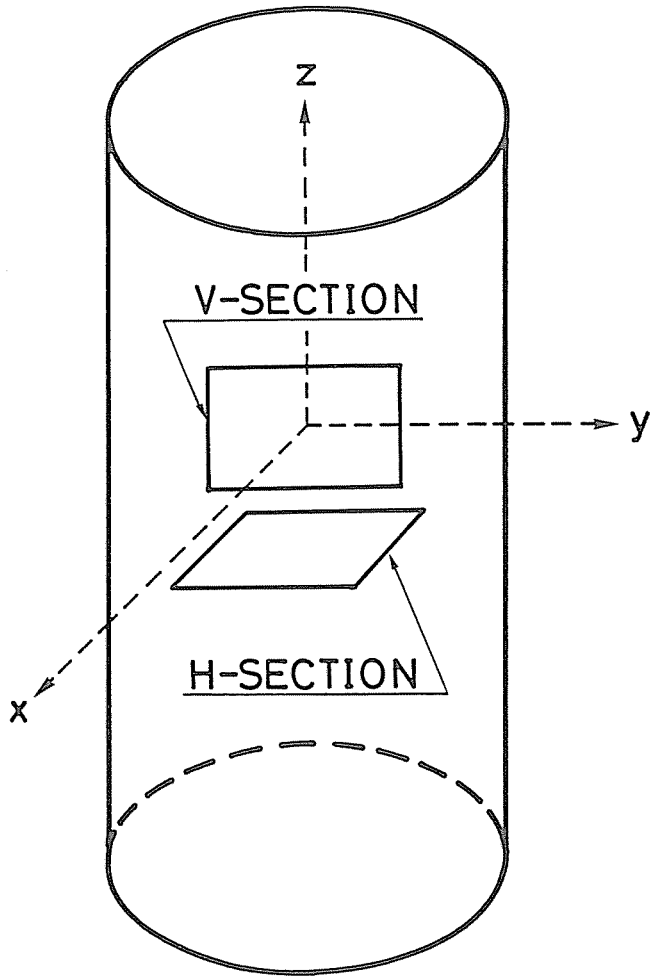

Fig.3-13 Preparation of sand sample for microscope photograph

Photo.3-5 shows the typical example of scanning electromicroscope photographs obtained from V- and H-sections of the sand samples thus fixed by the bonding agent. These were the sand samples prepared from undisturbed I-sand specimen.

Measurements of the orientation and shape of particles was performed by tracing the sand particle boundaries on the photographic enlargements. As shown in Fig.3-14, the shortest dimension S_i, the longest dimension L_i and the angle θ_i between the apparent long axis of a particle (i) and the reference axis y on each section were measured in this study, and 250 particles were selected at random from the photographic enlargements.

The mean value of axial ratio (A.R.) which is regarded as a parameter indicating the particle shape was calculated by

$$A.R. = \frac{1}{n} \sum_{i=1}^{n} \left(\frac{S_i}{L_i} \right) \qquad (3\text{-}3)$$

where n is the number of particle (= 250). The value of A.R. ranges from 0 to 1. When the mean value of axial ratio approches unity, particles are considered to be close to spheres. The values of A.R. for K-, I- and T-sands obtained in the present study are given in Table 3-2, which shows that these sands have almost the same values of A.R. (= 0.6).

(a) V-section

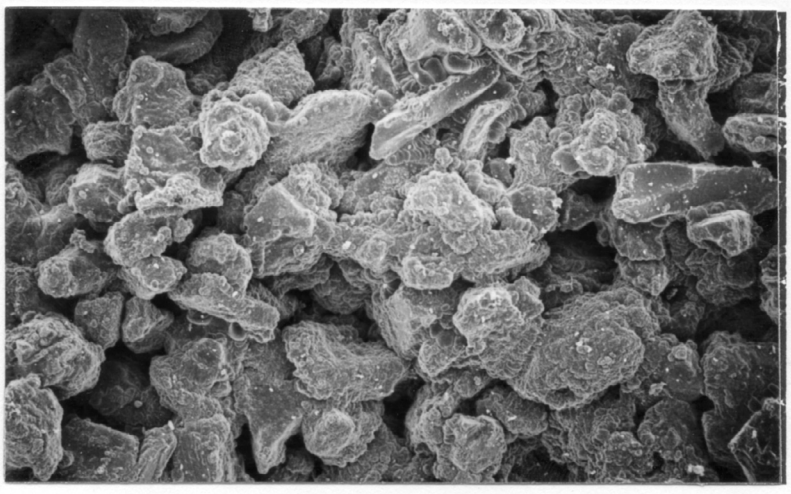

(b) H-section

Photo.3-5 Typical example of scanning electro-microscope photograph taken from undisturbed I-sand sample; (a) V-section, (b) H-section

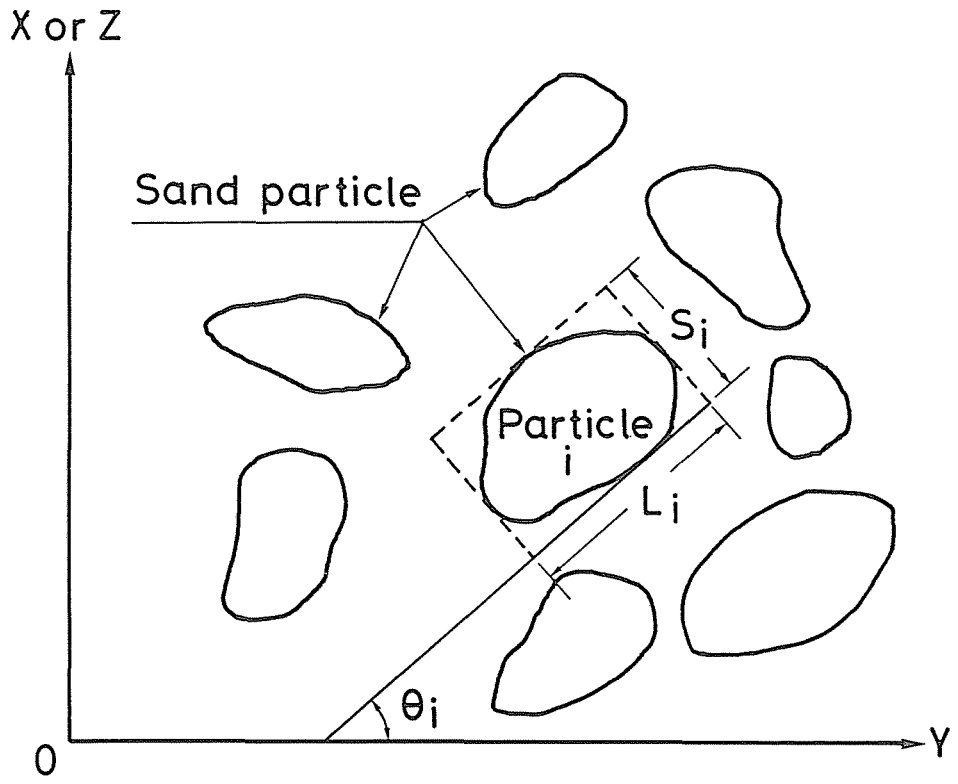

Fig.3-14 Definition of S_i, L_i and θ_i

Table 3-2 Values of A.R., V.M. and $\overline{\theta}$ measured in K-, I- and T-sand specimens

Sample name		D_r (%)	A.R.	V.M. (%)	$\overline{\theta}$ (deg.)
K-sand	Undisturbed specimen	98	0.64	V*: 50.3 H*: 5.9	V : 11.6 H : 7.9
	Tapped (R_D) specimen			V : 16.7 H : 9.9	V :-16.5 H : 31.0
I-sand	Undisturbed specimen	85	0.60	V : 40.0 H : 11.8	V : 3.5 H : 22.2
	MSP (R_B) specimen			V : 33.2 H : 2.7	V : 8.5 H : 41.9
	Rodded (R_C) specimen			V : 24.0 H : 8.4	V : 22.0 H :-21.2
T-sand	MSP (R_B) specimen	80	0.60	V : 36.3 H : 2.8	V : -2.9 H : 21.5
	Rodded (R_C) specimen	50		V : 19.4 H : 0.2	V : -8.0 H : -1.6

* V and H denote V-section and H-section, respectively.

Therefore, it may be said that K- and I-sands sampled from natural deposits are very similar to T-sand which consists mainly of flat or rod-like particles.

As mentioned above, the orientations of apparent long axes of sand particles were evaluated by measuring θ_i value of 250 particles for vertical and horizontal sections. In this study, the orientations of their particles for each section were determined by assigning them to one of the twelve 15° intervals between 0° and 180°. The choice of 15° intervals was based on the total number of particles in the tracing sample and compatibility of confidence level (accuracy) in fabric and property determination. The number of particles in each of the intervals was separately totalled, and then computed as percentages of the total number of particles in the tracing sample. These percentage values were then plotted on polar coordinate graph paper as rose diagrams shown in Fig.3-15. In these figures, the solid lines represent the orientations for V-section and the broken lines the orientations for H-section. If all particles were randomly oriented, the plot will be a circle shown in the figures.

In order to examine the intensity of fabric anisotropy, the mean vector direction $\bar{\theta}$ and vector magnitude V.M. defined by Curray (1956) were calculated according to:

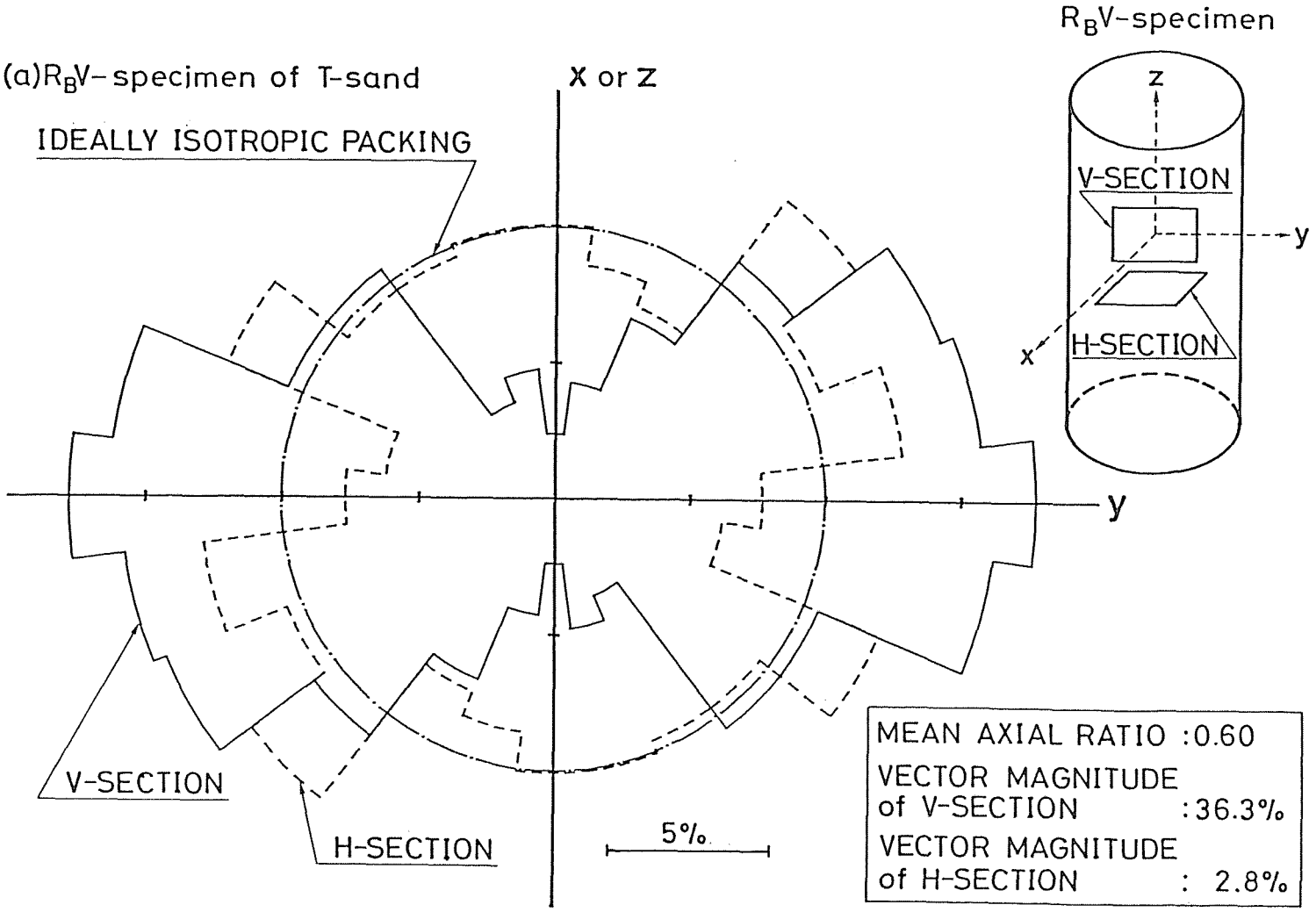

Fig.3-15(a) Rose diagrams to show orientations of particle long axes in T-sand specimen with D_r of 80 % prepared by MSP method (R_B method)

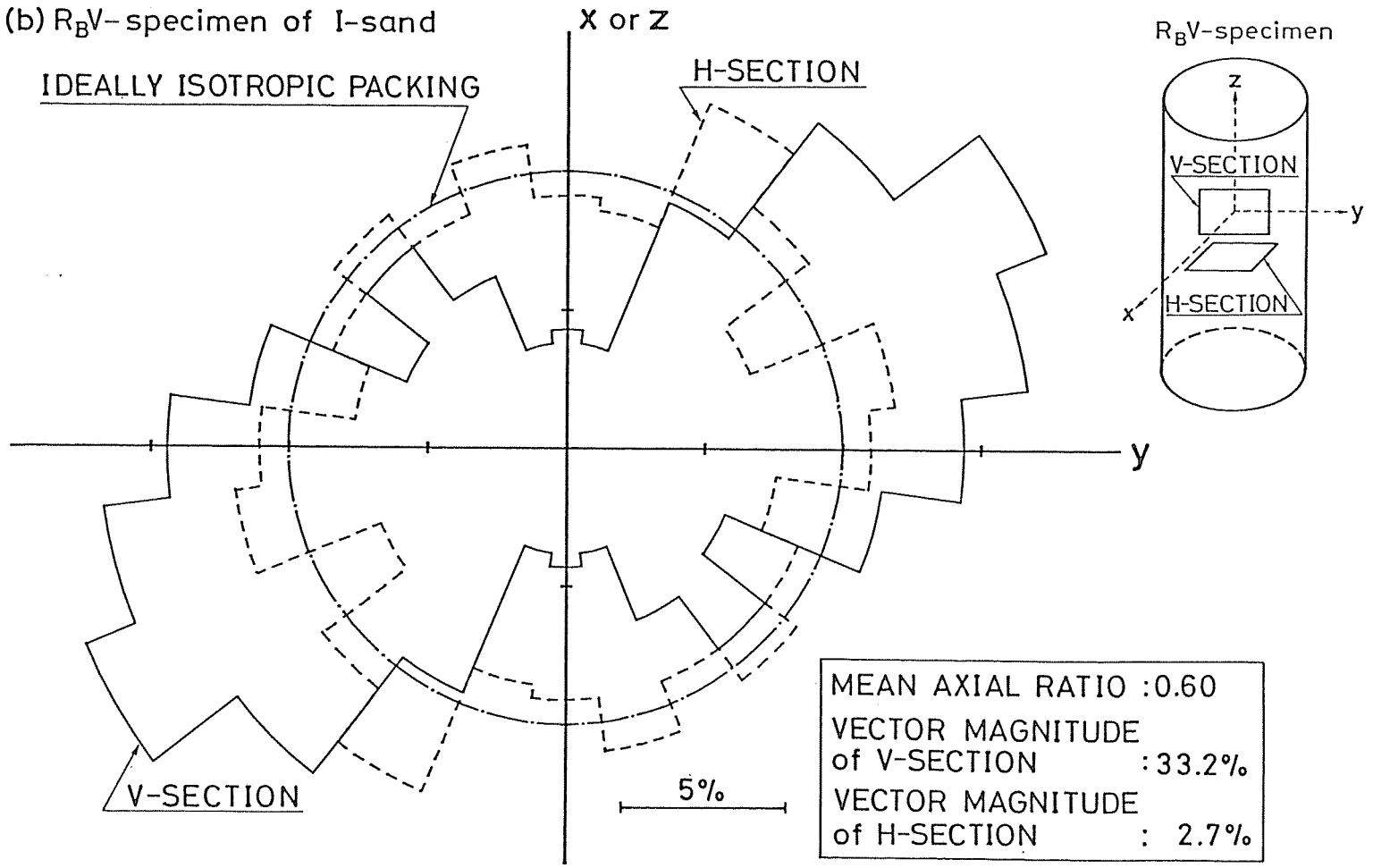

Fig.3-15(b) Rose diagrams to show orientations of particle long axes in I-sand specimen with D_r of 85 % prepared by MSP method (R_B method)

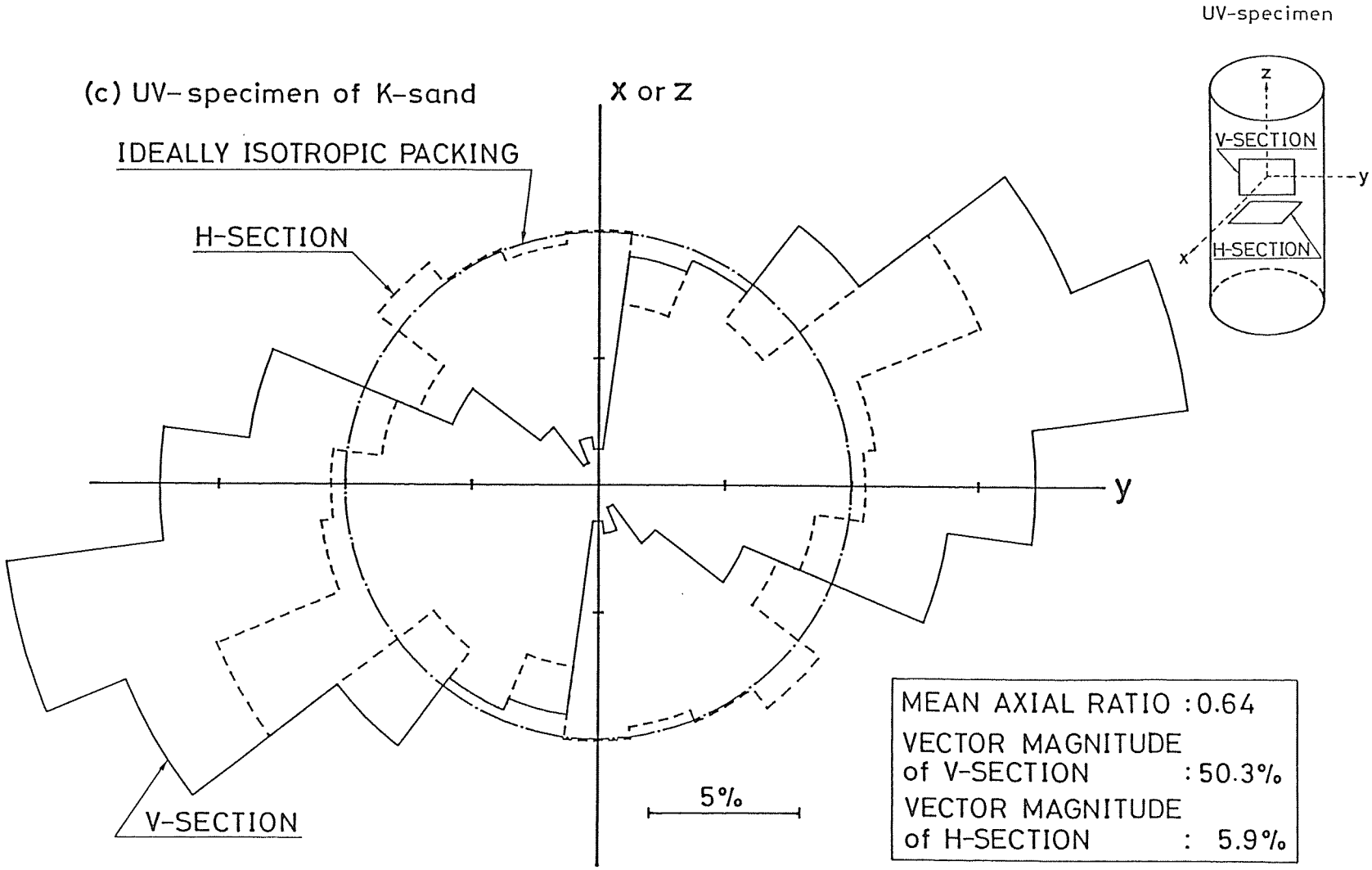

Fig.3-15(c) Rose diagrams to show orientations of particle long axes in undisturbed K-sand specimen with D_r of 98 % obtained from block sample

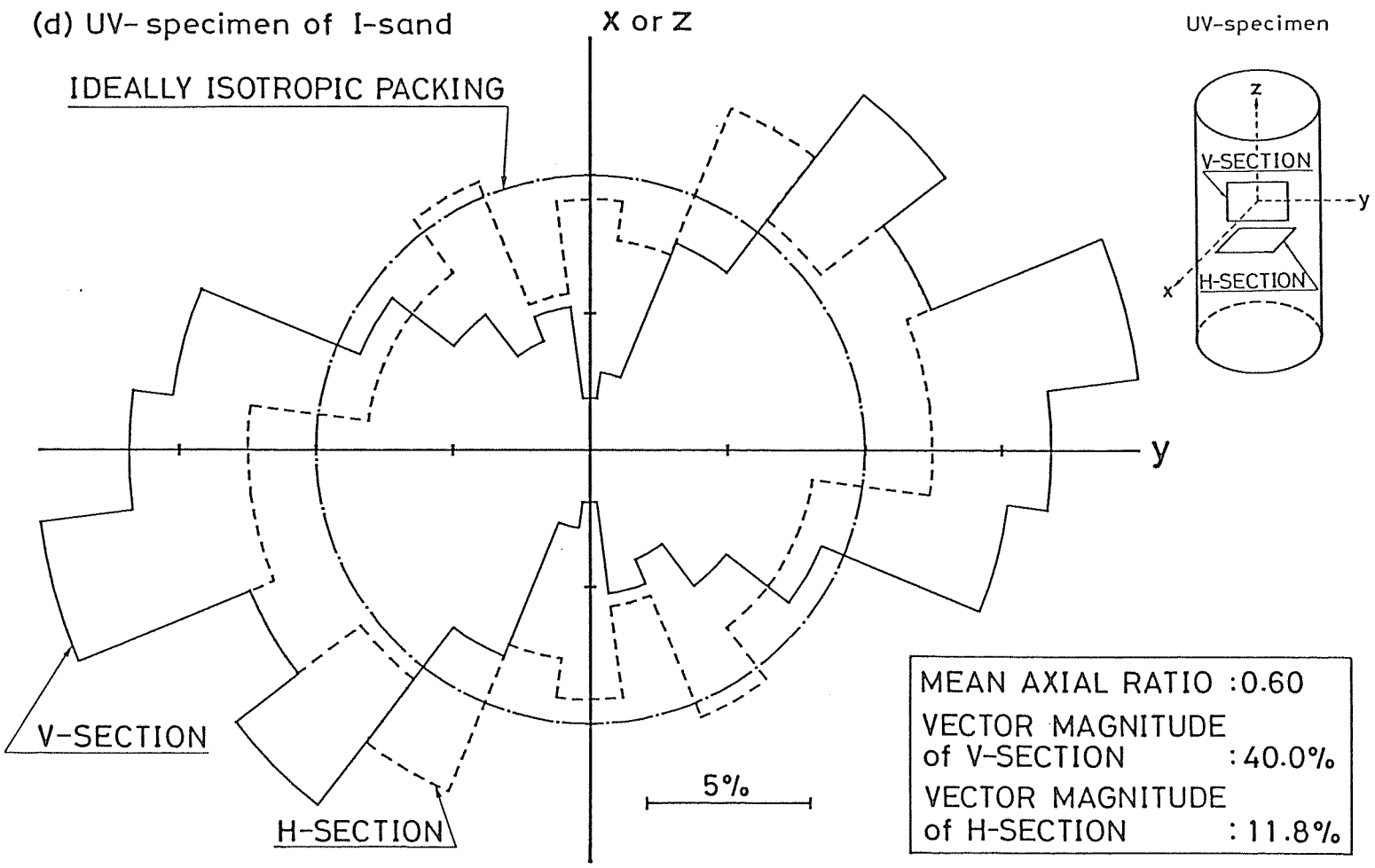

Fig.3-15(d) Rose diagrams to show orientations of particle long axes in undisturbed I-sand specimen with D_r of 85 % obtained from block sample

$$\bar{\theta} = \frac{1}{2} \arctan \frac{\sum_{i=1}^{n} \sin 2\theta_i}{\sum_{i=1}^{n} \cos 2\theta_i} \qquad (3\text{-}4)$$

$$V.M. = \sqrt{\left(\sum_{i=1}^{n} \sin 2\theta_i \right)^2 + \left(\sum_{i=1}^{n} \cos 2\theta_i \right)^2} \cdot \frac{100}{n} \ (\%) \qquad (3\text{-}5)$$

where n is the number of measurements and $\bar{\theta}$ denotes the inclination angle of the preferred direction to the reference axis y. The value of V.M. varies from 0 to 100 %. V.M. = 0 % corresponds to completely random orientation of particle long axes, whereas V.M. = 100 % corresponds to all long axes having exactly the same direction. The values of $\bar{\theta}$ and V.M. measured in the undisturbed sands and triaxial test specimens prepared by the various methods are summarized in Table 3-2.

For the vertical section of T-sand specimen prepared by MSP method (R_B method), $\bar{\theta} = -2.9^\circ$. This means that the apparent long axes in the sand specimen were preferably parallel to the horizontal direction, which was used as reference axis. The value of V.M. was calculated to be 36.3 % for the vertical section as shown in Table 3-2. This value of V.M. corresponds to a high degree of preferred particle orientation. Corresponding values of $\bar{\theta}$ and V.M. for the horizontal section of MSP specimen were 21.5° and 2.8 %, respectively. Thus, an almost completely random orientation of particles in the

horizontal plane was obtained. This tendency can be also confirmed in I-sand specimen reconstituted by MSP method (R_B method). The rose diagram and values of $\bar{\theta}$ and V.M. for R_A-specimen prepared by R_A method were almost the same as those for R_B-specimen, although their drawing was here abbreviated.

From these observations of sand fabric, it can be said that the sand specimen made by MSP method has strongly preferred orientations of particles in the vertical section of specimen and almost random orientations in its horizontal section. That is, the fabric of MSP specimen is of the orthotropic type with a vertical axis of rotational symmetry and horizontal planes of isotropy. This can be also seen in Figs.3-15(a) and (b). The existence of such fabric characteristics of sand sample prepared by pluviation of sand through air method such as MSP method has been reported by Oda (1972a), Oda and Koishikawa (1978) and Ochiai and Lade (1983).

Table 3-2 also indicates that the fabric characteristics of sand specimens prepared by R_C and R_D methods differ remarkably from those of MSP specimen.

It is worthy of note in Figs.3-15(c) and (d) and Table 3-2 that the fabric of sands sampled from two natural deposits is significantly anisotropic and its characteristic shows a very similar pattern to that of MSP specimen. These facts indicate that in-situ sands are always possessed of the fabric anisotropy due to their mode of deposition, and the feature of fabric anisotropy in K- and I-sands can be reproduced to a certain degree by MSP method proposed in this study.

3.6 Preliminary Examinations on Factors Influencing Shear Strength

Before commencing a series of laboratory tests, some preliminary examinations were made to estimate the accuracy of axial stress measurements and the reproducibility of the desired specimen densities.

Since it has been considered that errors in the measured axial load are caused mainly by the friction of loading piston when masuring with the load transducer outside the triaxial cell, the static drained triaxial compression and extension tests were conducted to compare the results obtained by the measurement of axial stress inside the triaxial cell with those obtained by the measurement outside. In this test program, T-sand was utilized.

Shown in Fig.3-16 is the plot of angle of shearing resistance ϕ_d (= arc sin $\{(\sigma_1-\sigma_3)_f/(\sigma_1+\sigma_3)_f\}$) vs. mean principal stress at consolidation p_c (= σ_c') obtained from the compression and extension tests on T-sand specimens formed by MSP method (R_A method). This figure indicates that the friction of loading piston may be of acceptable magnitude in the triaxial compression but, in the triaxial extension tests such type as of decreasing stress application, the errors in the calculated ϕ_d values may not be neglected except that p_c (= σ_c') = 392 kPa. That is, it may well be said that the

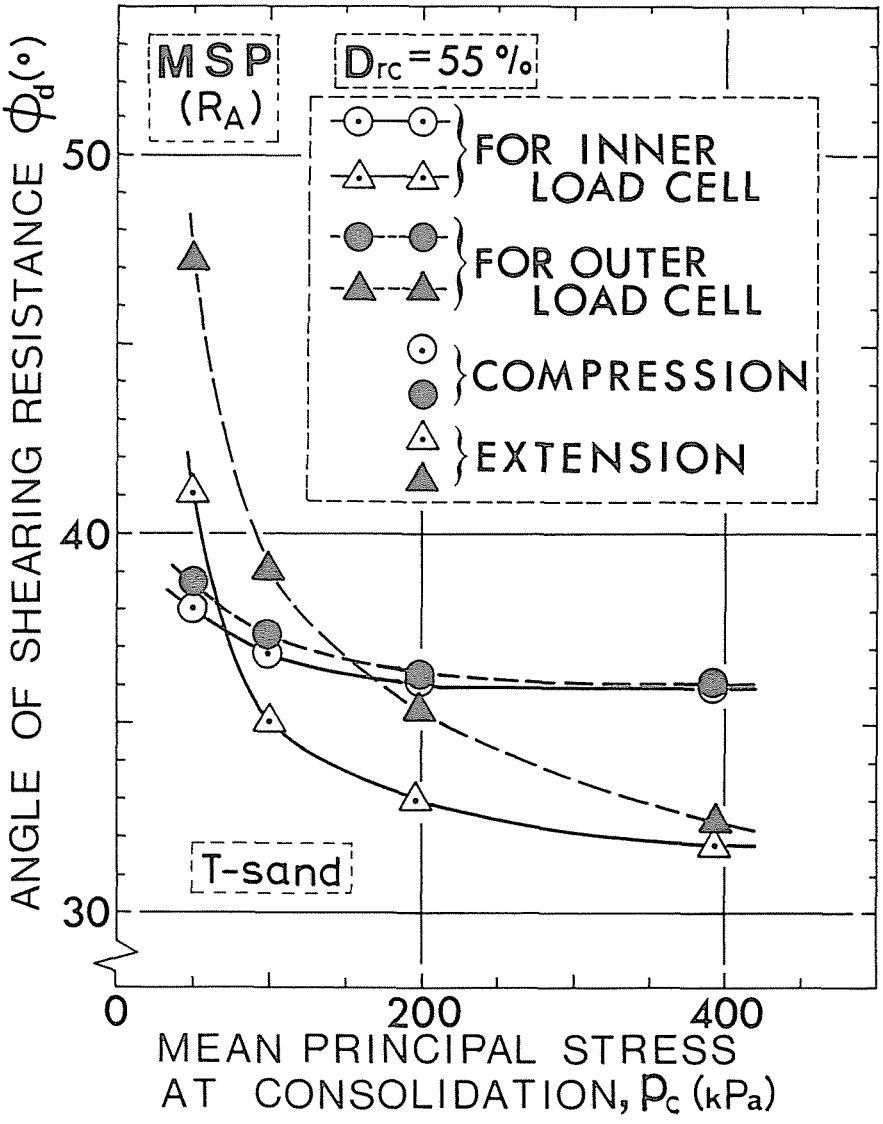

Fig.3-16 Effect of confining stress, friction of loading piston and stress system on the angle of shearing resistance

friction of loading piston can be by no means disregarded when testing the specimens under smaller confining pressure, especially in the extension test.

Fig.3-16 also shows that there is a remarkable reduction of ϕ_d with the increase of $p_c (= \sigma_c')$ from 49 to 392 kPa, notably in the extension test. Recently, Oda et al. (1978) performed a comprehensive series of plane strain tests and triaxial compression tests and observed a significant dependency of ϕ_d on $p_c (= \sigma_c')$, especially in the plane strain test. Although similar results were observed by De Beer (1965) and other research workers, further investigations are required for making a reasonable interpretation for the dependency of ϕ_d on $p_c (= \sigma_c')$.

Moreover, comparison of ϕ_d values between triaxial compression and extension tests shows that both of ϕ_d are not always equal to each other in magnitude. As shown later, ϕ_d are also affected by the sample preparation method. These experimental results indicate that the static shear strength of sand can be by no means estimated only by its density or void ratio.

Since non-uniformity may be introduced initially in the specimen, extreme care in making the specimens should be given. Table 3-3 shows a typical comparison of reproducibility and human error in the desired relative density ($D_r =$

Table 3-3 Reproducibility of desired relative density in various sample preparation methods

Method of preparation	Tech-nician	Number of samples	Average D_r (%)	Standard deviation	Coefficient of variation (%)
MSP	X	12	55.8	0.78	1.4
	Y	13	55.3	0.56	1.0
	Z	10	54.9	0.54	1.0
Rodding	X	11	54.2	1.10	2.0
	Y	10	55.4	1.82	3.3
	Z	11	55.0	1.43	2.6
Flask	Y	10	55.0	2.15	3.9
	Z	11	53.6	2.84	5.3
Tapping	X	12	53.9	2.45	4.5
	Z	13	55.3	2.10	3.8

55 %) three technicians prepared according to each sample preparation procedure. As can be seen from this table, such procedures as rodding (R_C), tapping (R_D) and flask methods lead to noticeable human errors and demand a tolerable skill in the attainment of higher reproducibility of D_r. It can be also seen that MSP method gives a higher reproducibility of D_r than other methods and is fairly free from human error. Considering the fact that higher human errors in making samples and lower reproducibility of D_r may lead to the non-uniformity of sample and low reliability of test results, it can be said that MSP method has the significant advantages over other possible methods.

To avoid the effect of variation of initial sample density from the desired one in comparing test data, the variations in D_{rc} of samples prepared by rodding (R_C), tapping (R_D) and flask methods were permitted to the extent within ±3 % from the aimed D_{rc} in this study.

CHAPTER 4 STATIC AND CYCLIC STRESS-STRAIN-STRENGTH BEHAVIORS OF RECONSTITUTED AND UNDISTURBED SANDS

4.1 Introduction

As mentioned previously, the sample preparation method (MSP method) proposed by the present author can give the sand specimens with a higher reproducibility of relative density and is fairly free from human error. However, it was also shown that MSP specimen possesses the fabric anisotropy in which the apparent long axis of the sand particles has strongly preferred orientations in the vertical section, but almost completely random orientations in the horizontal section (See CHAPTER 3). Accordingly, the mechanical behaviors of MSP specimen must become anisotropic ones.

This chapter will make the main features of the anisotropic mechanical properties of MSP specimen clear, by comparing with the test results of sand specimens formed by the different sample preparation methods which were described in the preceding paragraph.

Then, the significance of anisotropy in the static and cyclic stress-strain-strength properties of the undisturbed sands sampled from two natural deposits is also displayed in this chapter. Furthermore, whether or not the anisotropic

behavior of these undisturbed sands could be simulated in a laboratory testing is examined in detail.

The discussion in this chapter is based on the results of a series of static triaxial compression and extension tests and cyclic undrained triaxial tests.

4.2 Effect of Sample Preparation Method on Static and Cyclic Mechanical Properties

4.2.1 Stress-strain-dilatancy characteristics of sand specimen prepared by MSP method

In this and the following paragraphs, mechanical properties of T-sand is examined. Figs.4-1(a) and (b) show the effective stress ratio-shear strain-volumetric strain relationships for T-sand samples which are sheared in drained triaxial compression and extension stress conditions. These tests were conducted under σ_c' = 196 kPa and D_{rc}= 50 % or 70 %. Samples were formed by MSP method (R_A method) in which a desired relative density was achieved by adopting two combinations of nozzle diameter (d) and height of fall (h) as shown in these figures. As can be seen from these figures, the deformation-strength properties are in agreement with each other irrespective of the differences in combination of d and h. This fact could be also confirmed in the undrained conditions (See Figs.4-2(a) and (b)). It must be emphasized that the reproducibility of deformation-strength characteristics at the same density is by far higher in MSP specimens than in the specimens formed by rodding (R_C), tapping (R_D) and flask methods.

These results suggest that the fabric characteristics of MSP specimens (R_AV-specimens) are not altered by the height of fall and the rate of sand discharge as far as sand particles

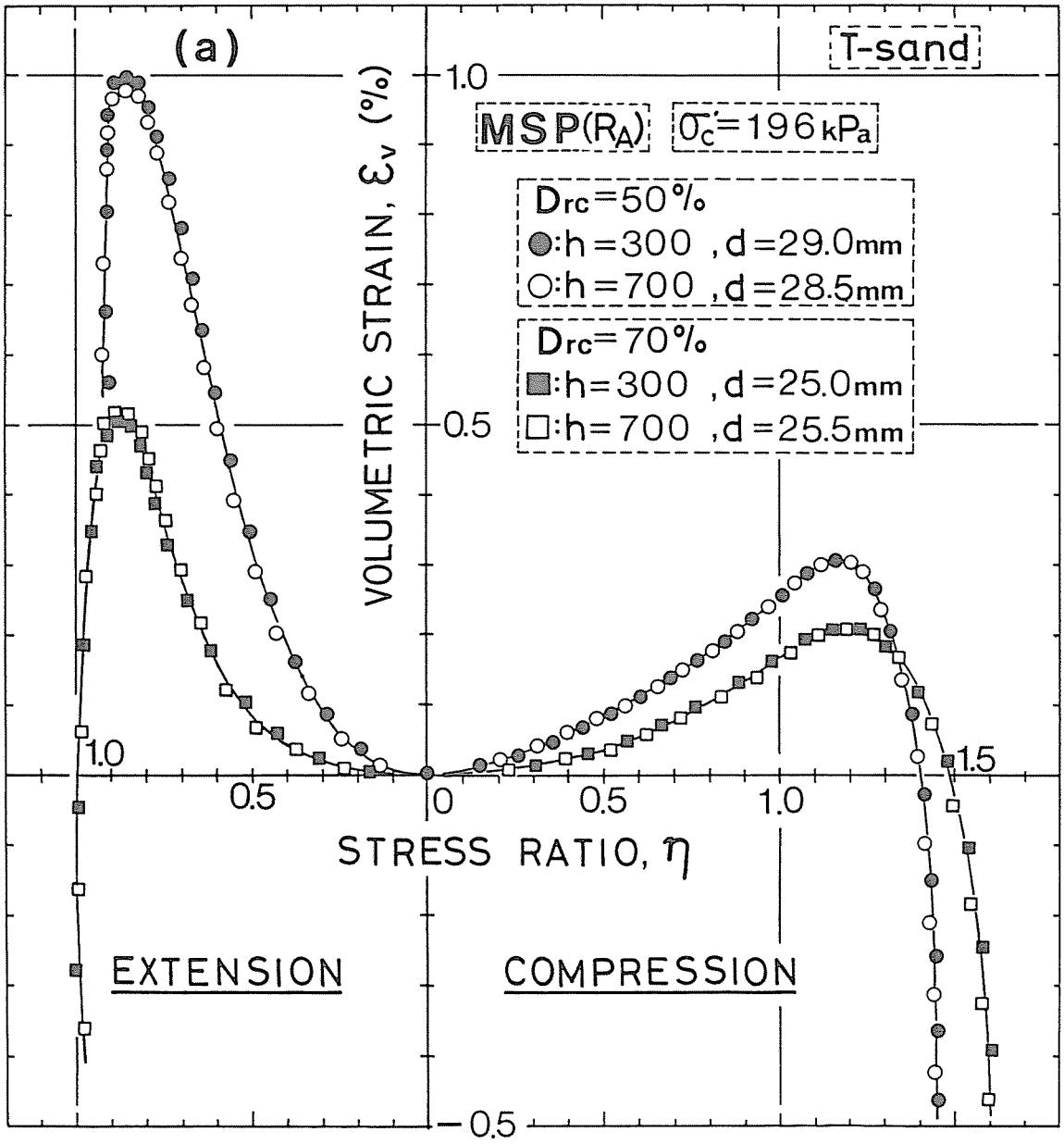

Fig.4-1(a) Effect of pluviation condition in MSP (R_A) method on drained stress-strain relationship (η vs. ε_v)

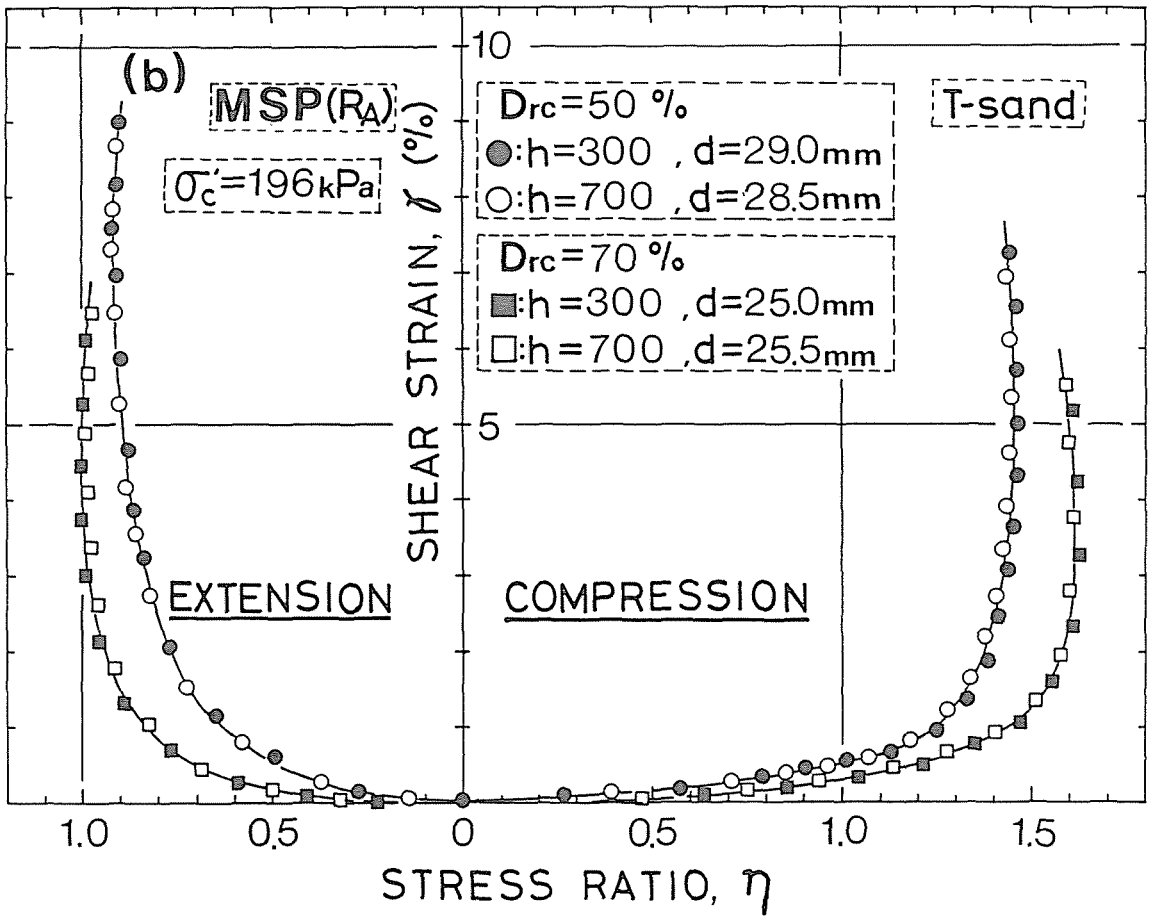

Fig.4-1(b) Effect of pluviation condition in MSP (R_A) method on drained stress-strain relationship (η vs. γ)

pluviate freely through air.

It can be also seen from Fig.4-1(a) that volume decreases during shear are more significant in the triaxial extension stress condition than in the triaxial compression stress condition. Similar tendency held valid in the triaxial tests with other stress paths which were conducted under the condition of p' $(=\sigma_c')$ = const. = 196 kPa and D_{rc} = 55 % as shown in Fig.4-3. These results indicate that the difference in the type of stress application, i.e. increasing or decreasing stress, gives little influence upon the significant difference between compression and extension tests regarding the dilatancy performance.

When MSP specimens were subjected to triaxial compression and extension stresses in undrained condition, similar results to those described above were observed as shown in Figs.4-2(a) and (b). From the observation of p' - q plot which represents the characteristics of pore water pressure development with the increase in shear stress, it can be found that a fairly high pore water pressure develops in extension test than in compression test. This tendency of the dilatancy almost coincides with that in drained condition.

In extension test, axial stress is equal to the minor principal stress, and the other two principal stresses are equal to each other in magnitude and the major one, whereas in compression test the intermediate principal stress is equal to the minor one. Thus there exists the difference with

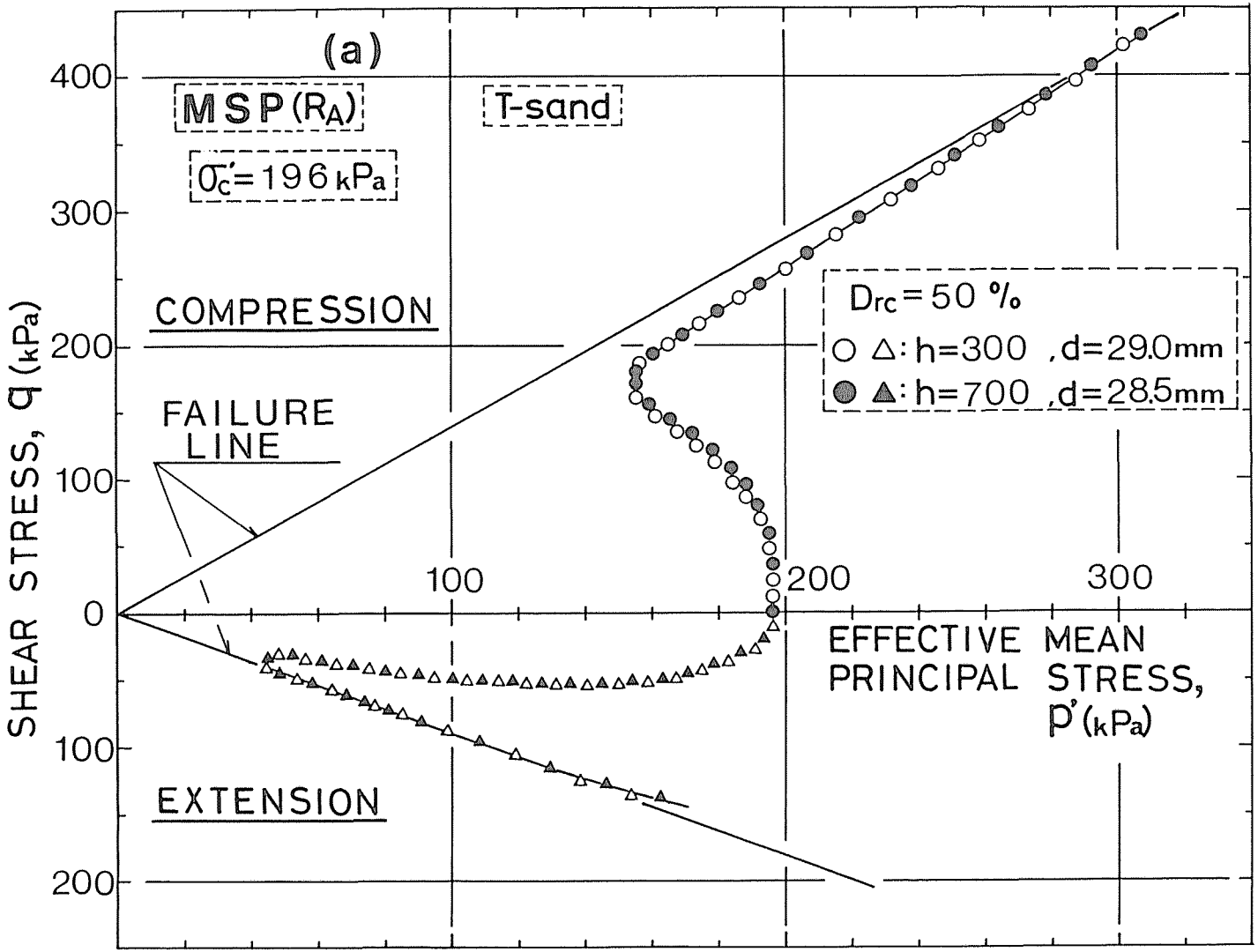

Fig.4-2(a) Effect of pluviation condition in MSP (R_A) method on undrained stress-strain relationship (q vs. p′)

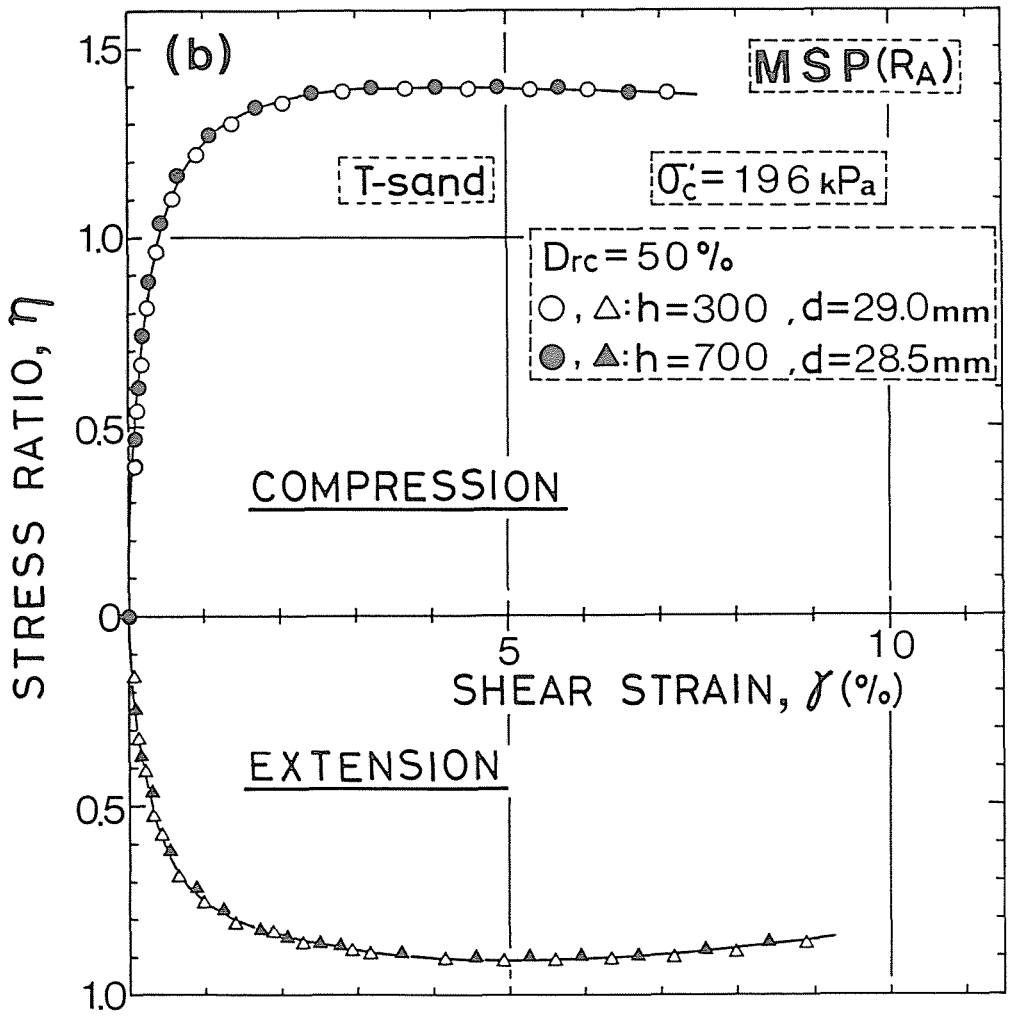

Fig.4-2(b) Effect of pluviation condition in MSP (R_A) method on undrained stress-strain relationship (η vs. γ)

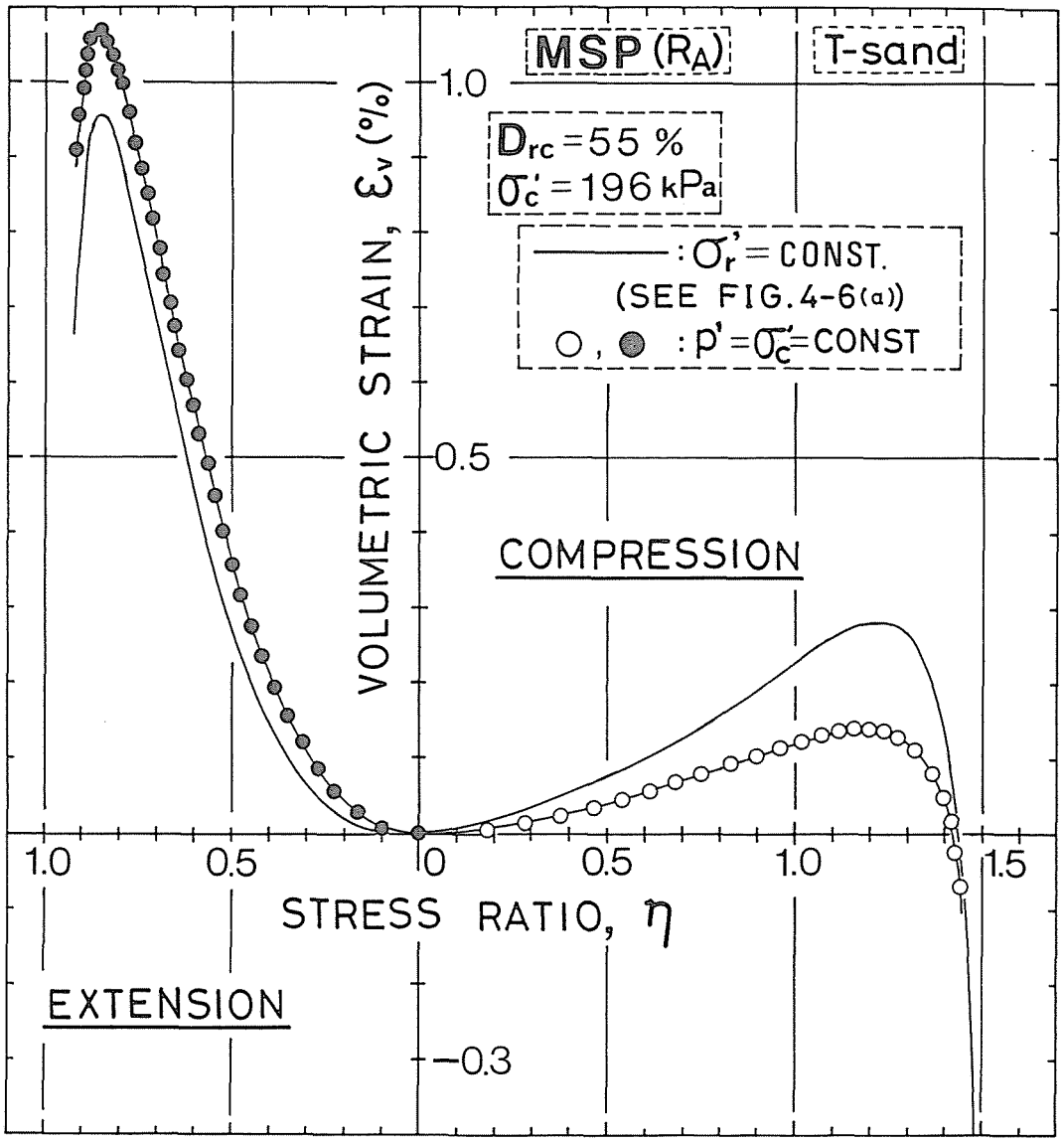

Fig.4-3 Comparison of dilatancy behaviors in p′= const. triaxial compression and extension tests to that in σ_r' = const. tests on MSP specimens

respect to stress system during shear in both compression and extension test. It would be expected, however, that the difference of dilatancy performance between compression and extension tests is not necessarily due only to the difference of stress system during shear, but also to the fabric anisotropy of specimens. As pointed out previously, when the specimens are formed by depositing sand under the action of gravitation, the specimen inherently acquires an anisotropic fabric. That is, the specimen prepared by MSP method in which sand particles are pluviated freely through air under the action of gravitation has strongly preferred orientations of particles in the vertical section of triaxial specimen and almost random orientations in its horizontal section (See CHAPTER 3). Therefore, it would be considered that the difference of deformation characteristics between the triaxial compression and extension tests does not have nothing to do with the fabric anisotropy of sand specimen. The anisotropic mechanical behaviors of MSP specimen will be discussed in detail in the following pages.

4.2.2 Comparison of static triaxial test results on specimens prepared by MSP and other methods

Shown in Figs.4-4(a) and (b) are the typical comparison of effective stress ratio-shear strain-volumetric strain relationships obtained from T-sand specimens which are prepared according to MSP (R_A), rodding (R_C) and tapping (R_D) methods. These figures indicate that the difference in deformation characteristics due to sample preparation method effects can be apparently observed and that the variation in dilatancy performance is more clear in the triaxial extension stress condition than in the triaxial compression stress condition. The difference of dilatancy characteristics between the triaxial compression and extension tests is the largest in the specimens formed by MSP (R_A) method. It can be also recognized that the difference of dilatancy characteristics between rodded and MSP specimens is the greatest in both triaxial compression and extension tests.

Table 4-1 gives the angle of shearing resistance ϕ_d and the volumetric strain at the maximum volume contraction during shear ε_{vmax} obtained in these test series. It can be seen from this table that ϕ_d values in both compression and extension tests are affected to a certain degree by the sample preparation method. In triaxial compression stress condition, it would be pointed out that MSP specimen behaves as if it had a more

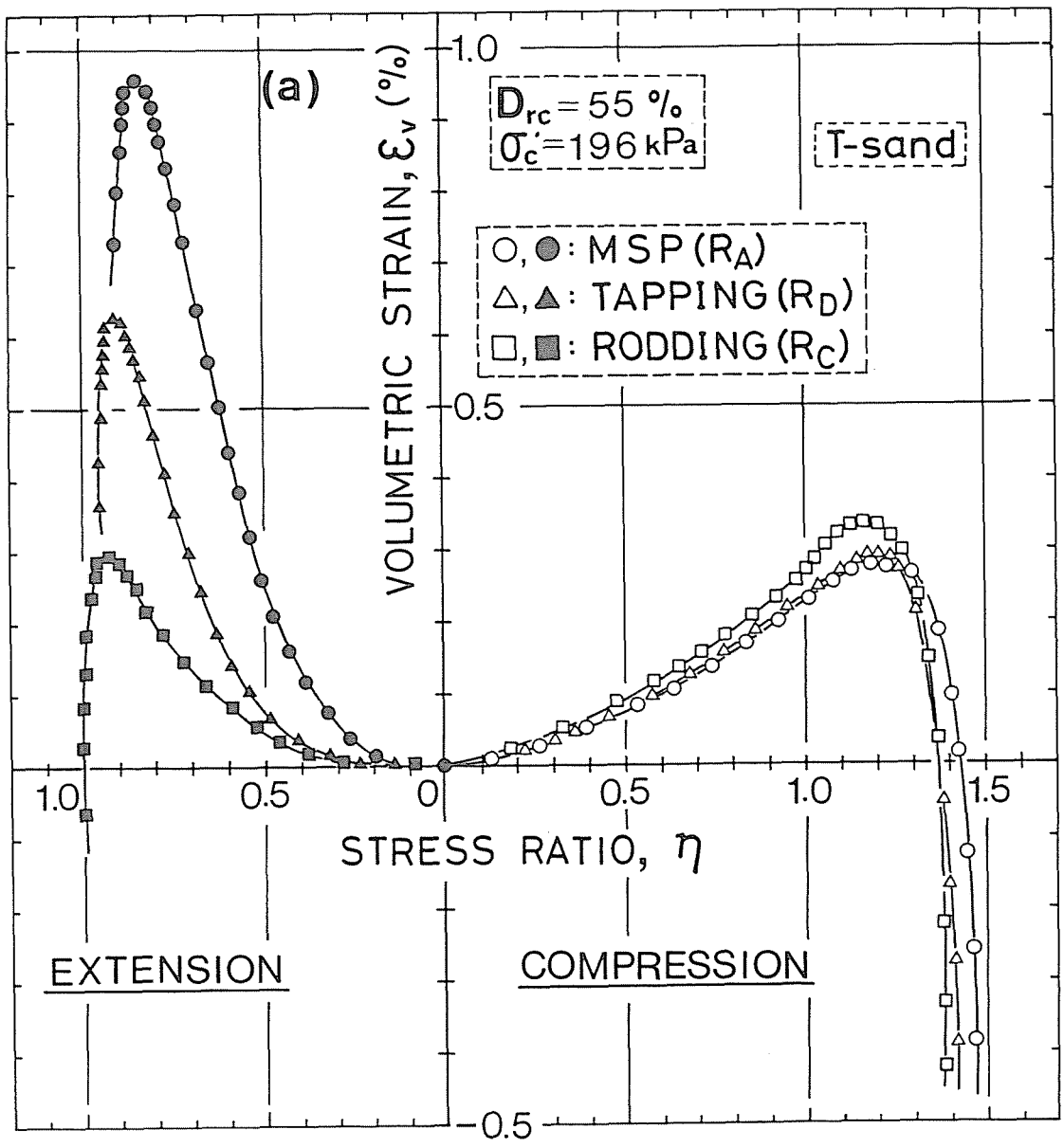

Fig.4-4(a) Variation in drained stress-strain relationship due to the effect of difference in sample preparation (η vs. ε_v)

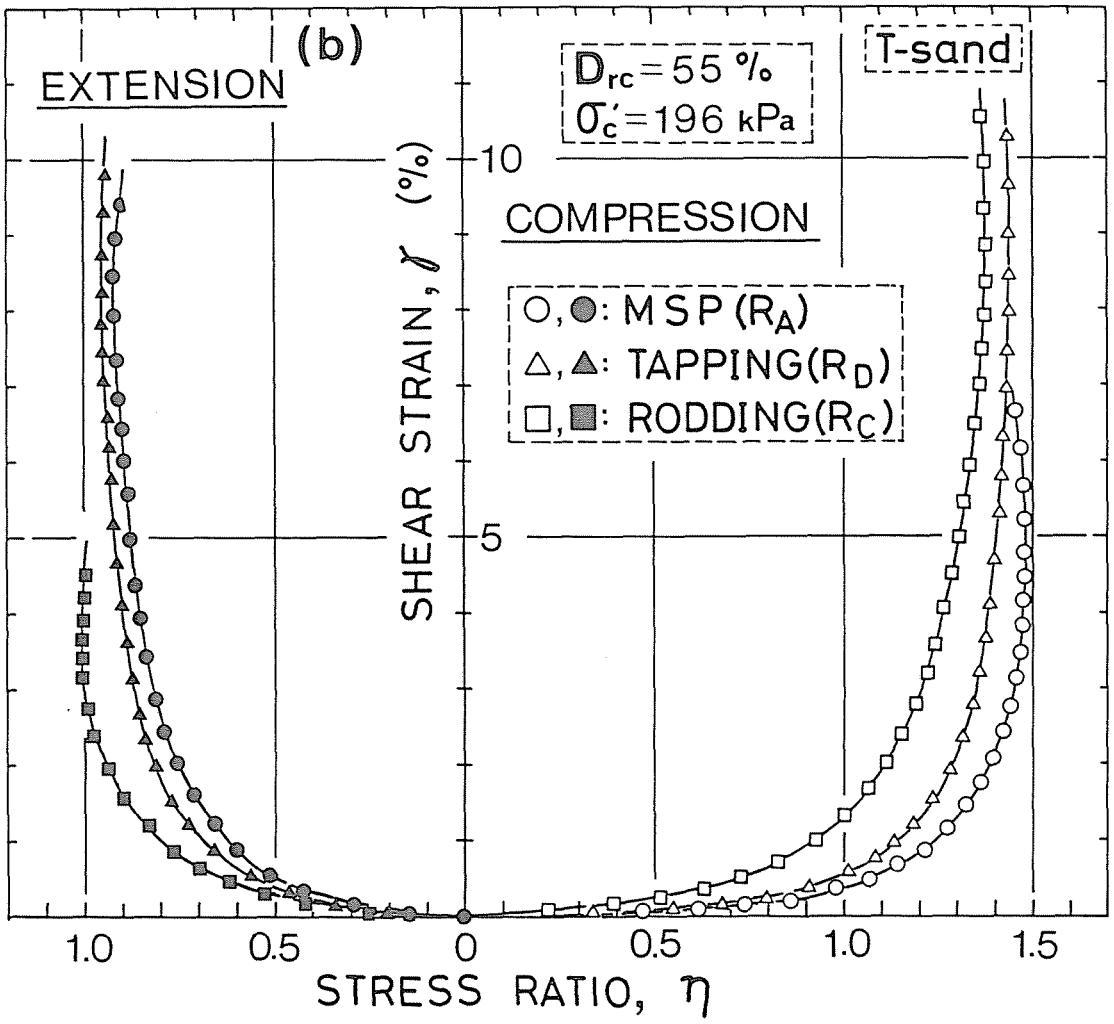

Fig.4-4(b) Variation in drained stress-strain relationship due to the effect of difference in sample preparation (η vs. γ)

Table 4-1 ε_{vmax} and ϕ_d obtained from drained triaxial compression and extension tests on specimens having relative density after consolidation at p_c = 196 kPa of 55 % prepared by MSP (R_A), rodding (R_C) and tapping (R_D) methods

Method of Preparation	Compression		Extension	
	ε_{vmax} (%)	ϕ_d (deg.)	ε_{vmax} (%)	ϕ_d (deg.)
MSP (R_A)	0.28	36.1	0.96	33.2
Rodding (R_C)	0.34	34.3	0.30	36.8
Tapping (R_D)	0.29	35.2	0.63	34.1

stable fabric, since its specimen has a smaller ε_{vmax}, a higher secant modulus and a larger ϕ_d value than those of other specimens. However, the mechanical behavior of MSP specimen in triaxial extension stress condition can be characterized by its larger ε_{vmax}, lower secant modulus and smaller ϕ_d value.

Such variations in deformation-strength characteristics obtained from the present study seem to be attributed to the difference of fabrics developed during sample preparation which could be seen in CHAPTER 3. These facts were also confirmed for the drained triaxial compression tests. For example, the different deformation characteristics of specimens having the same density but prepared by two different methods were found in the drained triaxial compression tests by Oda (1972b), who observed that the tapped specimen had a higher secant modulus than the plunged one. He also showed that the tapped specimen had a remarkable preferred orientation of long axis of particles to the horizontal plane whereas the plunged specimen did not and that this different mechanical behavior could be explained by differences in the fabrics of specimens.

The results of undrained triaxial tests on the specimen prepared by MSP (R_A), rodding (R_C) and tapping (R_D) methods are compared in Figs. 4-5(a) and (b). As can be seen from the figures, sample preparation method influences clearly on the undrained deformation characteristics. It seems apparent that the tendency of these sample preparation method effects

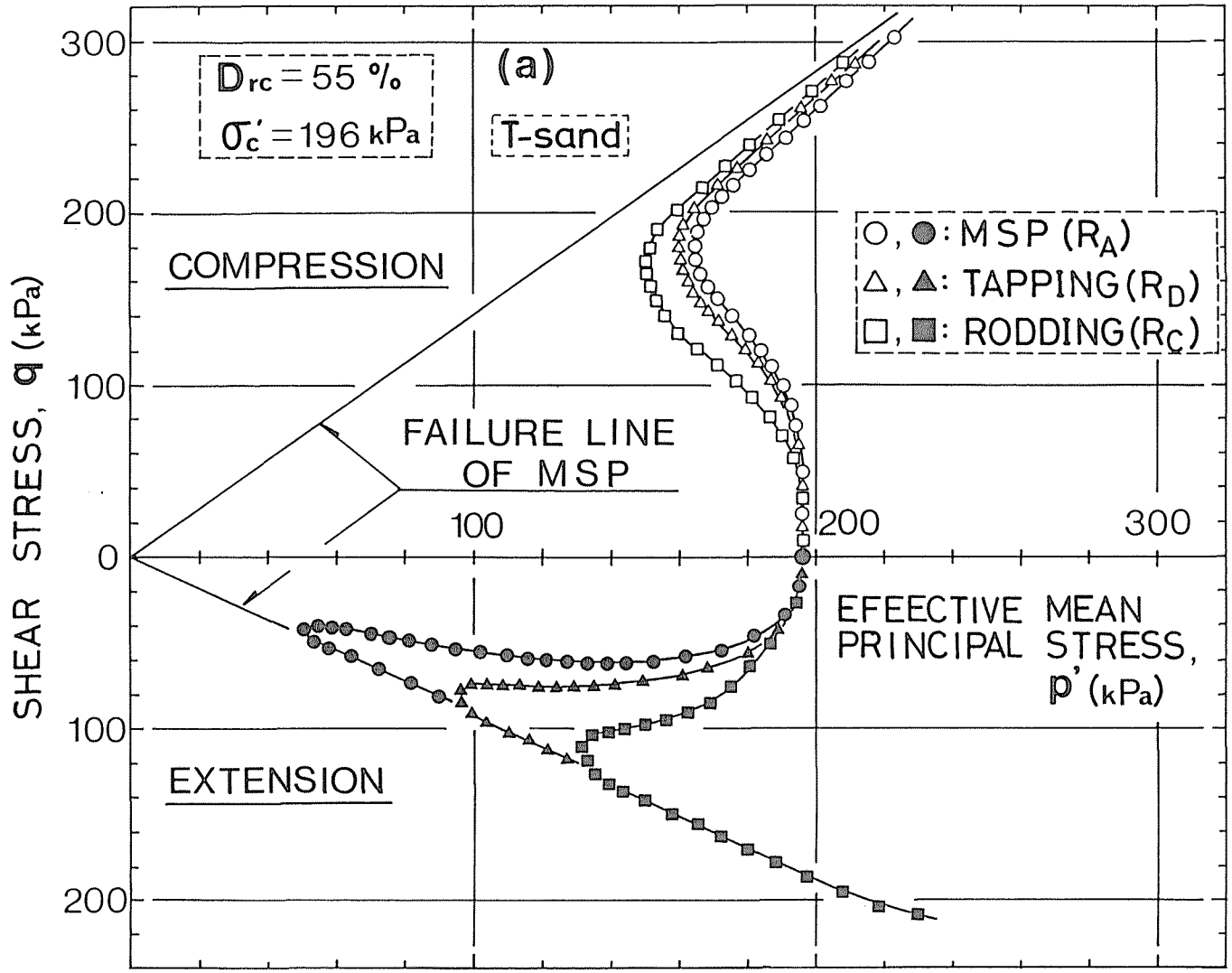

Fig.4-5(a) Variation in undrained stress-strain relationship due to the effect of difference in sample preparation (q vs. p′)

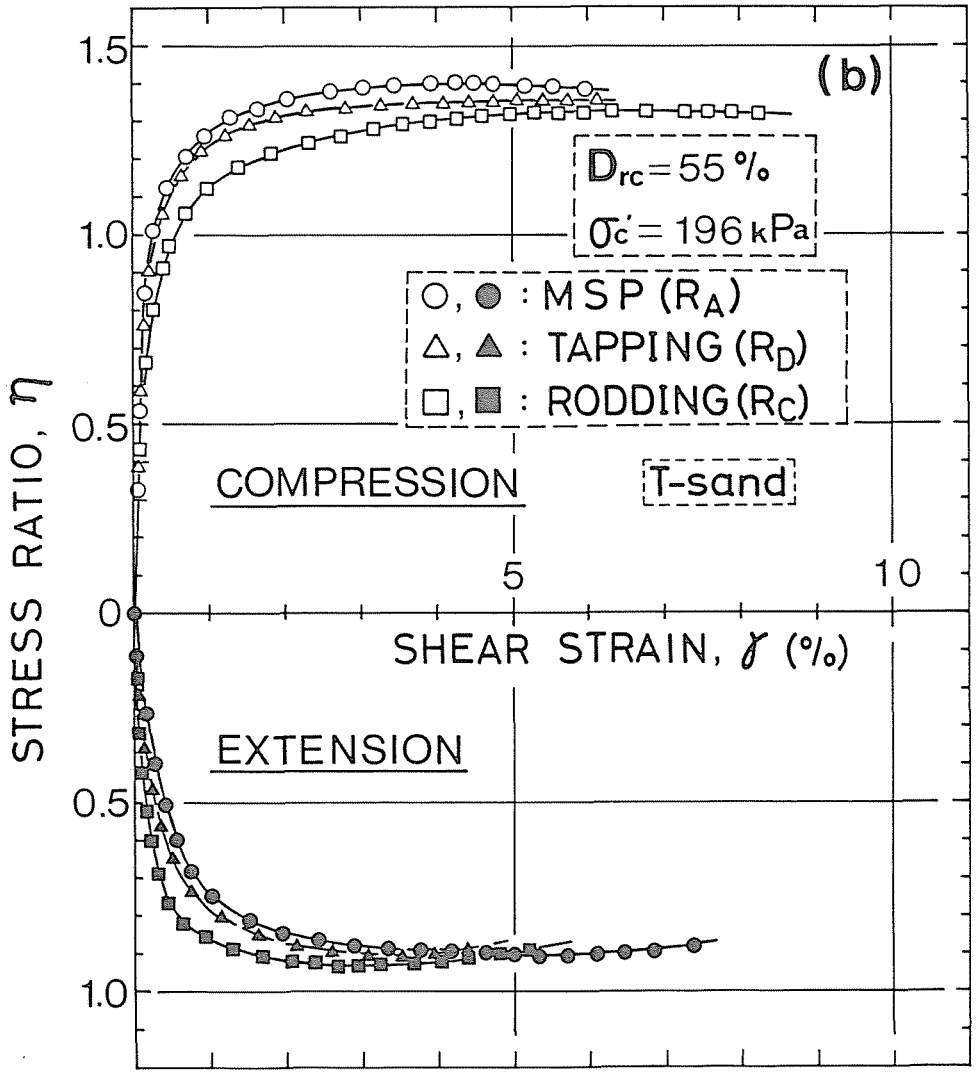

Fig.4-5(b) Variation in undrained stress-strain relationship due to the effect of difference in sample preparation (η vs. γ)

is almost identical to that in drained condition. That is, in both drained and undrained conditions it can be said that the effect of sample preparation method on the dilatancy characteristics of sands becomes more stronger in the extension stress condition under which the direction of the major principal stress is horizontal. At the same time, it would be considered that MSP method produces the specimens having the most significant anisotropic fabric which is stiffer in the vertical direction of pluviation than in the horizontal direction.

Shown in Figs.4-6(a) and (b) are the comparison of test results between flask and MSP (R_A) methods. In both drained and undrained conditions, no significant difference of dilatancy performance in the triaxial compression and extension tests can be seen between the two methods and it does not seem that there is such fundamental difference as would influence the test result. This fact shows that there is no difference in the fabric characteristic of the specimens made by such method as pluviation through air under the action of gravitation.

From the experimental results mentioned above, it can be pointed out that though the effects of anisotropic fabric induced in making the sample on the static deformation-strength properties are significant, variations in dilatancy performance are more dramatic, especially in the triaxial extension tests.

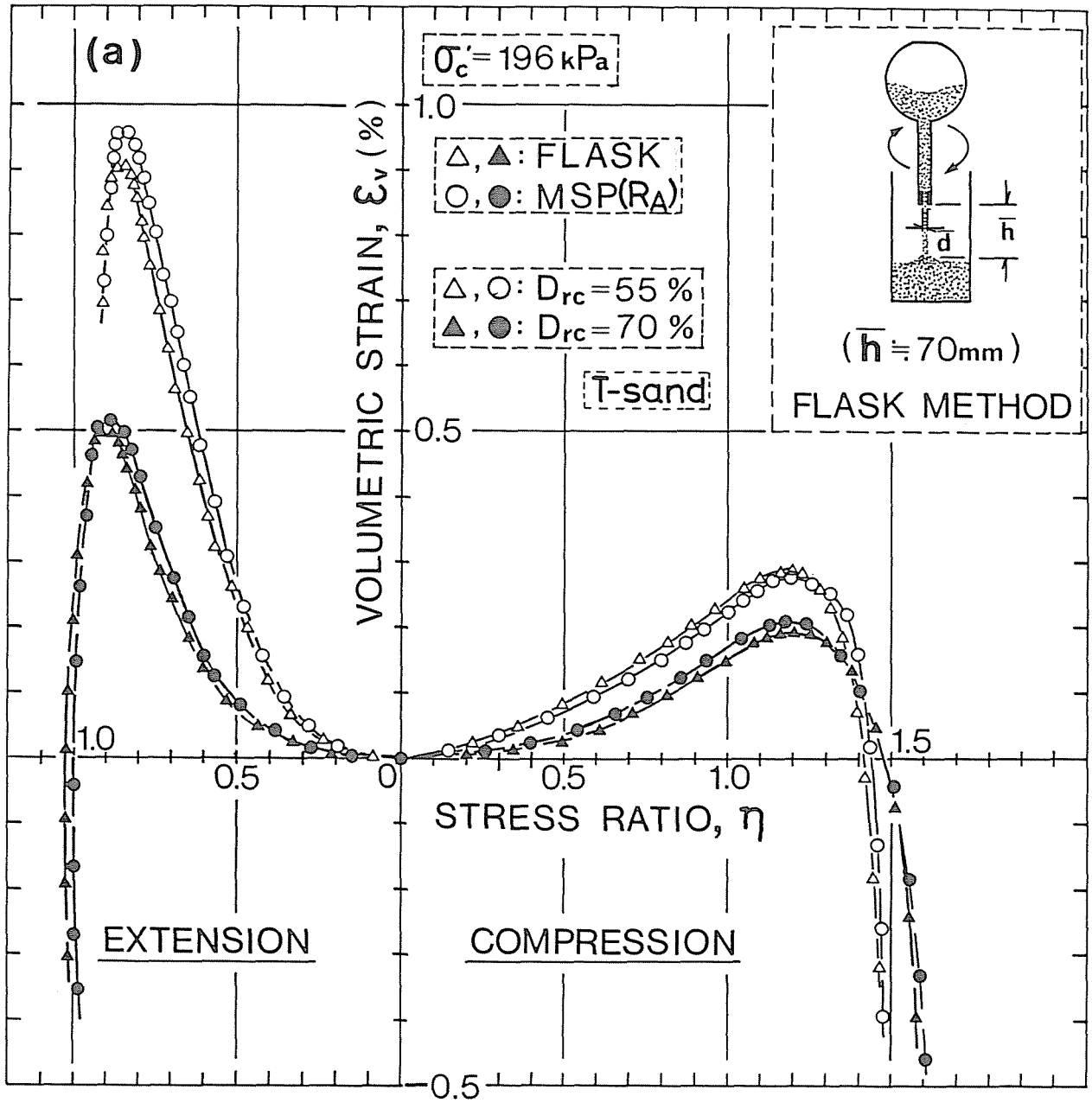

Fig.4-6(a) Comparison of dilatancy behaviors obtained from triaxial compression and extension tests on specimens prepared by MSP (R_A) and flask methods (η vs. ε_v)

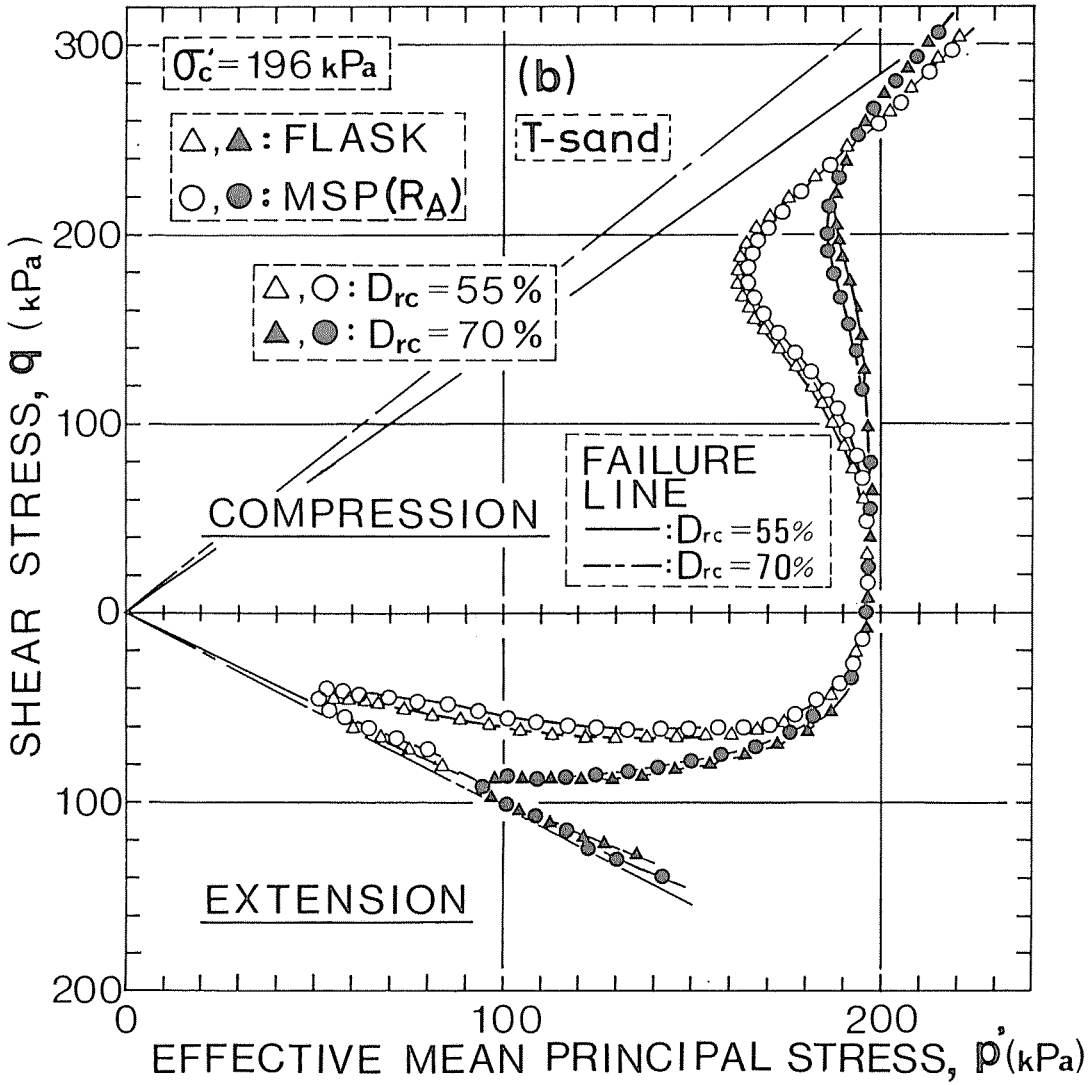

Fig.4-6(b) Comparison of dilatancy behaviors obtained from triaxial compression and extension tests on specimens prepared by MSP (R_A) and flask methods (p'vs. q)

4.2.3 Comparison of cyclic undrained triaxial test results on specimens formed by MSP and other methods

It has been apparent that the influence of sample preparation method on the static dilatancy characteristics is important, notably in the triaxial extension test as mentioned above. Cyclic undrained triaxial tests were performed in order to examine how the difference of sample preparation method affects the cyclic undrained strength.

Shown in Fig.4-7 is a typical result of statically cycled triaxial test on the specimens prepared by MSP (R_A) and rodding (R_C) methods, in which both specimens were isotropically consolidated to $\sigma_c' = 196$ kPa and then triaxial compression and extension with the same shear stress amplitude ($q = 55$ kPa) was repetitively applied. It should be remembered here that the most significant difference in both the drained and undrained deformation characteristics obtained from the static triaxial tests due to sample preparation method effects is found when MSP and rodded specimens are compared.

As can be seen from this figure, the difference of undrained effective stress paths during cyclic loading is remarkable. The stress paths demonstrated in Fig.4-7 show that the pore water pressure developed in the extensional side of the first loading cycle is by far higher in MSP specimen than in rodded specimen and that this tendency is preserved

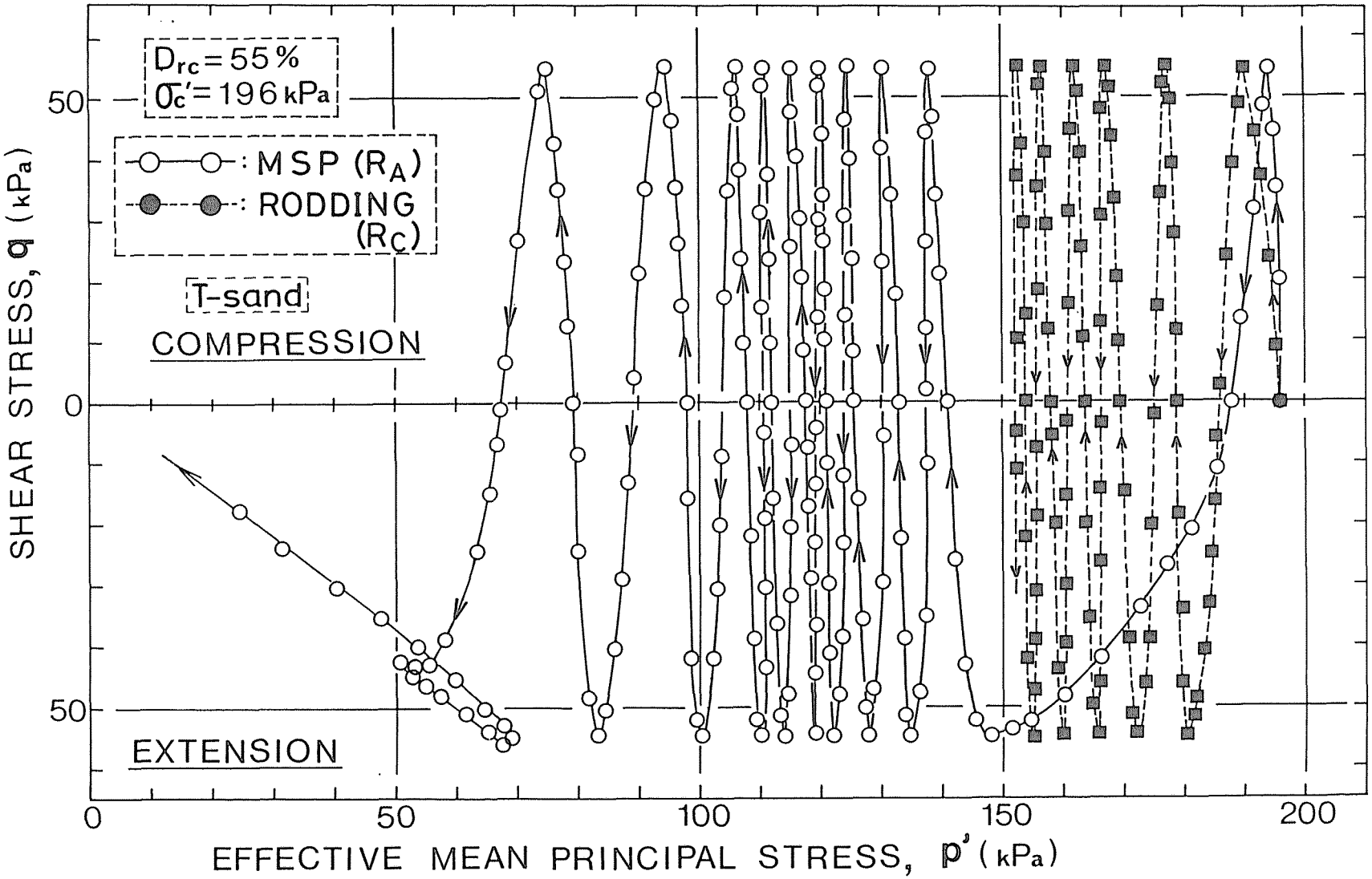

Fig.4-7 Comparison of undrained effective stress paths for MSP and rodded specimens under statically cyclic stresses

to a certain degree in the subsequent loading cycles. It is worthy of note that a predominant development of pore water pressure accompanied by a larger shear strain in the extensional side such as observed above can lead to a smaller resistance to liquefaction. Comparison of Figs.4-7 and 4-5(a) shows that the liquefaction behavior of specimen prepared by the same method is intimately related to the static dilatancy characteristics of each specimen.

From these results and the previous considerations, it can be said that not only static dilatancy characteristic but also liquefaction behavior at given density are extremely sensitive to the fabric characteristics of sand sample.

A typical comparison of cyclic undrained strength values obtained from cyclic triaxial tests on the specimens having D_{rc} of 55 % prepared by three different methods is shown in Fig.4-8 for the failure defined as initial liquefaction. This figure shows that there is a remarkable variation in cyclic undrained strength due to sample preparation method effects. It can be also seen from the figure that cyclic undrained strength is the lowest for MSP specimen and the highest for rodded specimen, although the scattering of data is relatively large in rodded and tapped specimens. It should be noted that the lowest cyclic undrained strength of MSP specimen is attributed to its anisotropic fabric which induces a predominant development of pore water pressure in the extensional side. It is

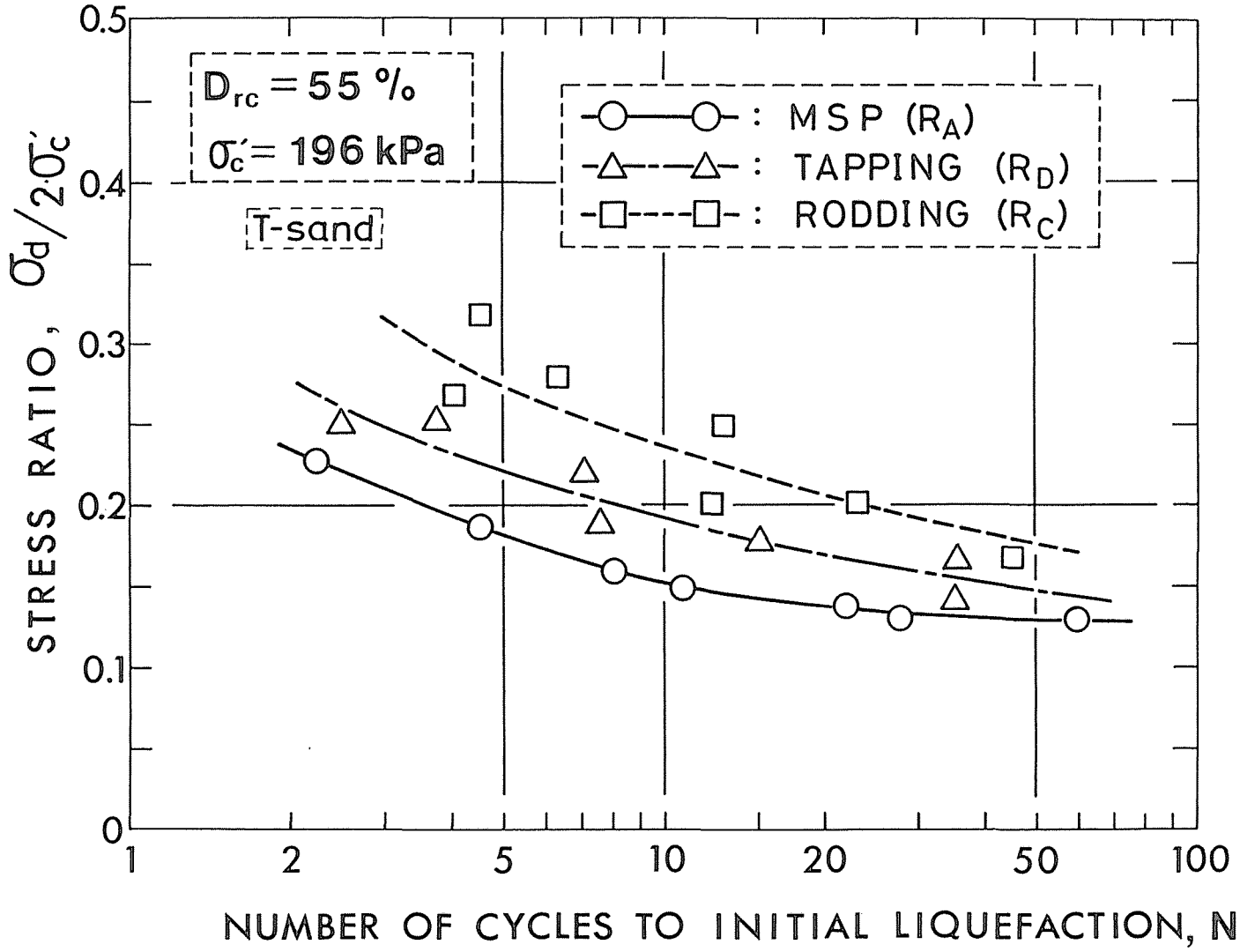

Fig.4-8 Comparison of cyclic stress ratio vs. number of loading to initial liquefaction for MSP, rodded and tapped specimens

clear that the significant variations in the static dilatancy properties due to the differences in the fabric characteristics of specimen, especially in the extensional side as shown in Figs.4-4(a) and 4-5(a) contribute to a considerable degree to the differences in the cyclic undrained strength values.

Recently, Silver et al. (1980) have examined the influence of sand sample preparation methods on the cyclic undrained strength of simple shear and triaxial tests. Two different sample preparation methods they adopted were wet tamping method suggested by Ladd (1978) and pluviation through air method which is called as flask method in the present study. They have found that according to strength comparison based on the stress ratio defined as the maximum cyclic shear stress divided by the effective mean principal stress at consolidation, cyclic undrained triaxial strength almost coincides with cyclic undrained simple shear strength for loose to medium dense specimens formed by pluviation through air method, although cyclic undrained strength of specimens prepared by wet tamping method was higher for triaxial tests than for simple shear tests. They have also pointed out that two different sample preparation methods do not make any difference on the cyclic undrained strength in the simple shear test. These results seem to suggest that the lowest value of undrained triaxial strength as obtained from MSP specimen corresponds to the liquefaction strength of in-situ horizontal sand deposits which could be simulated by the cyclic undrained

simple shear tests. It follows that the cyclic undrained triaxial strength values of the rodded and tapped specimens may give an over-estimate of the liquefaction strength in horizontal sand deposits.

In any case, the estimation of the in-situ liquefaction strength values from the cyclic undrained triaxial tests seems to be possible by adopting a pertinent sample preparation method in the laboratory. It is particularly expected that the triaxial tests on specimen prepared by pluviation of sand particles such as MSP method will give to a certain degree a good indication of the static and cyclic deformation characteristics in naturally deposited sands.

4.3 Anisotropy in Static and Cyclic Mechanical Properties of MSP Specimen

In order to simply examine the degree of mechanical anisotropy of sand specimens prepared by three methods adopted in this study, the isotropic consolidation and swelling tests in which cell pressure is varied between 4.9 kPa and 588 kPa were conducted. As shown in Fig.4-9, test results observed during two cycles of consolidation and swelling are represented as the relationship of volumetric strain ε_v and three times axial strain $3\varepsilon_a$.

It has been suggested by El-Sohby (1969) that such plotting as this figure is useful for representing a simple demonstration of the degree of anisotropy. In the triaxial specimen with the isotropic fabrics, ε_v must be equal to $3\varepsilon_a$. On the other hand, in the triaxial specimen having such anisotropic fabric as deformability is more significant in the horizontal direction than in the vertical direction, ε_v must be larger than $3\varepsilon_a$.

As can be seen in Fig.4-9, in the specimens prepared by MSP (R_A) and tapping (R_D) methods, ε_v is slightly larger than $3\varepsilon_a$ in any loading stages. Although this fact seems to support the intuitive idea that the behavior of the specimens formed by these two methods is anisotropic; specimens are more stiffer in the vertical direction than in the horizontal direction, it should be noted that the deviation from isotropic line

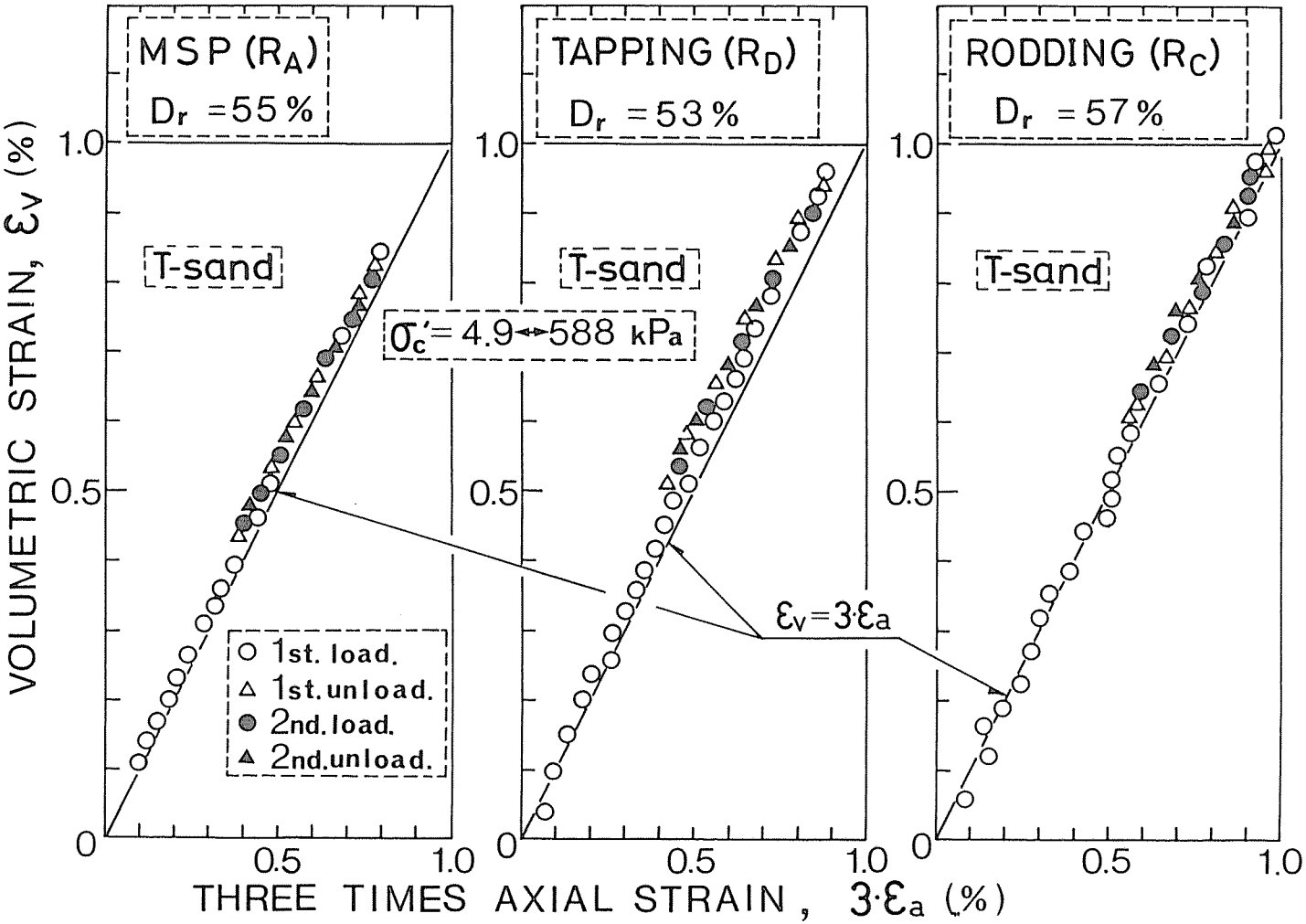

Fig.4-9 Volumetric strains vs. three times axial strain obtained from isotropic consolidation-swelling test on MSP, rodded and tapped specimens

($\varepsilon_v = 3\varepsilon_a$) is small and there is no significant difference of the relationship of ε_v and $3\varepsilon_a$ in both specimens. And also, in the specimens prepared by rodding (R_C) method, the deviation from isotropic line is negligible although experimental results are more scattered than in the specimens prepared by MSP method.

The comparison of test results on the specimens formed by three different preparation methods shows that such a remarkable difference as can be observed in the deformation characteristics during shear tests does not appeared as to $\varepsilon_v - 3\varepsilon_a$ relationship. It would be considered that variations in mechanical behavior due to the fabric characteristics of specimen cannot be detected clearly at this type of plot.
In other words, it seems apparent that to demonstrate quantitatively the anisotropic behavior in shear deformation by this plotting is extremely difficult.

It is possible in the present study to evaluate the dependency of mechanical properties of sand on the fabric anisotropy, by directly comparing under the same stress system the test results of R_BV- and R_BH-specimens which are formed by MSP method (R_B method).

Figs.4-10(a) and (b) show the effective stress ratio-axial strain-volumetric strain relationships for R_BV- and R_BH-specimens of T-sand which were sheared in drained triaxial

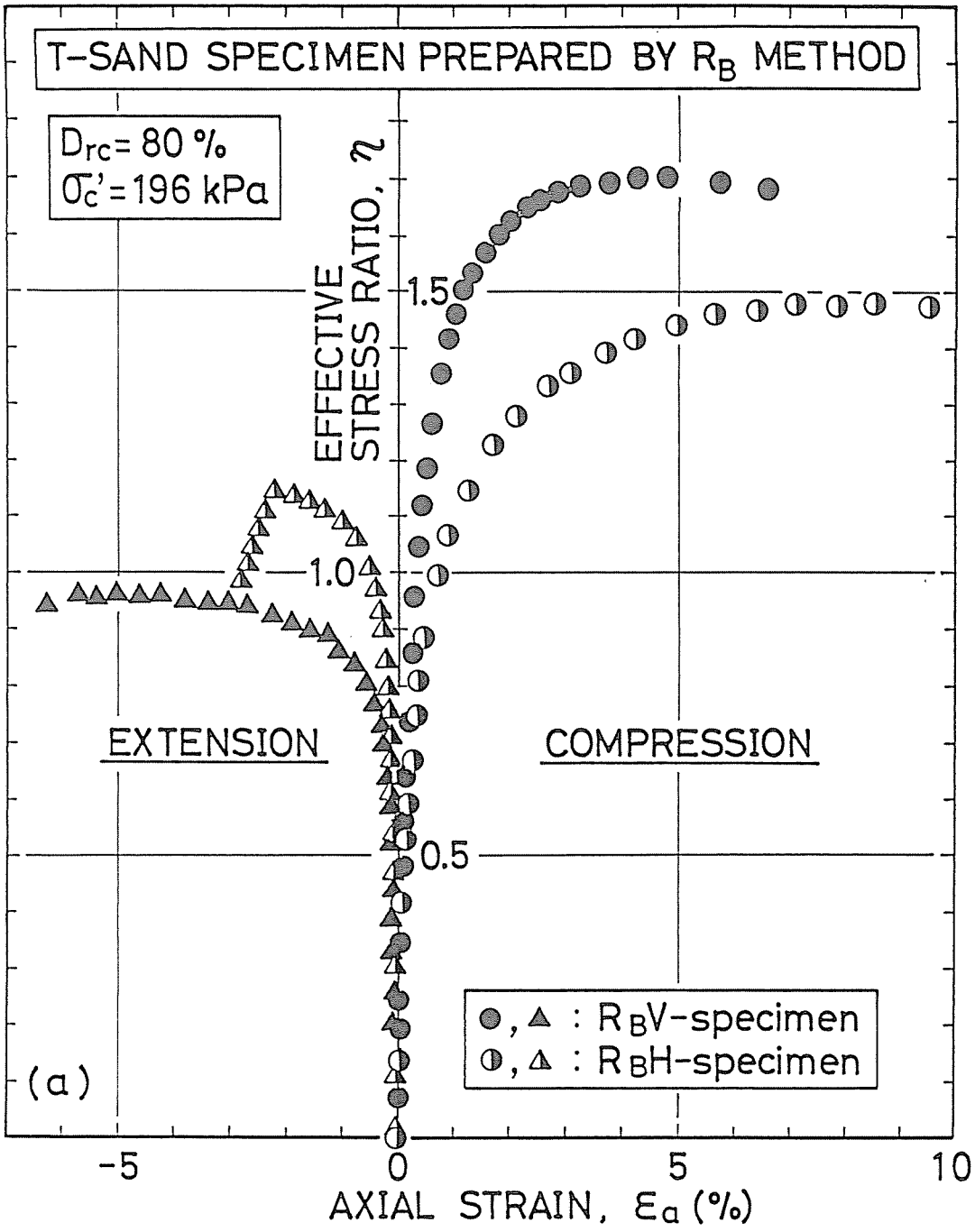

Fig.4-10(a) Comparisons of drained stress-strain relationships for R_BV- and R_BH-specimens of T-sand (η vs. ε_a)

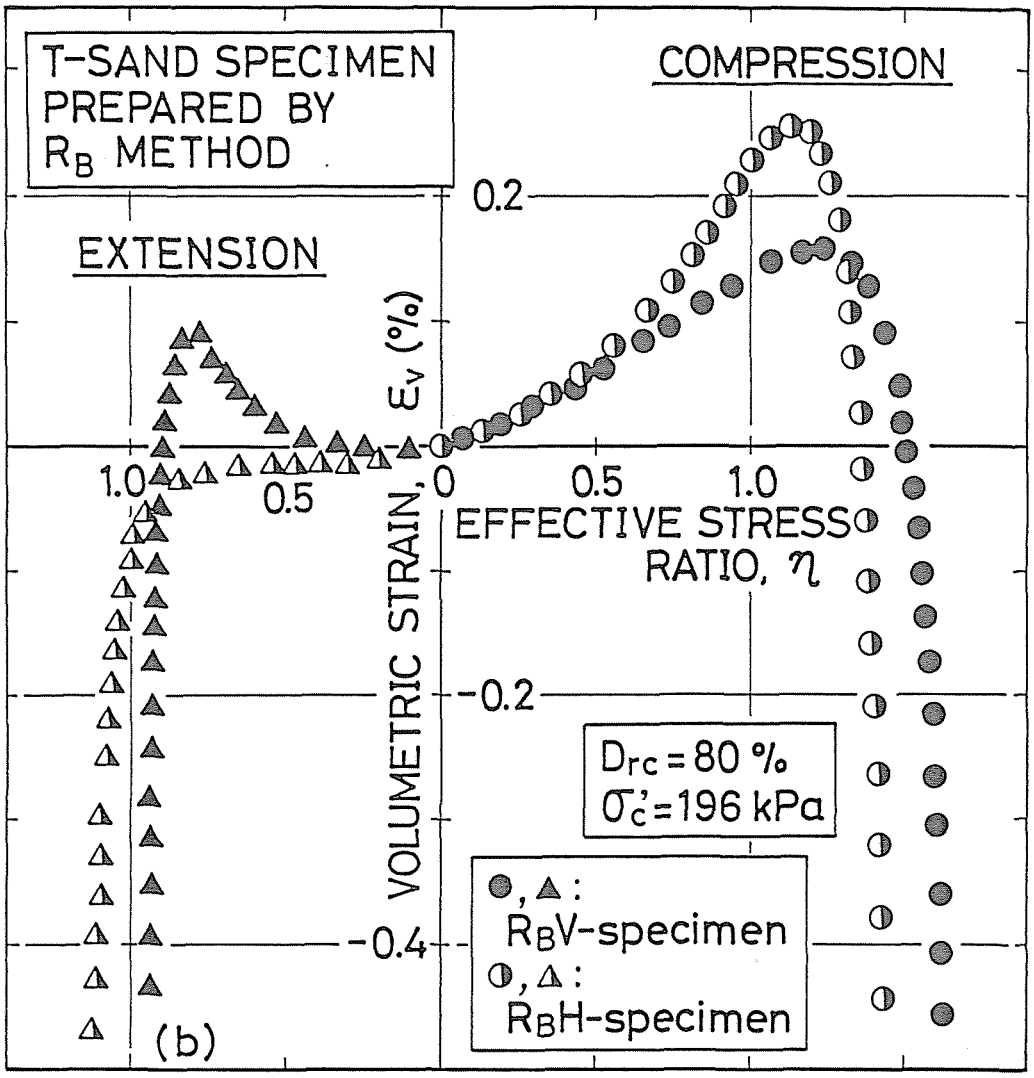

Fig.4-10(b) Comparisons of drained stress-strain relationships for R_BV- and R_BH-specimens of T-sand (η vs. ε_v)

compression and extension stress conditions. These tests were conducted under $\sigma_c' = 196$ kPa and $D_{rc} = 80$ %. Test results is not arranged based on the shear strain γ (Eq.(3-2)) but the axial strain ε_a for the following reason. It is considered that the radial strain ε_r of R_BV-specimen is almost the same for all radial directions of the triaxial specimen, but that of R_BH-specimen is different for different radial directions. Therefore, the reasonable shear strain γ for R_BH-specimen could not be estimated by Eq.(3-2) (See Fig.3-11).

Remarkable differences in the deformation-strength characteristics of both specimens can be seen in each stress condition. That is, in the triaxial compression stress condition under which the direction of the major principal stress is vertical, the deformability and volume contractility during shear of R_BH-specimen are more significant than those of R_BV-specimen. On the other hand, the tendency reverse to what is seen in the triaxial compression tests is observed in the triaxial extension stress condition with the major principal stress direction being radial.

Inasmuch as each test condition for both specimens is the same, the possible causes which may explain such changes in the deformation-strength properties must be the difference in the fabric characteristics (fabric anisotropy) due to the difference of cutting direction of triaxial specimens. As could be seen in Fig.3-15, the specimens made by pluviation of

sand through air method such as MSP method had the inherently anisotropic fabric due to the preferred orientations of particles in their vertical section. It can be considered that such fabric anisotropy may produce the anisotropic mechanical properties as observed in Fig.4-10 in which sand is more compressible and less extensible in the parallel direction to the bedding plane and conversely less compressible and more extensible in the normal direction to the bedding plane.

Shown in Figs.4-11 and 4-12 are the typical time histories obtained by the cyclic undrained triaxial tests performed under nearly equal value of cyclic stress ratio for R_BV- and R_BH-specimens of T-sand. Comparisons of the time histories for both specimens indicate that there exists a definite difference in the cyclic deformation performance between R_BV- and R_BH-specimens. That is, the predominant deformability is more significant in the extensional side for R_BV-specimen and in the compressional side for R_BH-specimen, as the cyclic undrained loading proceeds. Comparison of undrained effective stress paths shown in Figs. 4-12(a) and (b) also indicates that the pore water pressure developed in the extensional side is by far higher in R_BV-specimen than in R_BH-specimen.

The remarkable difference in deformation performance during cyclic loading such as observed above leads to a difference in the cyclic undrained triaxial strength. The relation-

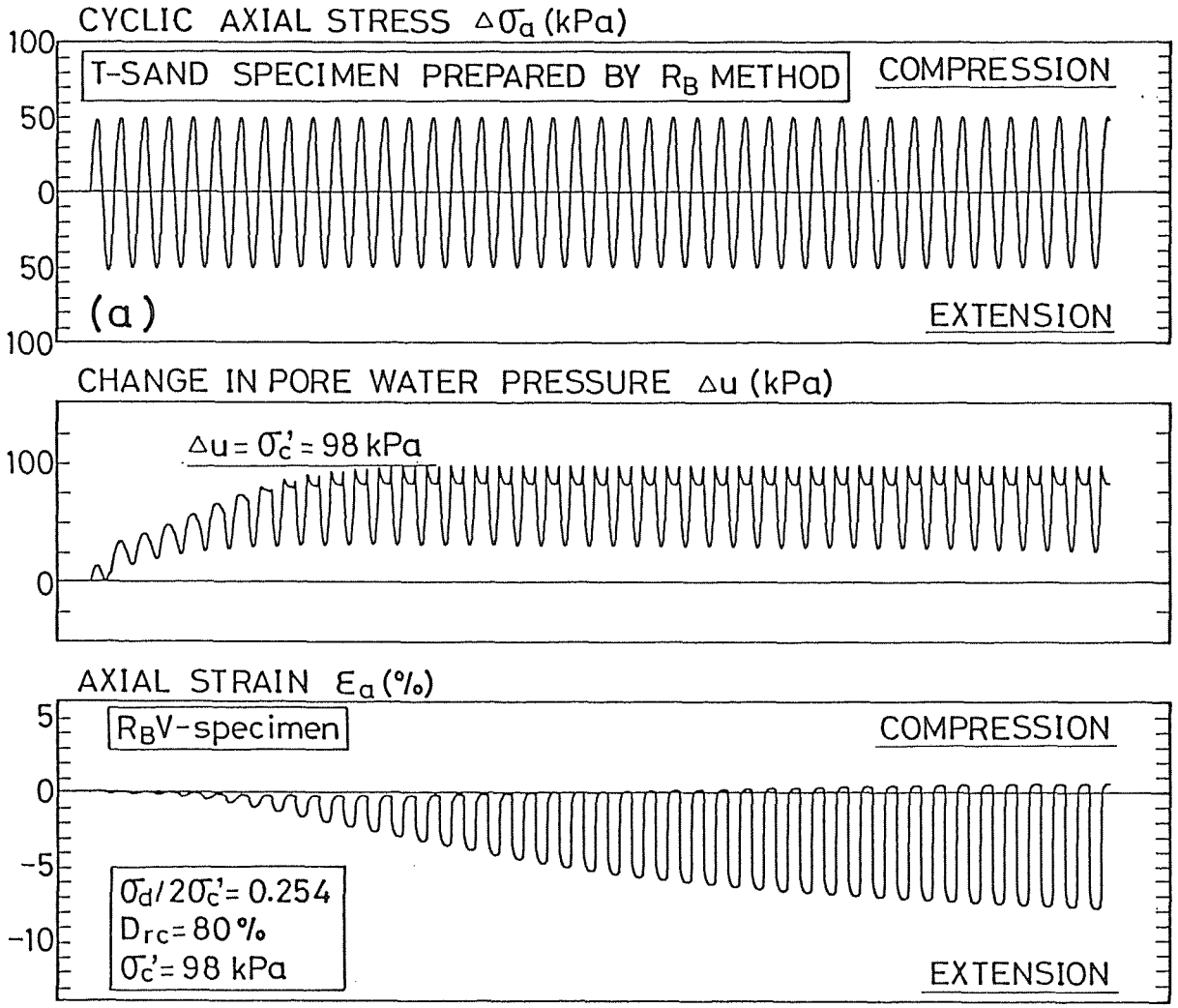

Fig.4-11(a) Time histories of cyclic axial stress, pore water pressure and axial strain for R_BV-specimen of T-sand

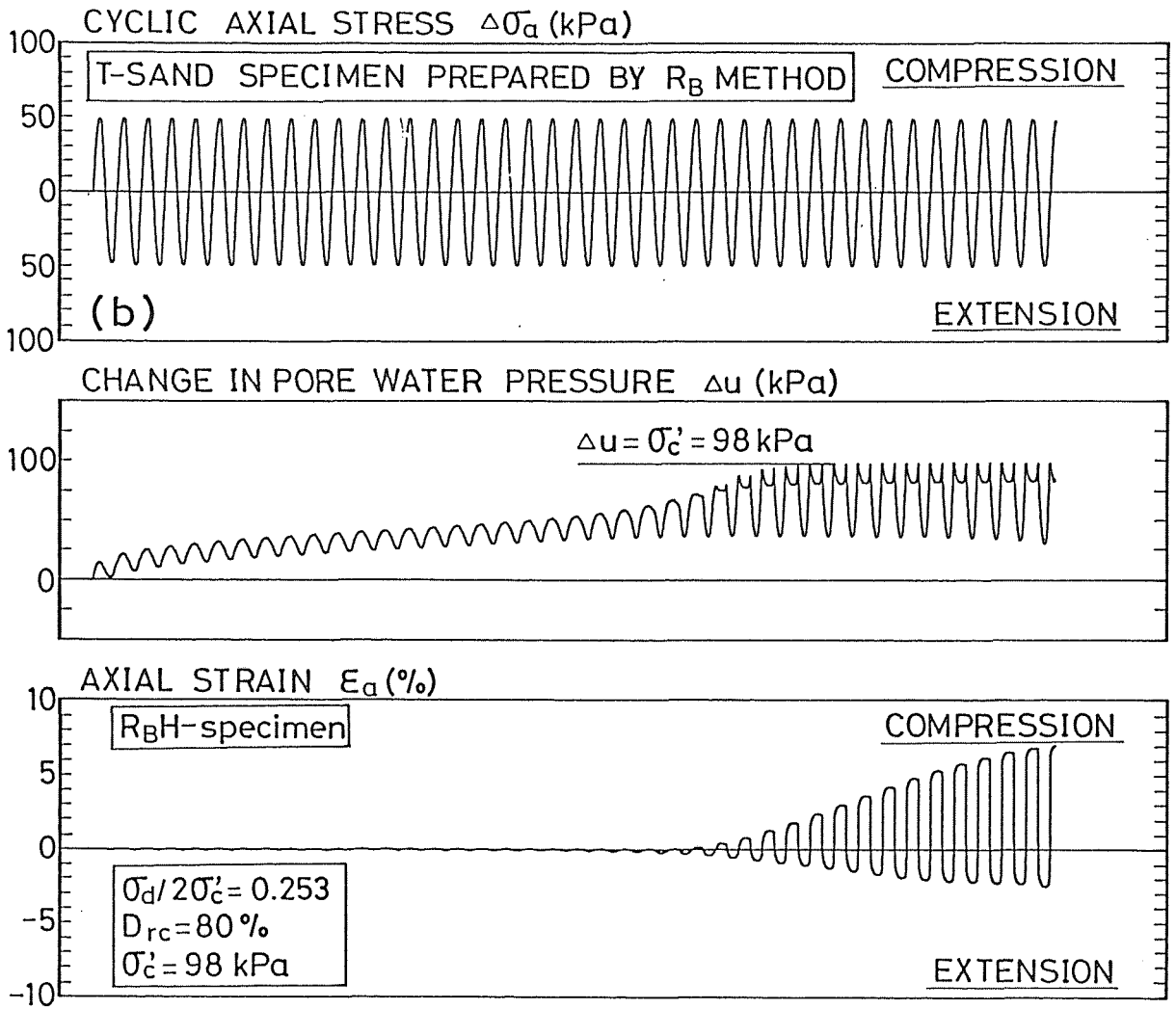

Fig.4-11(b) Time histories of cyclic axial stress, pore water pressure and axial strain for R_BH-specimen of T-sand

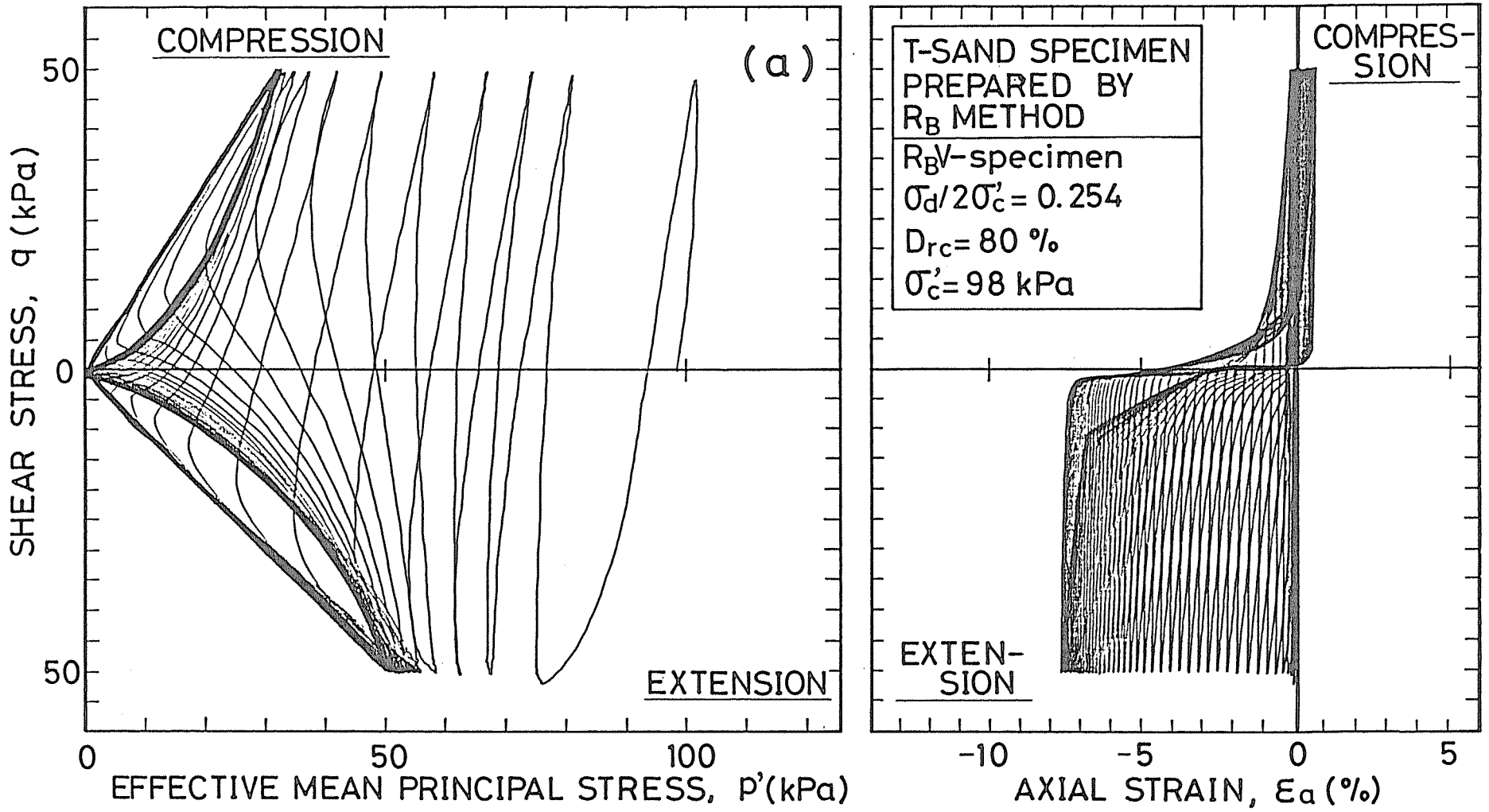

Fig.4-12(a) Time histories of undrained effective stress path and stress-strain relationship for R_BV-specimen of T-sand

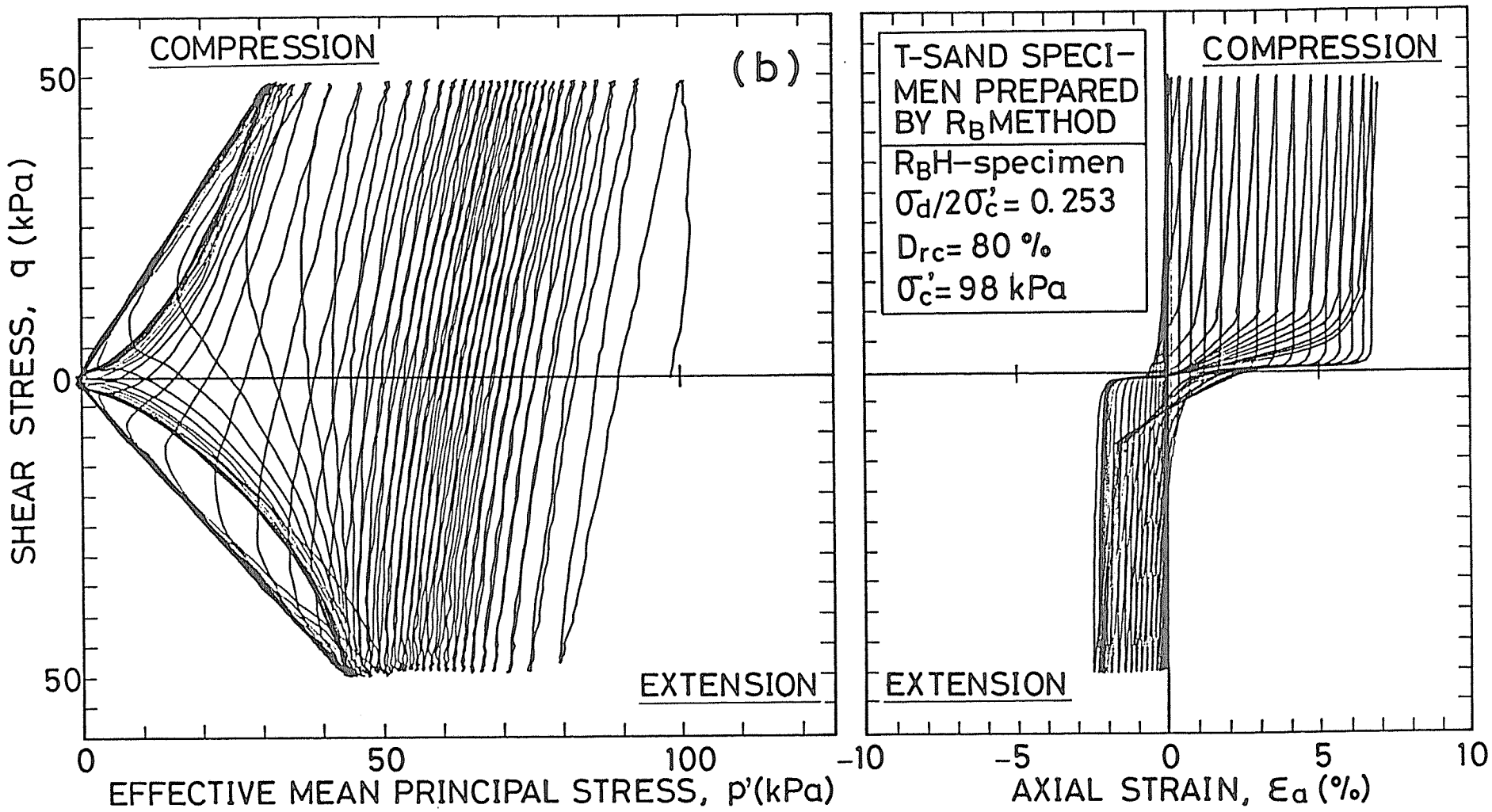

Fig.4-12(b) Time histories of undrained effective stress path and stress-strain relationship for R_BH-specimen of T-sand

ships between the cyclic stress ratio $\sigma_d/2\sigma_c'$ and the number of loading cycles N obtained from a series of cyclic undrained triaxial tests on R_BV- and R_BH-specimens of T-sand are compared in Figs.4-13(a) and (b). Fig.4-13(a) is arranged based on the number of loading cycles at which the values of double amplitude axial strain DA induced during cyclic loading are 1 %, 2 % and 5 % ($N = N_c$), and Fig.4-13(b) is shown for the failure defined as initial liquefaction ($N = N_l$). It can be seen in these figures that there exists a significant difference in cyclic undrained triaxial strength (cyclic strength) defined as cyclic stress ratio value inducing the initial liquefaction or 1 %, 2 % and 5 % double amplitude axial strains at any number of loading cycles between both specimens, and such cyclic strength values are always higher for R_BH-specimen than for R_BV-specimen. It could be pointed out that such variations in the cyclic undrained behaviors are almost identical to those in the static deformation-strength properties mentioned above which are attributed to the fabric anisotropy of specimen. Because it was found in the preceding paragraph that if the specimens are prepared by the same methods, the cyclic undrained behaviors of sand specimens are intimately related to their static dilatancy characteristics.

From these experimental results on sand artificially deposited, consequently, it can be said that not only static stress-strain-dilatancy characteristics but also cyclic undrained behaviors at given density are extremely dependent on the fabric anisotropy of sand.

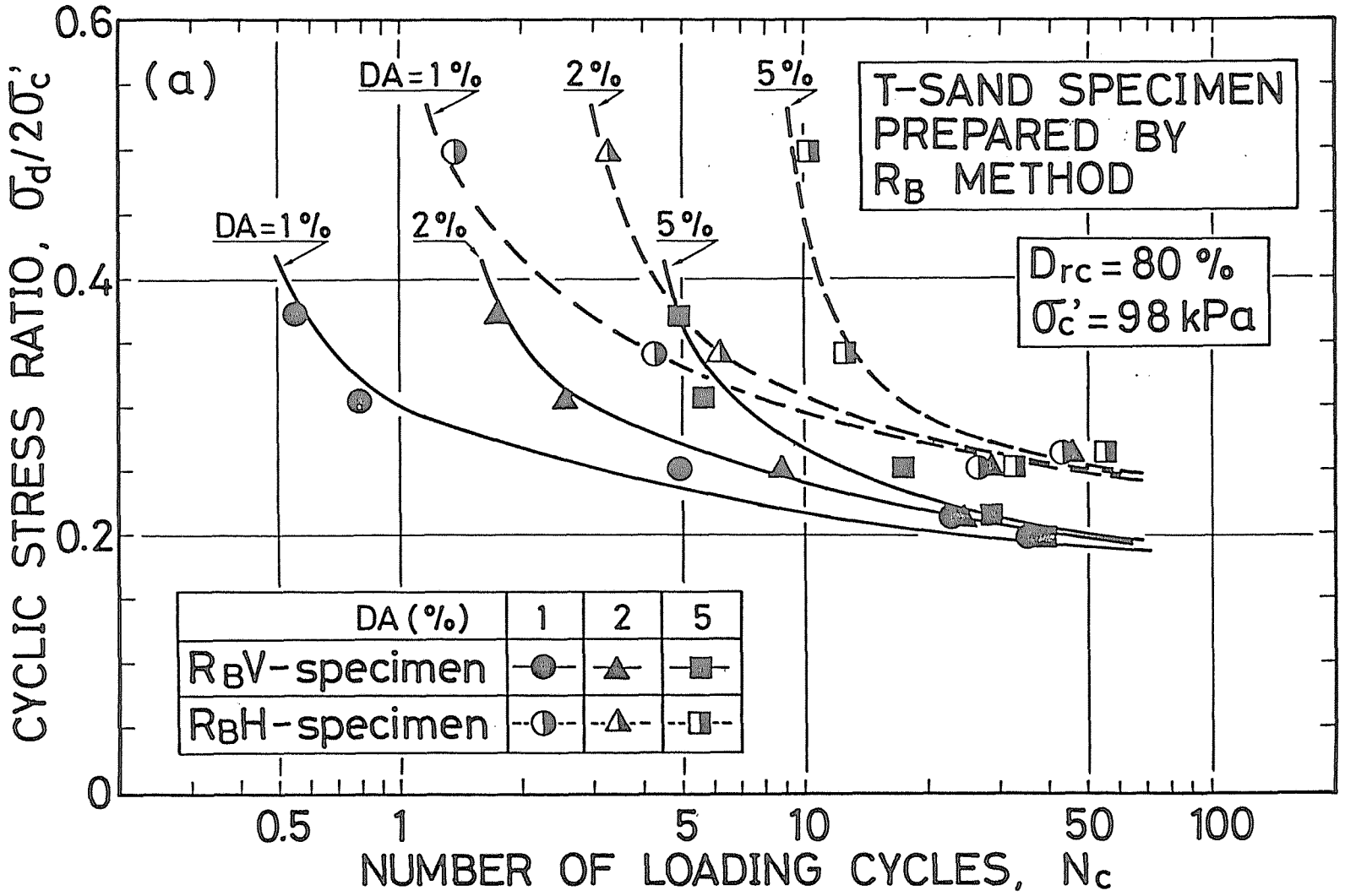

Fig.4-13(a) Comparison of cyclic undrained triaxial strengths for R_BV- and R_BH-specimens of T-sand (cyclic stress ratio vs. number of loading cycles to 1%, 2% and 5% double amplitude axial strains relationship)

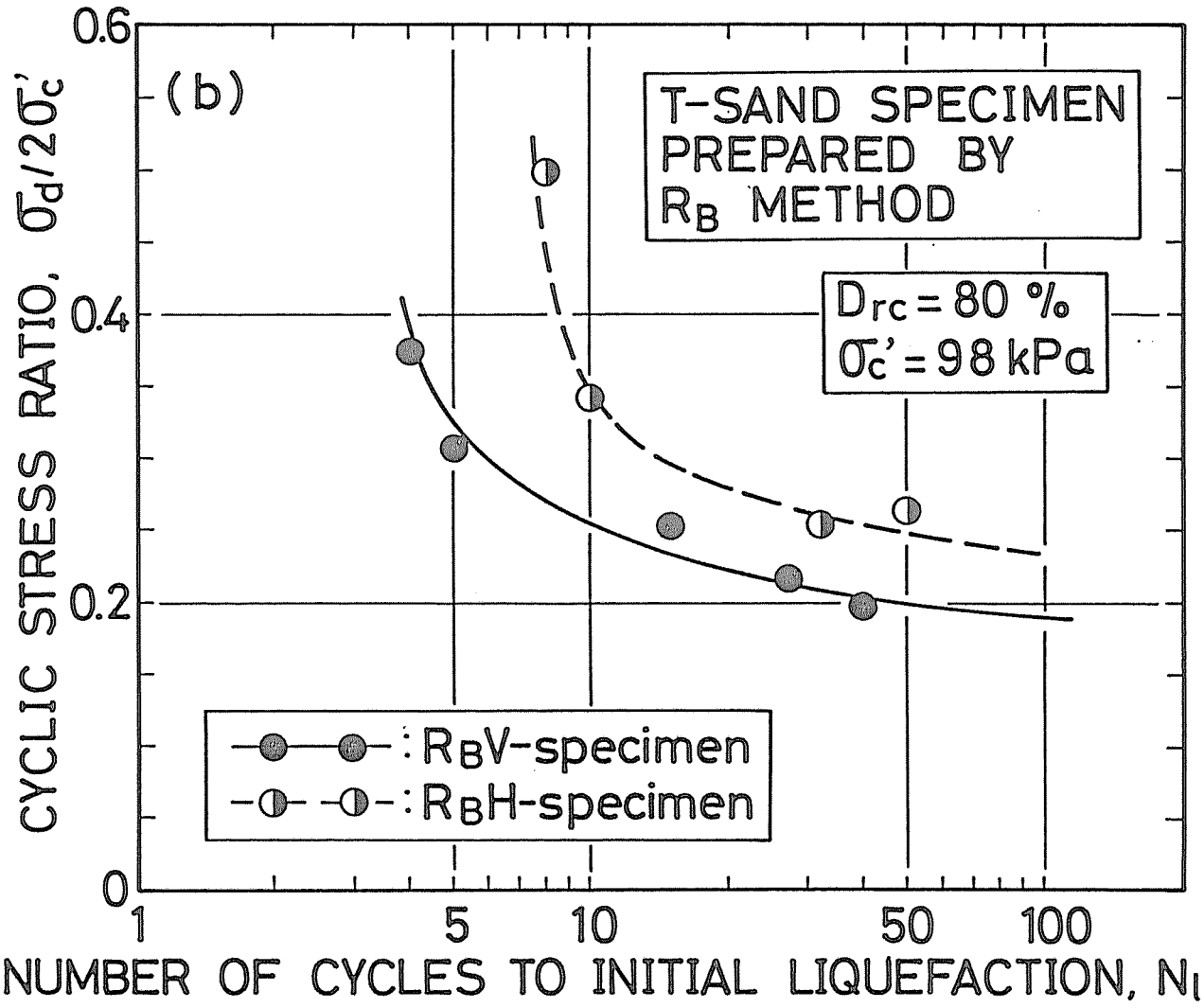

Fig.4-13(b) Comparison of cyclic undrained triaxial strengths for R_BV- and R_BH-specimens of T-sand (cyclic stress ratio vs. number of loading cycles to initial liquefaction relationship)

4.4 Anisotropy in Mechanical Properties and Its Simulation of Sands Sampled from Natural Deposits

4.4.1 Static deformation-strength properties of undisturbed sand

The significance of the anisotropy in mechanical behaviors of sand artificially deposited was explained in the preceding paragraph. In order to examine whether or not such anisotropic mechanical behaviors could exist in natural sand deposits, a series of static drained triaxial tests was performed for UV- and UH-specimens of undisturbed I-sand obtained by the block sampling. As mentioned previously (CHAPTER 3), the undisturbed triaxial specimens were consolidated isotropically to σ_c' of 98 kPa.

Figs.4-14(a) and (b) show the typical effective stress ratio-axial strain-volumetric strain relationships for both specimens cut from a block sample. Comparison of test results for each stress condition indicates that the difference of the static deformation-strength characteristics between both specimens can be apparently observed. Because in-situ sampling condition and laboratory sample treatments in the present study are completely the same for both UV- and UH-specimens, the only difference which exists between both specimens is that the axial direction of UV-specimen is selected to be the vertical

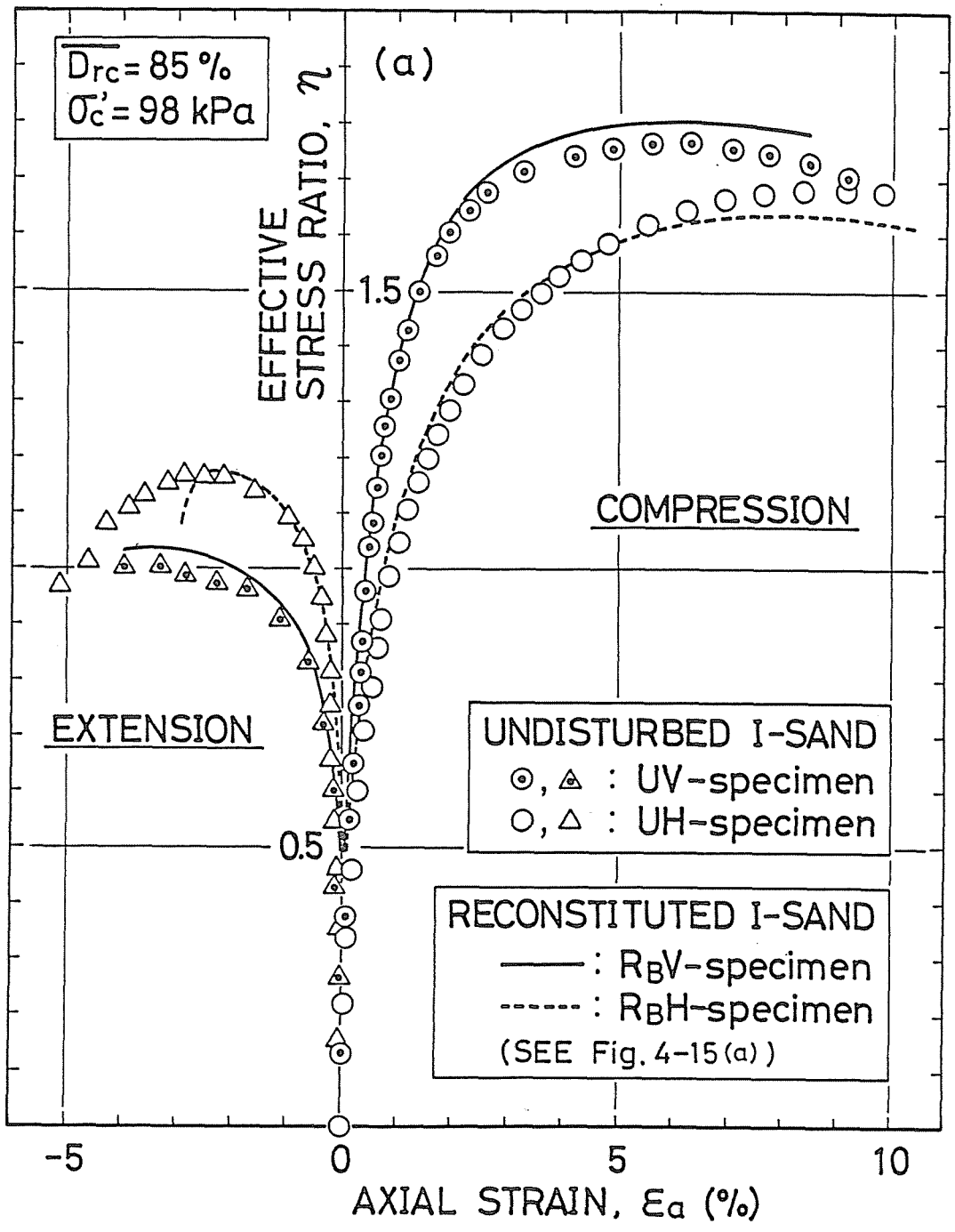

Fig.4-14(a) Change in drained stress-strain-dilatancy relationship of undisturbed I-sand due to the difference of cutting direction (η vs. ε_a)

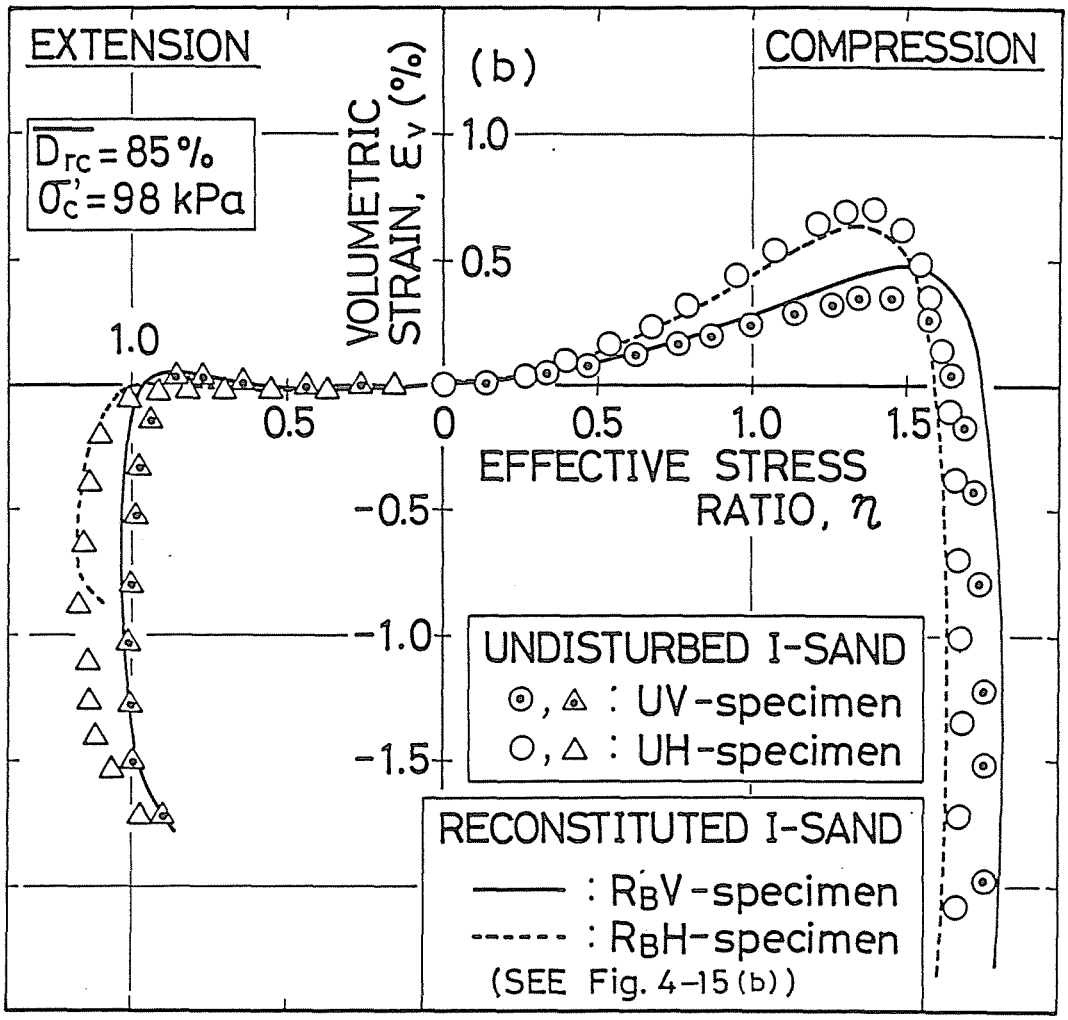

Fig.4-14(b) Change in drained stress-strain-dilatancy relationship of undisturbed I-sand due to the difference of cutting direction (η vs. ε_v)

direction in natural sand deposits and that of UH-specimen to be the horizontal direction in natural sand deposits. The experimental facts indicate that UV-specimen is by far more resistant to deformation when sheared under the triaxial compression condition and conversely less resistant to deformation when sheared under the triaxial extension condition than UH-specimen.

It can be recognized that such tendency of variations in the deformation-strength behaviors of sand sampled from natural deposits is very similar to that of dense T-sand prepared by pluviation of sand through air method (See Figs.4-10 (a) and (b)). It is also considered that anisotropy in static deformation-strength properties of undisturbed sand such as observed above is attributed to the anisotropic fabric of in-situ sand shown in Fig.3-15.

From these facts, it can be pointed out that the natural sand deposit examined in the present study is characterized by such anisotropic behaviors, in which sand is more compressible and less extensible in the horizontal direction than in the vertical direction, as those of artificially deposited sand by the pluviation of sand through air method in the laboratory.

4.4.2 Comparison of static deformation-strength properties between undisturbed and reconstituted specimens

In order to examine whether the anisotropic feature of mechanical properties for undisturbed sand could be simulated in the laboratory, static deformation-strength properties of I-sand specimens reconstituted to the same density as that of undisturbed sand by the various preparation methods were studied.

We can confirm in Fig.4-15 the facts hitherto known that the differences in reconstitution methods of sand sample have a considerable influence on the static deformation-strength behavior. However, it is worthy of note in Fig. 4-15 that the deformation-strength properties of R_BV- and R_BH-specimens made by R_B method (MSP method), among the reconstitution methods adopted in the present study, are similar to those of UV- and UH-specimens, respectively.

In order to make a direct comparison between both behaviors for each stress condition, the effective stress ratio-axial strain-volumetric strain relationships for R_BV- and R_BH-specimens are depicted in Figs.4-14(a) and (b) with solid and broken lines, respectively. It can be seen in Fig.4-14 that there exists a good coincidence between R_BV- and UV-specimens and R_BH- and UH-specimens in each triaxial stress condition. These facts indicate that a better reproduction of anisotropic

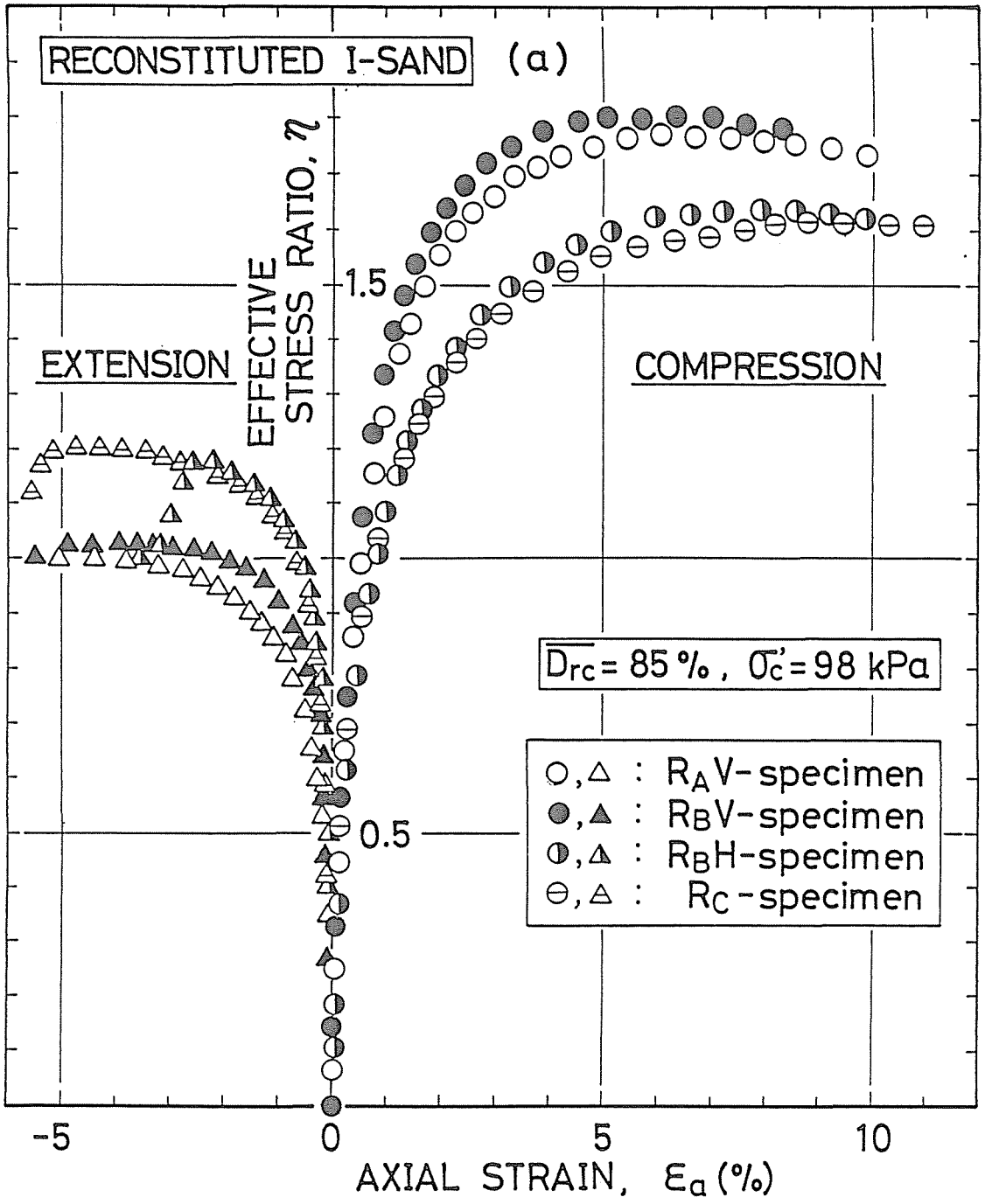

Fig.4-15(a) Variation in drained stress-strain-dilatancy relationship of reconstituted I-sand due to the effect of difference in sample preparation method (η vs. ε_a)

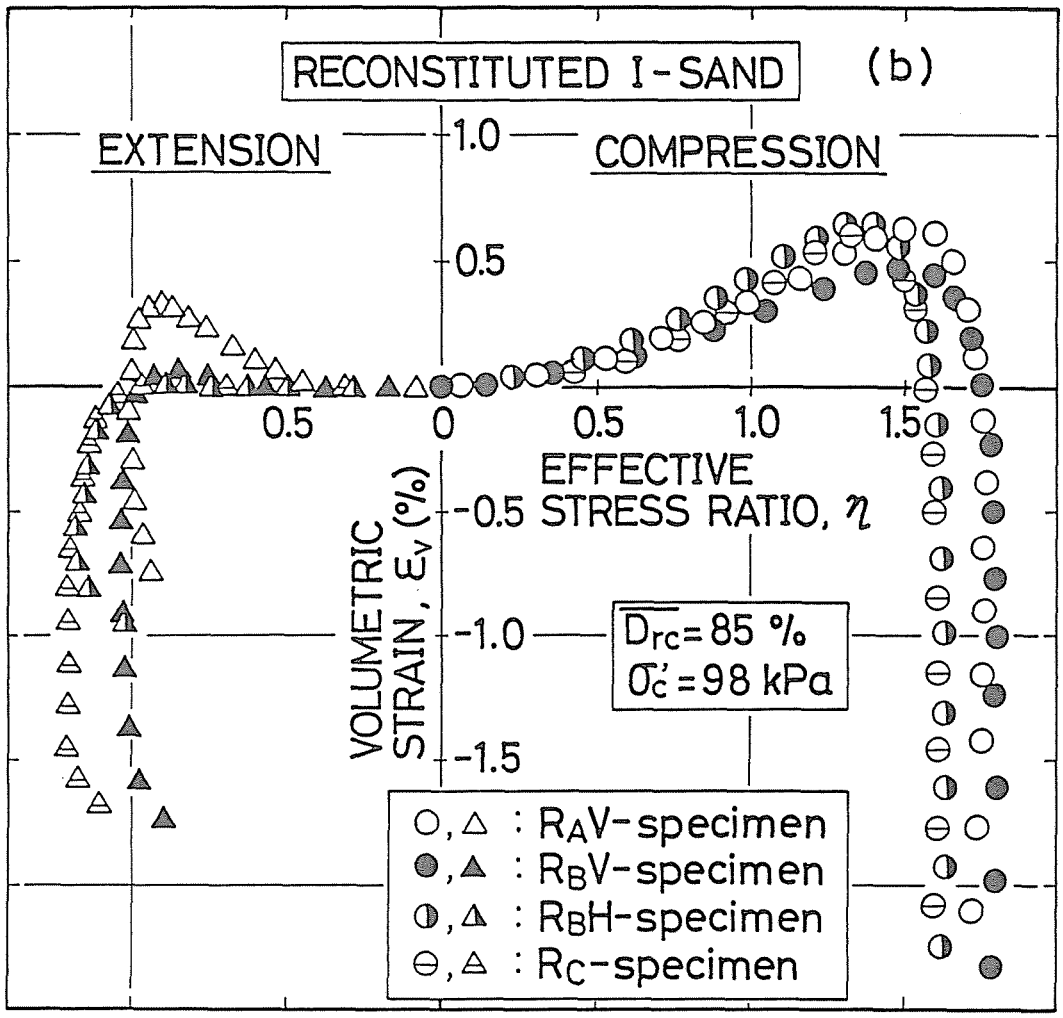

Fig.4-15(b) Variation in drained stress-strain-dilatancy relationship of reconstituted I-sand due to the effect of difference in sample preparation method (η vs. ε_v)

triaxial shear behaviors in natural sand deposits is possible by adopting the pluviation of sand through air method such as MSP method (R_B method) in the laboratory.

The only difference between R_A and R_B methods seems whether or not the sand specimen is temporarily frozen during its preparation process. Because it was indicated by preliminary examinations (Miura et al., 1982a) that the cutting process of the specimens from a frozen sand block had no significant effects on the results of static triaxial compression and extension tests. Accordingly, it is considered that the comparison of R_AV- and R_BV-specimens enables to detect an influence of the freeze-thaw sequence on the deformation-strength properties of sand. It can be confirmed, by comparing the deformation-strength properties of R_AV-specimen with those of R_BV-specimen in Figs.4-15(a) and (b), that the influence of the freeze-thaw sequence on the stress-strain-dilatancy characteristics of I-sand is only slight under the triaxial compression stress condition, but could not be disregarded especially in the dilatancy characteristics under the triaxial extension stress condition. That is, the trend of volume contraction during shear of sand specimen subjected previously to the freeze-thaw sequence is significantly restrained in the triaxial extension stress condition. Figs.4-16(a) and (b) indicate that such influence of the freeze-thaw sequence can be also observed in the dilatancy characteristics of T-sand.

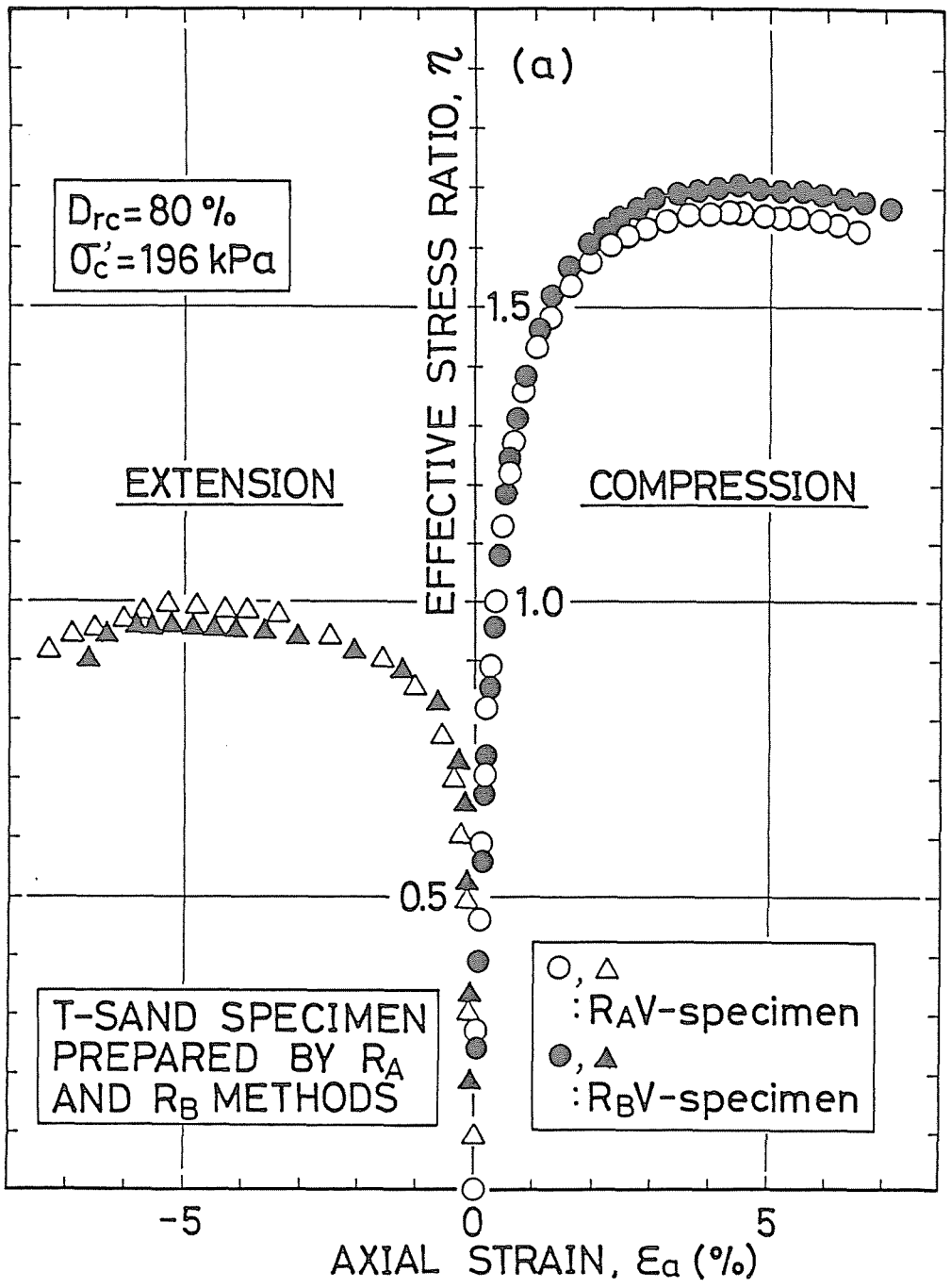

Fig.4-16(a) Effect of freeze-thaw sequence during sample preparation on drained stress-strain-dilatancy relationship of T-sand (Test data of R_BV-specimen are the same as those in Fig.4-10(a)) (η vs. ε_a)

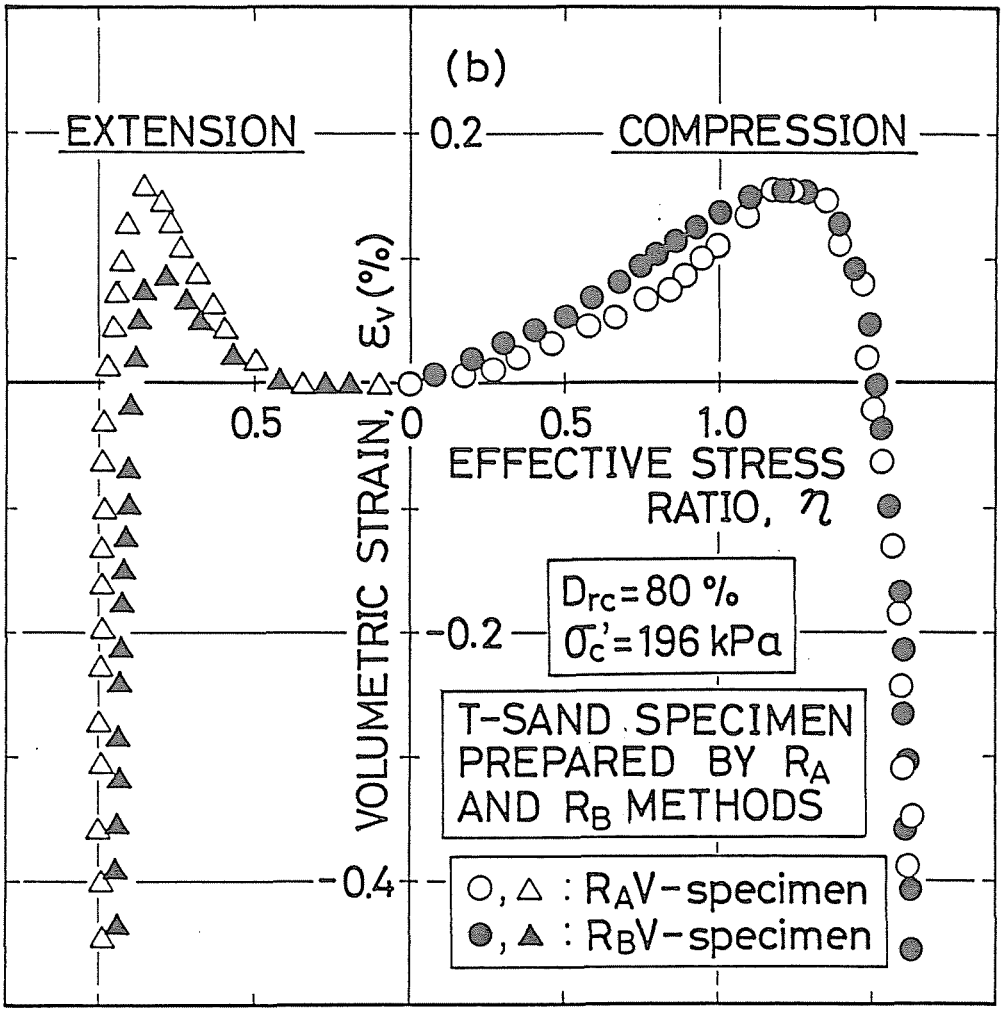

Fig.4-16(a) Effect of freeze-thaw sequence during sample preparation on drained stress-strain-dilatancy relationship of T-sand (Test data of R_BV-specimen are the same as those shown in Fig.4-10(b)) (η vs. ε_v)

As described previously (CHAPTER 3), no measurable volume change of sand due to the freeze-thaw sequence was observed in this study. It was also confirmed by the characterization of sand fabric that the fabric characteristics of R_AV-specimen are almost similar to those of R_BV-specimen. However, the facts described above indicate that the freeze-thaw sequence is able to make a delicate difference in the dilatancy characteristics of sand specimen, in which the particles have strongly preferred orientations in its vertical section, under the triaxial extension stress condition.

The influence of the freeze-thaw sequence will be further discussed in the later paragraph.

4.4.3 Cyclic undrained behaviors of undisturbed sand

Shown in Figs.4-17, 4-18, 4-19 and 4-20 are the comparisons of typical time histories of cyclic axial stress, pore water pressure, axial strain, undrained effective stress path and stress-strain relationship for UV- and UH-specimens of K-sand and I-sand. The comparison between the cyclic undrained behaviors of UV- and UH-specimens for both sands indicates that there exists such a remarkable difference in the pattern of axial strain and pore water pressure development observed in T-sand (Figs.4-11 and 4-12). That is, the axial strain induced by cyclic loading is more predominant in the extensional side for UV-specimen and reversely in the compressional side for UH-specimen. It may be seen in both undisturbed sands that the pore water pressure development of UH-specimen is by far higher in the compressional side than of UV-specimen. From the considerations on the results of static triaxial tests for undisturbed sand and for T-sand described in the preceding paragraph, these variations in cyclic undrained behaviors seem to be attributed to the existence of fabric anisotropy in natural sand deposits shown in Figs.3-15 (c) and (d).

It should be noted that K-sand which contains fine particles of around 3 % can be characterized by such anisotropic cyclic behavior as that of I-sand and T-sand which do not

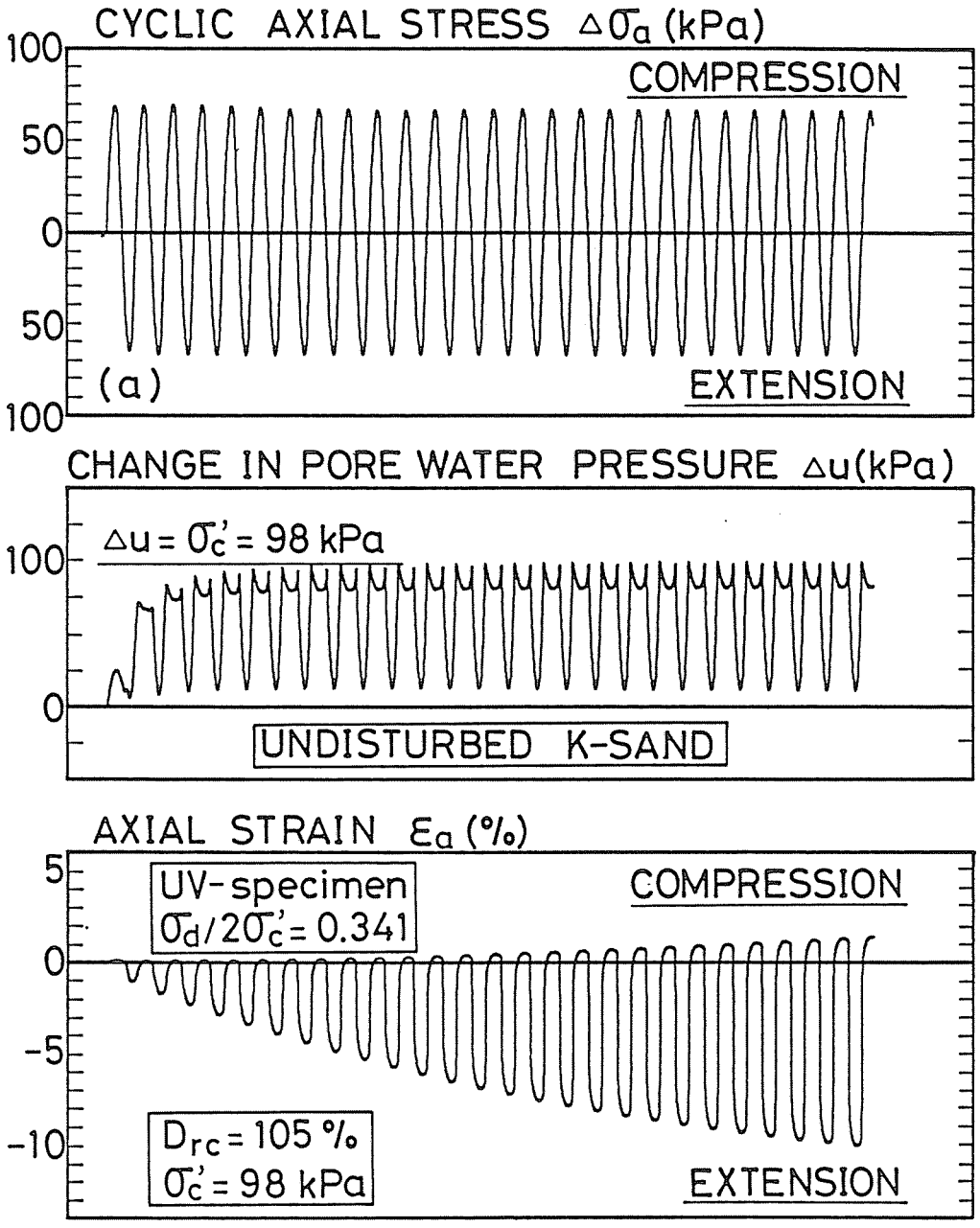

Fig.4-17(a) Time histories of cyclic axial stress, pore water pressure and axial strain for UV-specimen of undisturbed K-sand

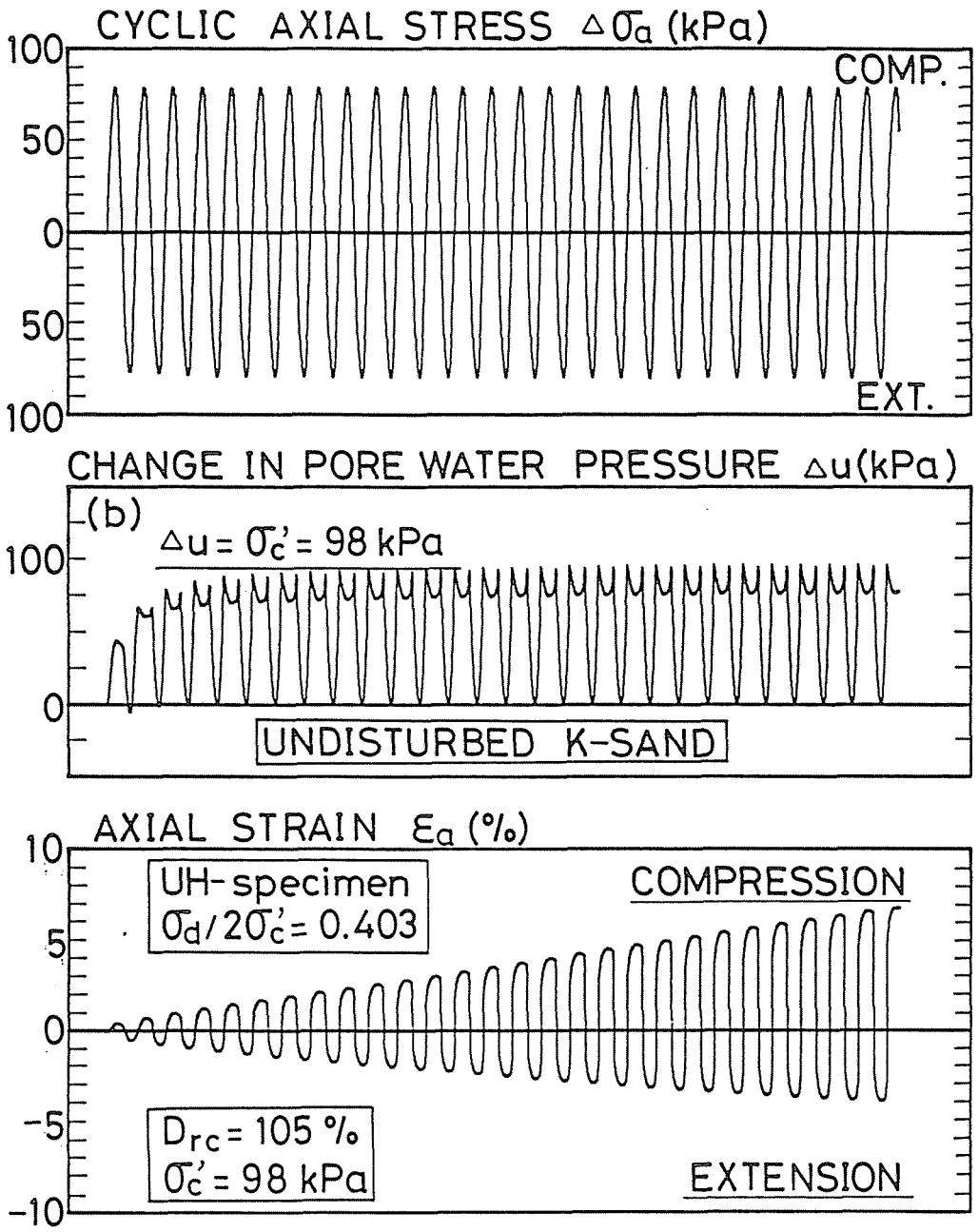

Fig.4-17(b) Time histories of cyclic axial stress, pore water pressure and axial strain for UH-specimen of undisturbed K-sand

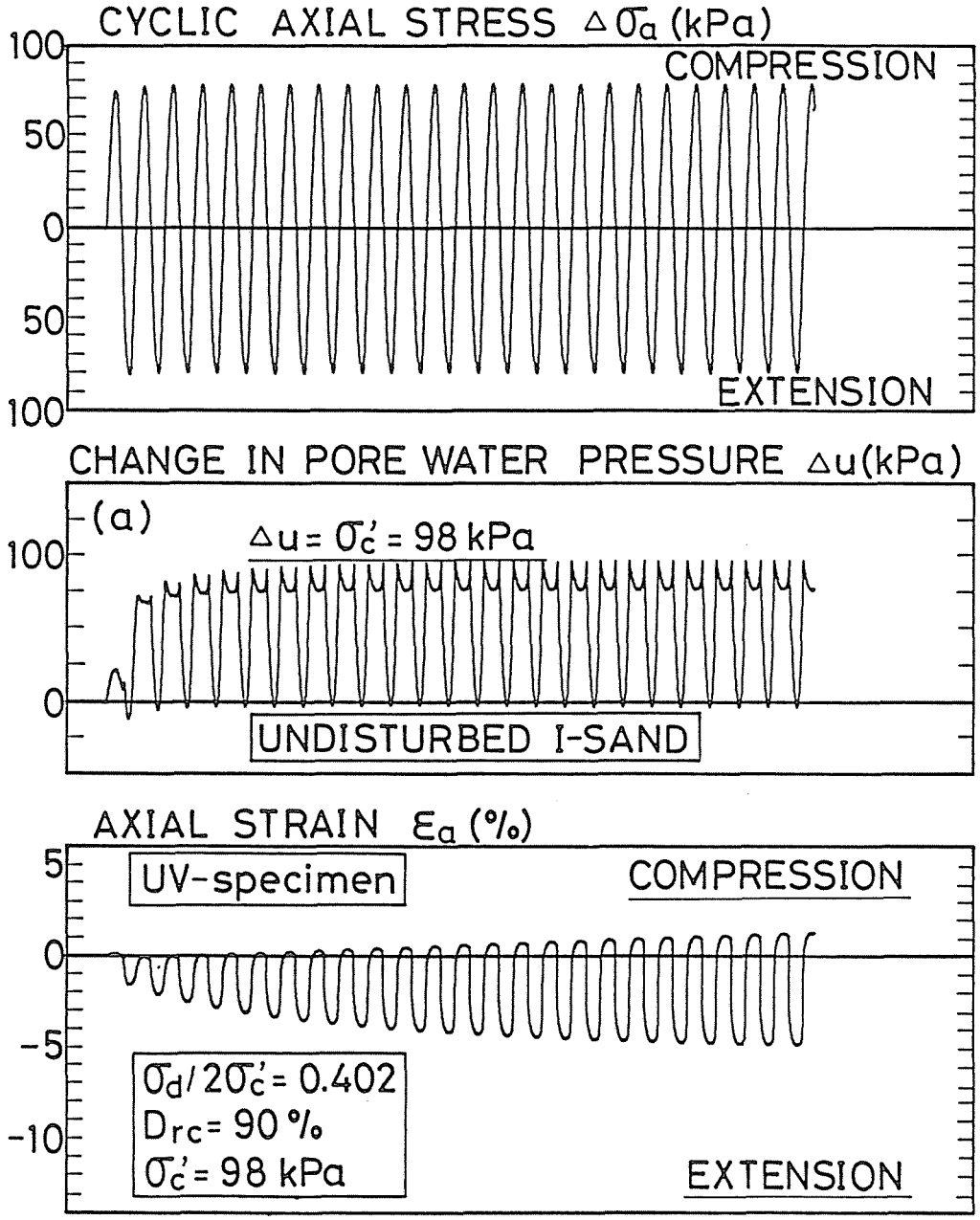

Fig.4-18(a) Time histories of cyclic axial stress, pore water pressure and axial strain for UV-specimen of undisturbed I-sand

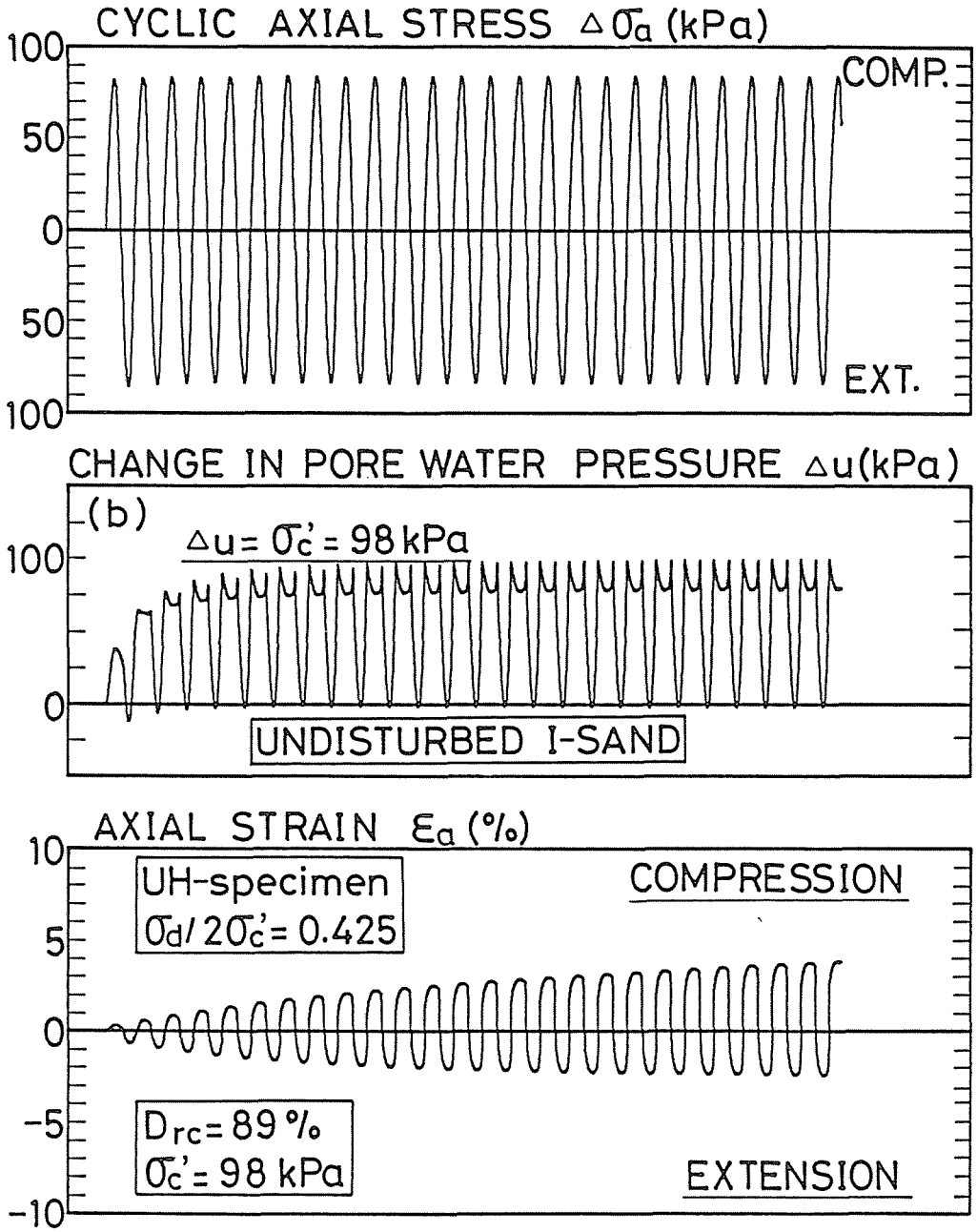

Fig.4-18(b) Time histories of cyclic axial stress, pore water pressure and axial strain for UH-specimen of undisturbed I-sand

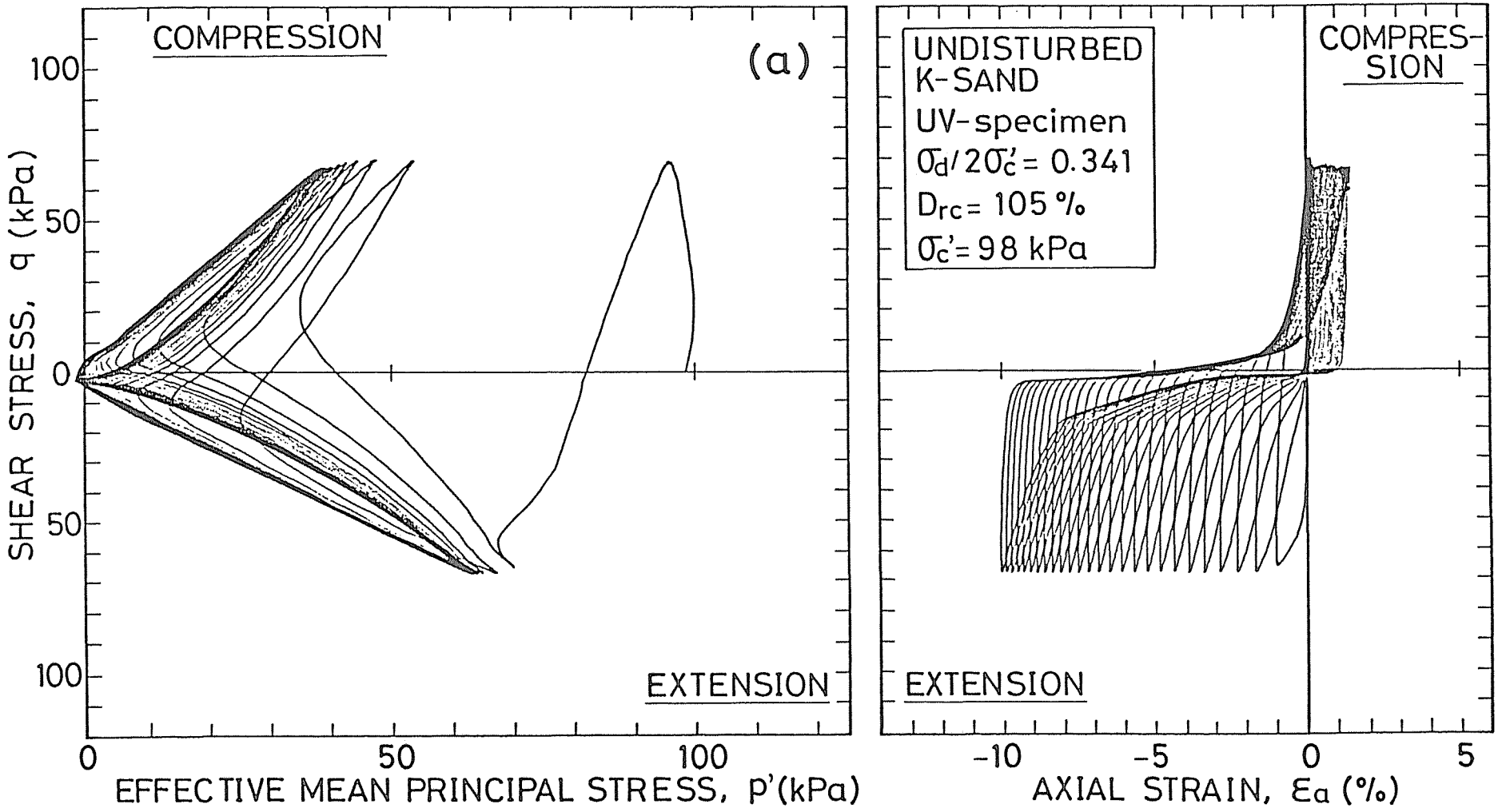

Fig.4-19(a) Time histories of undrained effective stress path and stress-strain relationship for UV-specimen of undisturbed K-sand

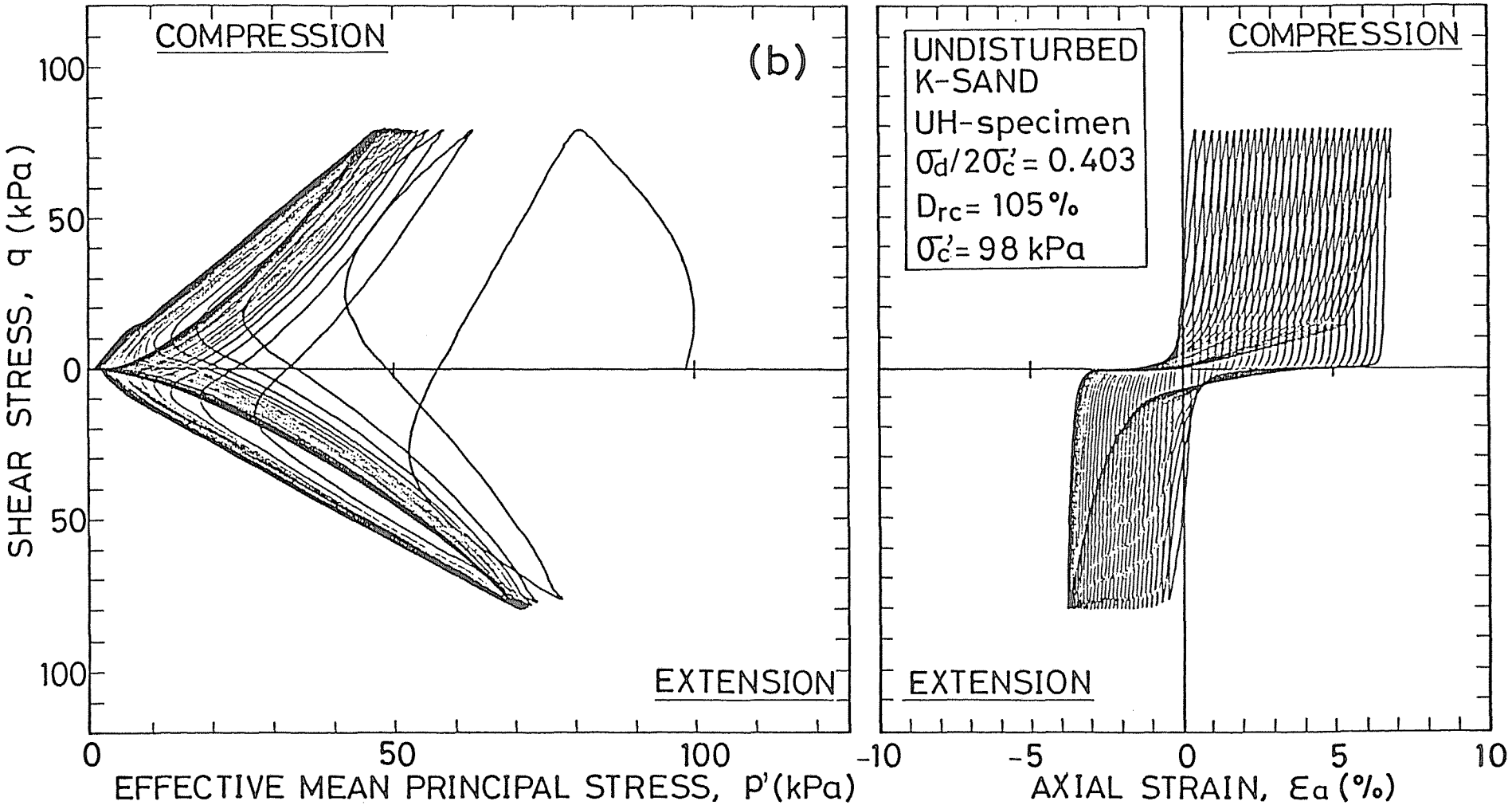

Fig.4-19(b) Time histories of undrained effective stress path and stress-strain relationship for UH-specimen of undisturbed K-sand

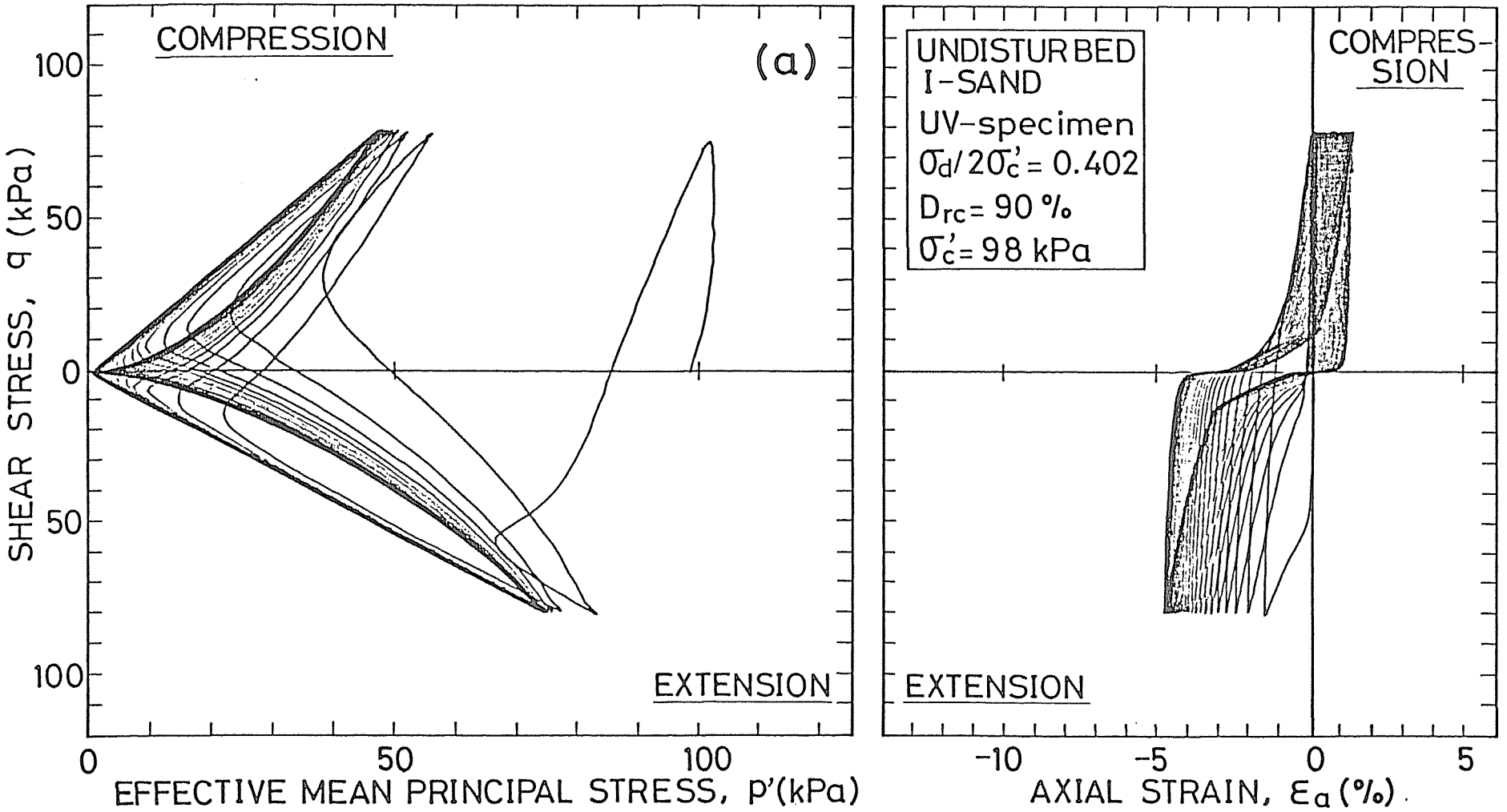

Fig.4-20(a) Time histories of undrained effective stress path and stress-strain relationship for UV-specimen of undisturbed I-sand

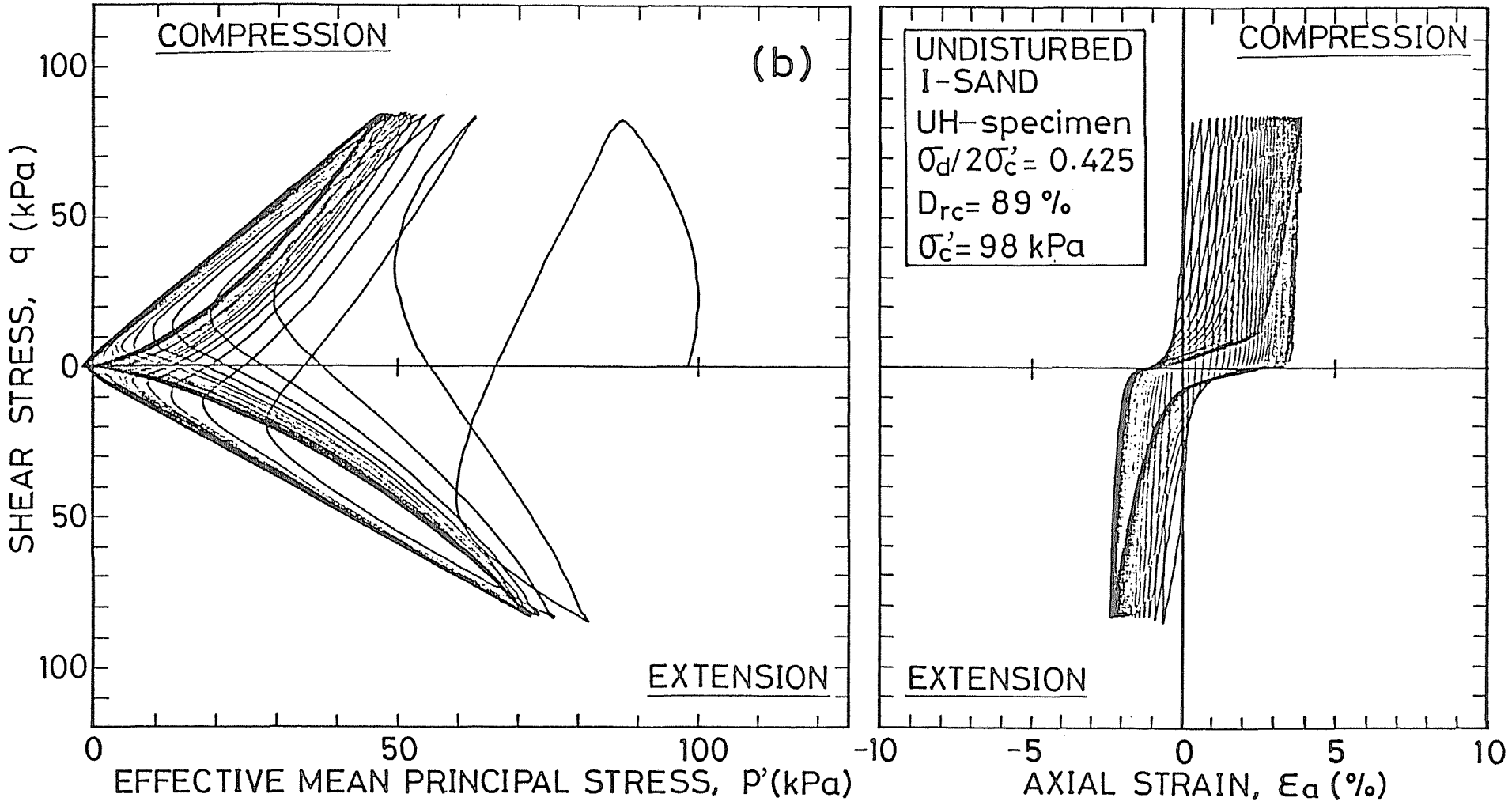

Fig.4-20(b) Time histories of undrained effective stress path and stress-strain relationship for UH-specimen of undisturbed I-sand

involve any fine particles. This indicates that the anisotropy of mechanical properties due to the fabric anisotropy induced during depositing process exists not only in naturally or artificially deposited clean sand, but also in naturally deposited sand which contains fine particles to some extent.

Figs.4-21 and 4-22 show that the variation in cyclic deformation performance such as observed above makes a remarkable difference in the cyclic undrained triaxial strength. As can be seen in Figs.4-21(a) and 4-22(a), the comparison of cyclic stress ratio $\sigma_d/2\sigma_c'$ which induces DA of 1 %, 2 % and 5 % at the same number of loading cycles between both specimens shows that in both K-sand and I-sand the values of $\sigma_d/2\sigma_c'$ of UH-specimen are higher than those of UV-specimen, especially for smaller number of loading cycles.

These experimental results mean that the cyclic undrained triaxial strength evaluated by UV-specimens whose axial direction is chosen to coincide with the in-situ vertical direction becomes lower than that evaluated by UH-specimens whose axial direction is chosen to coincide with the in-situ horizontal direction. It can be also confirmed that these trends of undisturbed K-sand and I-sands are very similar to those of T-sand shown in Fig.4-13. On the other hand, for the cyclic undrained triaxial strength defined as initial liquefaction, such a remarkable difference as detected in T-sand (Fig.4-13 (b)) is not observed in both undisturbed sands, whereas UH-

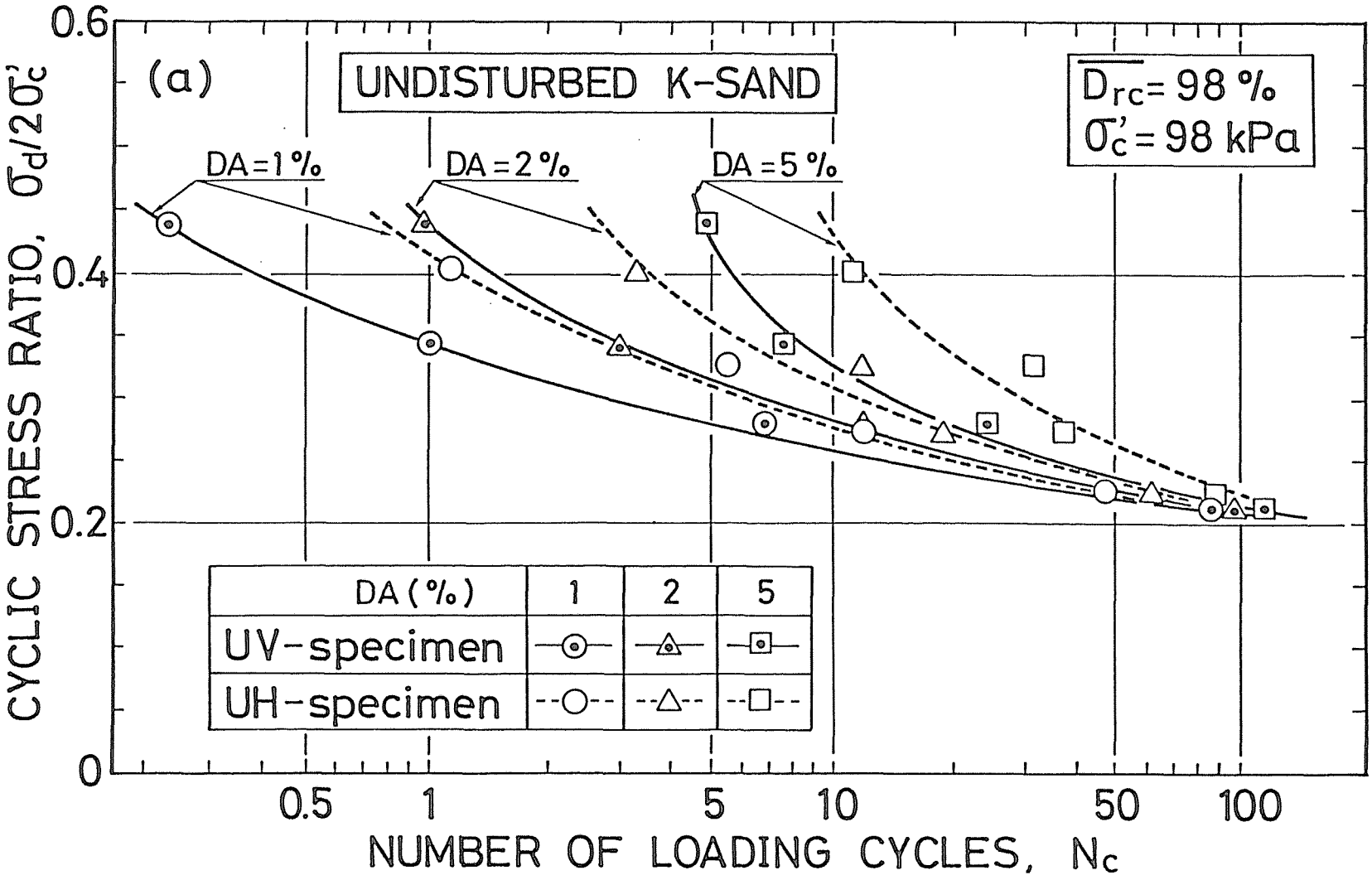

Fig.4-21(a) Comparison of cyclic undrained triaxial strength for UV- and UH-specimens of undisturbed K-sand (Cyclic stress ratio vs. number of loading cycles to 1%, 2% and 5% double amplitude axial strains relationship)

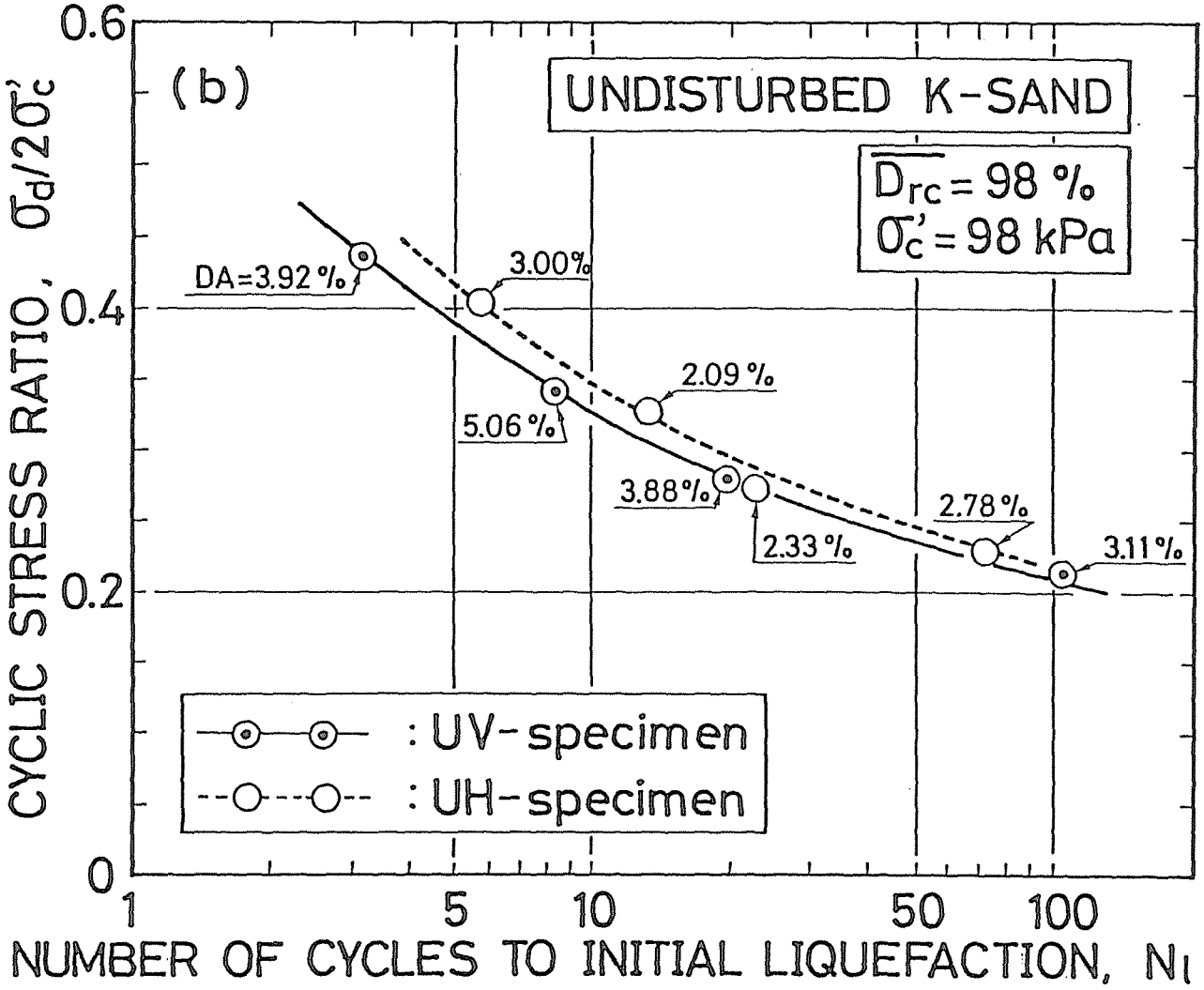

Fig.4-21(b) Comparison of cyclic undrained triaxial strength for UV- and UH-specimens of undisturbed K-sand (Cyclic stress ratio vs. number of loading cycles to initial liquefaction relationship)

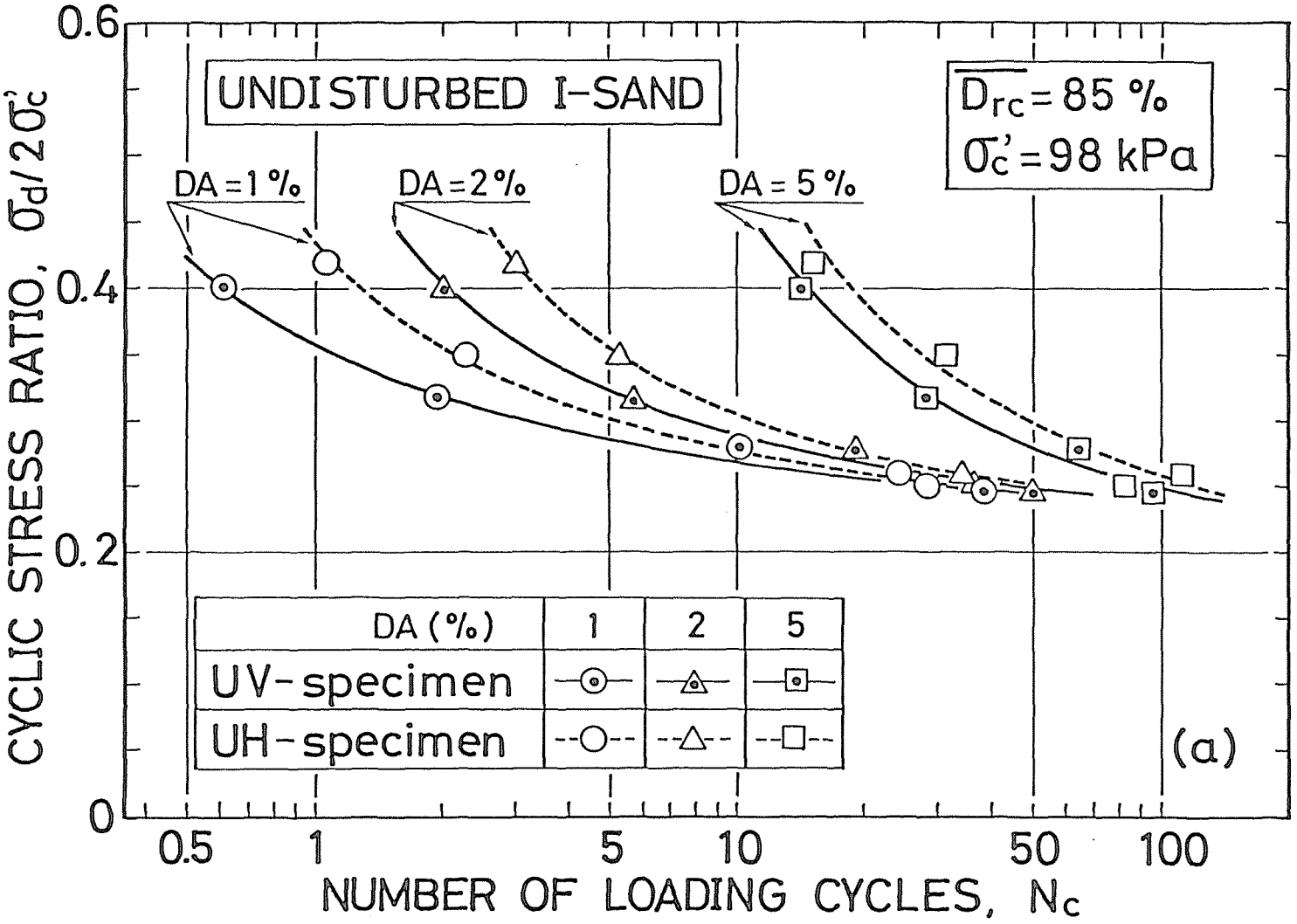

Fig.4-22(a) Comparison of cyclic undrained triaxial strength for UV- and UH-specimens of undisturbed I-sand (Cyclic stress ratio vs. number of loading cycles to 1%, 2% and 5% double amplitude axial strains relationship)

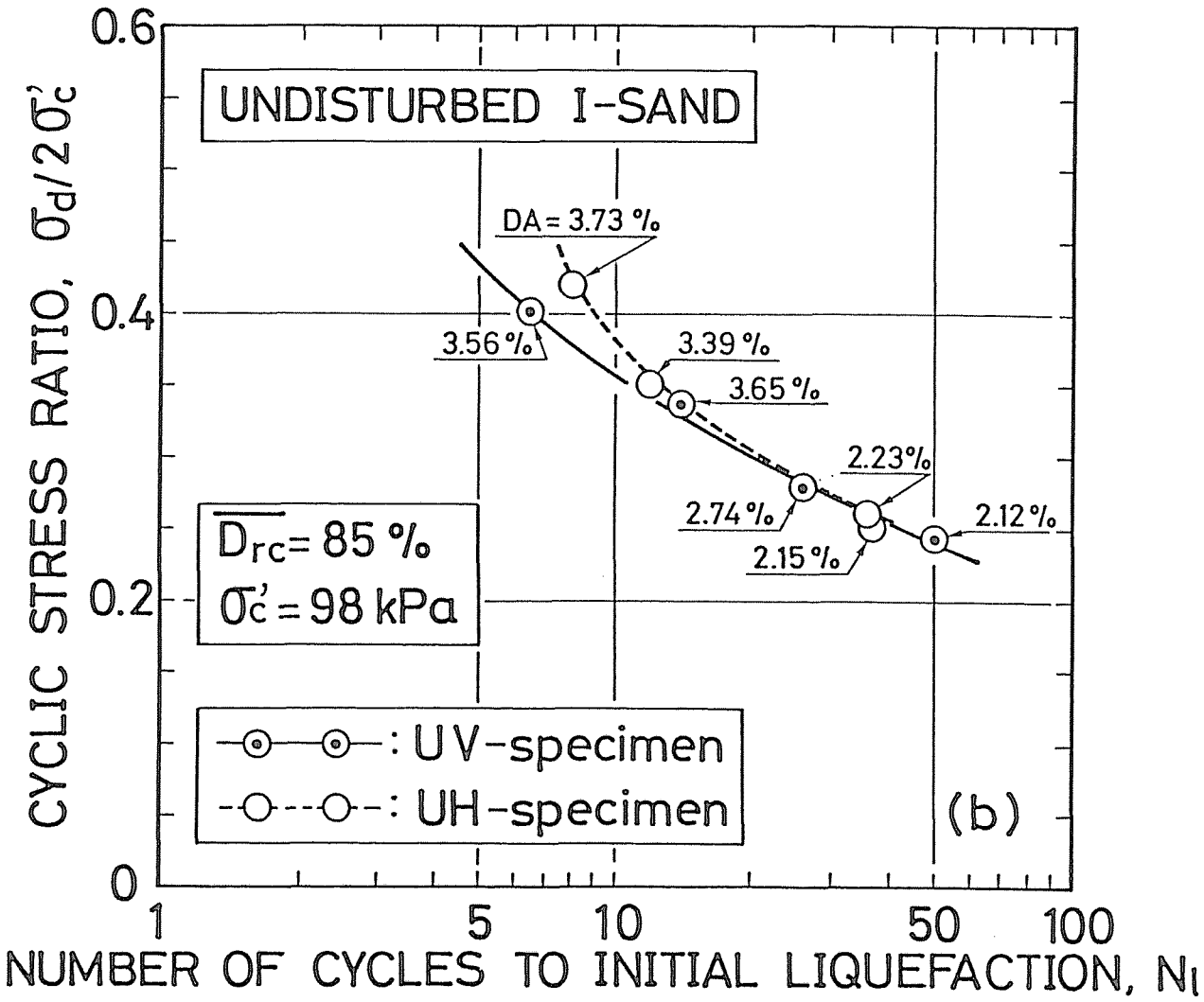

Fig.4-22(b) Comparison of undrained triaxial strength for UV- and UH-specimens of undisturbed I-sand (Cyclic stress ratio vs. number of loading cycles to initial liquefaction relationship)

specimens seem produce slightly higher cyclic strength value than UV-specimens as shown in Figs.4-21(b) and 4-22(b).

From these experimental results and the considerations in the preceding paragraphs, it should be said that the cyclic undrained triaxial behavior of the natural deposits depends strongly on their anisotropic fabrics and its features are very similar to those of specimen prepared by the method of pluviation of sand through air such as MSP method.

4.4.4 Comparison of cyclic undrained behaviors between undisturbed and reconstituted specimens

Because it can be apparently confirmed in the preceding section that the changes in the cyclic undrained triaxial behavior of sands sampled from the natural deposits show a similar pattern to those of artificially deposited sand, the adoption of a suitable reconstitution method in a laboratory is expected to enable a reproduction of anisotropic feature of cyclic undrained behavior for the undisturbed sand. In this section, the above possibility is studied by examining the cyclic undrained behaviors of K-sand and I-sand specimens reconstituted by the various methods.

The cyclic stress ratio vs. the number of loading cycles to initial liquefaction relationships for K-sand reconstituted by rodding (R_C) and tapping (R_D) methods are shown comparing with those for undisturbed K-sand in Fig.4-23. The specimens reconstituted by R_A and R_B methods were not adopted for K-sand, because the method of pluviation of sand through air could not produce the uniform K-sand specimen with higher relative density ($\overline{D_{rc}} = 98$ %) as explained in the preceding chapter. As can be seen in Fig.4-23, the cyclic undrained triaxial strengths of reconstituted K-sand are overall lower than those of undisturbed K-sand. Although the cyclic undrained triaxial strength value of R_C-specimen is relatively approximate to that

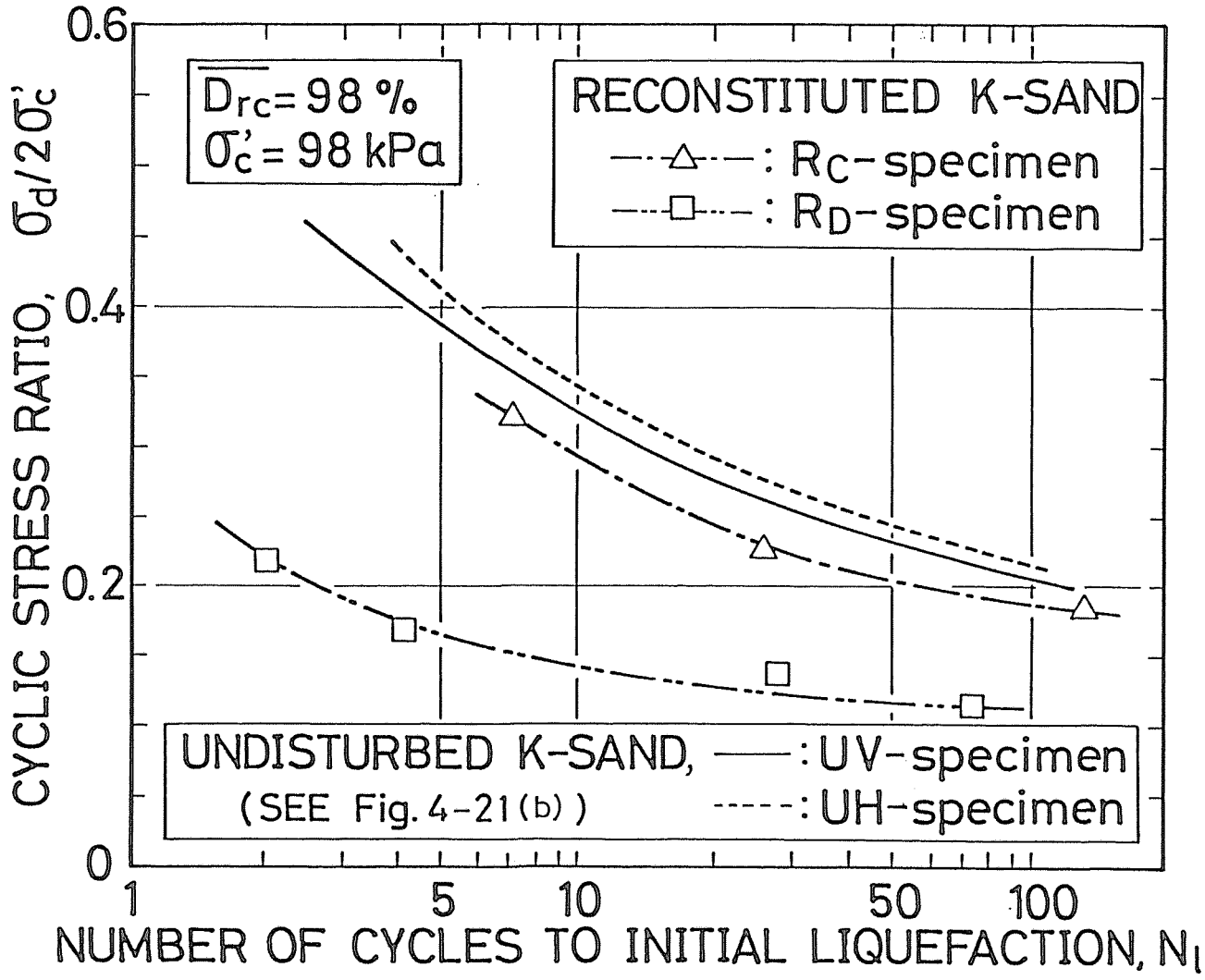

Fig.4-23 Comparison of cyclic stress ratio vs. number of loading cycles to initial liquefaction relationships for reconstituted and undisturbed specimens of K-sand

of undisturbed K-sand, we should not discuss the adequacy of R_C method disregarding the fact that the time history patterns of R_C-specimens whose typical drawings are given in Figs.4-24 (a) and (b) differ remarkably from those of undisturbed sands. These results seem indicate that R_C and R_D methods cannot produce K-sand specimen with the anisotropic fabric which may induce the anisotropic cyclic behavior such as observed in Figs.4-19 and 4-21.

Shown in Fig.4-25 are the cyclic stress ratio vs. the number of loading cycles to initial liquefaction relationships for I-sand reconstituted by R_A, R_B and R_C methods, comparing with those for undisturbed I-sand. As described in the preceding paragraphs, the method of pluviation of sand through air such as R_A and R_B methods can be easily applied to I-sand. It is worthy of note that the cyclic undrained triaxial strength values of R_BV- and R_BH-specimens are almost the same as those of UV- and UH-specimens, respectively.

In order to examine in detail the deformation performances during cyclic undrained loading of I-sand specimens reconstituted by R_B method, their time histories of cyclic axial stress, pore water pressure, axial strain, undrained effective stress path and stress-strain relationship are shown in Figs. 4-26 and 4-27. It can be seen that R_BV-specimen is by far more deformable in the extensional side and the deformation of R_BH-specimen is more predominant in the compressional side.

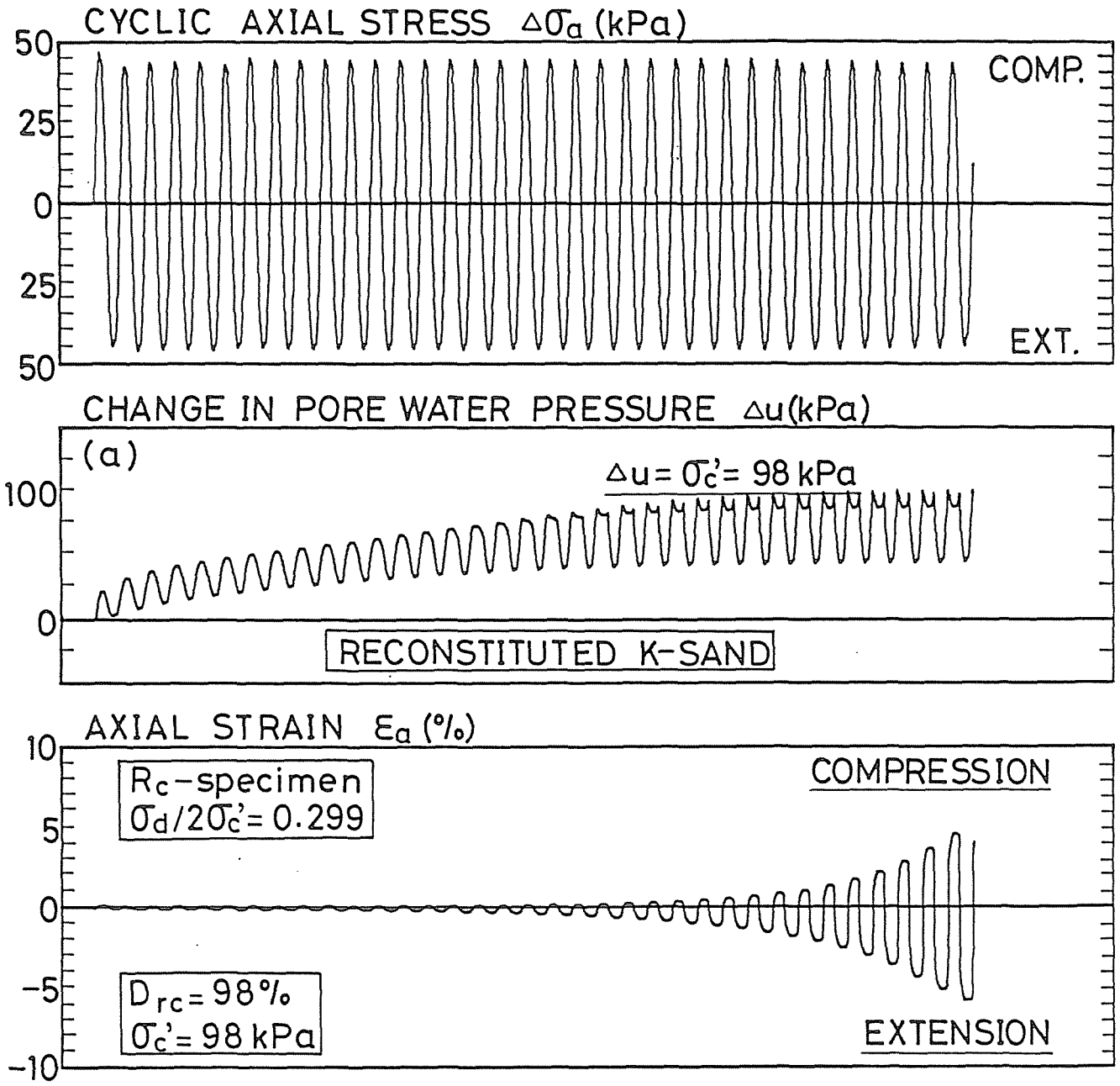

Fig.4-24(a) Time histories of cyclic axial stress, pore water pressure and axial strain for K-sand specimen reconstituted by R_C method (rodding method)

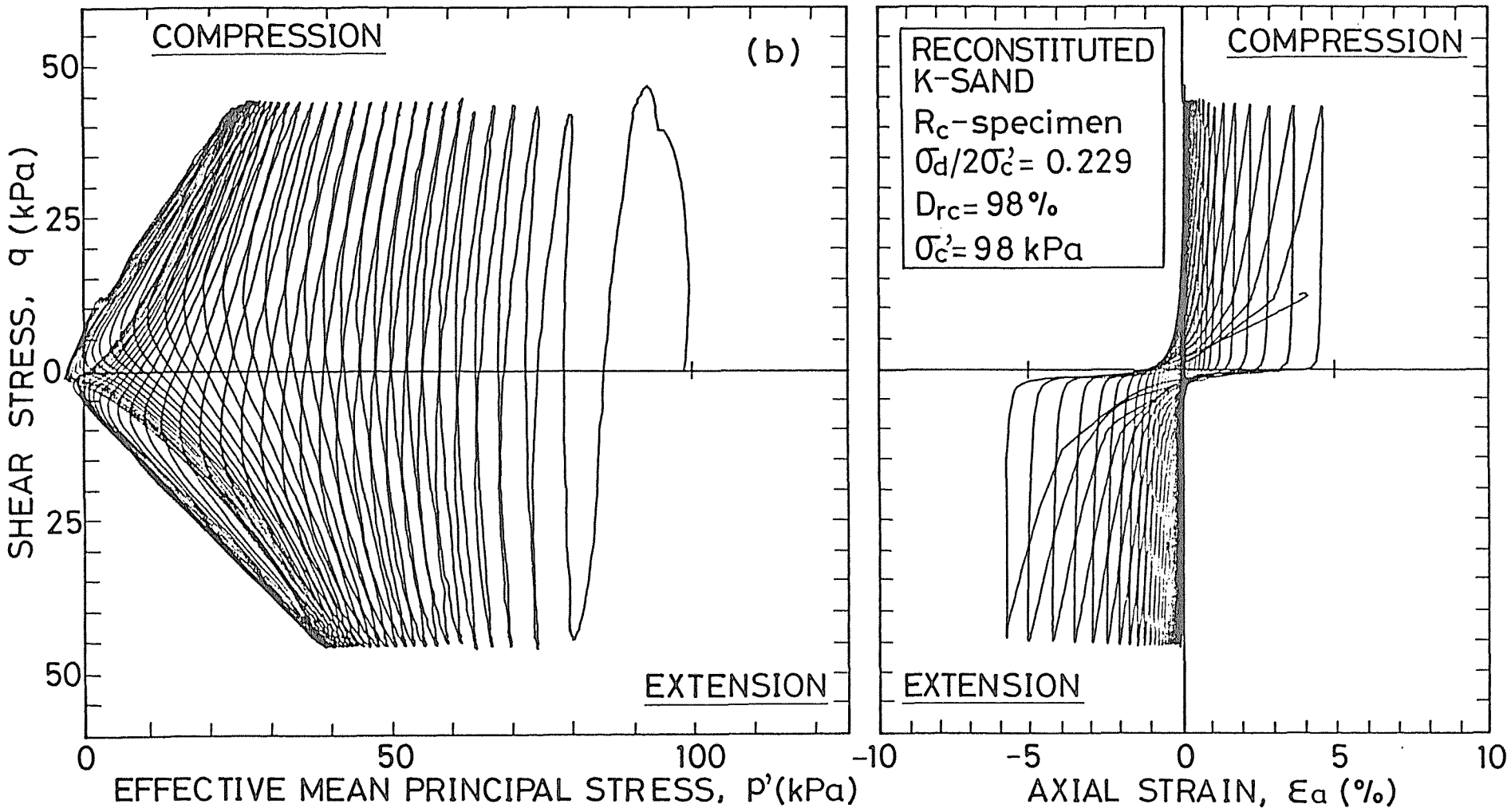

Fig.4-24(b) Time histories of undrained effective stress path and stress-strain relationship for K-sand specimen reconstituted by R_C method (rodding method)

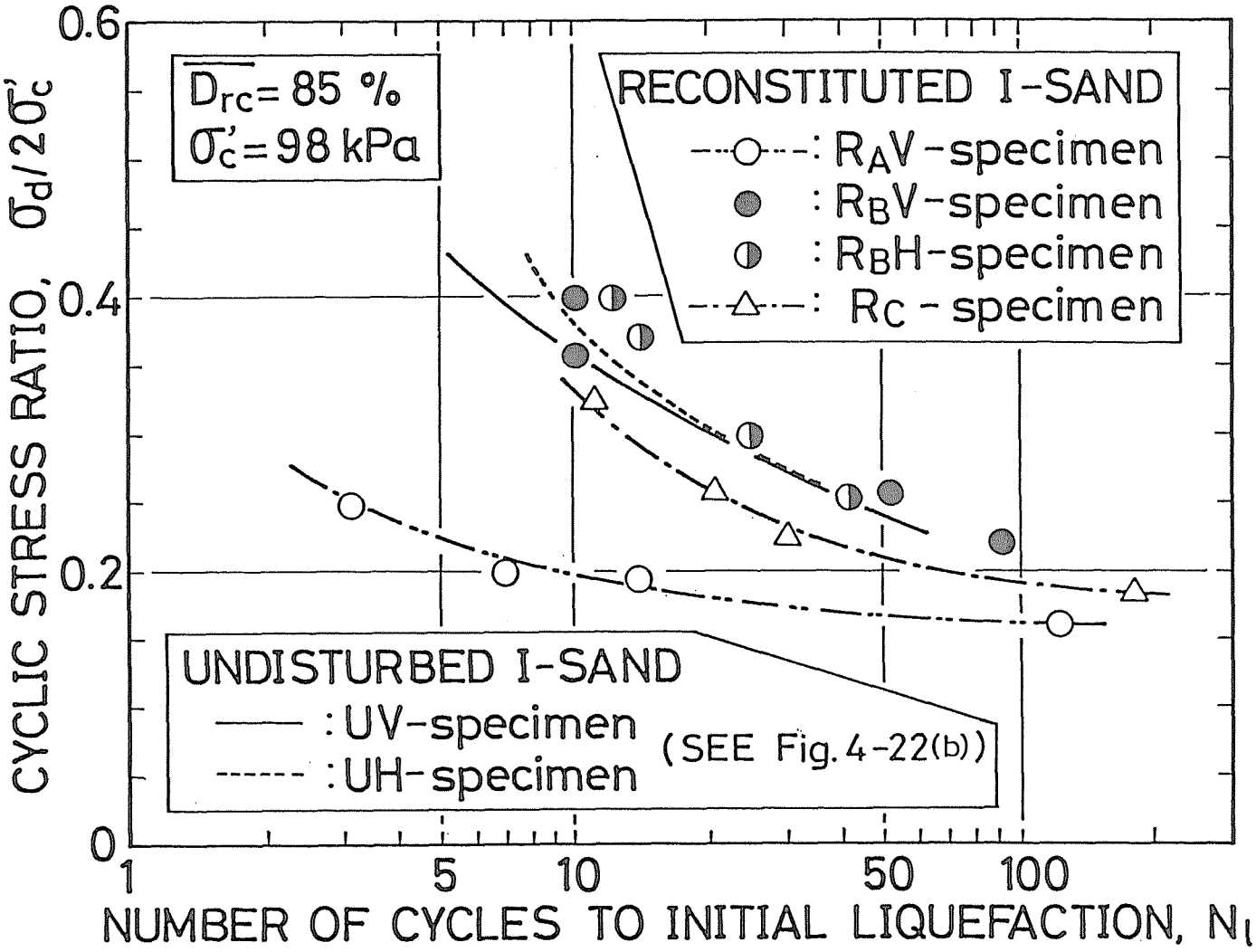

Fig.4-25 Comparison of cyclic stress ratio vs. number of loading cycles to initial liquefaction relationships for reconstituted and undisturbed specimens of I-sand

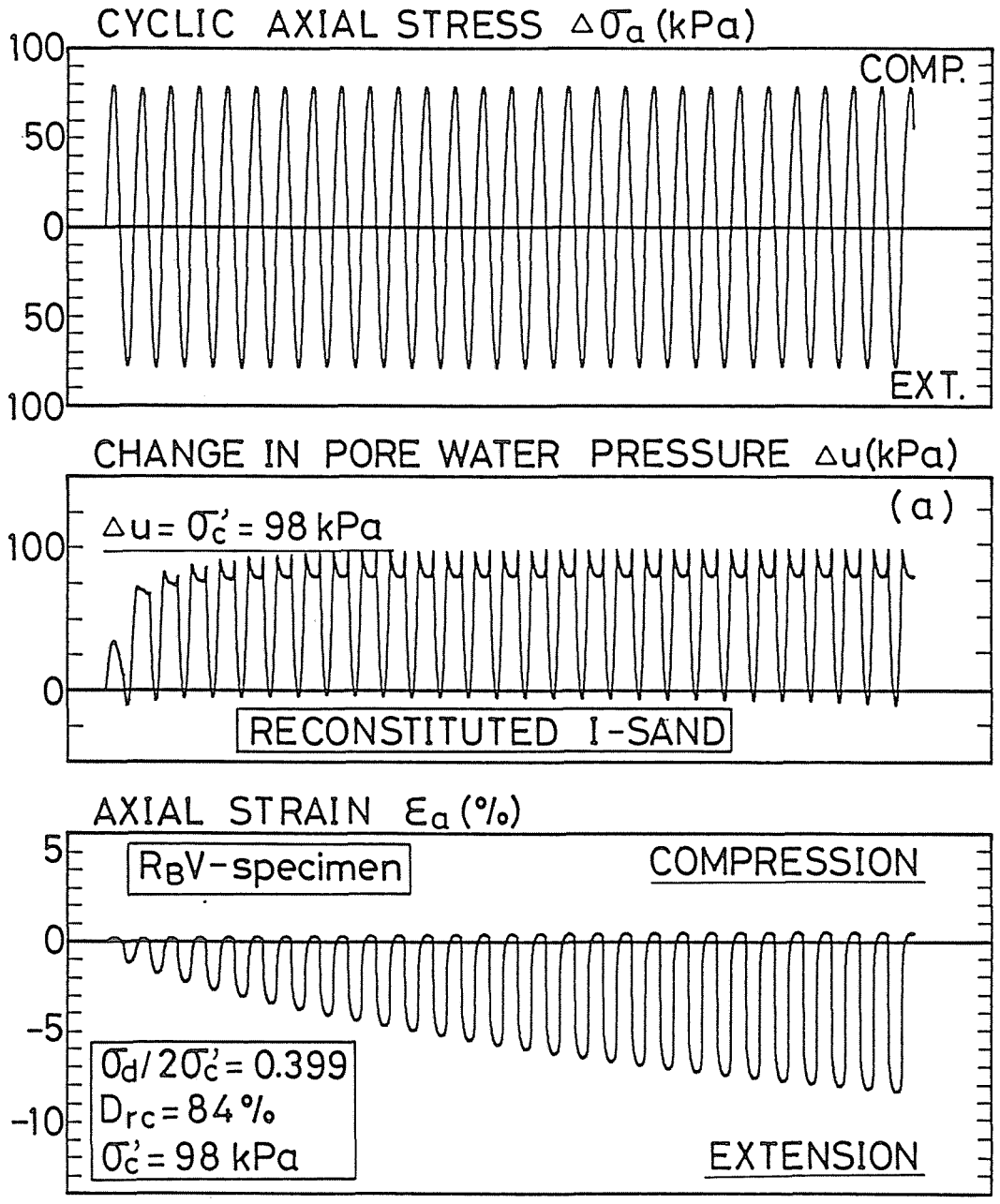

Fig.4-26(a) Time histories of cyclic axial stress, pore water pressure and axial strain for R_BV-specimen of I-sand reconstituted by R_B method (MSP method)

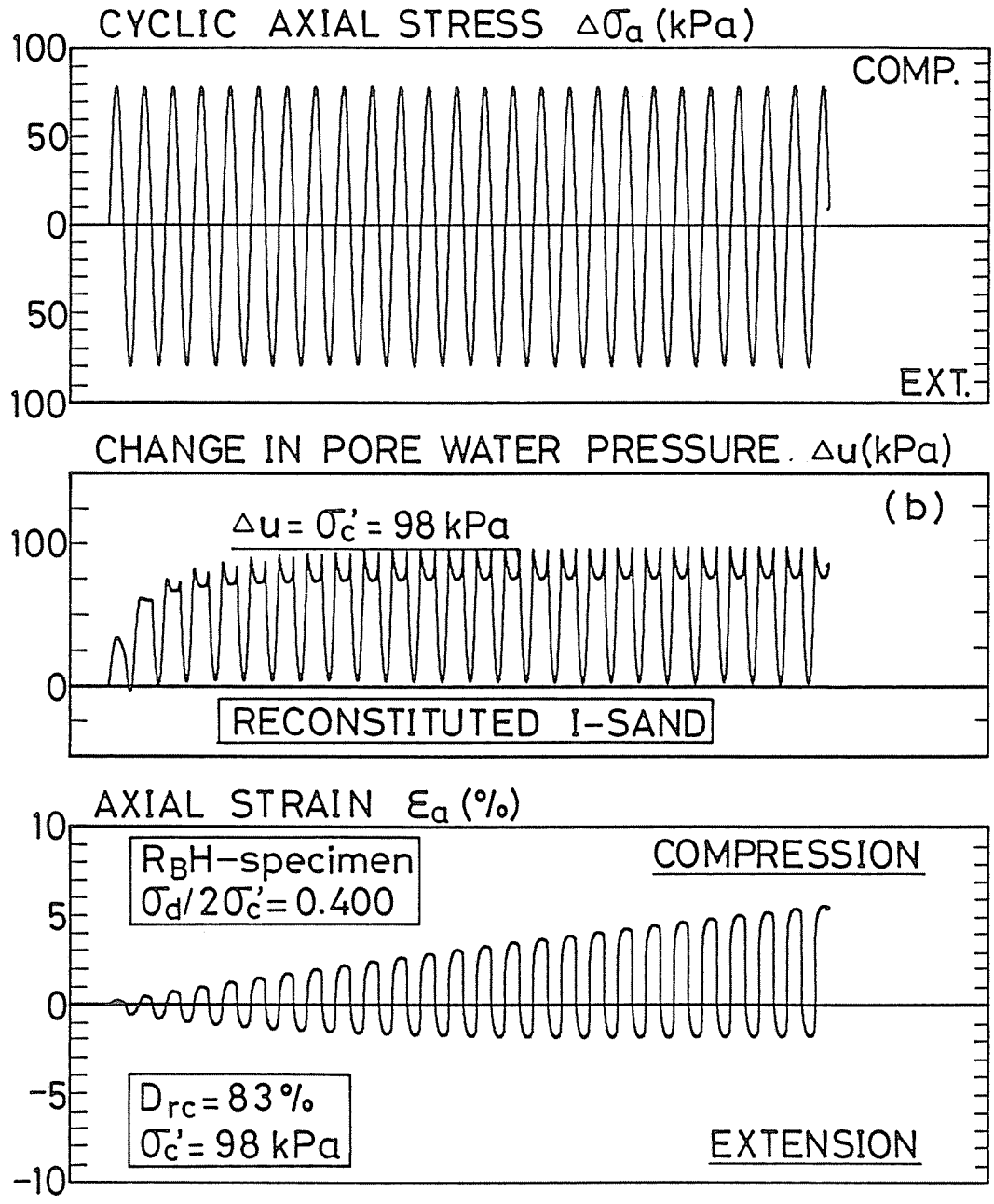

Fig.4-26(b) Time histories of cyclic axial stress, pore water pressure and axial strain for R_BH-specimen of I-sand reconstituted by R_B method (MSP method)

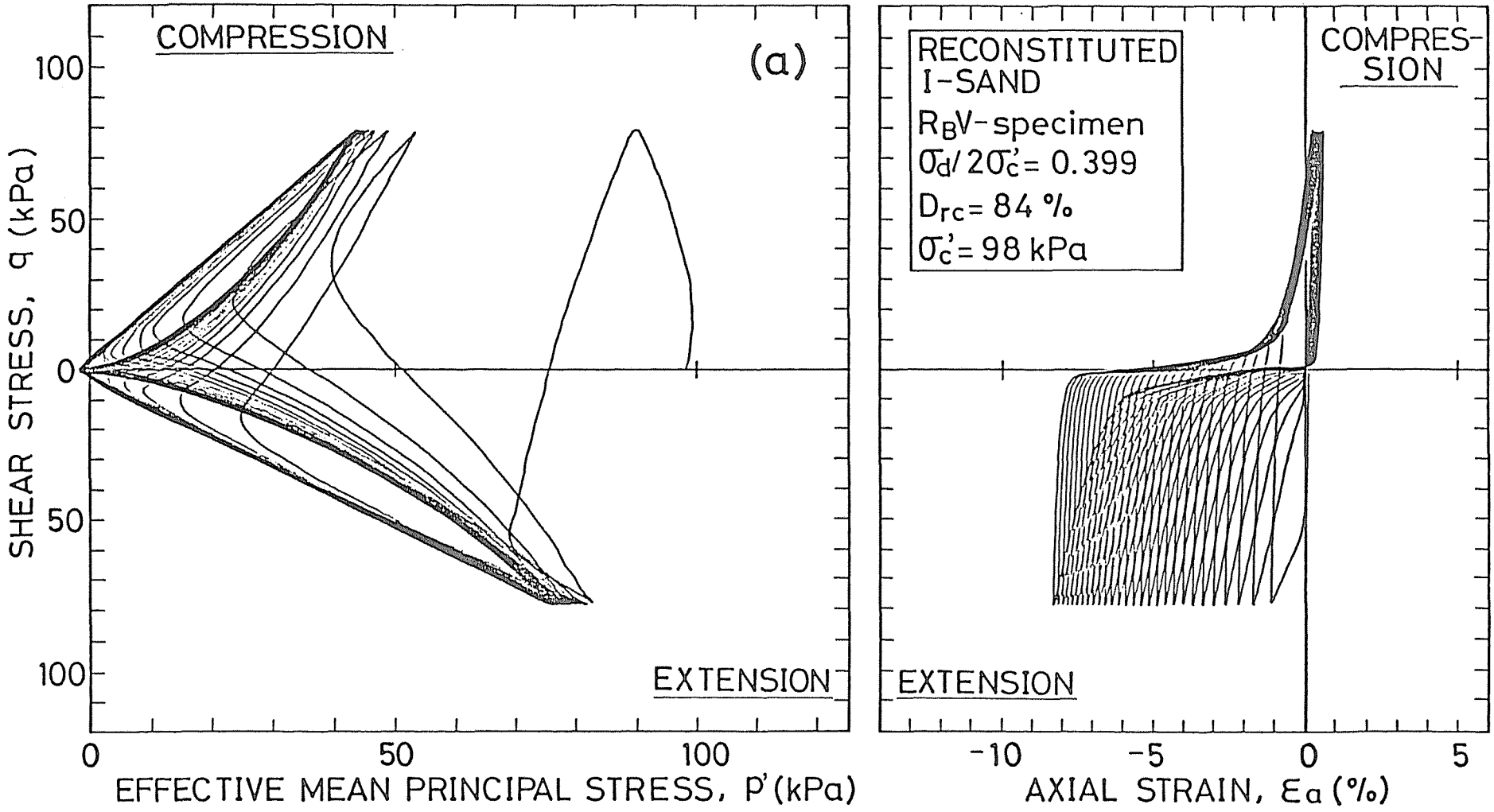

Fig.4-27(a) Time histories of undrained effective stress path and stress-strain relationship for R_BV-specimen of I-sand reconstituted by R_B method(MSP method)

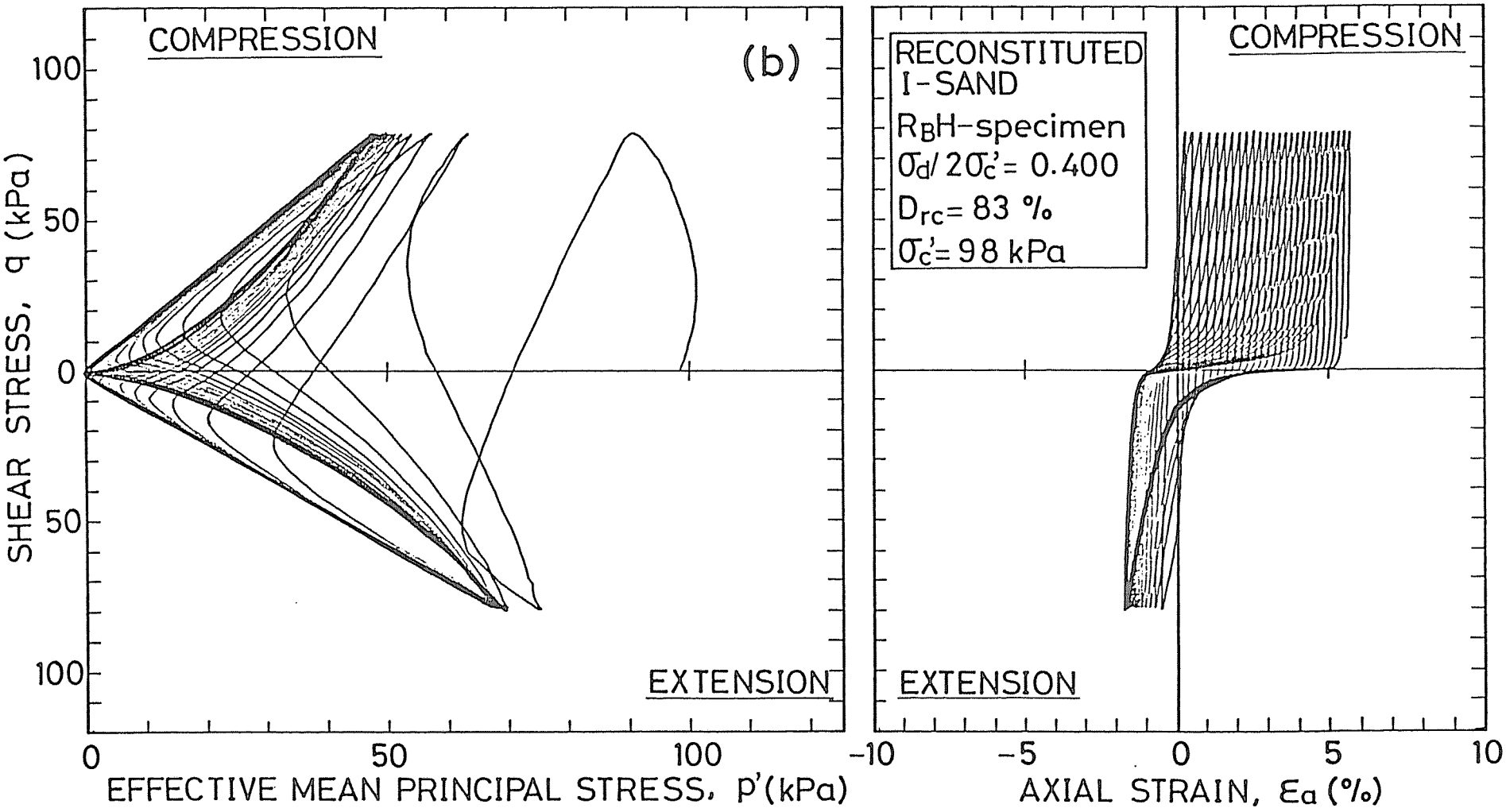

Fig.4-27(b) Time histories of undrained effective stress path and stress-strain relationship for R_BH-specimen of I-sand reconstituted by R_B method (MSP method)

It should be noted that the time history patterns of R_BV- and R_BH-specimens are very similar to those of UV- and UH-specimens, respectively. The cyclic stress ratio vs. the number of loading cycles required to reach 1 %, 2 % and 5 % double amplitude axial strains relationships for R_BV- and R_BH-specimens are shown comparing with those for UV- and UH-specimens in Figs.4-28(a) and (b). It can be also confirmed in Figs.4-28(a) and (b) that the cyclic undrained triaxial strengths of specimens reconstituted by R_B method agree well with ones of undisturbed I-sand specimens.

On the other hand, the cyclic undrained triaxial strength for R_AV-specimen of I-sand is significantly lower than UV-specimen as indicated in Fig.4-25, although the time history pattern for R_AV-specimen, whose typical drawings are given in Figs.4-29(a) and (b), is similar to that for UV-specimen. And also, the deformation performance (Figs.4-30 (a) and (b)) and the cyclic undrained triaxial strength for R_C-specimen are much different from those for undisturbed I-sand specimen, as observed in K-sand.

Taking account of these experimental results of I-sand, it would be expected that a better reproduction of the anisotropic cyclic undrained behavior of undisturbed K-sand specimen is also possible, if the reconstitution method such as pluviation of sand through air method could be applied to K-sand.

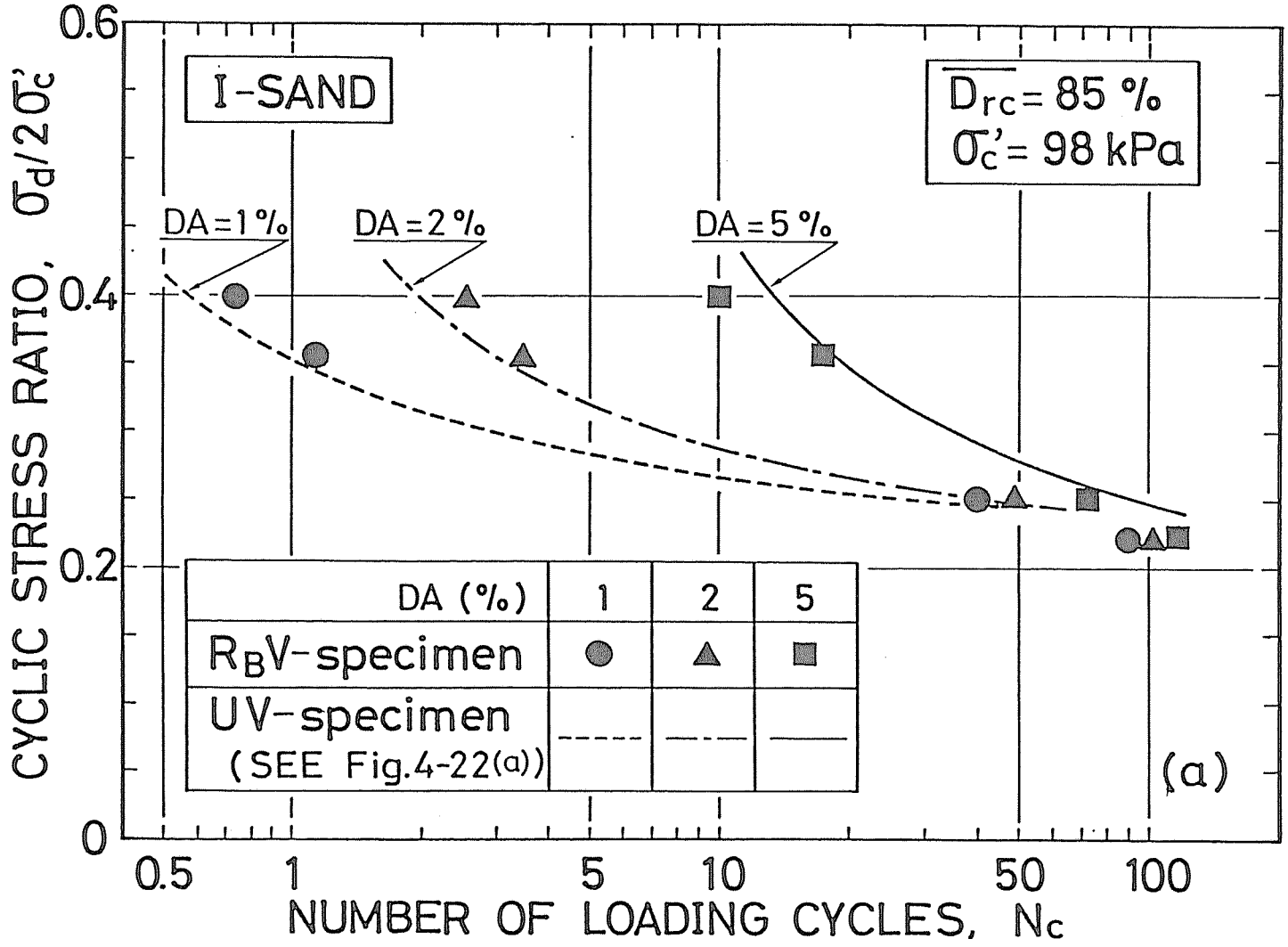

Fig.4-28(a) Comparison of cyclic stress ratio vs. number of loading cycles to 1%, 2% and 5% double amplitude axial strains relationships for reconstituted and undisturbed I-sand specimens between R_BV- and UV-specimens

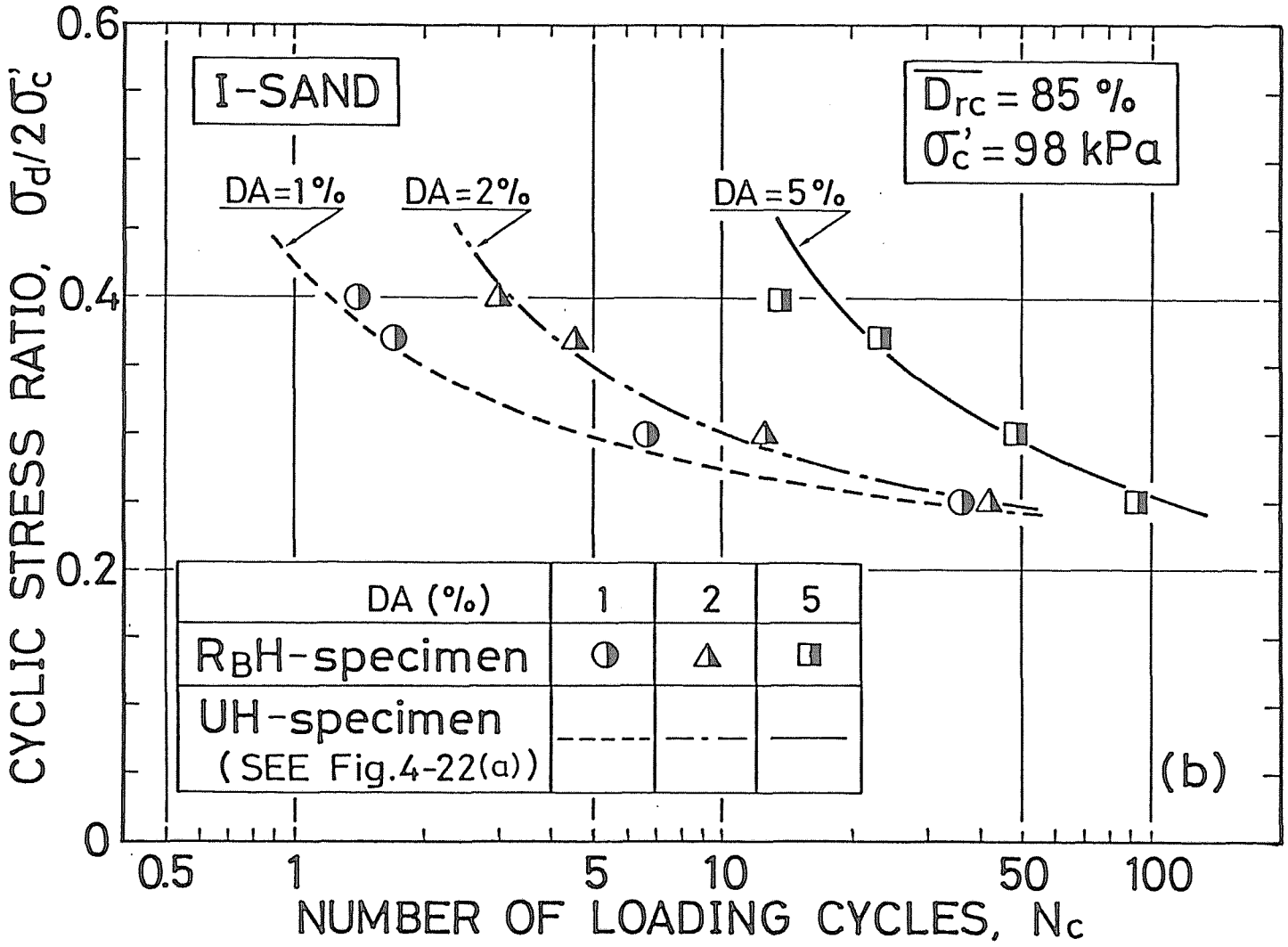

Fig.4-28(b) Comparison of cyclic stress ratio vs. number of loading cycles to 1%, 2% and 5% double amplitude axial strains relationships for reconstituted and undisturbed I-sand specimens between R_BH- and UH-specimens

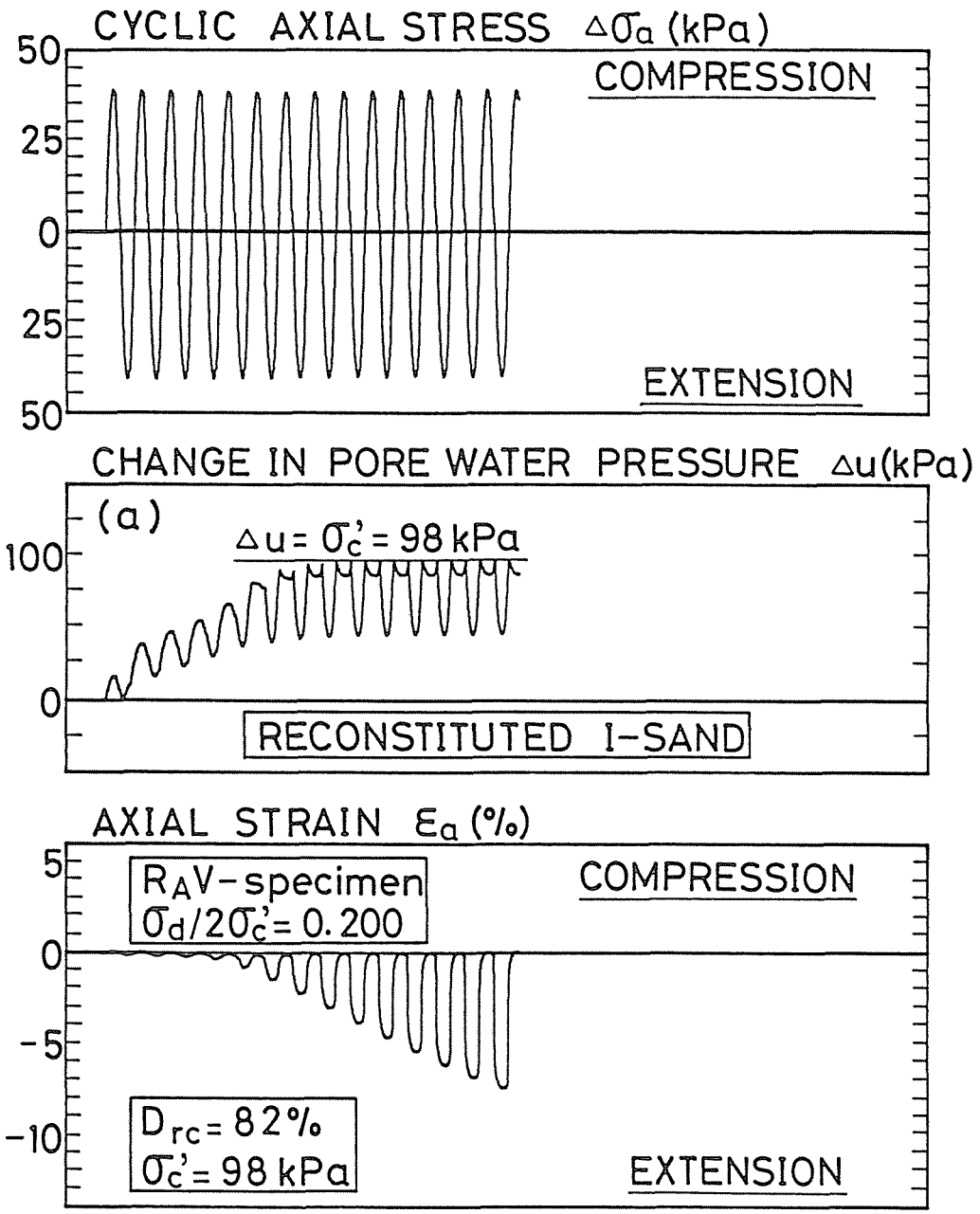

Fig.4-29(a) Time histories of cyclic axial stress, pore water pressure and axial strain for I-sand specimen reconstituted by R_A method (MSP method)

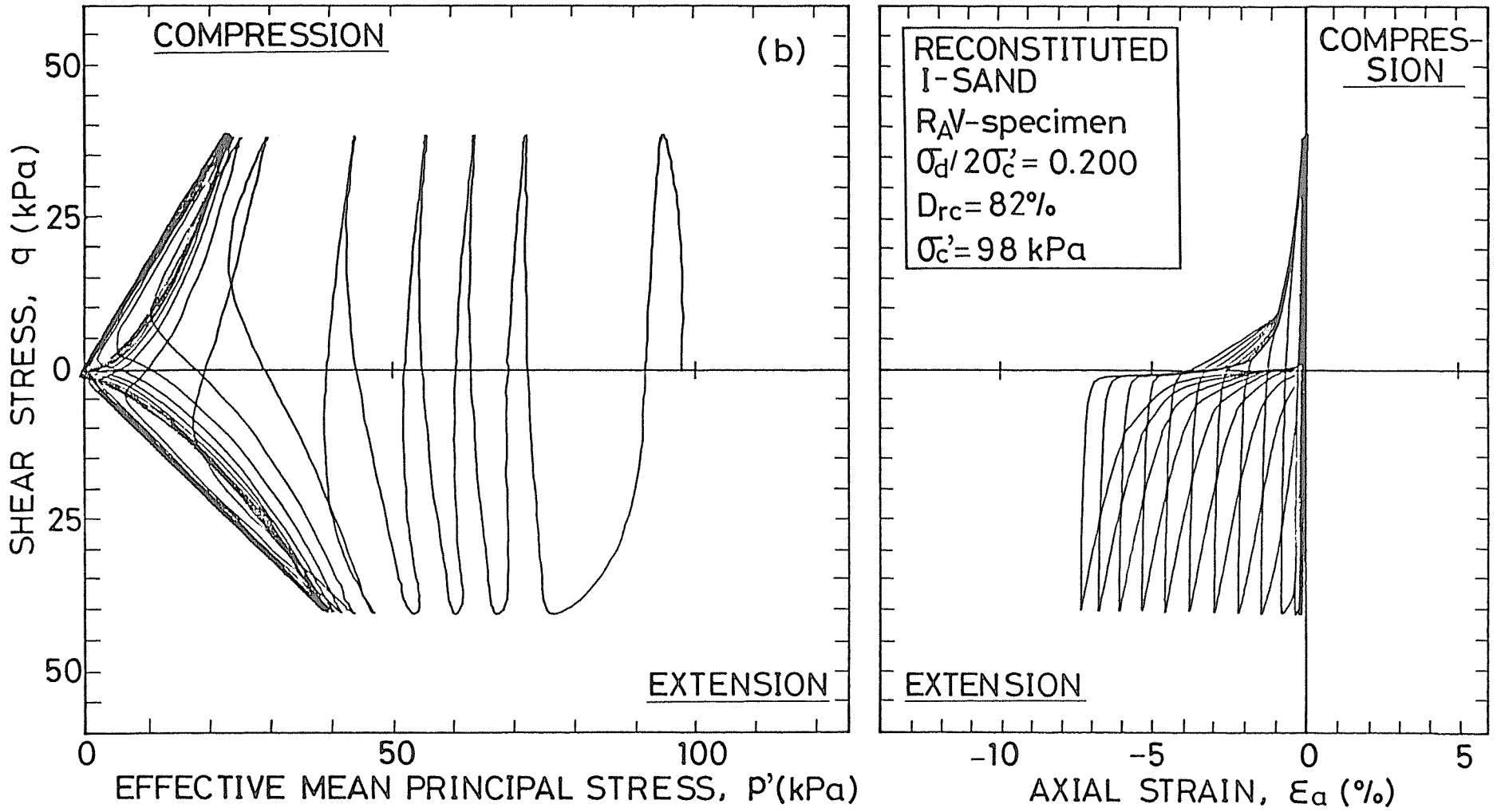

Fig.4-29(b) Time histories of undrained effective stress path and stress-strain relationship for I-sand specimen reconstituted by R_A method (MSP method)

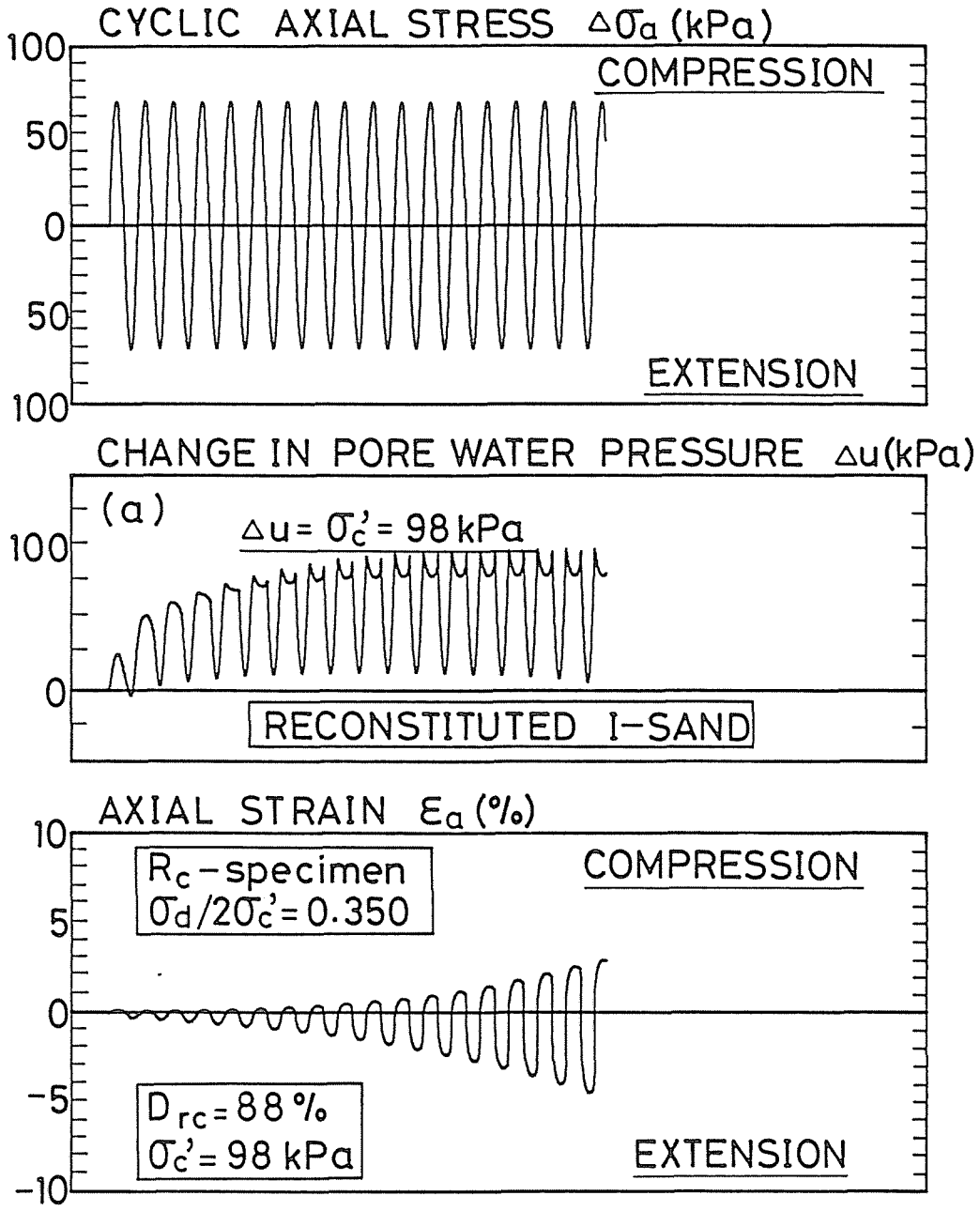

Fig.4-30(a) Time histories of cyclic axial stress, pore water pressure and axial strain for I-sand specimen reconstituted by R_C method (rodding method)

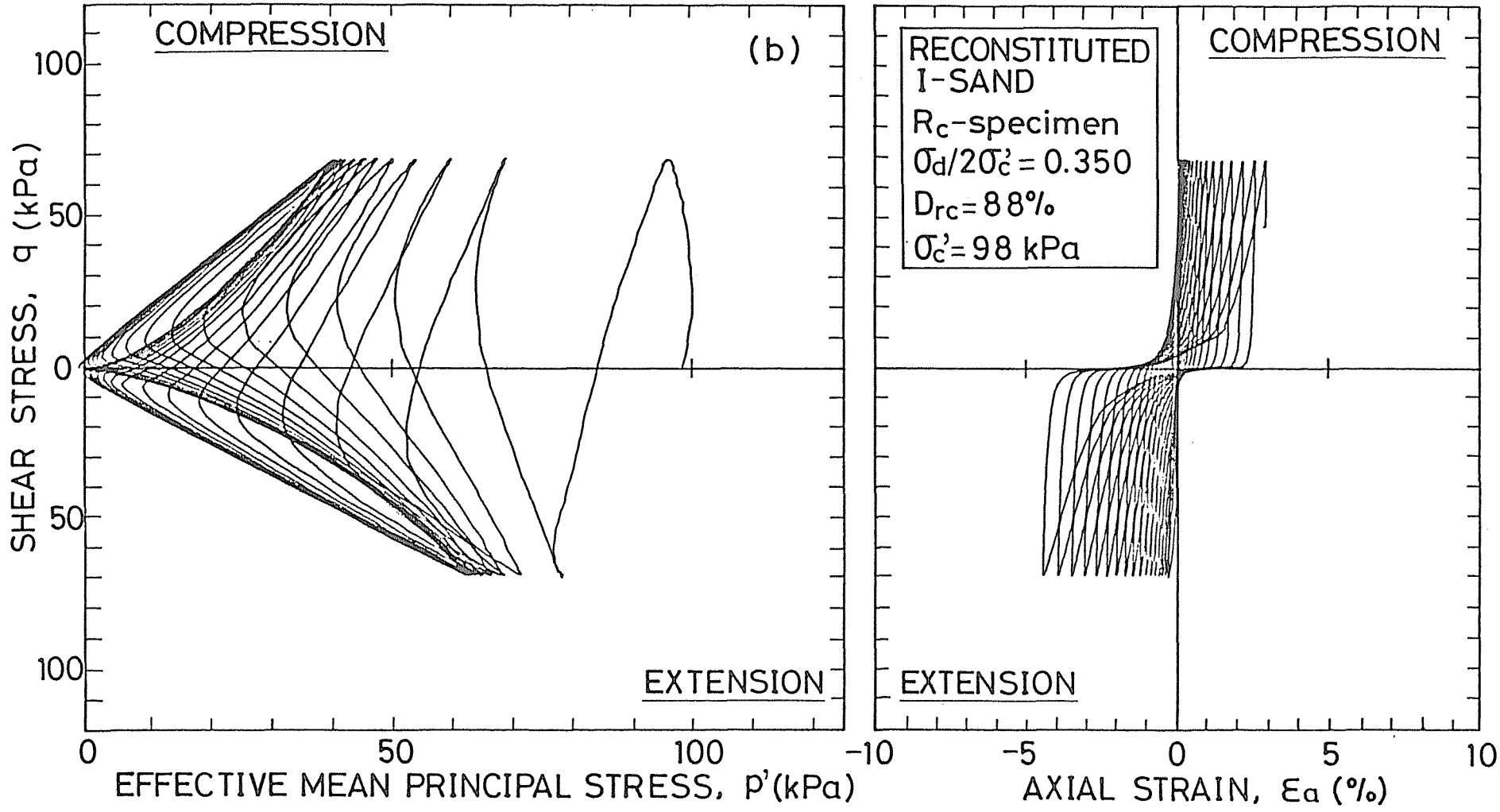

Fig.4-30(b) Time histories of undrained effective stress path and stress-strain relationship for I-sand specimen reconstituted by R_C method (rodding method)

4.4.5 Freeze-thaw sequence effects

Because the fabric characteristics of R_AV-specimen are almost the same as those of R_BV-specimen as described in the preceding paragraph, it may be considered that the remarkable difference in the cyclic undrained triaxial strength of R_AV- and R_BV-specimens of I-sand is mainly due to the effects of the freeze-thaw sequence. The results of cyclic undrained tests performed to examine the possible effects of the freeze-thaw sequence on the cyclic undrained triaxial strength of T-sand are shown in Figs.4-31(a) and (b). As observed in reconstituted I-sand, it can be also confirmed for T-sand that there exists a significant increase in the cyclic undrained triaxial strength due to the effect of the freeze-thaw sequence.

It should be remembered that the effects of the freeze-thaw sequence on the static deformation-strength characteristics of specimens with the preferred orientations of the sand particles in their vertical section appeared in such a way to restrain the trend of negative dilatancy (volume contraction) during shear under the triaxial extension stress condition. Such effects of the freeze-thaw sequence mean that if the sand specimen frozen previously is sheared under the undrained triaxial extension condition, the development of positive pore water pressure is restrained. From these

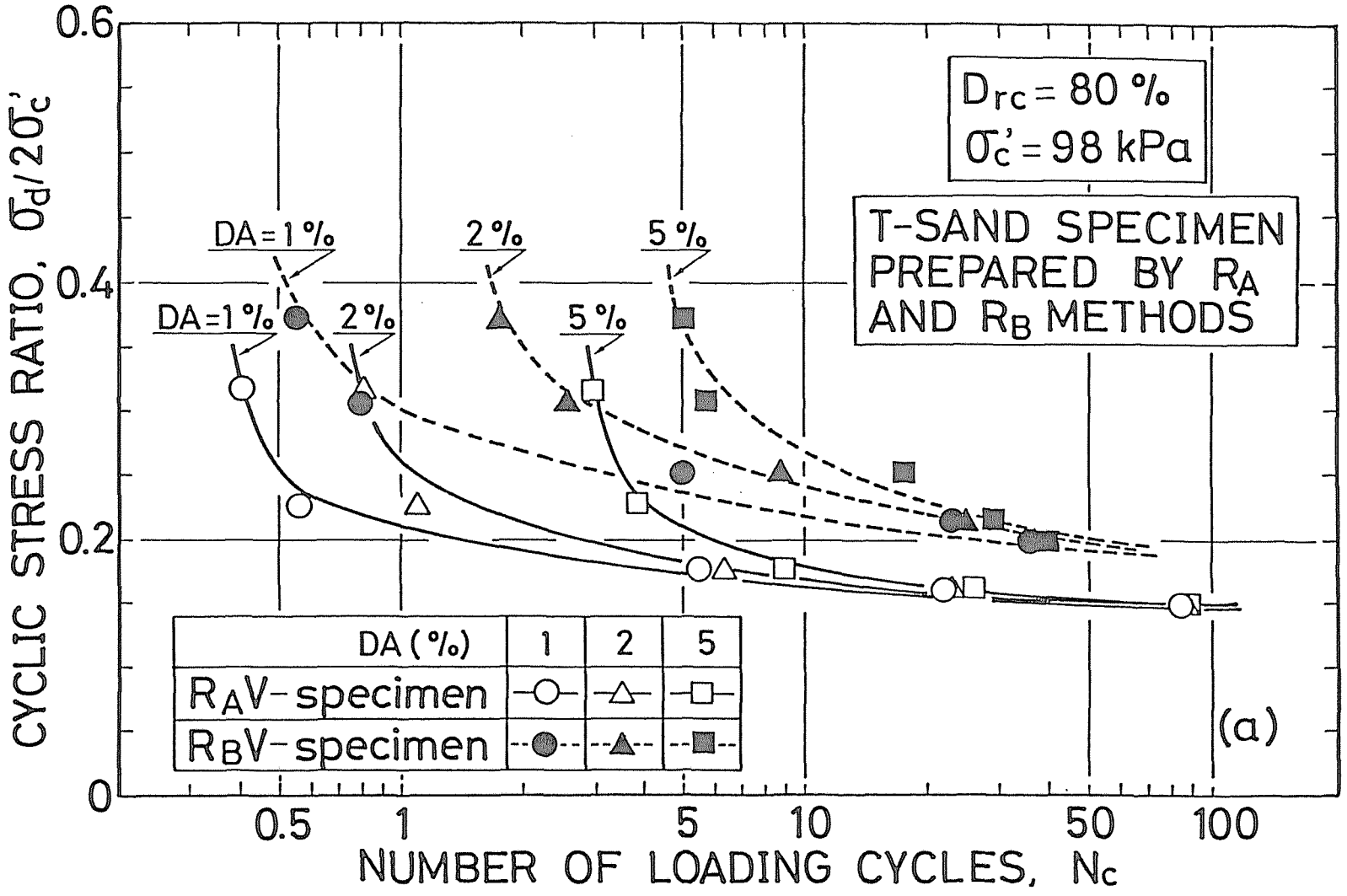

Fig.4-31(a) Effect of freeze-thaw sequence during sample preparation on cyclic undrained triaxial strength for T-sand (Cyclic stress ratio vs. number of loading cycles to 1%, 2% and 5% double amplitude axial strains relationship)

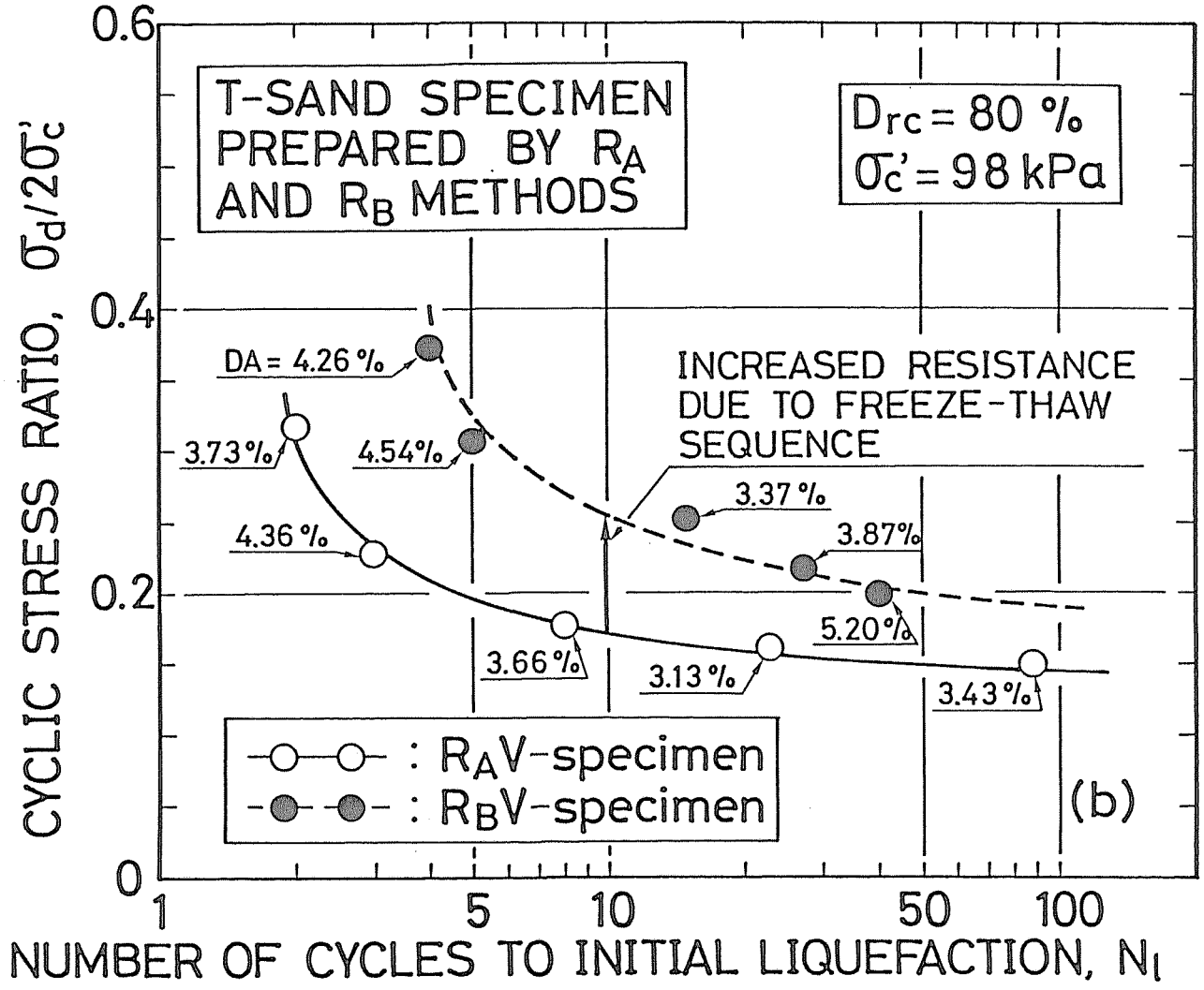

Fig.4-31(b) Effect of freeze-thaw sequence during sample preparation on cyclic undrained triaxial strength for T-sand (Cyclic stress ratio vs. number of loading cycles to initial liquefaction relationship)

experimental results and the facts that the cyclic undrained behavior of sand is intimately related to the static dilatancy characteristics, it is considered that the increase in the cyclic undrained triaxial strength due to the effect of the freeze-thaw sequence could be explained qualitatively by estimating the effects of the freeze-thaw sequence on the static dilatancy characteristics of sand.

It can be noted that the effects of the freeze-thaw sequence mentioned above are similar to those of overconsolidation on the cyclic undrained strength of sand which have shown by Ishihara and Takatsu (1979) and other researchers. Therefore, it may be expected that some change in the microfabrics of sand is induced by pseudo-overconsolidation effects due to the freeze-thaw sequence. The experimental results of the reconstituted sands described above indicate that the cyclic undrained triaxial strength of undisturbed sands obtained in the present study may not represent the perfectly true one of the natural sand deposits. However, whether or not this interpretation is true or whether another one is required cannot be known until further research is done.

In any case, this study clarified that the natural sands which could be hopefully sampled to a certain degree by block sampling method by freezing possessed the strong anisotropy in the mechanical properties due to their fabric anisotropy, and that a better reproduction of the anisotropic

static and cyclic deformation-strength characteristics of the natural sand was possible by adopting in the laboratory a sample preparation method (R_B method) which might simulate the in-situ block sampling procedure.

CHAPTER 5 THREE-DIMENSIONAL STRESS-STRAIN RELATIONSHIP FOR SAND WITH ANISOTROPIC FABRIC

5.1 Introduction

Recent geotechnical problems in practice such as bearing capacity and liquefaction analysis of sandy grounds have required a complete knowledge of the prefailure stress-strain-dilatancy characteristics of sand. In order to estimate the in-situ behavior of sands from laboratory test results, it is essential to test them under exactly the same conditions as exist in-situ. At the same time, it should be noted that natural cohesionless soils possess the anisotropic mechanical properties which may be attributed to the fabric characteristics formed by the parallel alignments of particles induced during depositing process as demonstrated previously.
A noteworthy fact presented in this investigation has been that deformability of sand specimen is lower in the direction of sand deposition (the in-situ vertical direction) than in the direction perpendicular to it (the in-situ horizontal direction) and thus deformation behavior of sand varies with the direction even for the same combination of principal stresses.

Although a theoretical investigation of a means to sys-

tematize such complicated phenomena of sands is important, these anisotropic deformation characteristics cannot be modeled by any existing theories (e.g., Lade and Duncan, 1975; Nishi and Esashi, 1978) which assumed the sand specimen to be isotropic in its mechanical properties.

Presented herein are a new three-dimensional mechanical model for anisotropic sands derived with the help of the concept of non-associated flow rule on the elasto-plasticity and the verification with respect to the measured data of two true triaxial tests which were performed by Yamada and Ishihara (1979) and the present author.

5.2 True Triaxial Test Apparatus and Material

Examination of some basic postulations for the elasto-plasticity and the verification of the derived general stress-strain relationship are based on the data of the true triaxial tests which were carried out by Yamada and Ishihara (1979) and the present author.

In the test program of Yamada and Ishihara (1979), Fuji river sand which is referred in this paper to as " F-sand " was utilized. It consists of subrounded to subangular particles in the size range of 0.074 ^{mm} to 2.0 ^{mm}. The cubical triaxial shear test apparatus used by Yamada and Ishihara (1979) is shown in Fig.5-1. The apparatus is capable of applying three principal stresses σ_x, σ_y, σ_z independently to specimens of $100 \times 100 \times 100$ ^{mm} in size. The cubical triaxial cell was formed by assembling six wall units face to face around the spacing frame. Each unit was equipped with a pressure chamber comprising a flexible rubber on the front surface and a rigid brass lid on the back. Pressurized water controlled by an air regulator was supplied to the pressure chambers to transfer loads to the specimen. Each principal strain was measured by monitoring the amount of water flowing into or out of the pressure chamber by means of a volume change gauge. When saturated specimen was tested under drained condition, the volume change could also be measured by monitoring the

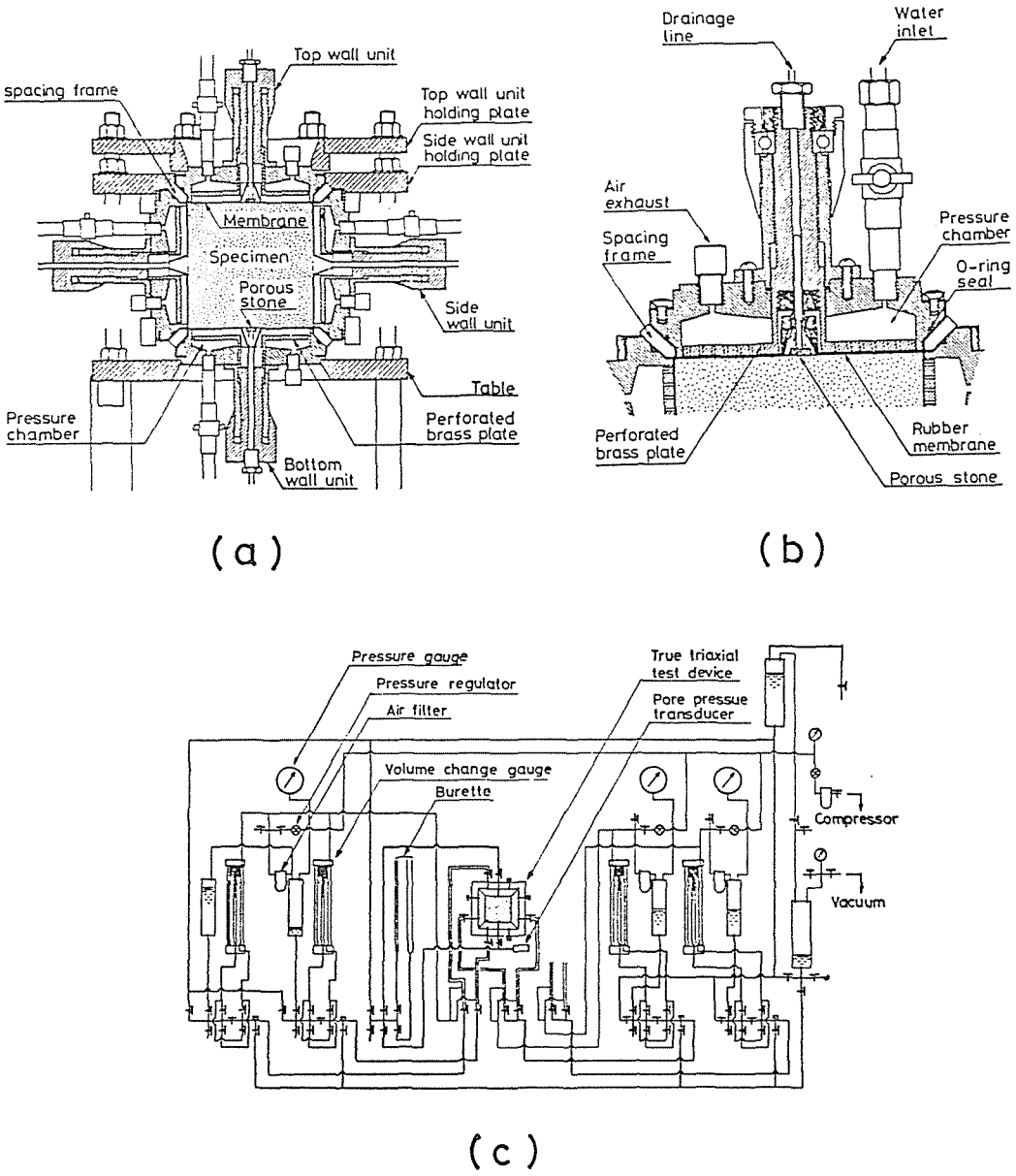

Fig.5-1 True triaxial test apparatus employed by Yamada and Ishihara (1979); (a) cross section of the true triaxial test device, (b) details of cross section of the wall unit, (c) air-water system for applying and measuring stresses

amount of water flowing into or out of the specimen. In the case of the undrained test, pore water pressure was measured with the use of an electric pressure transducer installed in the drainage line.

In their true triaxial test on F-sand with relative density after consolidation D_{rc} of around 34 %, all of the specimens were formed by pouring the saturated sand in a funnel-shaped reservoir into the cubical chamber filled with de-aired water. It could be considered that this sample preparation method is relatively similar to tapping (R_D) method described previously. F-sand specimens were consolidated to an effective mean principal stress p_c of 98 kPa and were then subjected to some shear stresses under the condition of $p = p_c = \text{const.}$

In the true triaxial test by the present author, the true triaxial apparatus which was explained in CHAPTER 3 was utilized, and T-sand was used. As described previously, three principal stresses σ_x, σ_y, σ_z could be applied independently through hydraulic pressure (cell pressure), rubber pressure bag and rigid platen, respectively. T-sand specimen with D_{rc} of 53 % in this study were prepared by MSP (R_A) method which enables to simulate the feature of the fabric anisotropy in the natural sand deposits as demonstrated in CHAPTER 3. All of T-sand specimens were consolidated to p_c of 196 kPa. Shear condition of T-sand is the same as that of F-sand.

To avoid the effect of variation of initial specimen density from the desired one, the variations in D_{rc} of T-sand specimens were limited to the extent within ± 2 %.

The differences in both true triaxial tests and in the physical properties of both sands used are summarized in Table 5-1. In both tests, there are considerable differences with respect to physical properties of sands, relative density, consolidation pressure, sample preparation method and loading system. Though the variations of deformation behaviors due to these differences can be observed in both tests, it will be clear in the later part of this chapter that both sand specimens produce the anisotropic mechanical properties which are attributed to the fabric characteristics formed during sample preparation.

Table 5-1 Summary of true triaxial test conditions, sample preparation methods and physical properties of sands used by Yamada and Ishihara (1979) and the present author

True triaxial tests	Specimen dimensions (mm)	Loading systems	Sand used	Sample preparation method	p_c (kPa)	D_r (%)	G_s	e_{max} / e_{min}	D_{50} (mm) / U_c
Yamada and Ishihara (1979)	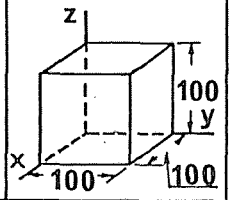	x, y, z: pressure bag	Fuji river sand (F-sand)	pluviation and tapping under water	98	34	2.73	1.03 / 0.48	0.40 / 2.14
Present author	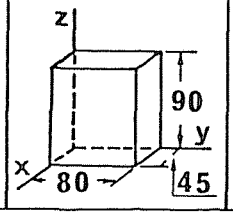	x: hydraulic pressure y: pressure bag z: rigid platen	Toyoura sand (T-sand)	MSP (R_A)	196	53	2.65	0.992 / 0.625	0.21 / 1.36

5.3 Representation of Stress and Strain Parameters and Test Scheme

According to observations of the fabric characteristics of sand specimens, the method of pluviation of sand through air such as MSP method seems to produce the sand specimen with the fabric characterized by the orthotropic property that the apparent long axis of the sand particles has strongly preferred orientations in the vertical section, but almost completely random orientations in the horizontal section. Consequently, we can consider the vertical axis to be axis of symmetry for the orthotropic sand specimens. It is convenient for the explanation of these orthotropic sand specimens that the directions of stress and strain are indicated relative to the principal axes of the sand specimen. For this purpose, a Cartesian coordinate system in which the z-axis is chosen to coincide with the bedding direction of the specimen is employed as shown in Fig.5-2(a). Principal stresses and principal strains are labeled according to the directions in this coordinate system.

The three-dimensional stress point P (σ_x, σ_y, σ_z) shown in Figs.5-2(b) and (c) would be expressed by the normal and shear stresses on the octahedral stress plane, where shear stress q and normal stress p are defined as follows:

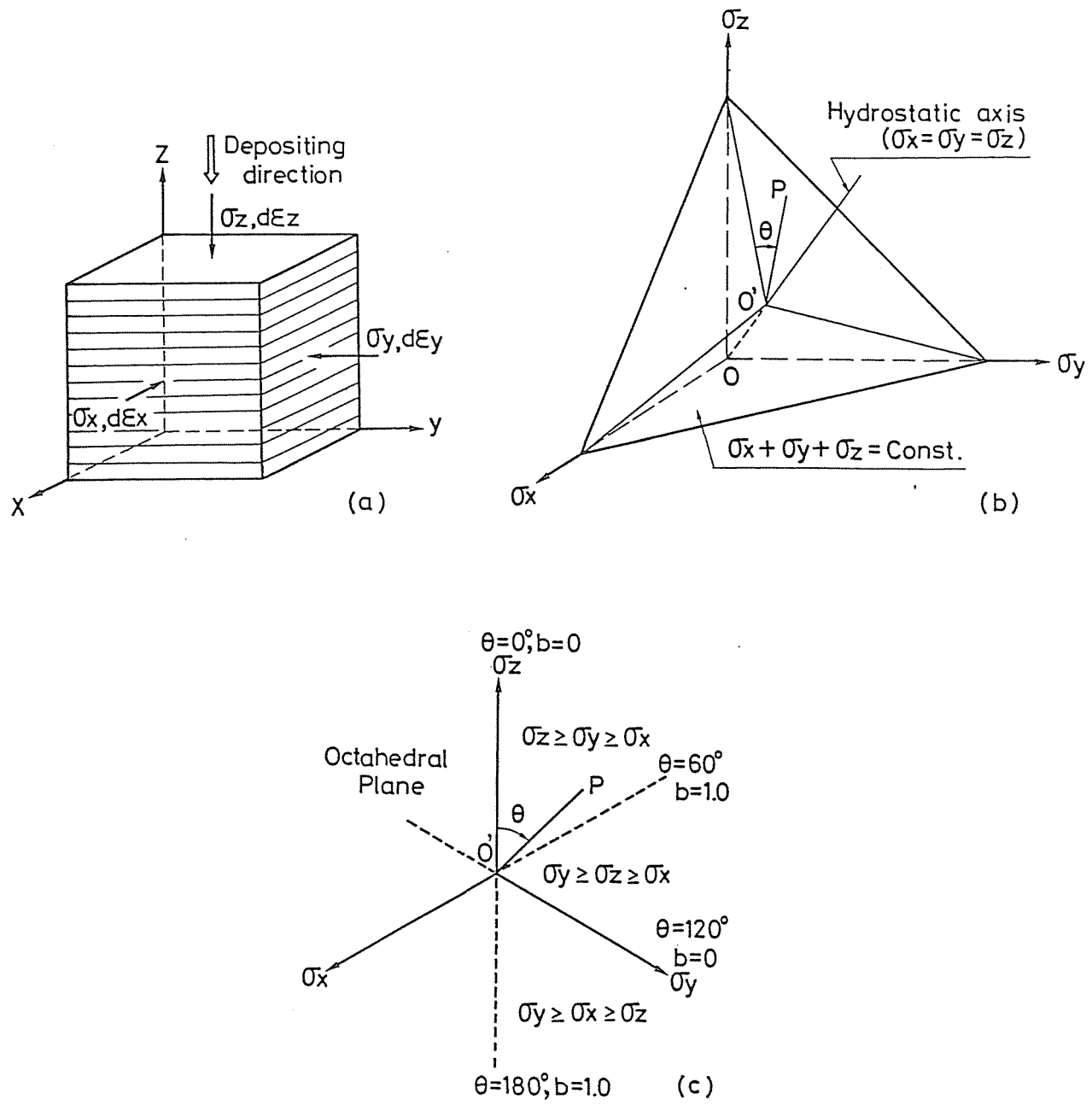

Fig.5-2 Representation of sand specimen and stress conditions; (a) orientation of orthotropic specimen relative to Cartesian coordinate system and definition of principal stress and strain increment, (b) octahedral stress system in principal stress space, (c) definition of parameter θ and stress paths employed in this study

$$p = \frac{1}{3}(\sigma_x + \sigma_y + \sigma_z) \qquad (5\text{-}1)$$

$$q = \frac{1}{\sqrt{2}}\{(\sigma_x - \sigma_y)^2 + (\sigma_y - \sigma_z)^2 + (\sigma_z - \sigma_x)^2\}^{\frac{1}{2}} \qquad (5\text{-}2)$$

These stresses imply the effective stress, since the tests are carried out under the drained condition. In the previous chapters, however, the effective stresses were designated with a prime on the respective notations.

The increments in volumetric and shear strains are also defined in conformity with the aforementioned stress parameters as follows:

$$d\varepsilon_v = d\varepsilon_x + d\varepsilon_y + d\varepsilon_z \qquad (5\text{-}3)$$

$$d\gamma = \frac{\sqrt{2}}{3}\{(d\varepsilon_x - d\varepsilon_y)^2 + (d\varepsilon_y - d\varepsilon_z)^2 + (d\varepsilon_z - d\varepsilon_x)^2\}^{\frac{1}{2}} \qquad (5\text{-}4)$$

where $d\varepsilon_x$, $d\varepsilon_y$ and $d\varepsilon_z$ are the principal strain increment components in x-, y- and z-directions. Compressive strains are positive quantities.

In the case of symmetrical stress condition such as applied in the conventional triaxial compression and extension tests on MSP specimen (i.e. R_AV-specimen), p, q, $d\varepsilon_v$ and $d\gamma$ coincide with ones denoted by Eqs.(3-1) and (3-2), respectively.

The directions of shear stresses on the octahedral stress plane are expressed by the angle θ which is measured clockwise from the σ_z-axis to the stress point P as shown in Figs.5-2(b) and (c) and is calculated as follows:

$$\tan\theta = \frac{\sqrt{3}\,(\sigma_y - \sigma_x)}{2\sigma_z - \sigma_x - \sigma_y} \qquad (5\text{-}5)$$

The relative magnitude of the intermediate principal stress is indicated by b-value, which is expressed as follows:

$$b = \frac{\sigma_2 - \sigma_3}{\sigma_1 - \sigma_3} \qquad (5\text{-}6)$$

where σ_1, σ_2 and σ_3 are the major, intermediate and minor principal stresses, respectively. The b-value may vary between 0 and 1.0, and it has the relation to the parameter θ as indicated in Fig.5-3. It would be considered from the independency of b-value on the order of the magnitude of principal stresses σ_x, σ_y and σ_z that b-value is a parameter

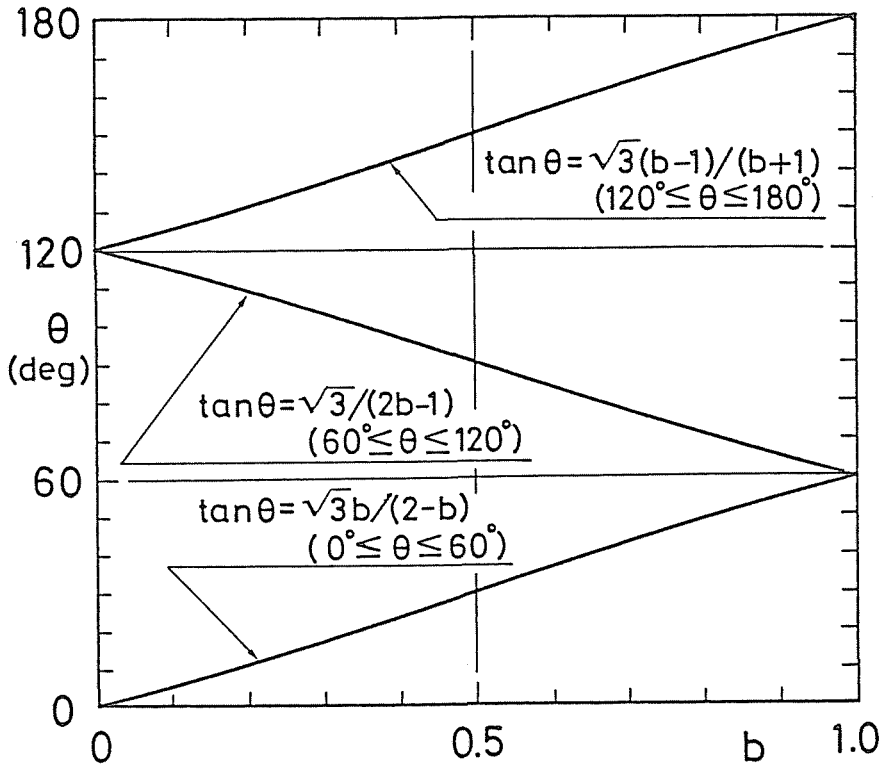

Fig.5-3 Parameter θ vs. b-value relationship in any stress system. For the ranges of θ between 0° and 60°, 60° and 120°, and 120° and 180°, b-balues are calculated as follows:

$$b = (\sigma_y - \sigma_x)/(\sigma_z - \sigma_x) \qquad (0^\circ \leq \theta \leq 60^\circ)$$

$$b = (\sigma_z - \sigma_x)/(\sigma_y - \sigma_x) \qquad (60^\circ < \theta \leq 120^\circ)$$

$$b = (\sigma_x - \sigma_z)/(\sigma_y - \sigma_z) \qquad (120^\circ < \theta \leq 180^\circ)$$

which prescribes the stress system during shear.

The true triaxial tests in this study were performed with constant values of θ or b, i.e. shear stresses increase monotonically along some stress path extending straight in radial directions on the octahedral stress plane. The stress path chosen were limited to the right-hand-side of the octahedral stress plane, since the orthotropic sand specimen are considered to have isotropic properties in xy-plane. Consequently, the deformation characteristics of sands in the range of $\theta = 0^\circ$ to 180° are investigated in the stress paths with an interval of $\theta = 15^\circ$ for F-sand and $\theta = 30^\circ$ for T-sand.

The discussion in this study is limited to the case in which the bedding plane coincides with the direction of the principal stresses.

5.4 Elastoplastic Stress-Strain Relationship

Strain increments $d\varepsilon_{ij}$ induced during consolidation and shear processes in the granular material such as sand could be divided into elastic strain increments $d\varepsilon^e_{ij}$ and plastic strain increments $d\varepsilon^p_{ij}$ as follows:

$$d\varepsilon_{ij} = d\varepsilon^e_{ij} + d\varepsilon^p_{ij} \qquad (i,j = 1,2,3) \qquad (5\text{-}7)$$

in which $d\varepsilon^e_{ij}$ is calculated by the generalized Hooke's law. However, it is assumed under the shear condition of p = const. employed in this study that $d\varepsilon^e_{ij}$ produced in the shear process can be ignored. Consequently, strain increments due to the shear of sands could be estimated by the following flow rule (Hill, 1950):

$$d\varepsilon_{ij} = d\varepsilon^p_{ij} = h \frac{\partial g}{\partial \sigma_{ij}} df \qquad (5\text{-}8)$$

where f, g and h are yield, plastic potential and hardening functions, respectively. It is assumed in this study that the plastic strain increments caused by shear and consolidation can be treated independently, whereas the plastic strain increments due to consolidation can be evaluated in the same form as Eq.(5-8). The formulation of yield, plastic potential and hardening functions for sands will be presented in the following paragraphs.

5.4.1 Yield and plastic potential functions

Application of a load increment to sand yielding at a stress state induces the plastic deformation with work-hardening in the sand. In order to estimate these plastic deformation of sand, it is essential to establish the yield function which prescribes a closed surface or, in general, the yield surface, built up in the principal stress space by a combination of stresses. If plastic behavior of sand subjected to a sequence of load-increment can be assumed to be a succession of infinitely small yielding, the yield surface can be determined experimentally. For example, the experimental studies on these yielding properties by Pooroo-shasb et al. (1966), Cole (1967), Barden et al. (1969), Tatsu-oka and Ishihara (1974a) and Nishi and Esashi (1978) have shown that the yield loci for the sands in the various shear conditions are represented by straight lines or slightly curved lines with the convex shape for p-axis in the p - q plane.

Because of the simplicity in the formation of stress-strain relationship, it is assumed in the present study that the yield locus for shear of sand in the general stress conditions is straight lines in the p - q plane, i.e. constant lines of effective stress ratio η as in the past study (Miura et al., 1982b).

$$f = \eta = \left(\frac{q}{p}\right) \qquad (5\text{-}9)$$

In general, plastic strain increments depend upon the current stress state and previous strain history. At the same time, we can prescribe the directions of the principal strain increments with the help of the fact that the direction of the plastic strain increment is normal to the plastic potential plane established in the stress space. However, if we adopt the associated flow rule in which the yield function (Eq.(5-9)) is identical to the plastic potential function, the negative dilatancy (volume contraction) at the initial shear stage particular to the granular mass could not be explained.

Fig.5-4 shows the strain increments ($d\gamma$, $d\varepsilon_v$) measured under $p = p_c = \text{const.}$ (196 kPa) drained triaxial compression tests ($b = 0$, $\theta = 0^\circ$). Volumetric strain ε_v in Fig. 5-4 is only due to shear (dilatancy) because the effective mean principal stress is kept constant. Assuming that the yield surface represented in Fig.5-4 is identical with the plastic potential, volume change must show only expansion from starting of shear. Actual behavior is, however, different from it, and the direction of plastic strain increments changes inversely from early stage in shear up to failure

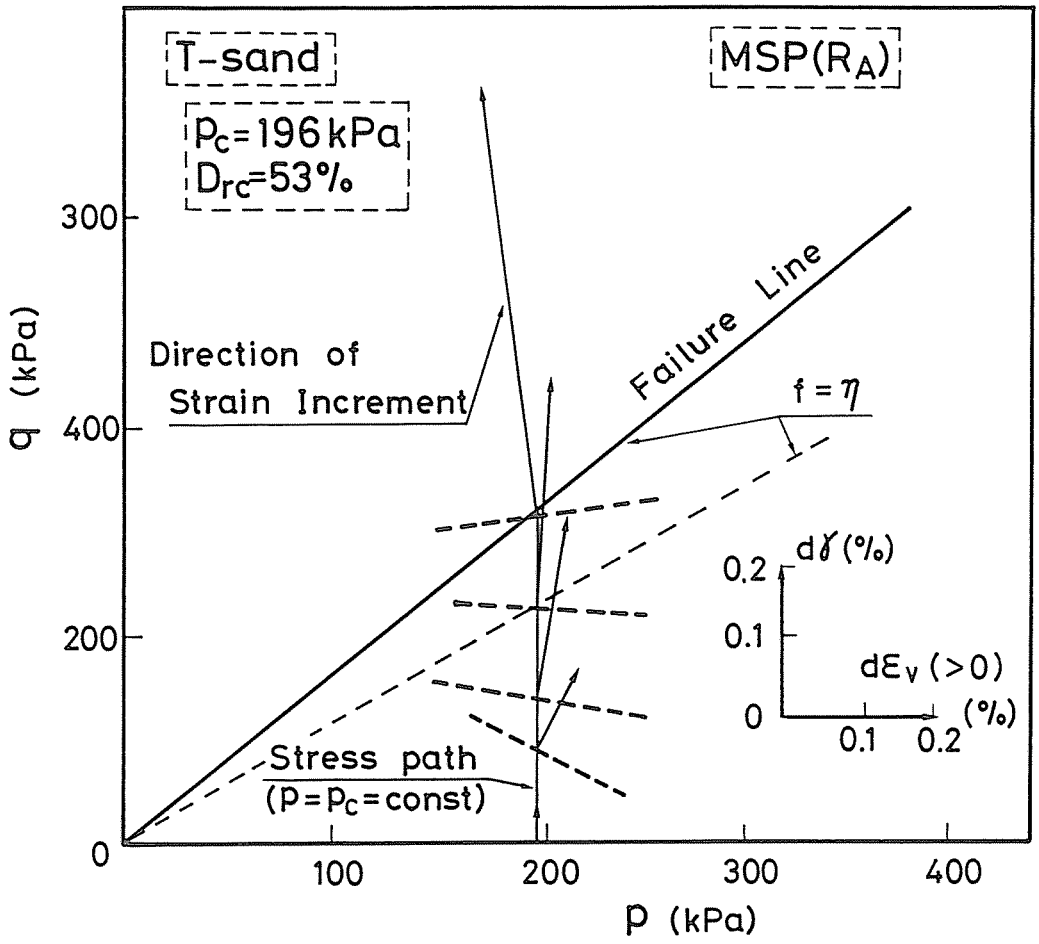

Fig.5-4 Changes in strain increment directions observed under $p = p_c = \text{const.}$ drained triaxial compression test

state. This fact means that the granular materials such as sands should be discussed based on the non-associated flow rule.

Roscoe et al. (1963) derived the elastoplastic stress-strain equation based on the associated flow rule and the concepts of the critical state and the state boundary surface. They also assumed in their developments that the dissipated energy per unit volume of soil, when undergoing deformation ($d\gamma$, $d\varepsilon_v$) at any state corresponding to a point on the state boundary surface, is $M \cdot p \cdot d\gamma$. That is,

$$p \cdot d\varepsilon_v + q \cdot d\gamma = M \cdot p \cdot d\gamma \qquad (5\text{-}10)$$

where the left-hand side represents the dissipated energy derived from the assumption in which the principal axes of stress and plastic strain increment coincide, and M is the η at critical state. Therefore, plastic strain increment ratio is given as follows:

$$\left(\frac{d\varepsilon_v}{d\gamma} \right) = M - \eta \qquad (5\text{-}11)$$

Figs.5-5(a) and (b) show the relationships between stress ratio and plastic strain increment ratio for F- and

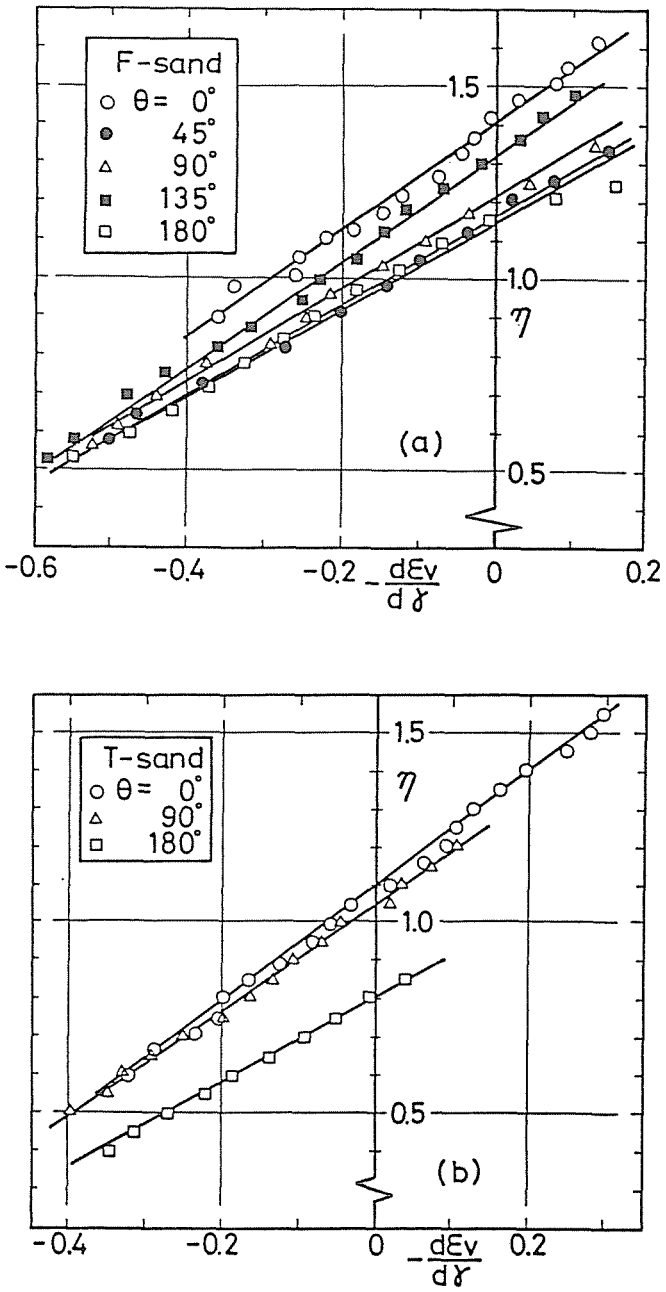

Fig.5-5 Relationships between stress ratio and plastic strain increment ratio in any stress paths; (a) F-sand (After data of Yamada and Ishihara (1979)), (b) T-sand

T-sands. In both tests, there is the unique linear relationship in the various stress paths, and it would be suggested that Eq.(5-10) or Eq.(5-11) is applicable for sand. However, the both test data depict that the linear gradient and the ordinate intercept are changed by Θ-value.

From these experimental results on the anisotropic sands under the general stress conditions, it is assumed that the plastic strain increment ratio is given in the form of the following equation:

$$\left(\frac{d\varepsilon_v}{d\gamma} \right) = C_d (m - \eta) \qquad (5\text{-}12)$$

in which C_d is the reciprocal of the linear gradient, and m is the η at the maximum volume contraction point during shear.

Dependency of C_d and m on the stress system and the fabric anisotropy is shown in Figs.5-6(a) and (b). It can be seen from the figures that both of C_d and m depend only on b-value, i.e. the stress system, but are independent of fabric anisotropy. It should be also noted that the product of C_d and m is always a constant not affected by the stress system and fabric anisotropy. Formulation of these parameters to b-value may be difficult as shown in Fig.5-6, but parameter m for the general stress conditions can be estimated through the shear-effective normal stress ratio on the spatial

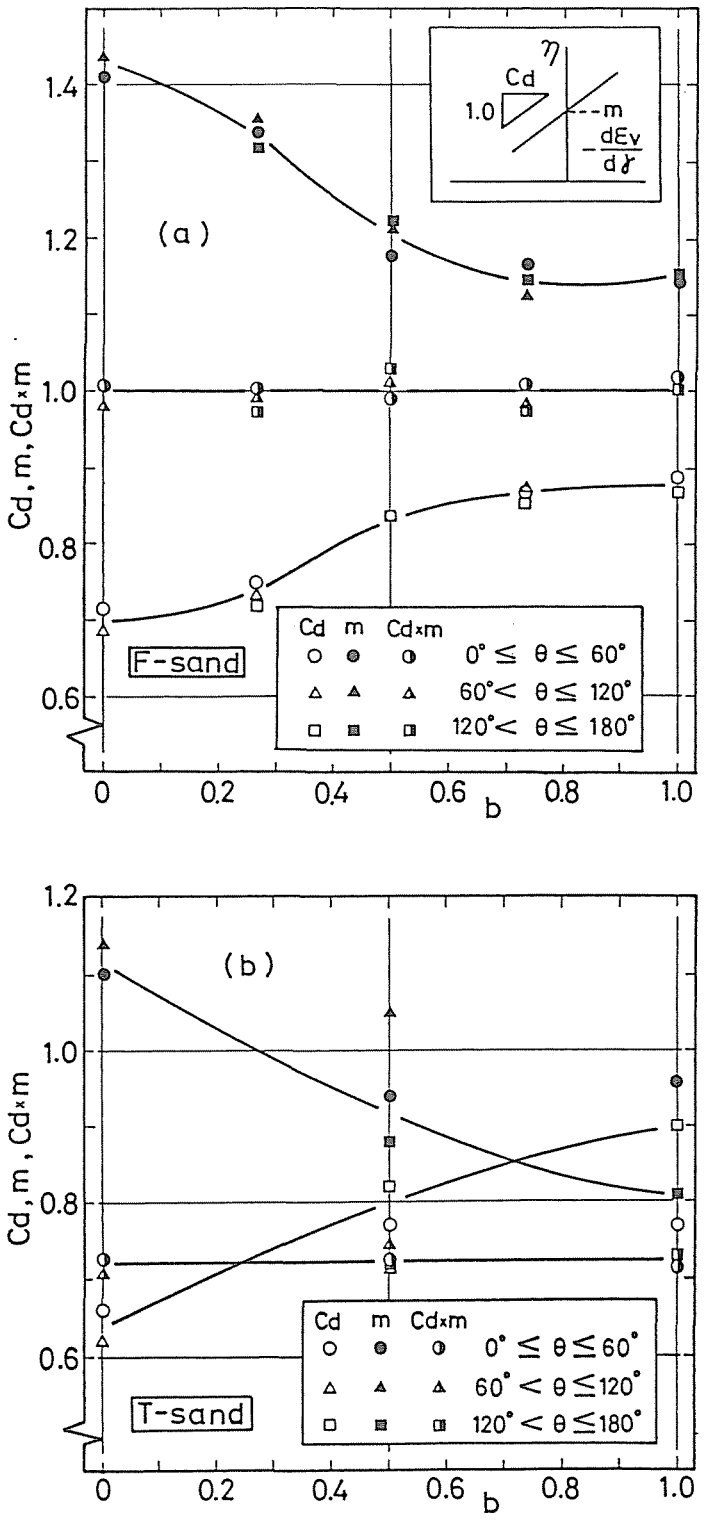

Fig.5-6 Parameters C_d and m vs. b-value and independency of $C_d \cdot m$ on stress system; (a) F-sand (After data of Yamada and Ishihara (1979), (b) T-sand

mobilized plane by Matsuoka and Nakai (1977) at maximum volume contraction $R\,(=(\tau/\sigma_N)_{at\ d\varepsilon_v=0})$. That is, the relationship between m and R is as follows:

$$R = (\tau/\sigma_N)_{at\ d\varepsilon_v=0} = \left(\frac{J_1J_2 - 9J_3}{9J_3}\right)^{\frac{1}{2}} = \left(\frac{6m^2 - 2m^3\cos3\theta}{27 - 9m^2 + 2m^3\cos3\theta}\right)^{\frac{1}{2}} \qquad (5\text{-}13)$$

where J_1, J_2 and J_3 are the first, second and third effective stress invariants, respectively. As can be seen in Fig.5-7, m is linearly related to R in both sands as

$$R = (1 - b)R_C + bR_E \qquad (5\text{-}14)$$

in which R_C and R_E are the values of R corresponding to the triaxial compression ($\theta = 0^\circ$) and the triaxial extension ($\theta = 180^\circ$) conditions, respectively. Thus, it may be possible by using the shear-effective normal stress ratio on the spatial mobilized plane (Matsuoka and Nakai, 1977) that the values of C_d and m at any stress system are evaluated from the measured ones of the triaxial compression and extension tests.

Relationship between stress ratio and plastic strain

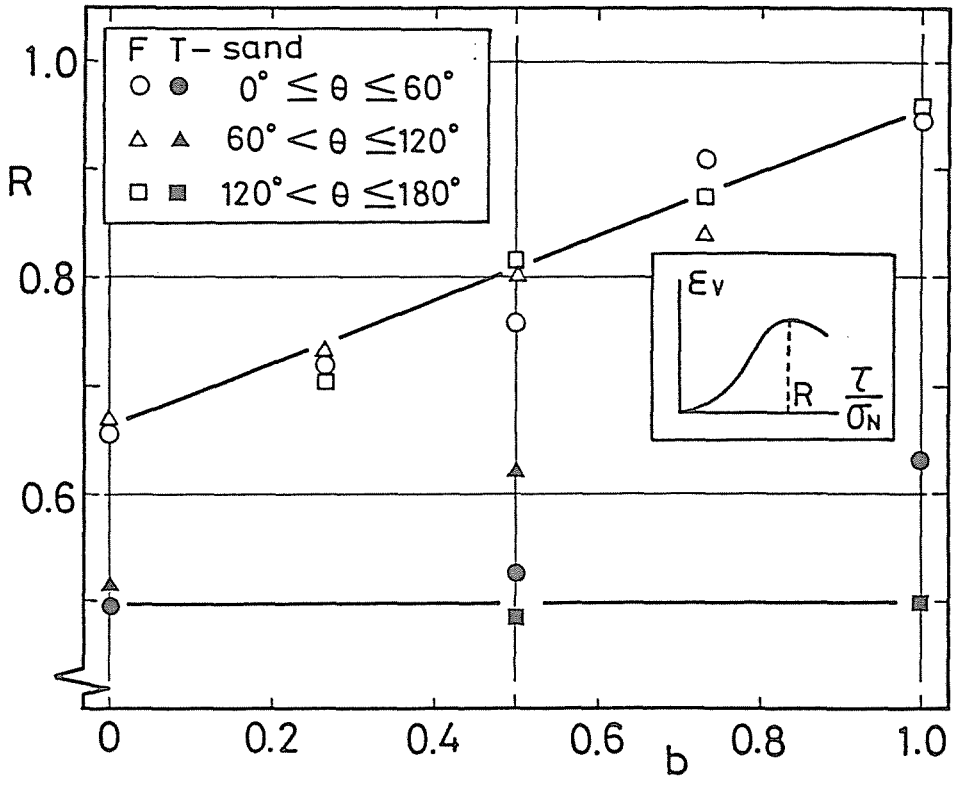

Fig.5-7 Stress ratio R at the maximum volume contraction during shear process vs. b-value in F- and T-sands (Test data of F-sand from Yamada and Ishihara (1979))

increment ratio generalized based on the above discussion introduces the plastic potential function g under the general stress conditions by the normality rule $(d\varepsilon_v/d\gamma)(dp/dq) = -1$ as follows:

$$g = \eta + \frac{C_d \cdot m}{1 - C_d} (1 - p^{C_d - 1}) \qquad (C_d \neq 1) \qquad (5\text{-}15)$$

$$g = \eta + m \cdot \ln p \qquad (C_d = 1) \qquad (5\text{-}16)$$

Fig.5-8 shows schematically the plastic potential function g represented by Eq.(5-15) or Eq.(5-16) in q - p plane. When a sand is sheared under p = const. condition after isotropic consolidation (p_c), the volume contraction occurs when η is smaller than m; i.e., $O' \rightarrow 1 \rightarrow 2$ in Fig.5-8, and the volume expansion occurs when η is larger than m; i.e., $2 \rightarrow 3$ in Fig.5-8, inducing the work-hardening. Therefore, dilatancy property of sand showing the volume contraction and volume expansion can be explained by means of such plastic potential function.

Change in the plastic potential surface or in the direction of plastic strain increment due to the difference of the shear stress system as represented by b-value can be evaluated by Eqs.(5-15) and (5-16). Fig.5-9 illustrates the change in plastic potential surface due to the difference of b-value for F-sand in p - q plane.

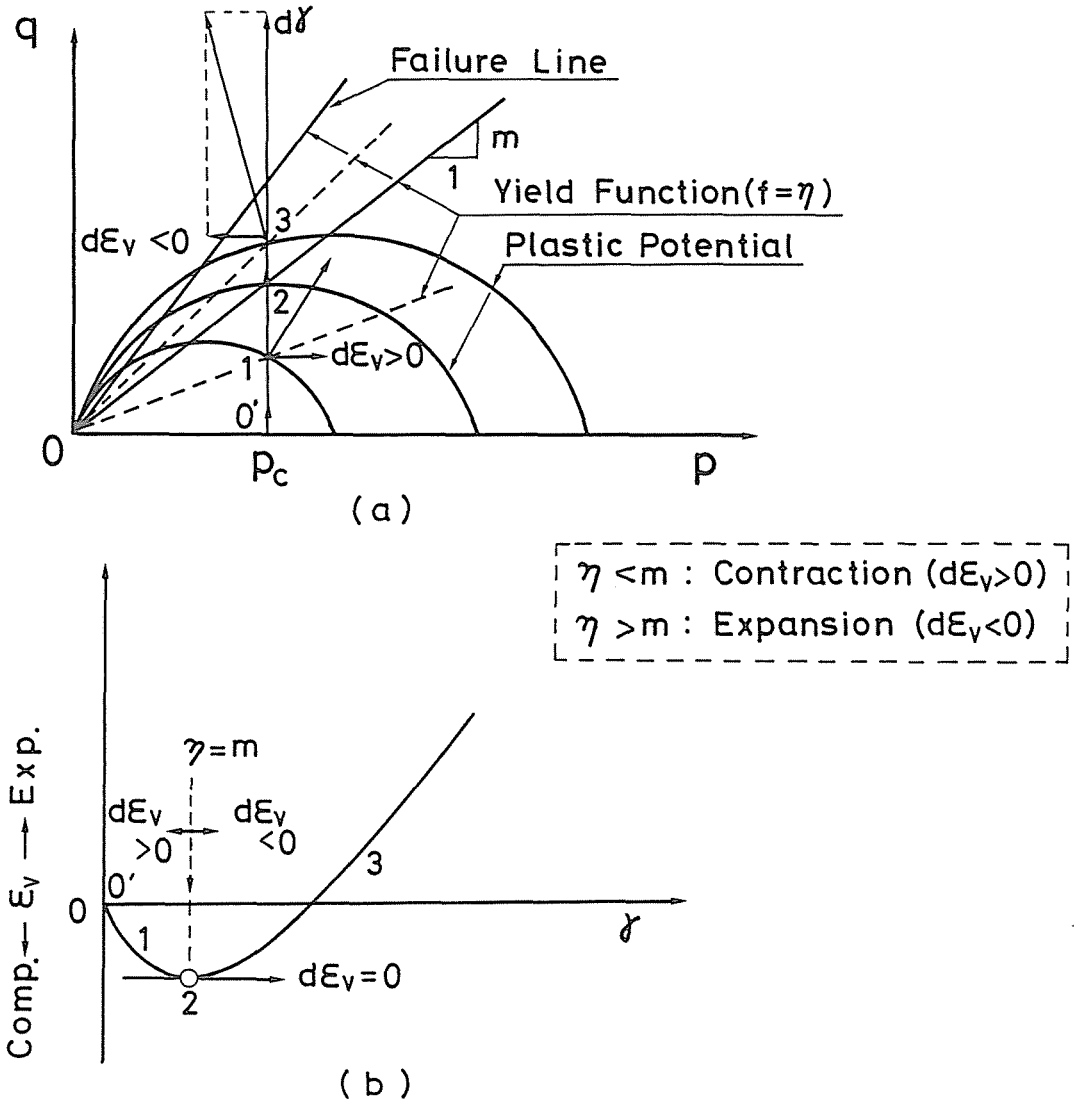

Fig.5-8 Plastic potential function expressing dilatancy property of sand

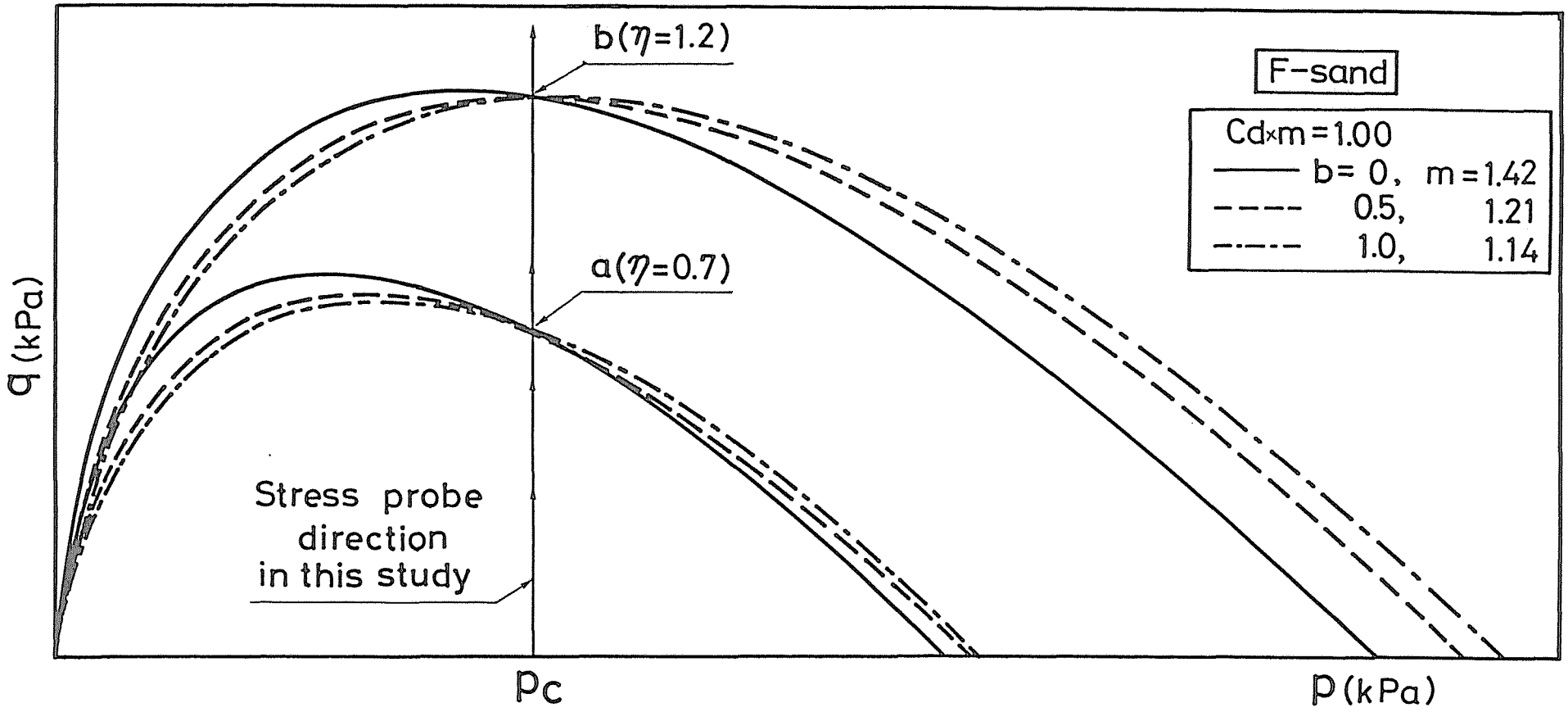

Fig.5-9 Change in plastic potential surface due to the difference of shear stress system for F-sand

5.4.2 Plastic strain work due to consolidation and shear and its relation to hardening function

In this and the following paragraphs, the plastic work, i.e. the dissipated energy within the sand element done by consolidation or shear, will be explained quantitatively, and it will be also presented that the plastic strain work plays the important role in establishing the hardening function for sands with anisotropic fabric under the general stress conditions.

From the result of the isotropic consolidation-swelling test on T-sand as shown in Fig.5-10, it can be suggested that deformation behavior in consolidation of sand would be characterized by the linear relationship between $\ln \varepsilon_v$ and $\ln p$. According to the elastoplastic consideration on these behavior, elastic volumetric strain increment $d\varepsilon_v^e$ and plastic volumetric strain increment $d\varepsilon_v^p$ developed during consolidation are given, referring to Fig.5-10(b), as follows:

$$d\varepsilon_v^e = k \cdot n \left(\frac{p_o}{p_k} \right)^1 \left(\frac{p}{p_o} \right)^n \frac{dp}{p} \qquad (5\text{-}17)$$

$$d\varepsilon_v^p = k \left(1 - n \right) \left(\frac{p}{p_k} \right)^1 \frac{dp}{p} \qquad (5\text{-}18)$$

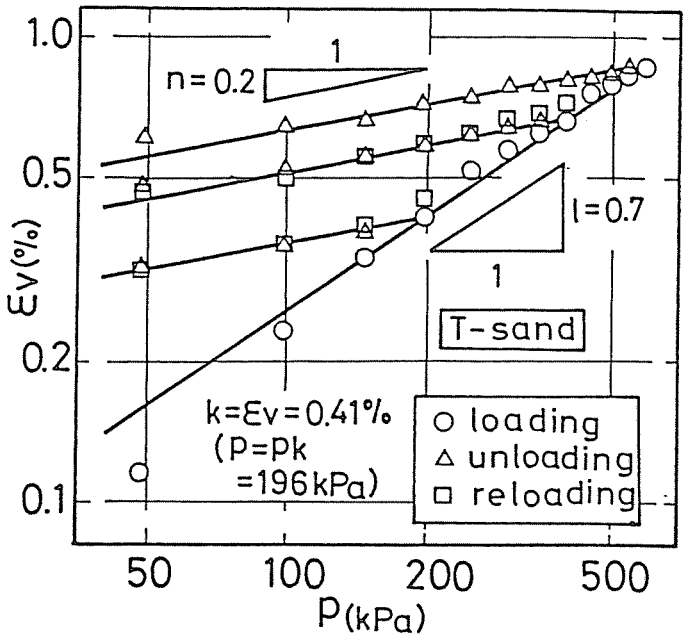

(a)

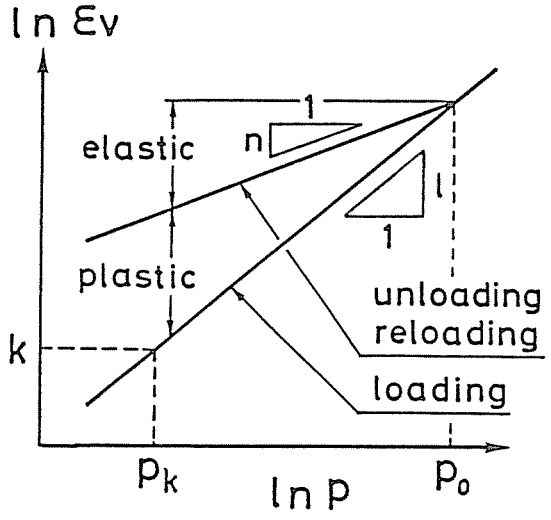

(b)

Fig.5-10 Relationship between volumetric strain and effective mean principal stress for T-sand in isotropic consolidation-swelling test

where the exponents l and n represent the slope of the consolidation and swelling curves, and k and p_o are the volumetric strain at $p = p_k$ and the pre-consolidation pressure, respectively. As explained in CHAPTER 4 (See Fig. 4-9), no measurable shear strain in the isotropic consolidation-swelling test can be observed even for MSP specimen which possesses the strong fabric anisotropy. Therefore, the associated flow rule can be applied for the consolidation process of sand.

Flow rule for the consolidation is not discussed in detail. From these experimental results, however, yield function f_c, plastic potential function g_c and hardening function h_c for the isotropic consolidation of sand can be denoted as follows:

$$f_c = g_c = p_k \tag{5-19}$$

$$h_c = k\,(1-n)\left(\frac{p}{p_k}\right)^{l}\frac{1}{p} \tag{5-20}$$

From Eq.(5-18), the plastic strain work increment done by the isotropic consolidation dW_I^p is obtained as follows:

$$dW_I^p = \sigma_x \, d\varepsilon_x + \sigma_y \, d\varepsilon_y + \sigma_z \, d\varepsilon_z = p \, d\varepsilon_v^p$$

$$= k \, (1 - n) \left(\frac{p}{p_k} \right)^1 dp \qquad (5\text{-}21)$$

Consequently, the plastic strain work done up to desired consolidation pressure p_c can be calculated by the following expression.

$$W_I^p = \int_0^{p_c} dW_I^p = \frac{1 - n}{1 + 1} \, k \left(\frac{p_c}{p_k} \right)^1 p_c \qquad (5\text{-}22)$$

On the other hand, the plastic strain work increment due to shear dW^p is generally given as follows:

$$dW^p = \sigma_x \, d\varepsilon_x + \sigma_y \, d\varepsilon_y + \sigma_z \, d\varepsilon_z = p \, d\varepsilon_v + q \, d\gamma \qquad (5\text{-}23)$$

Substitution of the principal strain increments which can be obtained from Eqs.(5-8), (5-9) and (5-15) or (5-16) into Eq.(5-4) gives the hardening function for shear as follows:

$$h = p \left(\frac{d\gamma}{d\eta} \right) \qquad (5\text{-}24)$$

It has been experimentally shown by Frydman (1976) that this hardening function can be represented as a unique function of plastic strain work during shear, irrespective of the consolidation pressure and the direction of shear stress.

$$h = A\,(W^p)^B \qquad (5\text{-}25)$$

where A is the h-value corresponding to W^p = 1 kPa and exponent B is the slope of the line in log-log plot. Figs. 5-11(a) and (b) show that hardening function h is a power function of W^p, and thus Eq.(5-25) is valid for F- and T-sands. However, the test data of both sands depict that parameter A and B change according to θ-value as shown in Figs.5-12(a) and (b). As it can be seen in these figures that parameter A and B vary lineraly with θ-value, the values of A and B in any stress system can be determined from ones of the conventional triaxial compression ($\theta = 0^\circ$) and triaxial extension ($\theta = 180^\circ$) tests. From the fact that parameters A and B depend strongly on θ-value, it can be pointed out that hardening parameter or, in general, hardening function is affected significantly by the fabric anisotropy of sand.

As indicated above, the establishment of the hardening function which can describe the anisotropic deformation behaviors of sands seems to be the most direct attack on the problem of fabric anisotropy of sands.

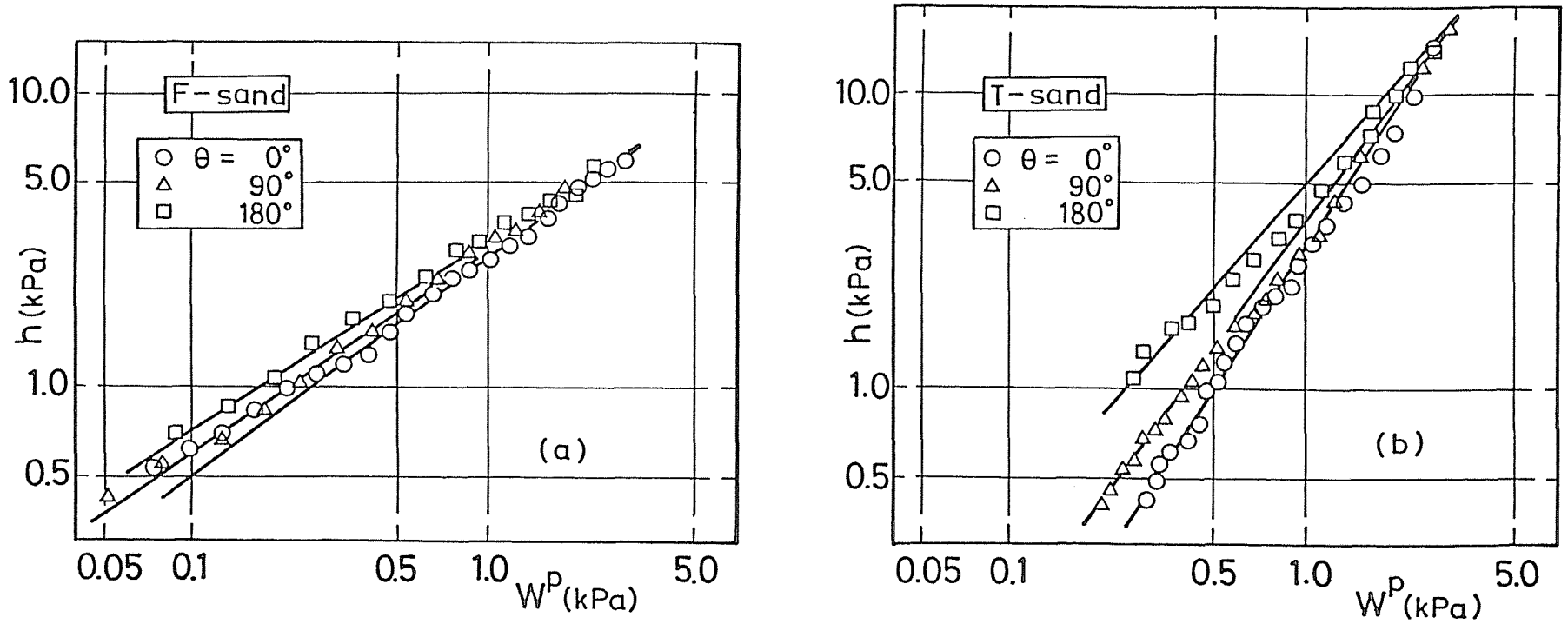

Fig.5-11 Relationships between hardening function (strain hardening parameter) and plastic strain work during shear process in any stress paths; (a) F-sand (After data of Yamada and Ishihara (1979)), (b) T-sand

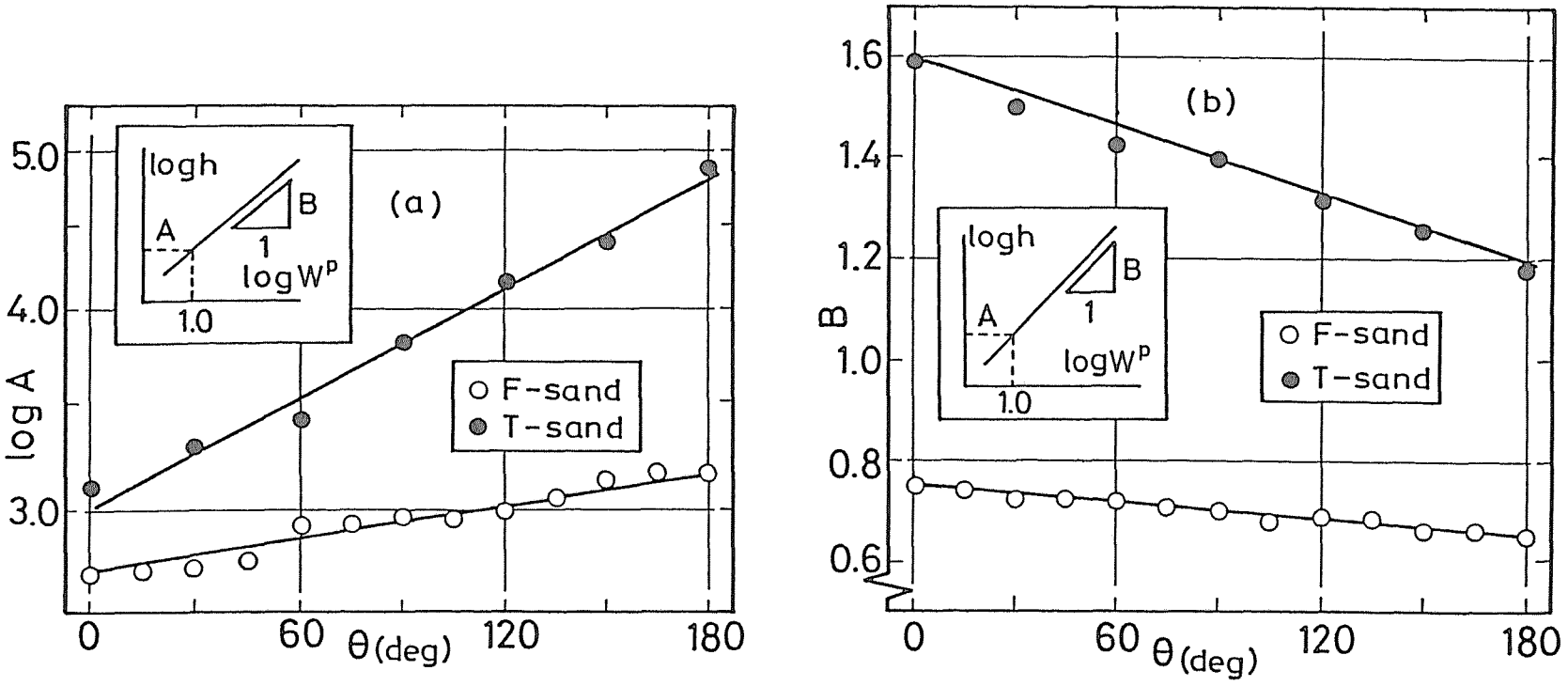

Fig.5-12 Changes in parameters A and B due to difference of stress system; (a) A vs.θ, (b) B vs. θ (Test data of F-sand from Yamada and Ishihara (1979))

5.4.3 Hardening function for anisotropic sand under the general stress conditions

The hardening function of Eq.(5-25) is extended to take the occurrence of the anisotropic principal strains in the three-dimensional stress condition into account, based on the concept of compounded mobilized plane by Matsuoka (1974). Matsuoka's theory is not only concise and but also convenient for analyzing the strains under three different stresses. Tatsuoka (1980) has also applied this theory to derive the stress-strain relationship for anisotropic sands.

Fig.5-13 illustrates the conceptional view in which each of the principal strain increments $d\varepsilon_x$, $d\varepsilon_y$ and $d\varepsilon_z$ is divided into three two-dimensional stress systems fixed with respect to fabric of a sand element concerned. According to the concept of compounded mobilized plane, each of the principal strain increments is denoted by a summation of the different strain increments in two two-dimensional stress systems to which each of them belongs, i.e.,

$$d\varepsilon_i = d\varepsilon_{iij} \left(\text{or } d\varepsilon_{iji} \right) + d\varepsilon_{iki} \left(\text{or } d\varepsilon_{iik} \right) \quad (5\text{-}26a)$$

$$d\varepsilon_j = d\varepsilon_{jij} \left(\text{or } d\varepsilon_{jji} \right) + d\varepsilon_{jjk} \left(\text{or } d\varepsilon_{jkj} \right) \quad (5\text{-}26b)$$

$$d\varepsilon_k = d\varepsilon_{kik} \left(\text{or } d\varepsilon_{kki} \right) + d\varepsilon_{kjk} \left(\text{or } d\varepsilon_{kkj} \right) \quad (5\text{-}26c)$$

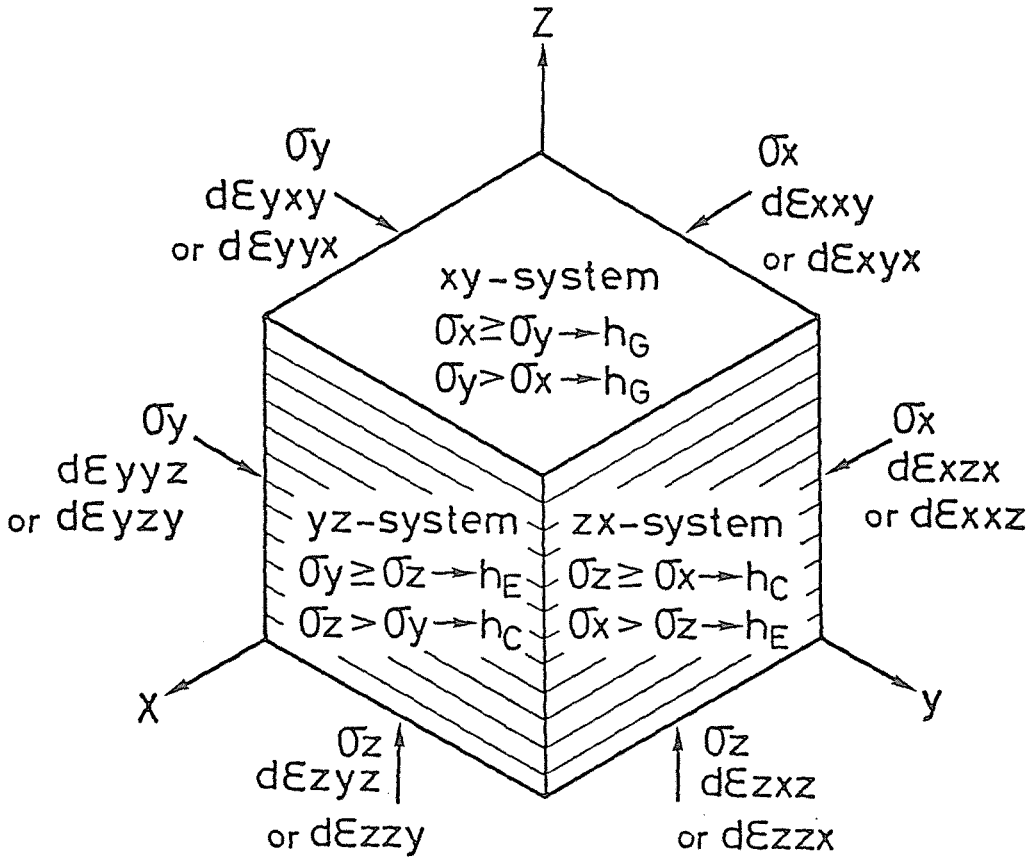

Fig.5-13 Three two-dimensional stress and strain increment systems

where suffixes i, j and k do not represent the indices of tensor, but one out of x, y and z without duplication of uses. First suffix notation in the right-hand side of the above equation denotes the directions of the principal strain increments. Second and third suffixes denote the two-dimensional stress systems to which each of divided principal strain increments belongs, and they are taken according to the magnitude of two principal stresses concerned. For example, Eq.(5-26a) shows that principal strain increments $d\varepsilon_i$ can be denoted by a summation of the principal strain increment induced in the ij-stress system or ji-stress system ($d\varepsilon_{iij}$ at $\sigma_i \geq \sigma_j$ or $d\varepsilon_{iji}$ at $\sigma_j > \sigma_i$) and the principal strain increment induced in the ki-stress system or ik-stress system ($d\varepsilon_{iki}$ at $\sigma_k \geq \sigma_i$ or $d\varepsilon_{iik}$ at $\sigma_i > \sigma_k$).

It is assumed in this paper that the principal strain increments divided in each of the two-dimensional stress systems can be calculated under the general stress conditions by selecting the hardening function corresponding to the magnitude relation of two principal stresses concerned as follows:

$$d\varepsilon_{iij} = D_{ij}\, h_{ij}\, \frac{\partial g}{\partial \sigma_i}\, df \qquad (\sigma_i \geq \sigma_j) \qquad (5\text{-}27a)$$

$$d\varepsilon_{iji} = D_{ij}\, h_{ji}\, \frac{\partial g}{\partial \sigma_i}\, df \qquad (\sigma_j \geq \sigma_i) \qquad (5\text{-}27b)$$

in which

$$\frac{\partial g}{\partial \sigma_i} = \frac{1}{3p}\left(\frac{9}{2\eta}\frac{\sigma_i - p}{p} + C_d(m - \eta)\right) \tag{5-28}$$

$$D_{ij} = \frac{|\sigma_i - \sigma_j|}{|\sigma_i - \sigma_j| + |\sigma_i - \sigma_k|} \tag{5-29}$$

The plastic potential function g and the yield function f of Eq.(5-27) are determined not only by two principal stresses (σ_i and σ_j) but also by another principal stress σ_k. Consequently, in order to estimate, for example, $d\varepsilon_{iij}$ for the two-dimensional stress system of σ_i and σ_j, it is necessary to evaluate the effects of σ_k. D_{ij} is newly introduced to consider the effects of third principal stress, and it can be given easily by designating the stress system during shear process. Moreover, h_{ij} or h_{ji} can be determined concretely taking account of the fabric characteristics of sand and the magnitude relation of two principal stresses in each of the two-dimensional stress systems. Thus, the concept of compounded mobilized plane proposed originally by Matsuoka (1974) is applied to the present study with the modification mentioned above.

If we express the hardening functions corresponding to the triaxial compression ($\theta = 0^\circ$) and triaxial extension

($\theta = 180^\circ$) conditions as h_C and h_E, respectively, the following equations are given from Eq.(5-25).

$$h_C = A_C \left(W^p \right)^{B_C} \tag{5-30}$$

$$h_E = A_E \left(W^p \right)^{B_E} \tag{5-31}$$

where A_C, B_C, A_E and B_E can be obtained from the conventional triaxial compression and extension tests.

As can be seen in Fig.5-13, in yz- and zx-planes which have the definite anisotropic fabrics characterized by preferably parallel alignments of sand particles to horizontal direction, h_C or h_E would be selected according to the magnitude relation of two principal stresses concerned. From the aforementioned point of view on the sand specimen with orthotropic fabric such as MSP specimen and Fig.5-13, xy-plane (i.e., horizontal plane) can be assumed to be approximately in the isotropic state with respect to its mechanical property. Hardening function h_G corresponding to $\theta = 90^\circ$ should be adopted in xy-plane regardless of the magnitude relation of σ_x and σ_y, since we assume the hardening function to be dependent mainly on the fabric anisotropy of sand specimen as mentioned above.

It is assumed in this paper that h_G can be evaluated by h_C and h_E as follows:

$$h_G = (h_C h_E)^{\frac{1}{2}} = \{ A_C A_E (W^p)^{B_C+B_E} \}^{\frac{1}{2}} \qquad (5\text{-}32)$$

From the above explanations, the hardening functions for each of the two-diemnsional stress systems can be represented, referring to Fig.5-13, by the following expressions.

$$h_{xy} = h_{yx} = h_G \qquad (5\text{-}33a)$$

$$h_{yz} = h_{xz} = h_E \qquad (5\text{-}33b)$$

$$h_{zx} = h_{zy} = h_C \qquad (5\text{-}33c)$$

After all, it follows that hardening function h_i corresponding to each of the principal strain increments has been newly established by superposing the strain increments induced in each of the two-dimensional stress system as follows:

$$d\varepsilon_i = h_i \frac{\partial g}{\partial \sigma_i} df \qquad (5\text{-}34)$$

where h_i is given by comparing above equation with Eqs.(5-26) and (5-27) by the following expression.

$$h_i = D_{ij}\, h_{ij}\ (\text{or } h_{ji}) + D_{ik}\, h_{ki}\ (\text{or } h_{ik}) \qquad (5\text{-}35)$$

The concrete form of hardening function h_i can be easily determined by assigning θ-value, and h_x, h_y and h_z are represented for the stress system $0^\circ \leq \theta \leq 180^\circ$ by the following expressions.

$$\left.\begin{aligned} h_x &= D_{xy}\, h_{yx} + D_{xz}\, h_{zx} = D_{xy}\, h_G + D_{xz}\, h_C \\ h_y &= D_{yz}\, h_{zy} + D_{yx}\, h_{yx} = D_{yz}\, h_C + D_{yx}\, h_G \\ h_z &= D_{zx}\, h_{zx} + D_{zy}\, h_{zy} = D_{zx}\, h_C + D_{zy}\, h_C = h_C \end{aligned}\right\} \quad (0^\circ \leq \theta \leq 60^\circ) \qquad (5\text{-}36a)$$

$$\left.\begin{aligned} h_x &= D_{xy}\, h_{yx} + D_{xz}\, h_{zx} = D_{xy}\, h_G + D_{xz}\, h_C \\ h_y &= D_{yz}\, h_{yz} + D_{yx}\, h_{yx} = D_{yz}\, h_E + D_{yx}\, h_G \\ h_z &= D_{zx}\, h_{zx} + D_{zy}\, h_{yz} = D_{zx}\, h_C + D_{zy}\, h_E \end{aligned}\right\} \quad (60^\circ < \theta \leq 120^\circ) \qquad (5\text{-}36b)$$

$$\left.\begin{aligned} h_x &= D_{xy}\, h_{yx} + D_{xz}\, h_{xz} = D_{xy}\, h_G + D_{xz}\, h_E \\ h_y &= D_{yz}\, h_{yz} + D_{yx}\, h_{yx} = D_{yz}\, h_E + D_{yx}\, h_G \\ h_z &= D_{zx}\, h_{xz} + D_{zy}\, h_{yz} = D_{zx}\, h_E + D_{zy}\, h_E = h_E \end{aligned}\right\} \quad (120^\circ < \theta \leq 180^\circ) \qquad (5\text{-}36c)$$

in which D_{xy}, D_{xz}, D_{yz}, D_{yx}, D_{zx} and D_{zy} are the parameters related only to θ-value, and they can be denoted, referring

to Eq.(5-29), as follows:

$$D_{xy} = \frac{|\sin\theta|}{|\sin\theta| + |\sin(\theta - 120^\circ)|} \qquad (5\text{-}37a)$$

$$D_{xz} = \frac{|\sin(\theta - 120^\circ)|}{|\sin(\theta - 120^\circ)| + |\sin\theta|} \qquad (5\text{-}37b)$$

$$D_{yx} = \frac{|\sin\theta|}{|\sin\theta| + |\sin(\theta - 60^\circ)|} \qquad (5\text{-}37c)$$

$$D_{yz} = \frac{|\sin(\theta - 60^\circ)|}{|\sin(\theta - 60^\circ)| + |\sin\theta|} \qquad (5\text{-}37d)$$

$$D_{zx} = \frac{|\sin(\theta - 120^\circ)|}{|\sin(\theta - 60^\circ)| + |\sin(\theta - 120^\circ)|} \qquad (5\text{-}37e)$$

$$D_{zy} = \frac{|\sin(\theta - 60^\circ)|}{|\sin(\theta - 60^\circ)| + |\sin(\theta - 120^\circ)|} \qquad (5\text{-}37f)$$

5.4.4 Derived three-dimensional drained stress-strain relationship

Substitution of Eqs.(5-9), (5-15) or (5-16) and (5-36) into Eq.(5-34) gives the principal strain increments under the three-dimensional drained stress conditions $d\varepsilon_x$, $d\varepsilon_y$ and $d\varepsilon_z$. For example, each of the principal strain increments induced in the stress system $60^\circ < \theta \leq 120^\circ$ can be expressed by the following equations.

$$d\varepsilon_x = \left(\frac{\sin\theta}{\sin\theta + |\sin(\theta-120^\circ)|} \{ A_C A_E (W^p)^{B_C+B_E} \}^{\frac{1}{2}} + \frac{|\sin(\theta-120^\circ)|}{\sin\theta + |\sin(\theta-120^\circ)|} \cdot A_C (W^p)^{B_C} \right) \{ 3\cos(\theta-240^\circ) + C_d (m - \eta) \} \frac{d\eta}{3p} \qquad (5\text{-}38a)$$

$$d\varepsilon_y = \left(\frac{\sin(\theta-60^\circ)}{\sin\theta + \sin(\theta-60^\circ)} A_E (W^p)^{B_E} + \frac{\sin\theta}{\sin\theta + \sin(\theta-60^\circ)} \cdot \{ A_C A_E (W^p)^{B_C+B_E} \}^{\frac{1}{2}} \right) \{ 3\cos(\theta-120^\circ) + C_d (m - \eta) \} \cdot \frac{d\eta}{3p} \qquad (5\text{-}38b)$$

$$d\varepsilon_z = \left(\frac{|\sin(\theta-120^\circ)|}{\sin(\theta-60^\circ) + |\sin(\theta-120^\circ)|} A_C (W^p)^{B_C} + \frac{\sin(\theta-60^\circ)}{\sin(\theta-60^\circ) + |\sin(\theta-120^\circ)|} A_E (W^p)^{B_E} \right) \{ 3\cos\theta + C_d (m - \eta) \} \frac{d\eta}{3p} \qquad (5\text{-}38c)$$

The principal strain increments induced in the other stress systems $0^\circ \leq \theta \leq 60^\circ$ and $120^\circ < \theta \leq 180^\circ$ can be formulated in the similar expressions as indicated above, but their representations are abbreviated.

Parameters included in the proposed elastoplastic work-hardening model can be determined easily from the conventional triaxial compression and extension tests and the isotropic consolidation-swelling test.

In the following paragraph, the verification with respect to the measured data of the true triaxial tests performed by Yamada and Ishihara (1979) and the present author will be presented.

5.5 Comparison of Predicted with Observed Stress-Strain Relationship

As explained previously, parameters which prescribe the above stress-strain relationships under three different principal stresses can be evaluated by the data of the conventional triaxial compression and extension tests and the isotropic consolidation-swelling test. Parameters determined from these tests on F- and T-sands are summarized in Table 5-2. W_I^p is given through the isotropic consolidation-swelling test, while W_I^p for F-sand is estimated from the test data of Tatsuoka (1972).

Figs.5-14(a) to (m) and Figs.5-15(a) to (g) show the comparisons of the predicted and measured stress ratio vs. principal strains relationships for F- and T-sand, respectively. In these figures, the plots represent the observed values obtained from the true triaxial tests and the solid curves the stress-strain relationships derived in the preceding sections. The deformation characteristics of sands change complicately due to the synthetic effects of the differences of stress systems and the anisotropy of sand specimens. As can be seen in these figures, the predicted stress ratio vs. principal strains relationships explain well the measured values under three different principal stresses.

In both tests, it should be noted that, in the stress

Table 5-2 Model parameters for F- and T-sands (W_I^p for F-sand is determined from test data of Tatsuoka (1972) and other parameters from Yamada and Ishihara (1979))

Sample name	$C_d \cdot m$	m		A		B		W_I^p(kPa)
		m_C	m_E	A_C	A_E	B_C	B_E	
F-sand	1.00	1.42	1.14	2.75	3.15	0.75	0.65	0.003
T-sand	0.72	1.11	0.81	3.00	4.80	1.60	1.20	0.237

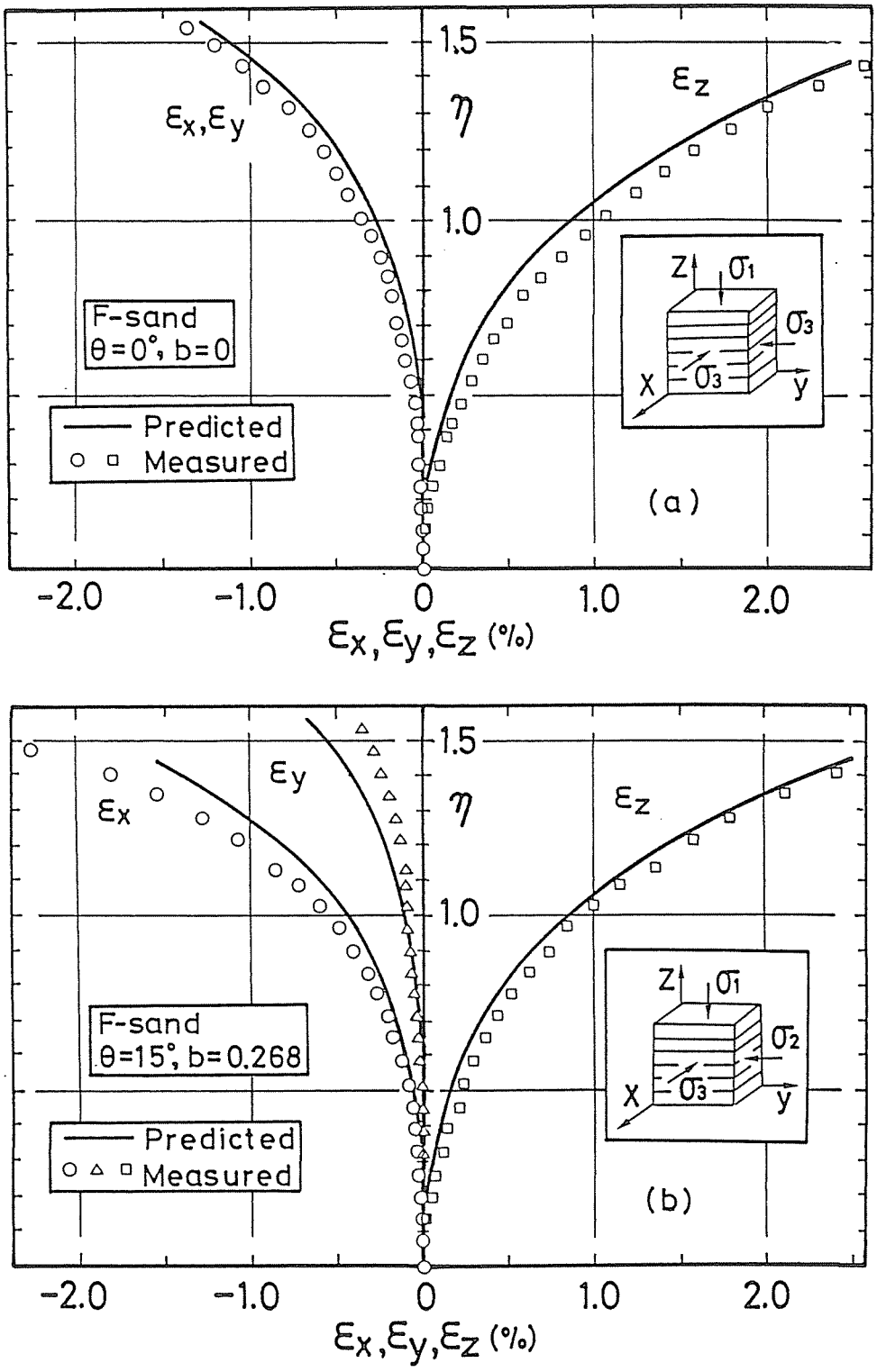

Fig.5-14 Comparisons of measured and predicted relationships between stress ratio and principal strains for F-sand in the stress paths with $\theta = 0^\circ$ (a) and $\theta = 15^\circ$ (b)

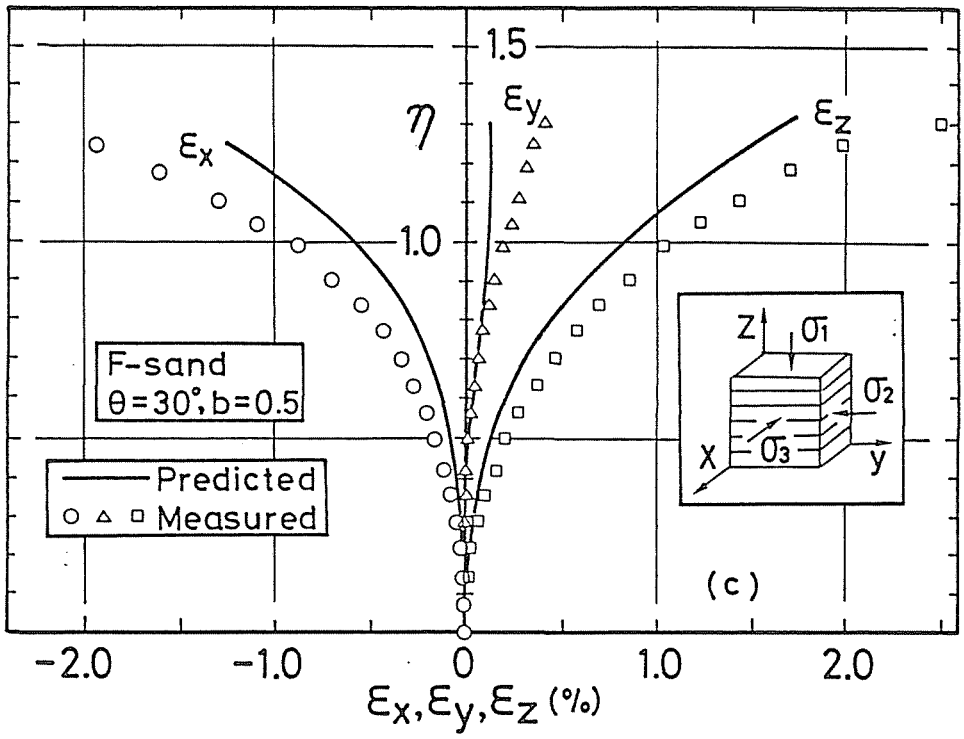

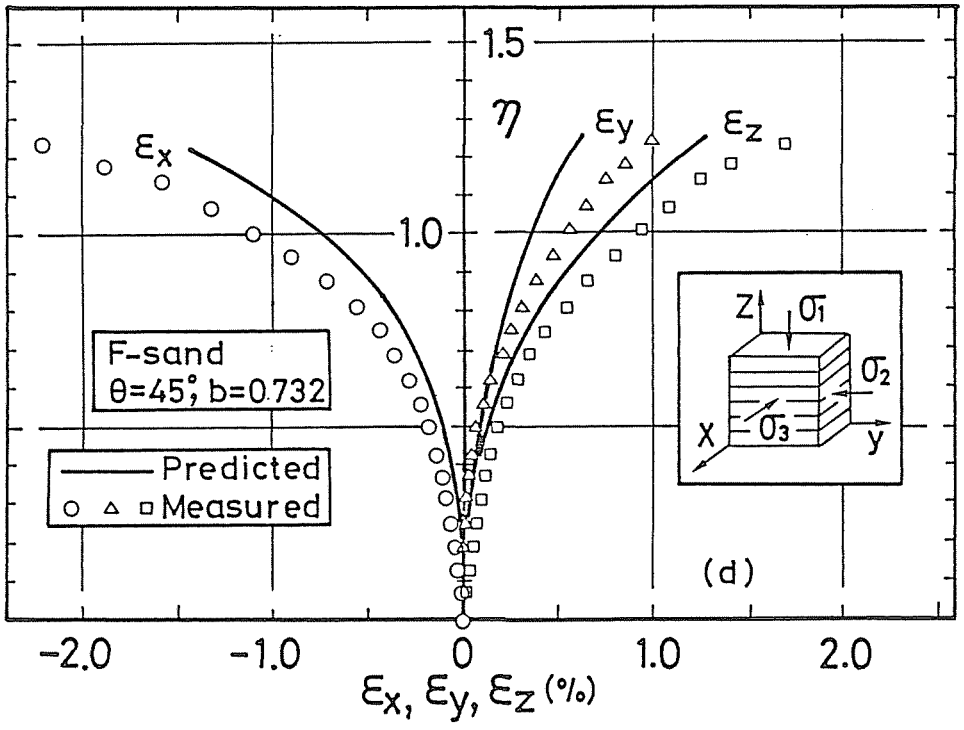

Fig.5-14 Comparisons of measured and predicted relationships between stress ratio and principal strains for F-sand in the stress paths with $\theta = 30^\circ$ (c) and $\theta = 45^\circ$ (d)

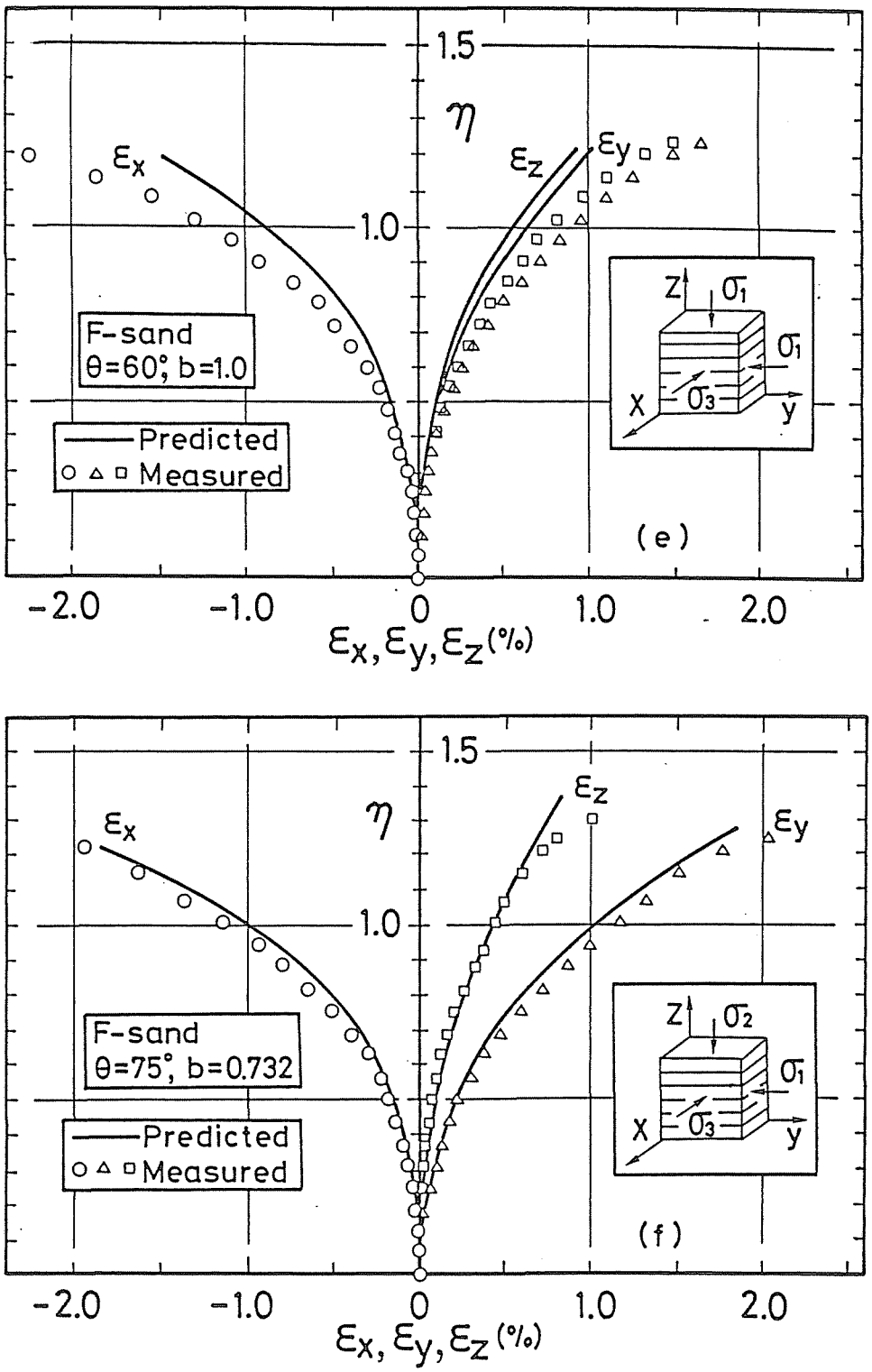

Fig.5-14 Comparisons of measured and predicted relationships between stress ratio and principal strains for F-sand in the stress paths with $\theta = 60^\circ$ (e) and $\theta = 75^\circ$ (f)

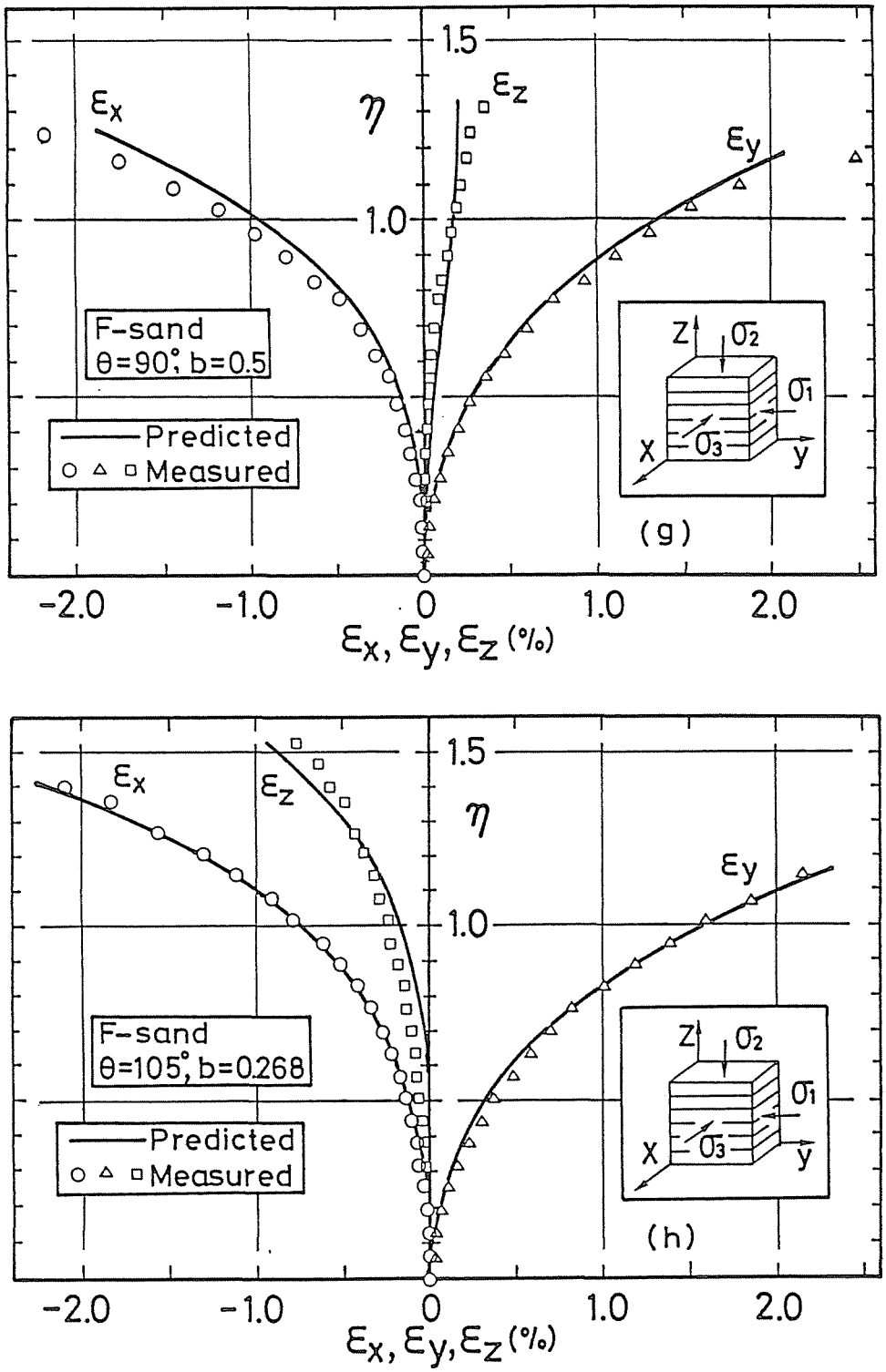

Fig.5-14 Comparisons of measured and predicted relationships between stress ratio and principal strains for F-sand in the stress paths with $\theta = 90^\circ$ (g) and $\theta = 105^\circ$ (h)

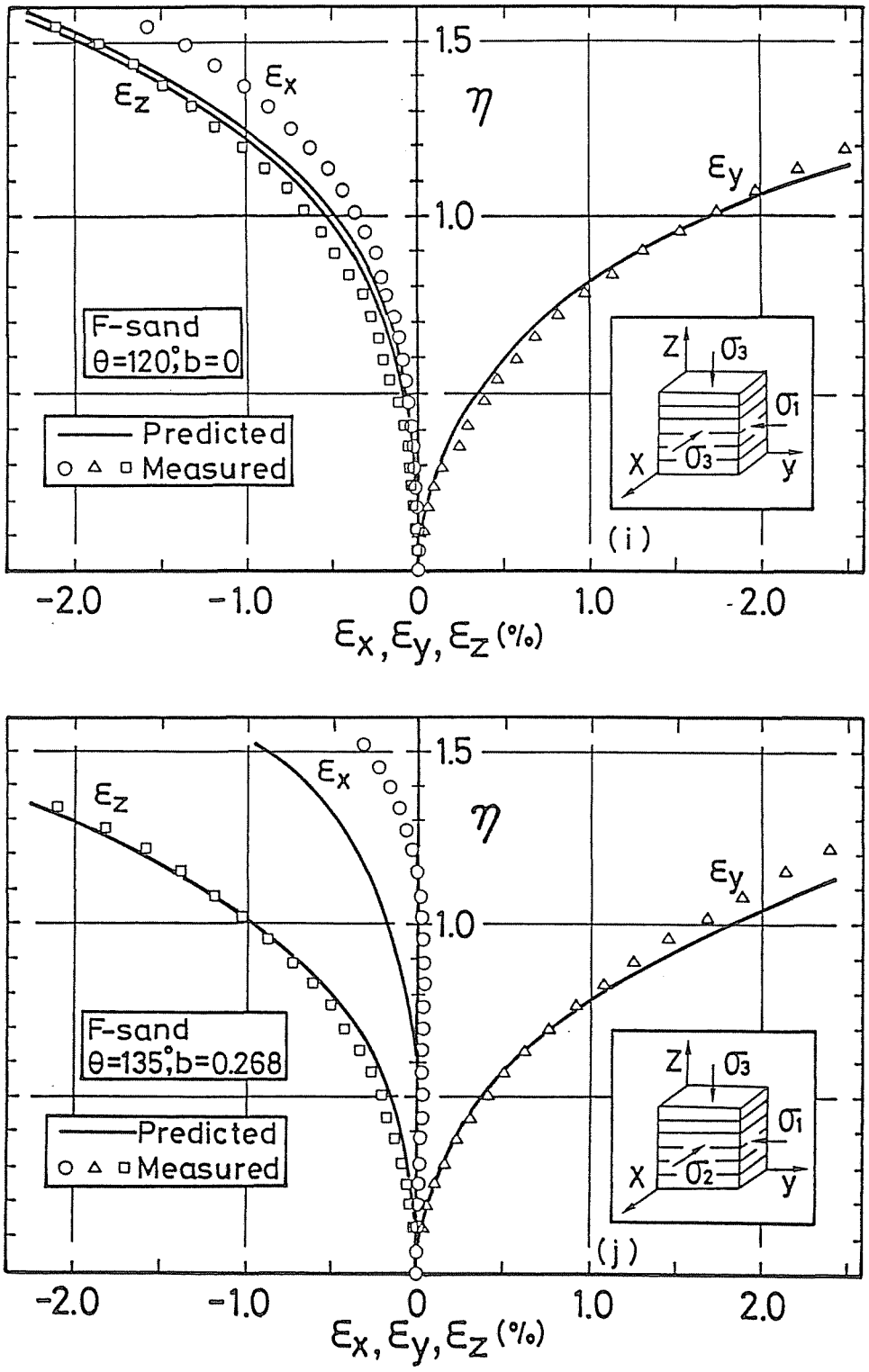

Fig.5-14 Comparisons of measured and predicted relationships between stress ratio and principal strains for F-sand in the stress paths with $\theta = 120°$ (i) and $\theta = 135°$ (j)

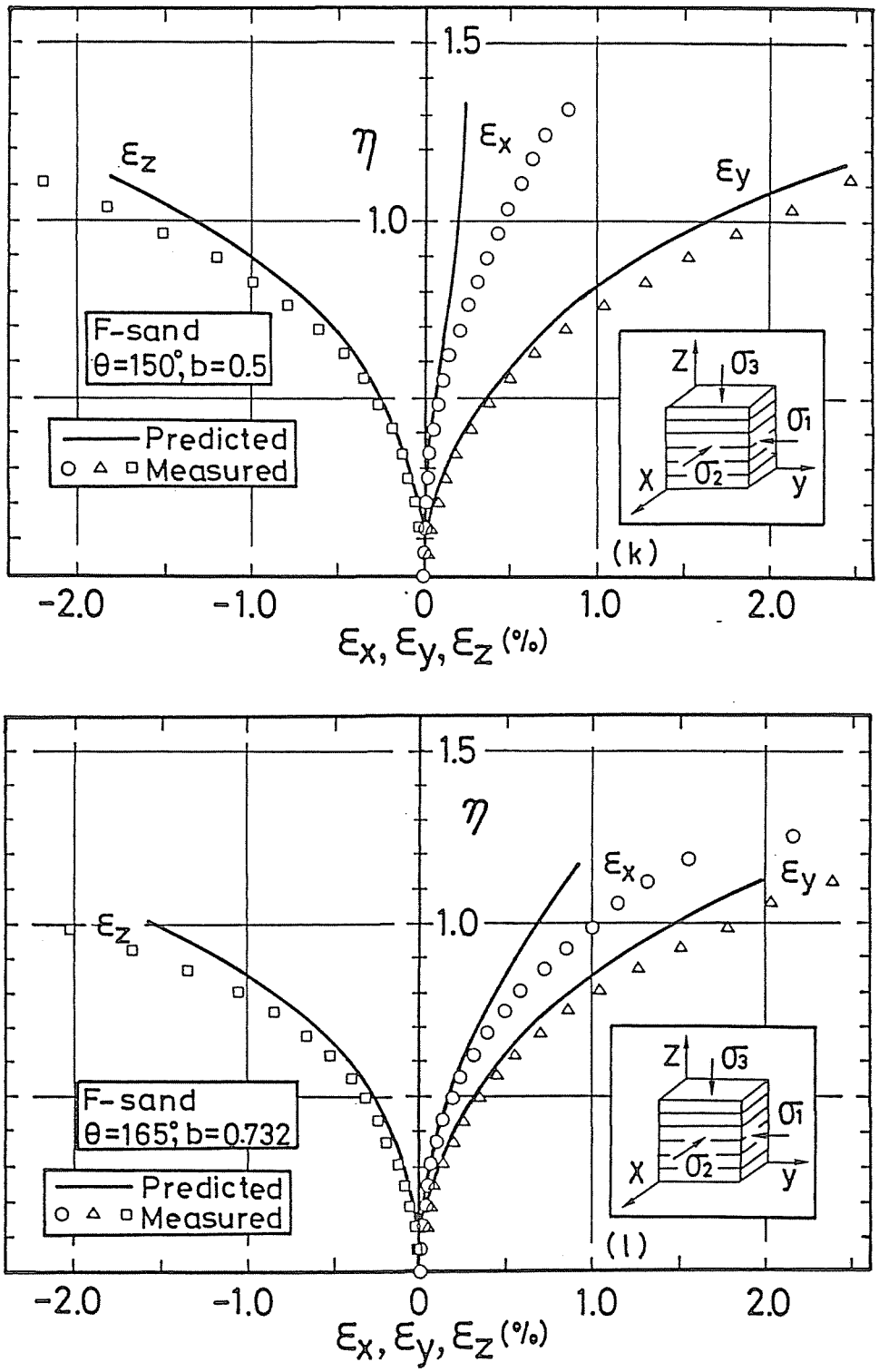

Fig.5-14 Comparisons of measured and predicted relationships between stress ratio and principal strains for F-sand in the stress paths with $\theta = 150°$ (k) and $\theta = 165°$ (l)

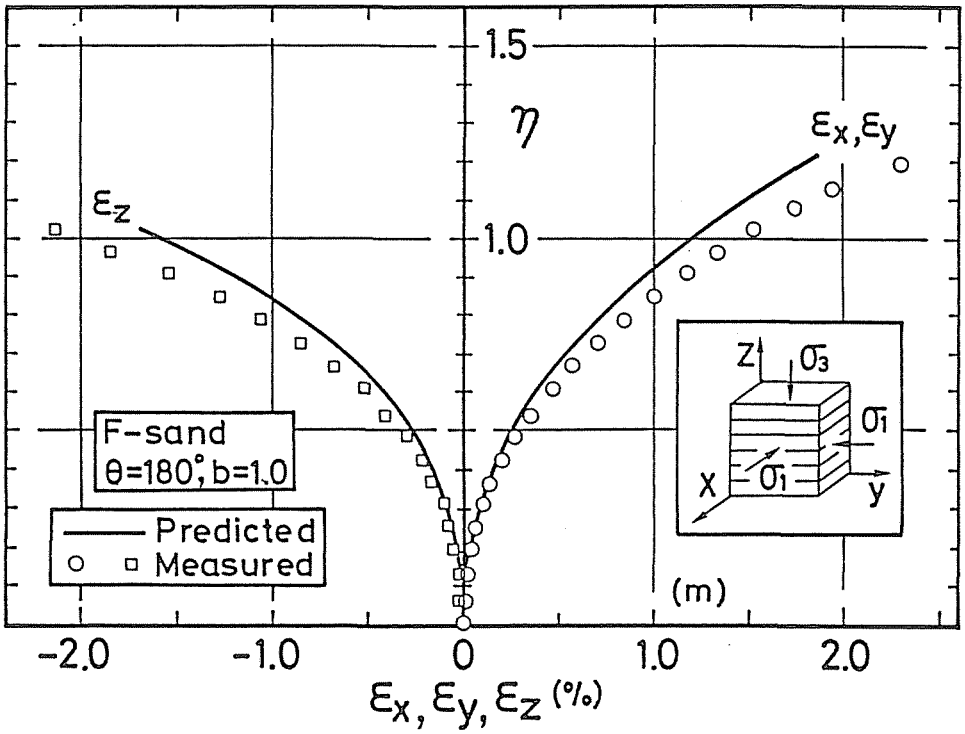

Fig.5-14 Comparison of measured and predicted relationships between stress ratio and principal strains for F-sand in the stress path with $\theta = 180°$ (m)

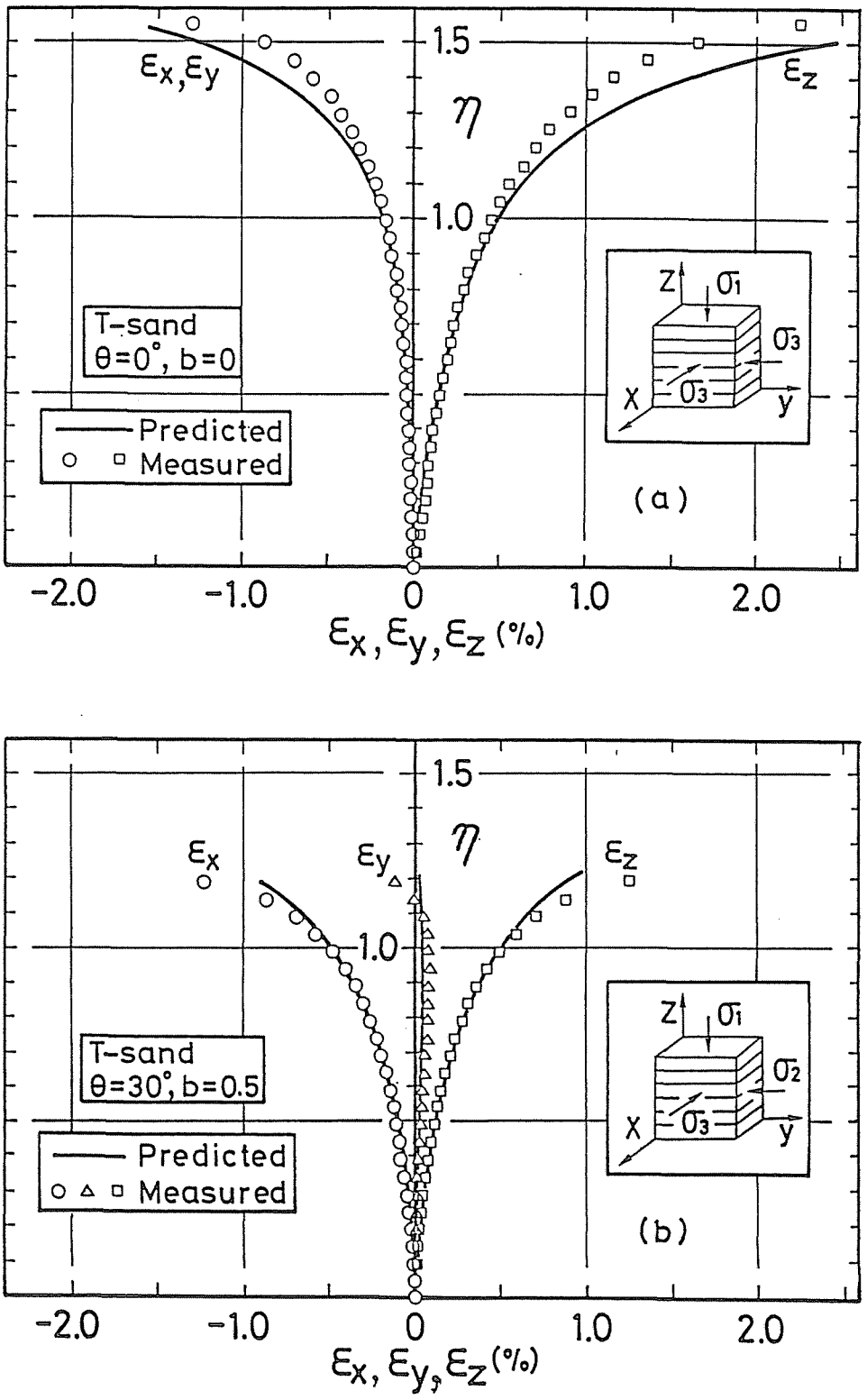

Fig.5-15 Comparisons of measured and predicted relationships between stress ratio and principal strains for T-sand in the stress paths with $\theta = 0^\circ$ (a) and $\theta = 30^\circ$ (b)

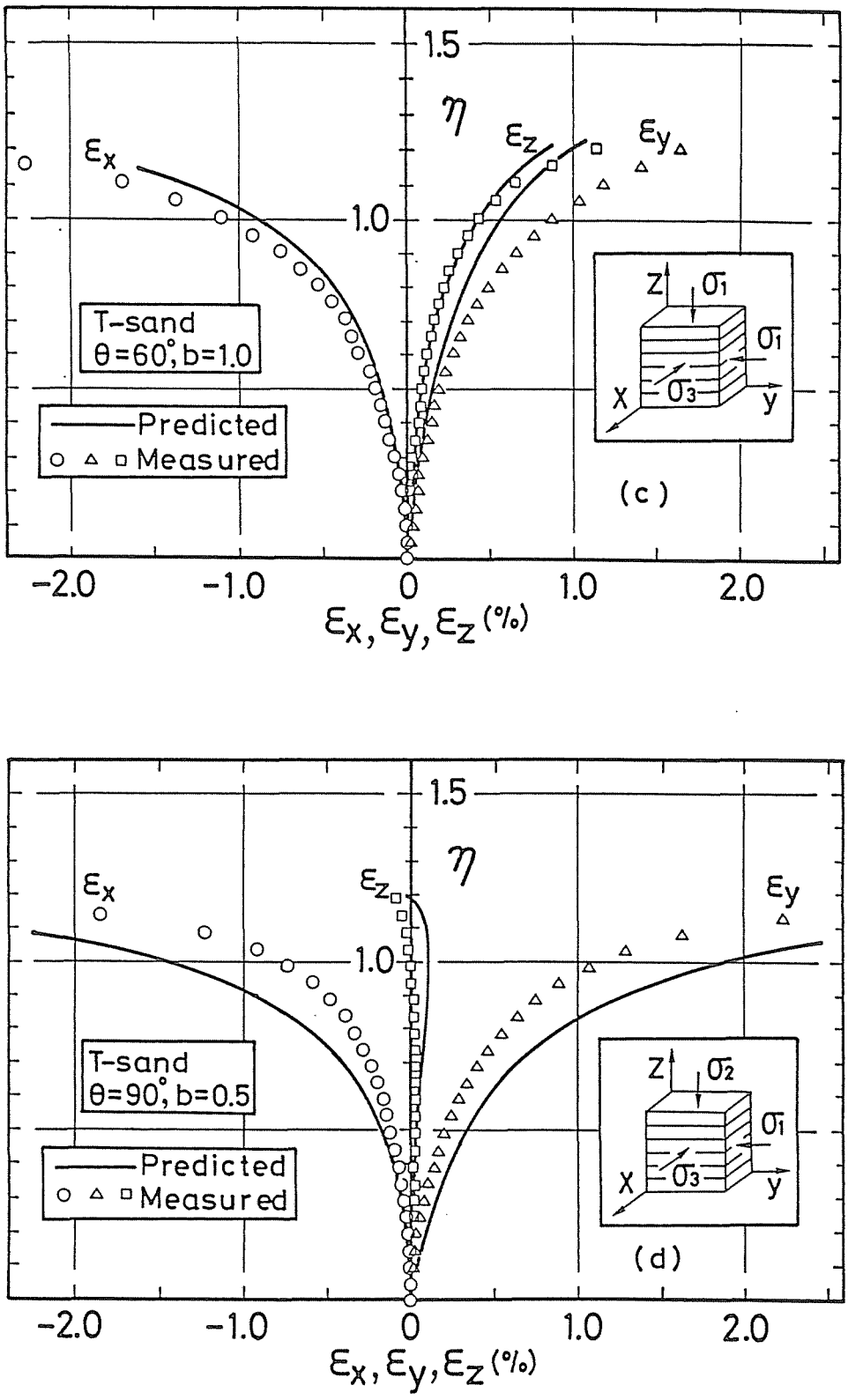

Fig.5-15 Comparisons of measured and predicted relationships between stress ratio and principal strains for T-sand in the stress paths with $\theta = 60°$ (c) and $\theta = 90°$ (d)

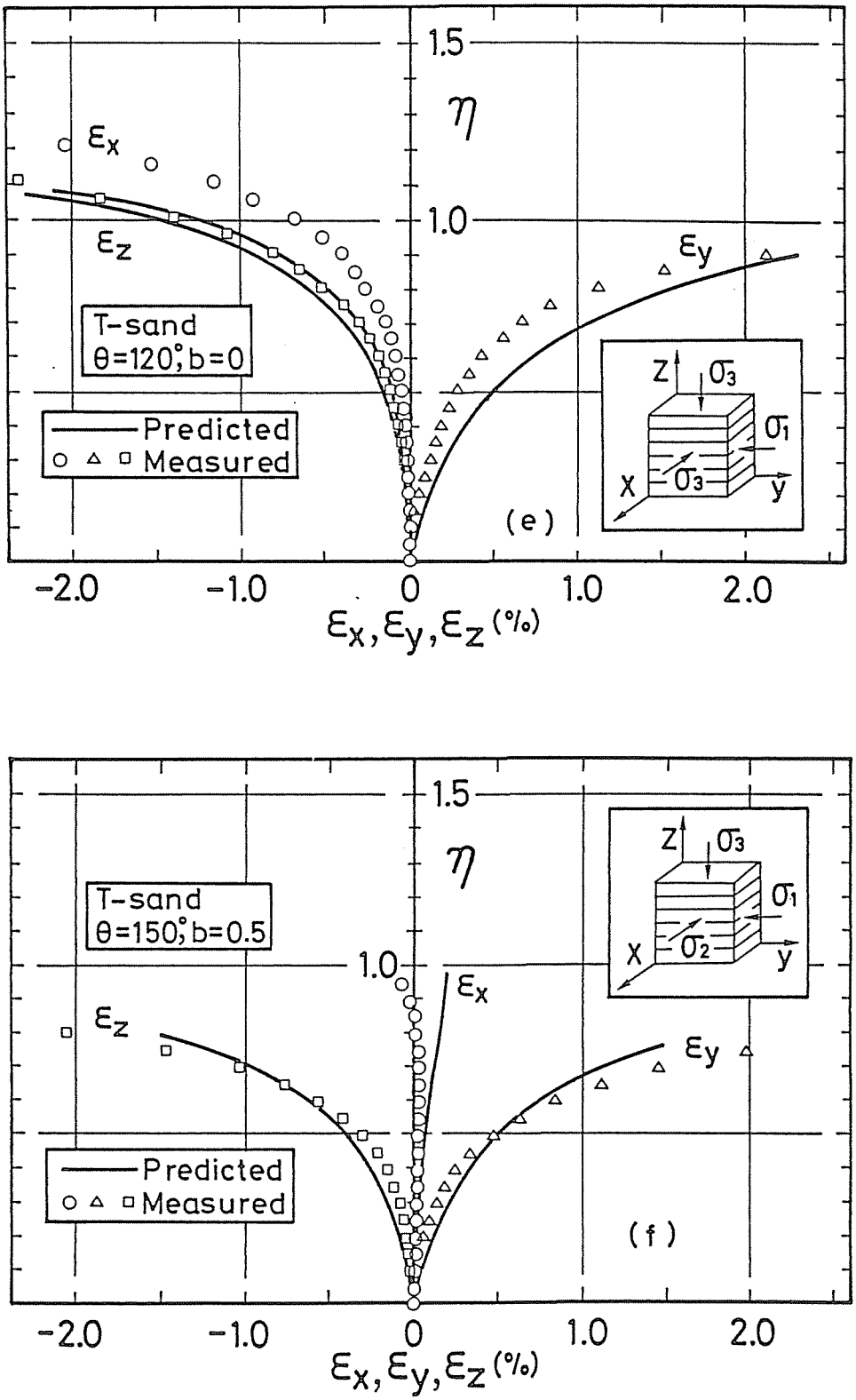

Fig.5-15 Comparisons of measured and predicted relationships between stress ratio and principal strains for T-sand in the stress paths with $\theta = 120°$ (e) and $\theta = 150°$ (f)

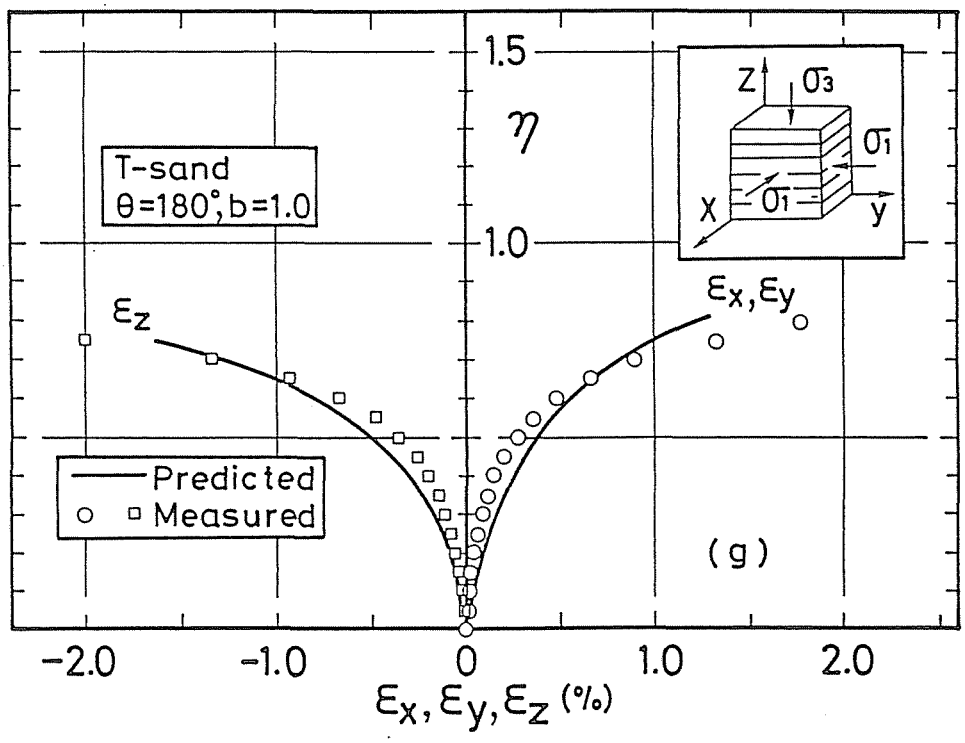

Fig.5-15 Comparison of measured and predicted relationships between stress ratio and principal strains for T-sand with $\theta = 180°$ (g)

conditions of $\theta = 60^\circ$ (triaxial extension tests shown in Fig. 5-14(e) and Fig.5-15(c)) and $\theta = 120^\circ$ (triaxial compression tests shown in Fig.5-14(i) and Fig.5-15(e)), there exists significant difference of the principal strain values induced in the directions with two equal principal stresses values. That is, though the stress systems in these tests are $\sigma_y = \sigma_z > \sigma_x$ ($\theta = 60^\circ$) and $\sigma_y > \sigma_z = \sigma_x$ ($\theta = 120^\circ$), the principal strains are induced with the tendency in which $\varepsilon_y > \varepsilon_z$ and $\varepsilon_x > \varepsilon_z$, respectively. These shear behaviors in both tests are due to the anisotropic mechanical properties of which sand specimens prepared by tapping and pouring or pluviation of sand method are more compressible in the x- and y-directions than in the z-direction and more extensible in the z-direction than in the x- and y-directions. It should be remembered that these anisotropic shear behaviors have been also confirmed for the in-situ natural sand deposits (See Figs.4-14(a) and (b)). The proposed mechanical model could predict qualitatively well the observed tendency as above, whereas degree of coincidence between predicted values and observed ones is slightly unsatisfactory.

Figs.5-16(a) and (b) show the comparisons of the predicted and measured shear strain vs. stress ratio under the stress conditions of $b = 0$ for F- and T-sands, respectively. On the other hand, the comparisons of the predicted and measured volumetric strain vs. stress ratio are shown in Figs.5-17(a)

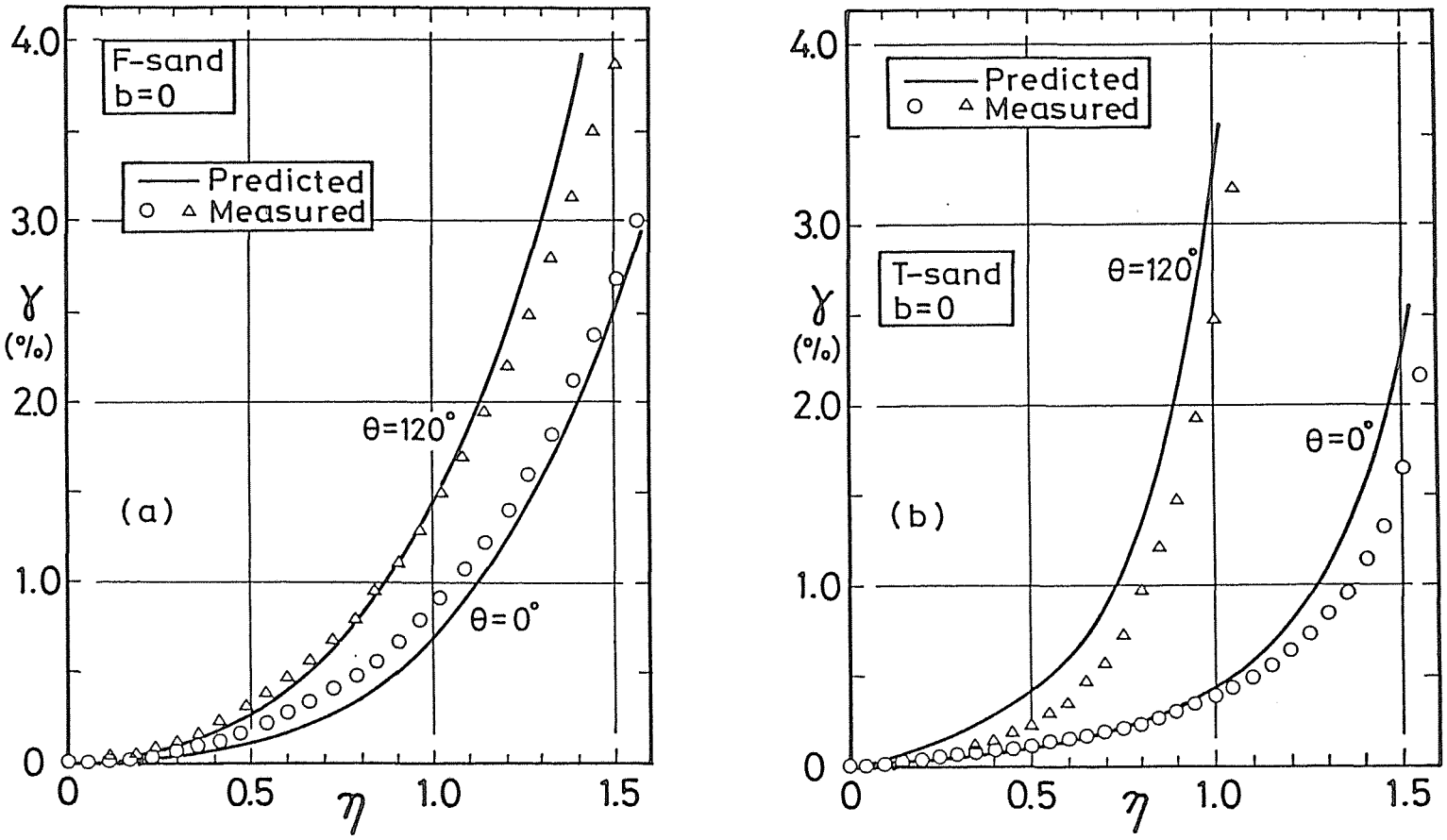

Fig.5-16 Comparisons of measured and predicted stress ratio-shear strain relationships in the test with the same b-value of 0 performed on; (a) F-sand (After data of Yamada and Ishihara (1979)), (b) T-sand

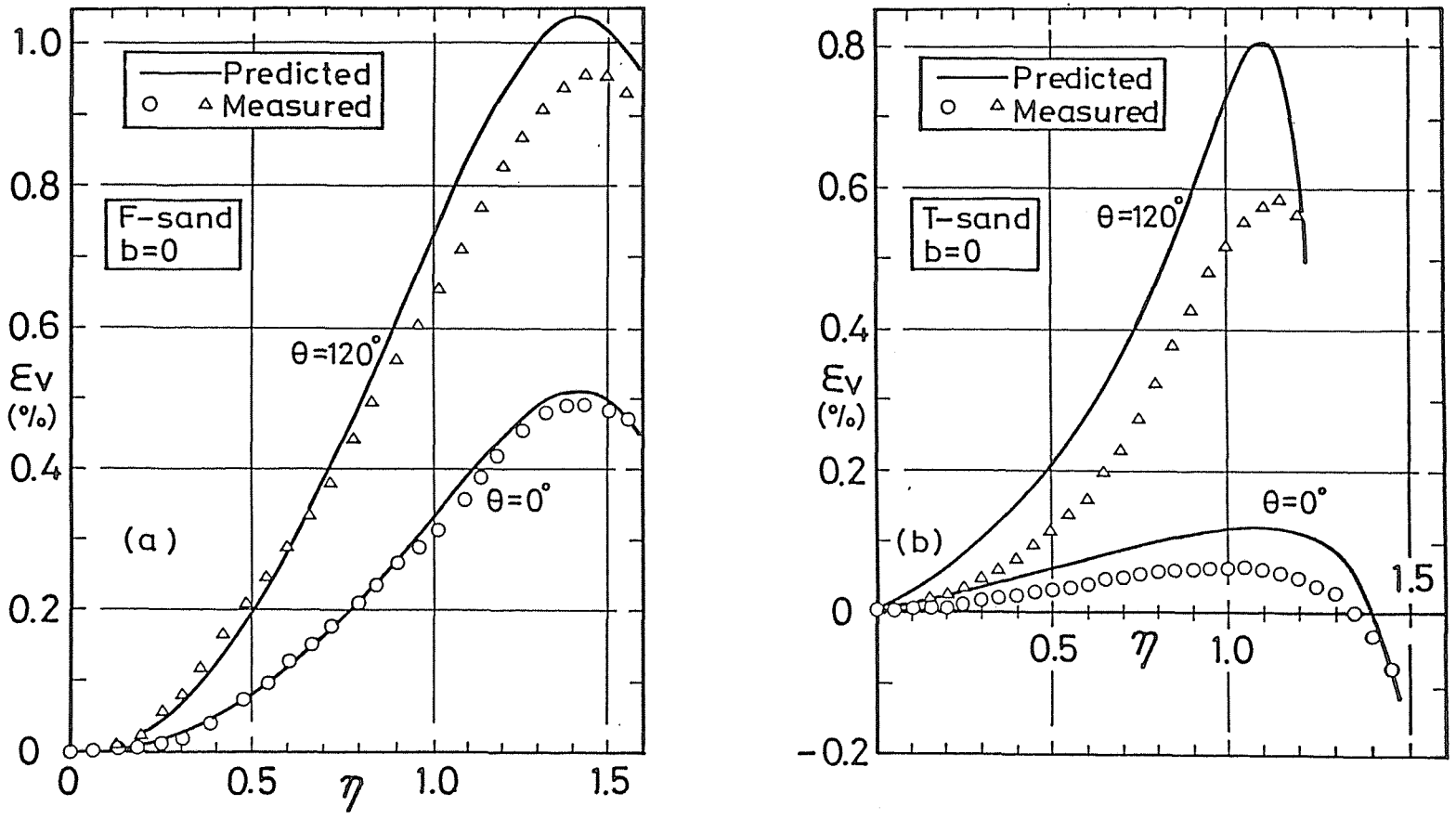

Fig.5-17 Comparisons of measured and predicted stress ratio-volumetric strain relationships in the test with the same b-value of 0 performed on; (a) F-sand (After data of Yamada and Ishihara (1979)), (b) T-sand

and (b) in the same way as shown in the above figures. As can be seen in these figures, this proposed model explains well such observed anisotropic property as deformation characteristics of sands specified by the same b-value can be never coincide by the effect of the inherent anisotropy of sand specimen and the sand specimen is more deformable in the tests with larger θ-values. In the case of other stress conditions for both sands, these facts can be also indicated (Miura et al., 1983a, b).

The relationships between θ-value and each of principal strains, shear strain and volumetric strain at the maximum volume contraction during shear process obtained from the tests on F- and T-sands are compared with the predicted ones in Figs. 5-18 to 5-20. Although it can be seen in these figures that the synthetic effects of the difference in stress system and the fabric anisotropy of specimens exert in the deformability of sands, predicted values by this model agree well with measured ones.

Figs.5-21(a) and (b) represent the comparisons of the predicted and measured equi-shear strain lines and directions of shear strain increment vectors projected on the octahedral stress planes in the range of relatively small shear strains for F- and T-sands. In these figures, the measured and predicted directions of shear strain increment vectors are exhibited by using arrows in the right-half- and left-half-sides

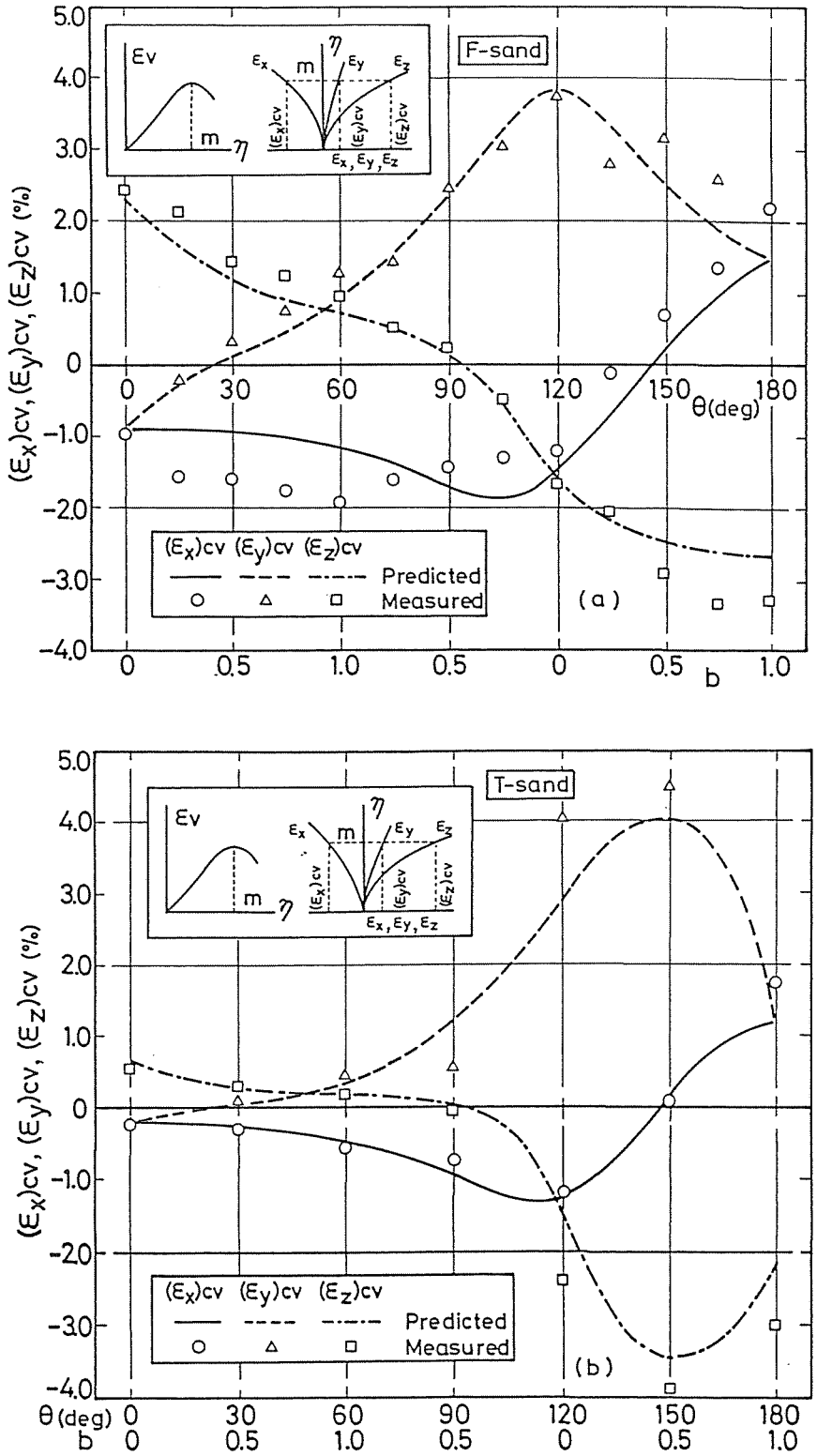

Fig.5-18 Comparisons of measured and predicted principal strains at maximum volume contraction during shear process vs. θ; (a) F-sand (After data of Yamada and Ishihara (1979)), (b) T-sand

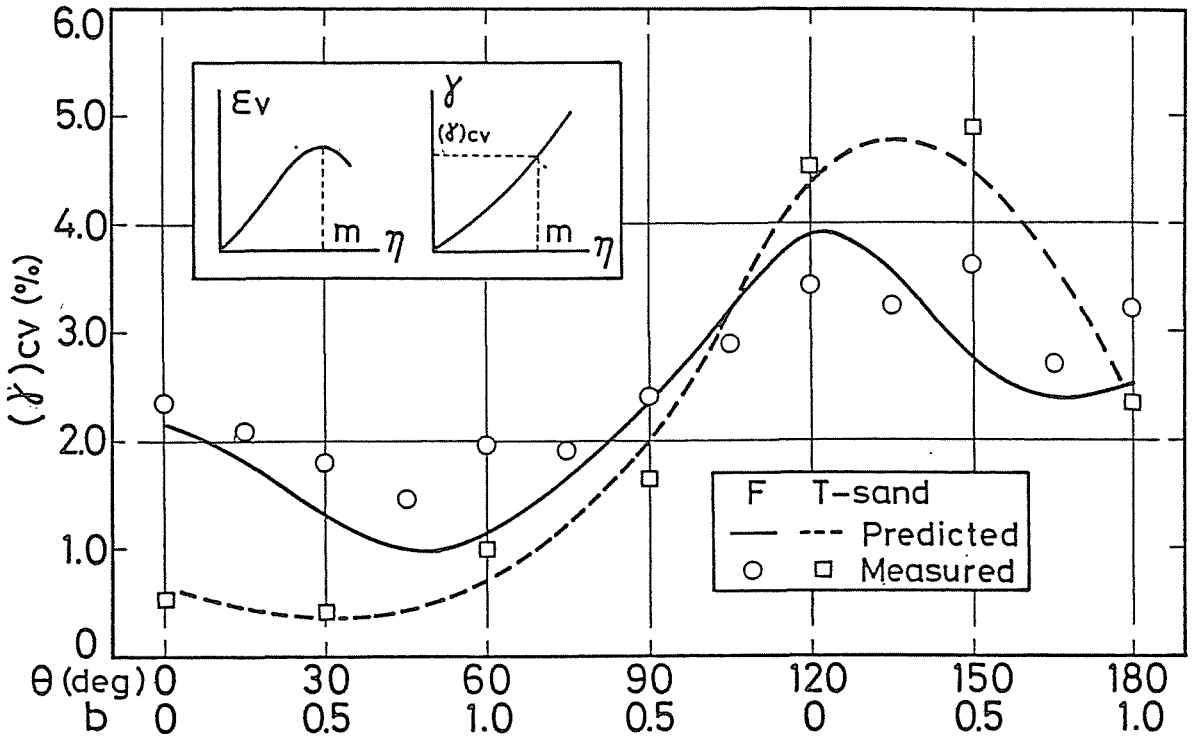

Fig.5-19 Comparisons of measured and predicted shear strain at the maximum volume contraction during shear process vs. θ for F- and T-sands (Test data of F-sand from Yamada and Ishihara (1979))

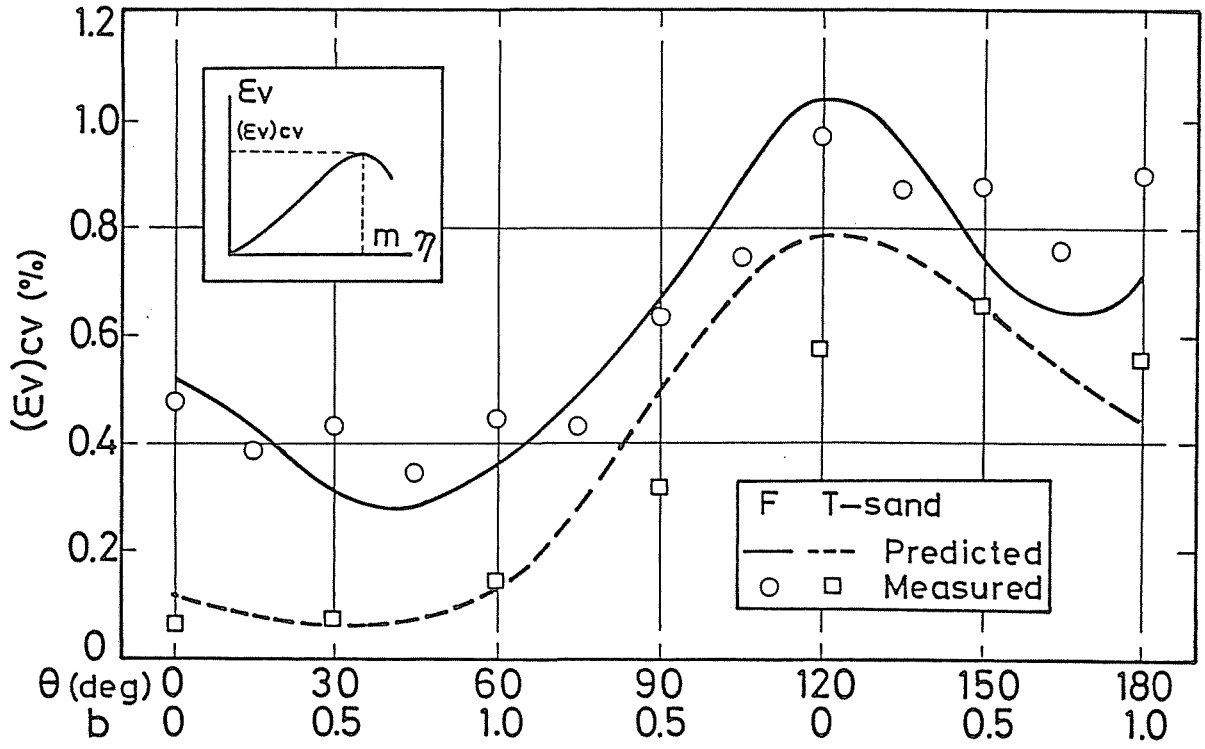

Fig.5-20 Comparisons of measured and predicted volumetric strain at the maximum volume contraction during shear process vs. θ for F- and T-sands (Test data of F-sand from Yamada and Ishihara (1979))

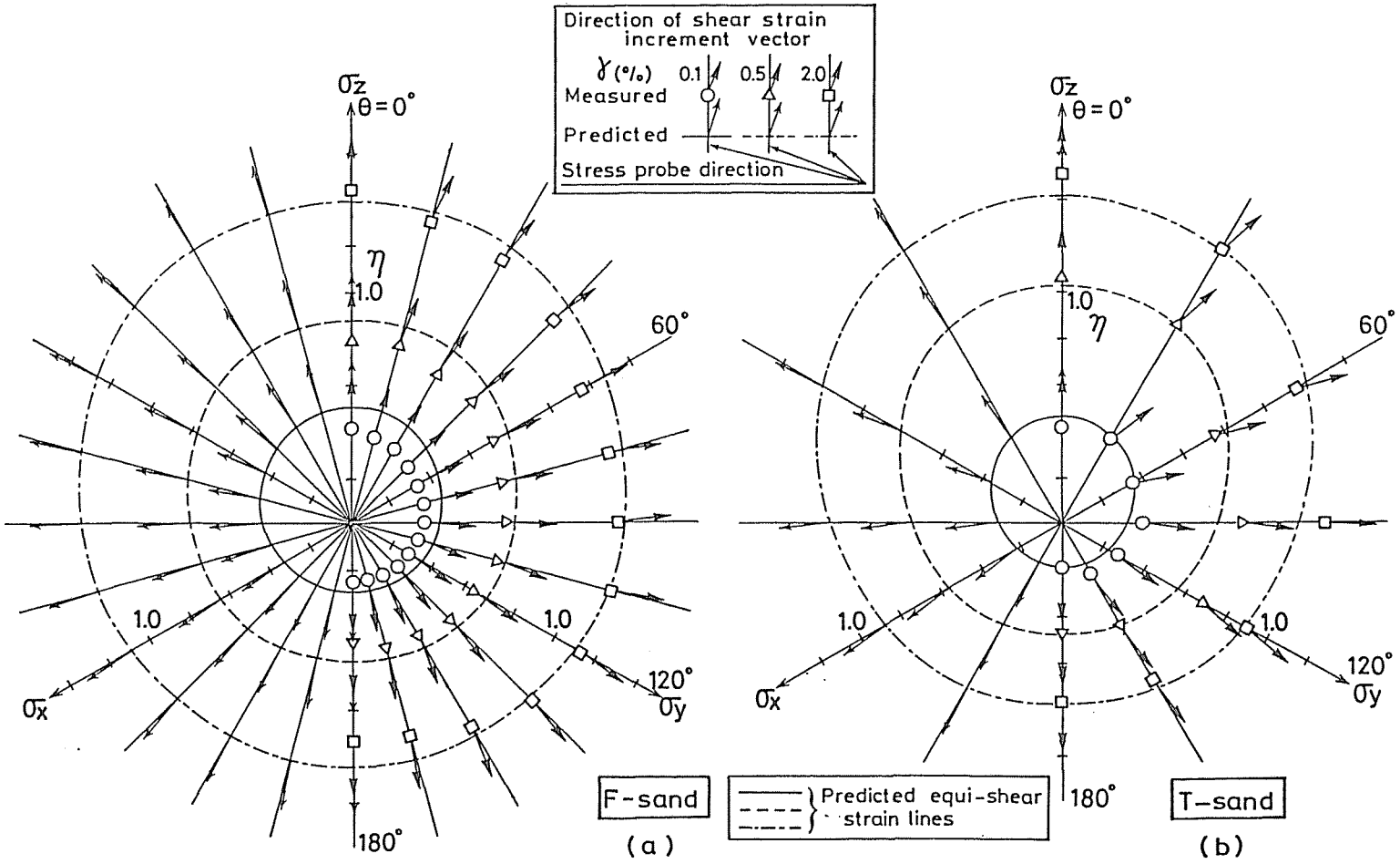

Fig.5-21 Comparisons of measured and predicted equi-shear strain lines and directions of shear strain increment vectors at prefailure projected on octahedral stress plane; (a) F-sand (After data of Yamada and Ishihara (1979)), (b) T-sand

of the octahedral stress plane, respectively. The shear strain increment vectors shown in Fig.5-21 must be oriented symmetrically with respect to the directions of $\theta = 60^\circ$ and 120°, if the sand specimen has the isotropic fabric. Because of the fabric anisotropy of sand specimens, however, the shear strain increment vectors observed in the tests deviate from the corresponding stress paths and are always more oriented in the clockwise direction. It may be considered from these figures that the equi-shear strain lines and the directions of shear strain increment vectors calculated by the present model reveal well the observed tendency.

Therefore, estimation is now possible on the drained stress-strain behaviors of the anisotropic specimen whose fabric characteristics are very similar to those of the in-situ natural sand deposits under the general stress conditions using the data obtained from the conventional triaxial compression and extension tests and the isotropic consolidation-swelling test.

5.6 Predicted Stress-Strain Behavior of Sand with Isotropic Fabric

As explained in the preceding paragraphs, deformation-strength behavior of sand is influenced strongly by the stress system and fabric anisotropy. In order to make quantitatively each of both influence factors clear, first of all, the deformation behavior of sand with the isotropic fabric must be examined. However, the laboratory examination concerning this subject is difficult to perform, since no entirely satisfactory method for preparing the uniform and isotropic sand sample has yet been developed. The proposed mechanical model could predict the three-dimensional deformation behavior of the isotropic sand, by substituting the isotropic hardening function h_G (corresponding to $\theta = 90^\circ$) for the hardening functions in each of three two-dimensional stress systems.

Figs.5-22(a) and (b) show the stress ratio vs. principal strains relationships under the stress conditions of $b = 0$ and 1 for F- and T-sands with the hypothetical isotropic fabric, respectively. Since both sands have the isotropic fabric, it is a natural course that there is no difference between the strain components which occur in the directions with the equal principal stresses.

Figs.5-23(a) and (b) represent the predicted volumetric strain vs. stress ratio relationships for the isotropic F- and

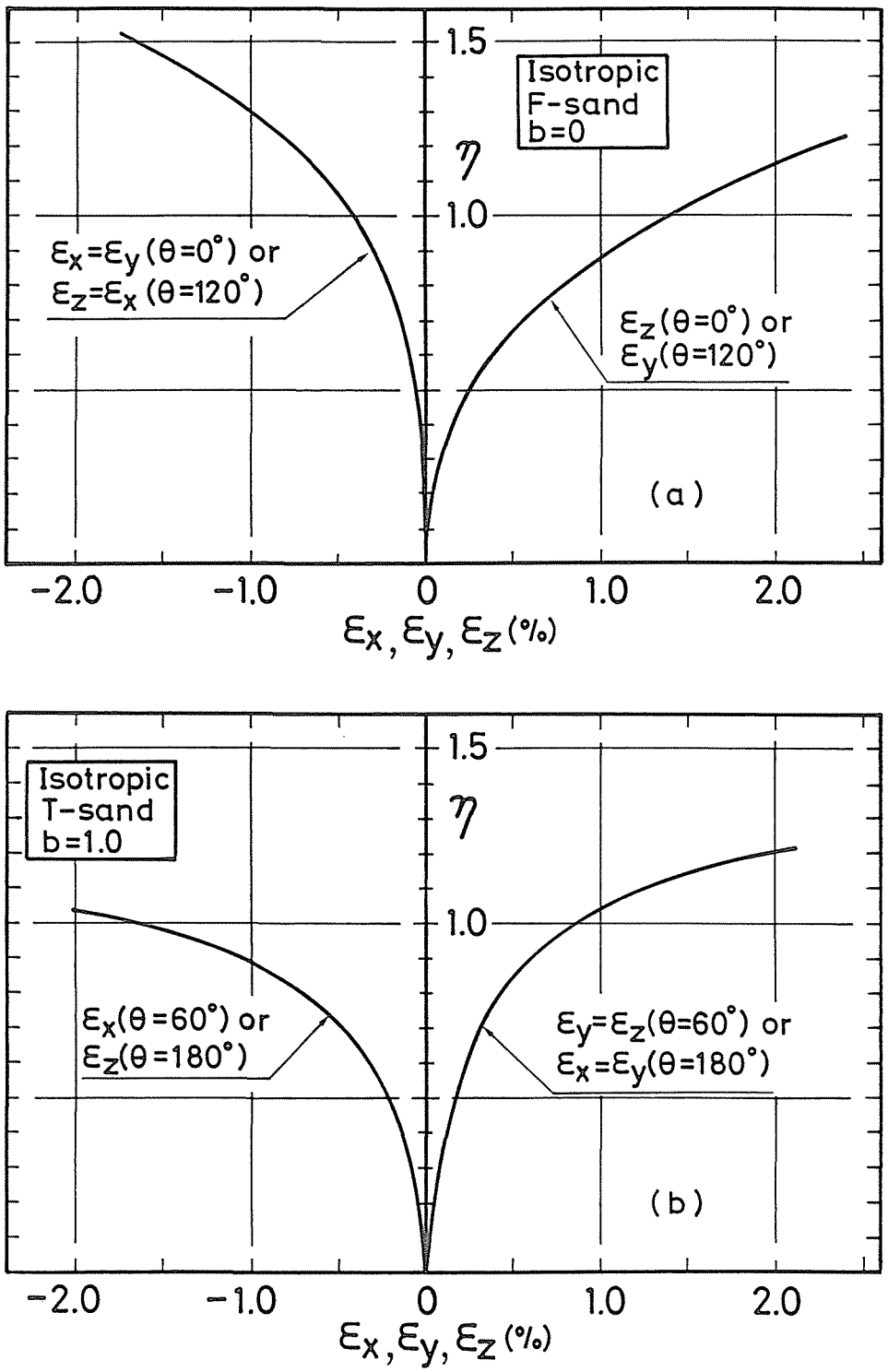

Fig.5-22 Predicted stress ratio vs. principal strains relationships for sand with isotropic fabric; (a) F-sand, (b) T-sand

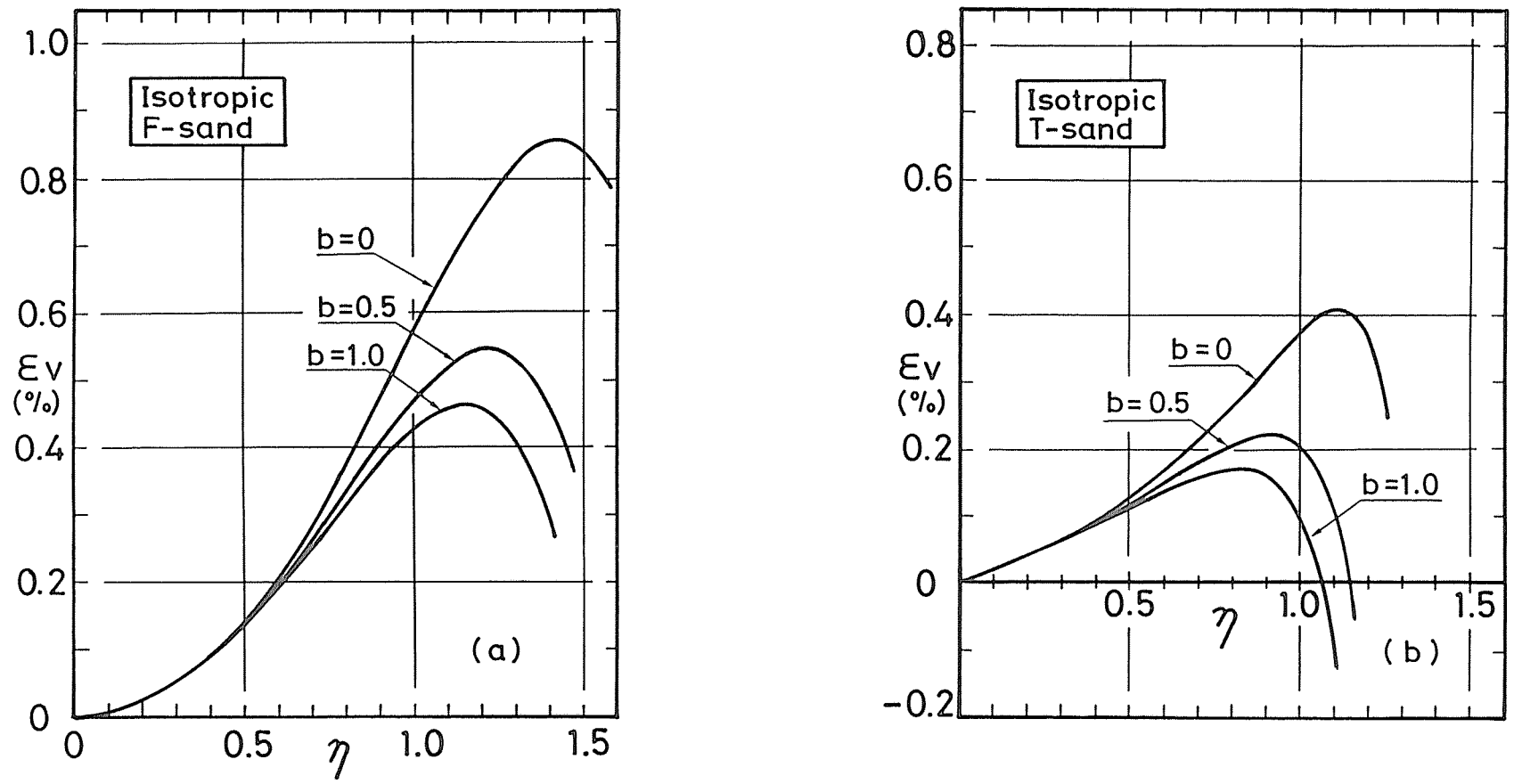

Fig.5-23 Predicted stress ratio vs. dilatancy relationships for sand with isotropic fabric; (a) F-sand, (b) T-sand

T-sands with b = 0, 0.5 and 1.0. Dilatancy behavior comparison of both isotropic sands suggests that the volume contraction during shear is the largest for the triaxial compression condition (b = 0) and the smallest for the triaxial extension condition (b = 1.0).

Shown in Fig.5-24 is the comparison of the shear strain and volumetric strain induced at the maximum volume contraction between the anisotropic and isotropic sands in any stress systems. It is confirmed in the figure that the fabric anisotropy of sand may produce the effects in which the strain occurrences are restrained at the stress systems with smaller θ-values than $70^\circ \sim 90^\circ$ and promoted at larger values than $70^\circ \sim 90^\circ$. Fig.5-24 also indicates that the influence of inherent anisotropy on the deformation behavior is more remarkable in T-sand than in F-sand.

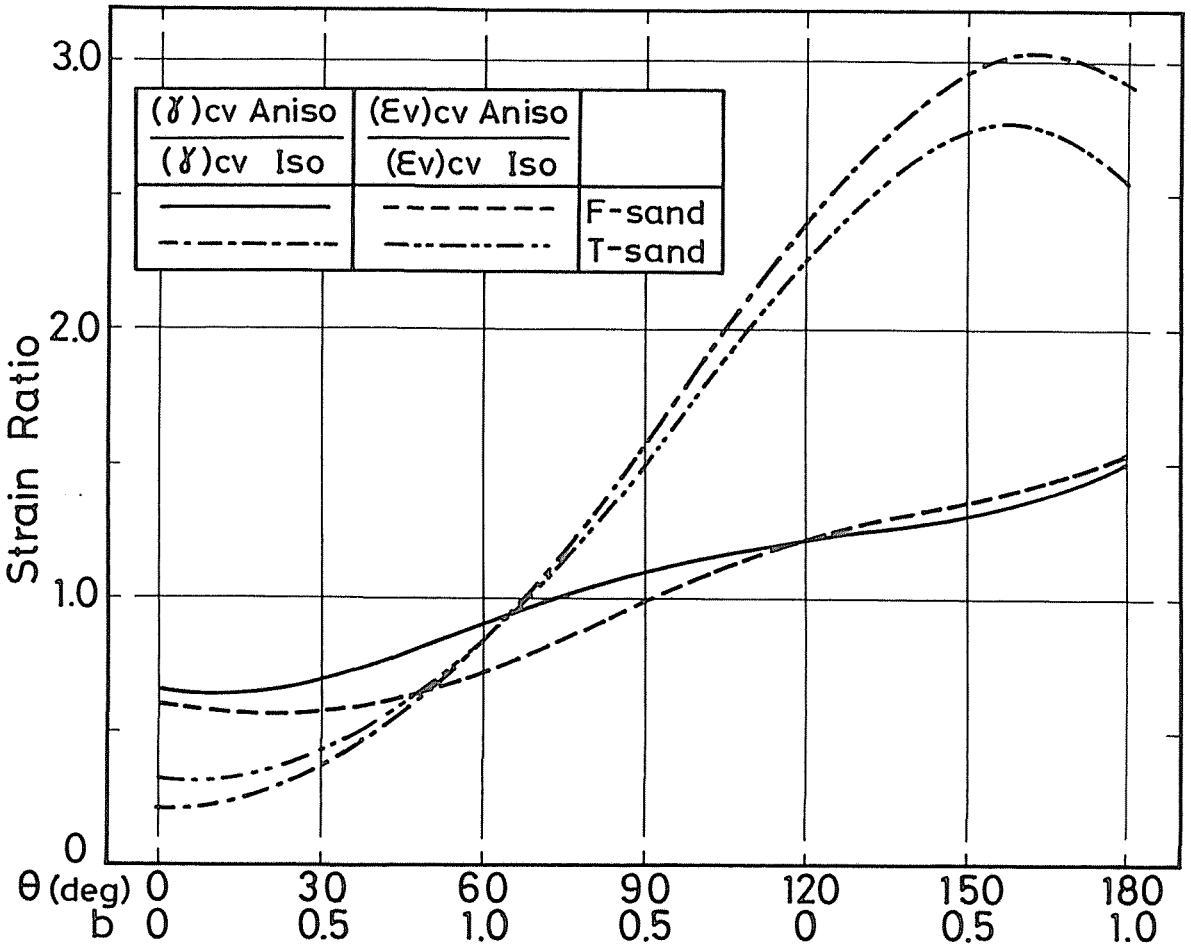

Fig.5-24 Influence of inherent anisotropy on the deformability of sands in any stress systems

CHAPTER 6 CONE PENETRATION CHARACTERISTICS AND ITS CORRELATION TO STATIC AND CYCLIC DEFORMATION-STRENGTH BEHAVIORS OF ANISOTROPIC SAND

6.1 Introduction

The data of sounding such as the standard penetration test and the cone penetration test has been employed as a convenient parameter to express the in-situ mechanical properties of sandy soils, despite its limitation as to lack of rigid standardization. For example, an indirect method, in which the angle of shearing resistance, deformability and liquefaction potential of cohesionless soils under the in-situ conditions are estimated through the value of relative density from the data of the sounding performed in the fields, has been universally adopted. As explained previously, the natural in-situ sand deposits possess the anisotropic mechanical properties which may be attributed to the fabric anisotropy formed by the parallel alignments of particles induced during depositing process. Therefore, these facts that the deformation-strength characteristics of sands are controlled not necessarily only by relative density but also by fabric anisotropy could be by no means ignored in the field of geotechnical engineering and should be also considered in the estimation of the

in-situ mechanical property from the data of sounding as the standard penetration test and the cone penetration test.

The study in this chapter is aimed to make the correlation between static cone penetration characteristics and mechanical properties for sand with anisotropic fabrics clear, since the static cone penetration test could be expected to detect continuously the changes in mechanical properties with the depth of sand grounds. Accordingly, in order to predict the in-situ anisotropic mechanical properties from the data of the cone penetration test, it is necessary to examine in detail whether the cone penetration test can trace out the anisotropy with respect to mechanical properties of sand or not.

Recently, the laboratory investigations of the effects of various factors on the cone penetration resistance of sands have been performed mainly by using the cone penetrometer. For example, Durgunoglu and Mitchell (1975a, b) have shown from the observation of failure mechanism in a sand deposit due to cone penetration that the penetrometer base characteristics influence on the cone penetration resistance values, and they have derived a penetration resistance equation which can take account of the penetrometer base characteristics.

Based on the experiments on the relations between cone penetration resistance and effective overburden pressure for sands with various relative densities, Schmertmann (1975) has proposed a method in which the angle of shearing resistance is estimated from the relative density evaluated by the cone

penetration resistance values. He has also pointed out the importance of the effects of overconsolidation on the cone penetration resistance in cohesionless soil.

More recently, the direct relationships between the results of static cone penetration tests in a calibration chamber and triaxial mechanical properties for sands have been examined by Chapman and Donald (1981) and Baldi et al. (1981, 1982).

Although the studies on the cone penetration resistance of sands have been widely executed as above mentioned, test data concerning the influence of fabric anisotropy on the cone penetration characteristics of cohesionless soils are extremely limited in number. In this chapter, the present author will discuss the effects of fabric anisotropy on the cone penetration characteristics and the correlation between the static and cyclic deformation-strength properties and the cone penetration characteristics for triaxial sand specimens formed by various preparation methods. Above all, the measured cone penetration resistances will be verified on the basis of the cavity expansion theory for sand proposed by Vesic (1972), and it will be indicated that anisotropic dilatancy characteristics due to cone penetration must be considered in its theoretical analysis.

6.2 Test Apparatus and Procedure

The testing equipment used in the present study belongs to a quite conventional triaxial type with the specimen size of 70 mm in diameter by 170 mm in height. In order to perform the static cone penetration tests on the specimens with the same stress conditions as those of the static and cyclic triaxial tests, a cone penetration system is incorporated into the conventional triaxial device, as shown in Fig.6-1(a). It would be considered that these improvements permit the direct comparisons between the data of the static and cyclic triaxial tests and the cone penetration tests, as both tests are carried out on the specimens with the same fabric characteristics. Loading ram in this apparatus is of the double-acting type in which the inner loading ram (A) and the outer loading ram (B) are movable independently. That is, loading ram (A) which is used for the cone penetration is fixed perfectly to loading ram (B), when performing the static and cyclic triaxial tests. On the other hand, in the static cone penetration test, the cone can be penetrated into the sand specimen by applying the loads to loading ram (A), while loading ram (B) is fixed to the top cap.

Fig.6-1(b) shows the cone set in the loading cap. The rubber O-rings fitted in the casing can intercept completely the inside of loading cap from the sand specimens during the

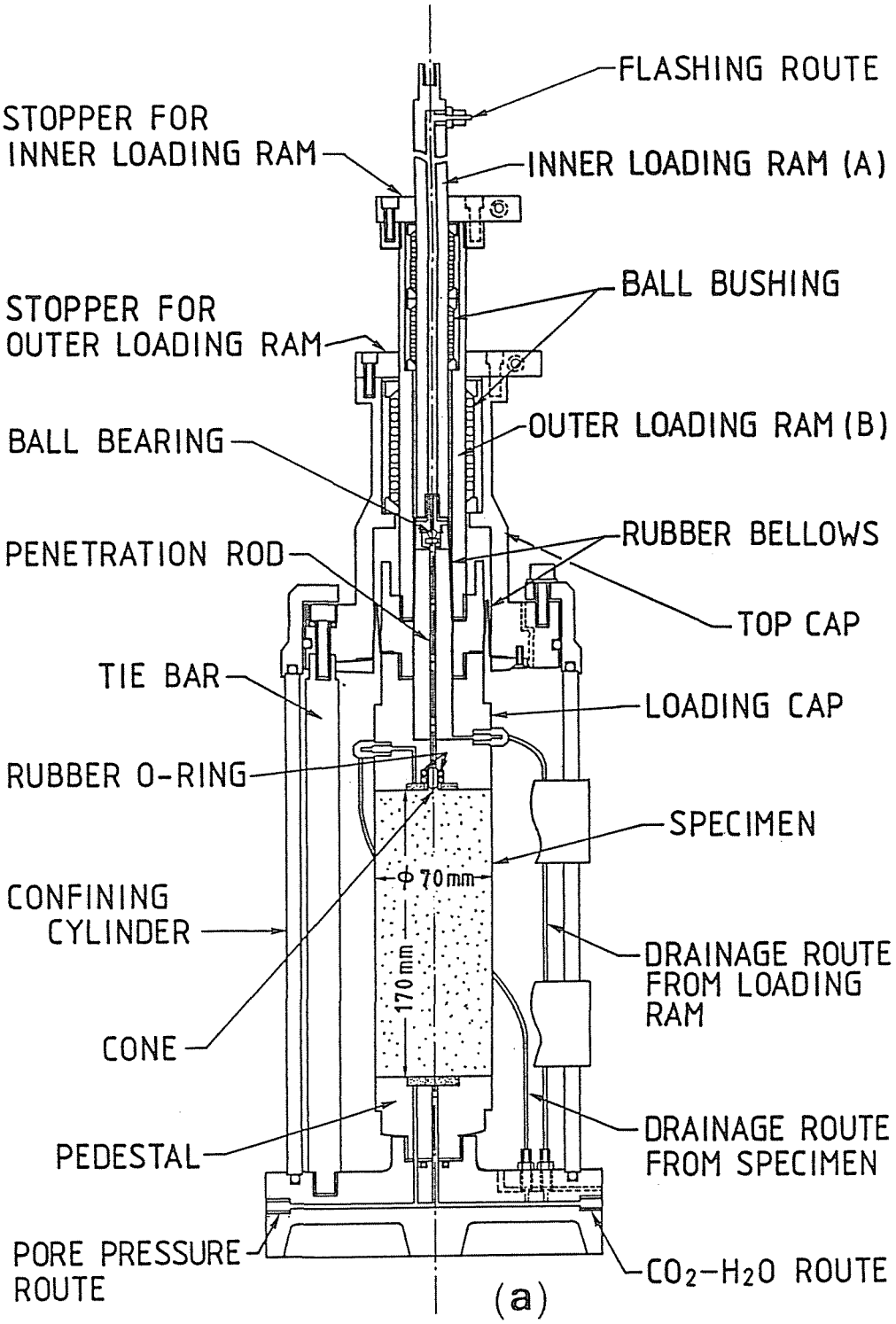

Fig.6-1(a) Schematic diagram of triaxial device improved for cone penetration test

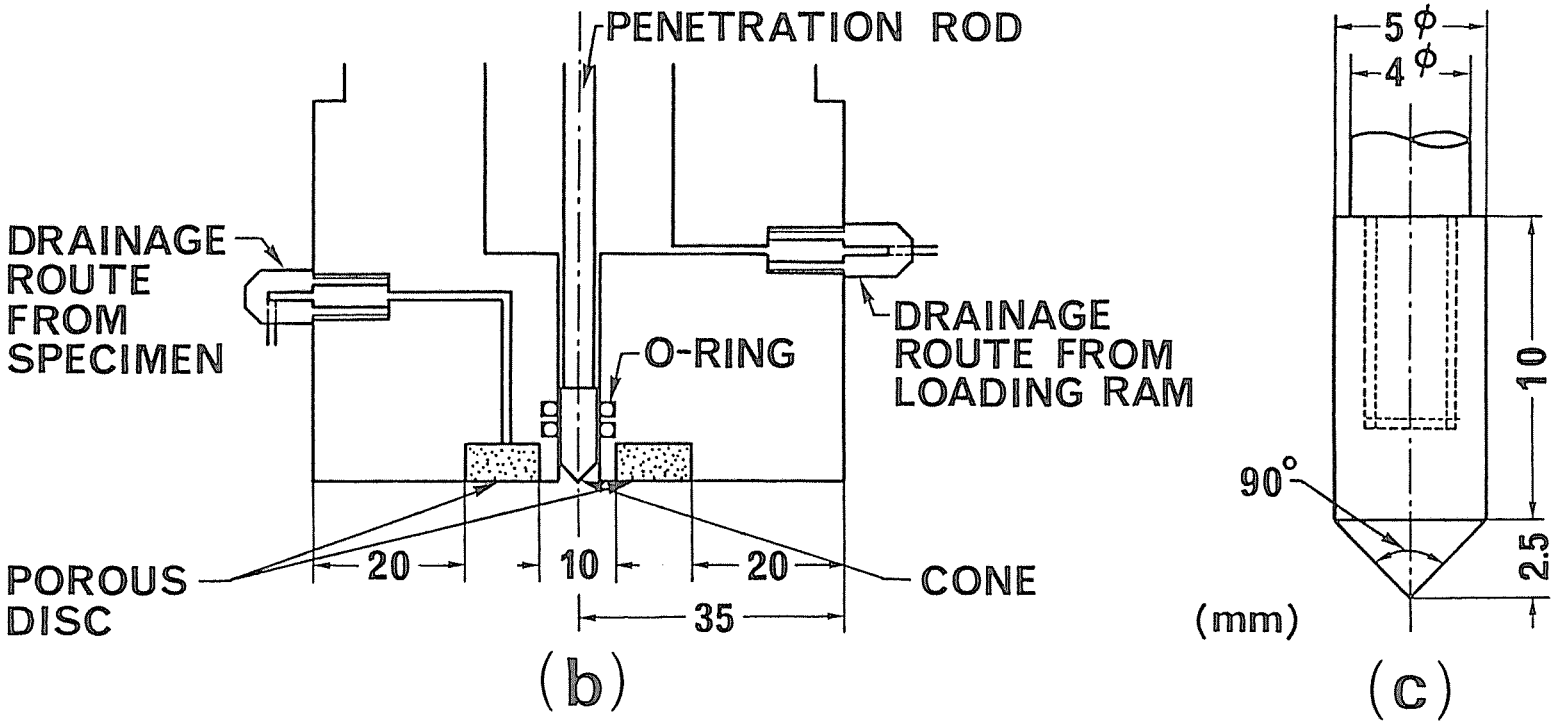

Figs.6-1(b) and (c) Details of loading cap (b) and point of cone (c) used in the present study

triaxial tests. Furthermore, the procedure with which the casing isolated from the external atmosphere by rubber bellows is filled with de-aired water and applied the same back pressure as that of specimen can prevent the stress release and the variation of the degree of saturation in the sand specimens during the cone penetration tests. The polished stainless steel cone employed in this study has an apex angle of 90°, as shown in Fig.6-1(c). Its diameter and sectional area are 5 ^{mm} and 19.6 $^{mm^2}$, respectively. The diameter of penetration rod is 4 ^{mm}. The shape and dimension of the cone mentioned above were determined based on the assumption of the expansion pattern of plastic zone due to cone penetration by Meyerhof (1961) and the diameter of triaxial specimen (70 ^{mm}) employed in the present study.

The discussion in this study is based on the test data of T-sand specimens which are prepared according to the sample preparation methods mentioned previously.

Static cone penetration test procedure

After each T-sand specimen was set up in the cell and then the cell pressure was raised to 19.6 kPa, carbon dioxide was percolated through the specimen for about 30 minutes. The frozen specimen is allowed to melt under the confining pressure of 19.6 kPa, before percolating the carbon dioxide. Subsequently, de-aired water was permeated into the voids at

a small differential head (4.9 kPa) so as to be free from the disturbance of initial fabrics. Back pressure of 196 kPa was, thereafter, applied for about one hour to insure the saturation of specimen. By this procedure, Skempton's B-value of greater than 0.98 was obtained in all specimens. Cell pressure was increased up to a desired value to give the isotropic stress condition. After consolidating for two hours, the cone penetration tests were performed, while the value of back pressure was maintained constant. These tests were carried out under the effective consolidation pressure σ_c' $(= p_c) =$ 196 kPa unless otherwise specified.

A series of static cone penetration tests on T-sand specimens with the relative densities after consolidation D_{rc} over the range from about 50 % to 100 % was conducted under the drained conditions at low penetration rate such as 2.8 mm per minute. Accordingly, no developments of the pore water pressure in the specimens due to cone penetration can be observed during the tests. The cone was penetrated continuously to the penetration depth of 100 mm which is defined in this study as the distance from the top of specimen. The penetration force and the amount of drainage from the specimen were measured at intervals of the penetration depth of 5 mm. Based on these measurements, the cone penetration resistance q_c and the volume change due to cone penetration ΔV were calculated.

The procedure for the static and cyclic triaxial tests

is the same as that explained in CHAPTER 3. A series of drained triaxial compression and extension tests was performed under the constant effective consolidation pressure (σ_c' ($= p_c$) = 196 kPa) for T-sand specimens with the values of D_{rc} over the range from about 50 % to 100 %. In cyclic undrained triaxial tests, D_{rc} after isotropic consolidation at σ_c' = 196 kPa was mainly selected as 55 %. To avoid the effect of variation of initial specimen density from the desired one, the variations in D_{rc} of all specimens were limited to the extent within ±3 %.

6.3 Effect of Fabric Characteristics on Cone Penetration Resistance

Figs.6-2(a) to (d) show the typical results of the cone penetration resistance q_c vs. penetration depth D_p relationships for sand specimens prepared by the various methods. R_D(H)-specimen in Fig.6-2(d), whose preparation method was not explained in CHAPTER 3, was cut from the frozen sand deposit in the container for R_B method (See Fig.3-6), so as to gain the coincidence of the axial direction of specimen with the horizontal direction of the sand container. This sand deposit was made according to R_D (tapping) method in which oven-dried T-sand was poured into the sand container in several layers with tapping its side wall, and the subsequent procedures were the same as those of R_B method.

The experimental results indicated in Fig.6-2 seem to support an intuitive concept popularly accepted in which the higher the density of sand is, the larger the values of cone penetration resistance. The obviously smaller penetration resistance values are observed in the initial stages of penetration. This is due to the incomplete formation of plastic zone around the cone. It can be seen in these figures that the complete formation of plastic zone around the cone which is achieved at a penetration depth gives the true penetration resistance value under the present shear condition.

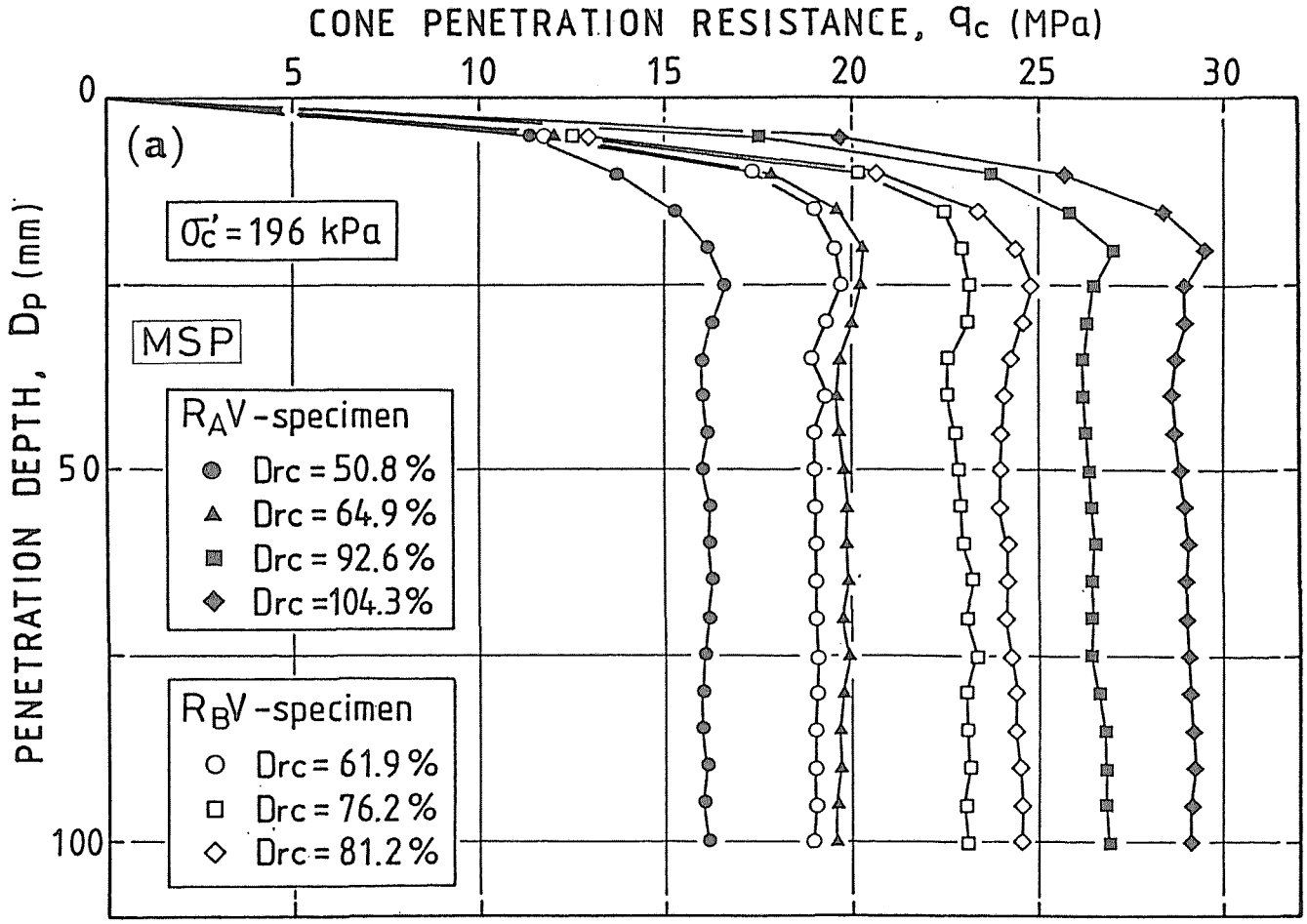

Fig.6-2(a) Typical test results of cone penetration resistance vs. penetration depth relationships for R_AV- and R_BV-specimens

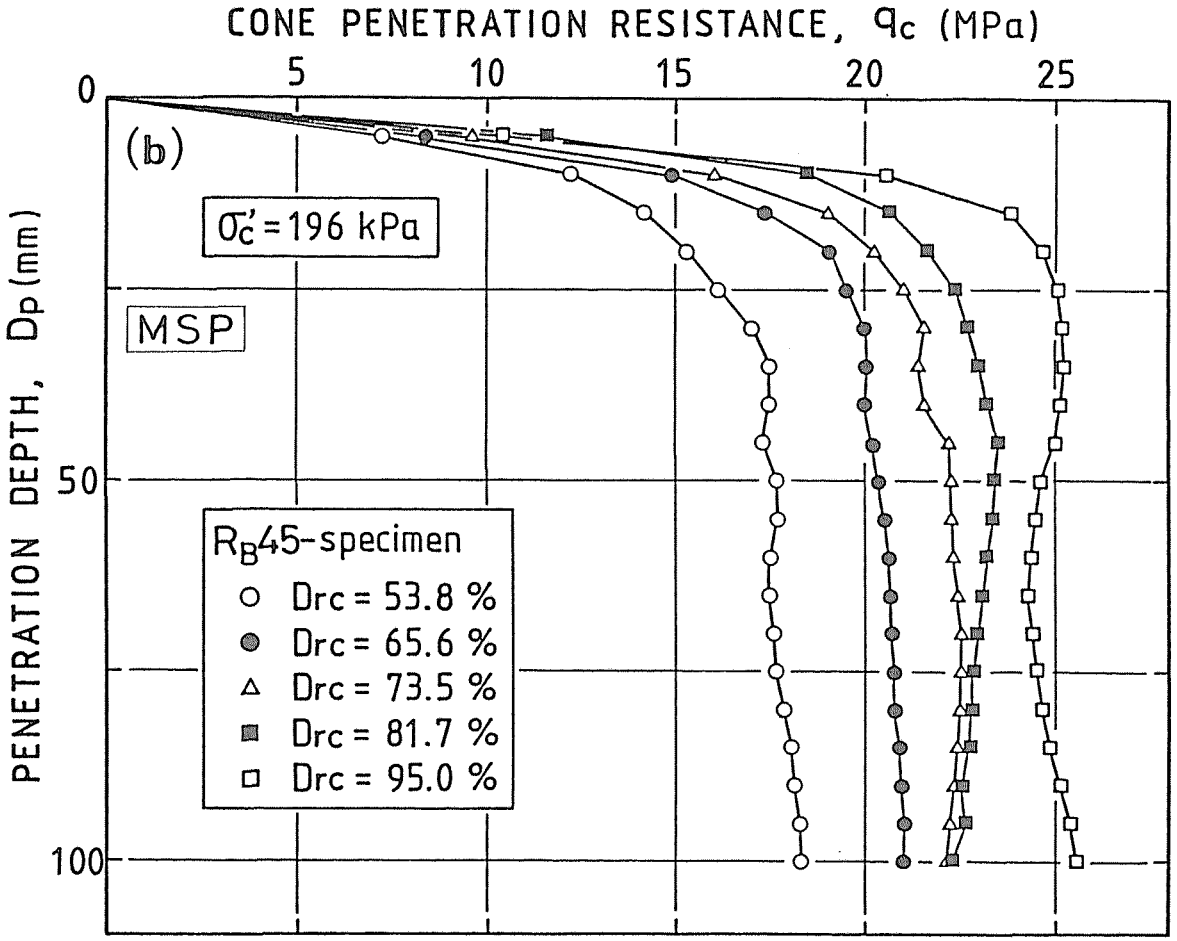

Fig.6-2(b) Typical test results of cone penetration resistance vs. penetration depth relationships for R_B45-specimens

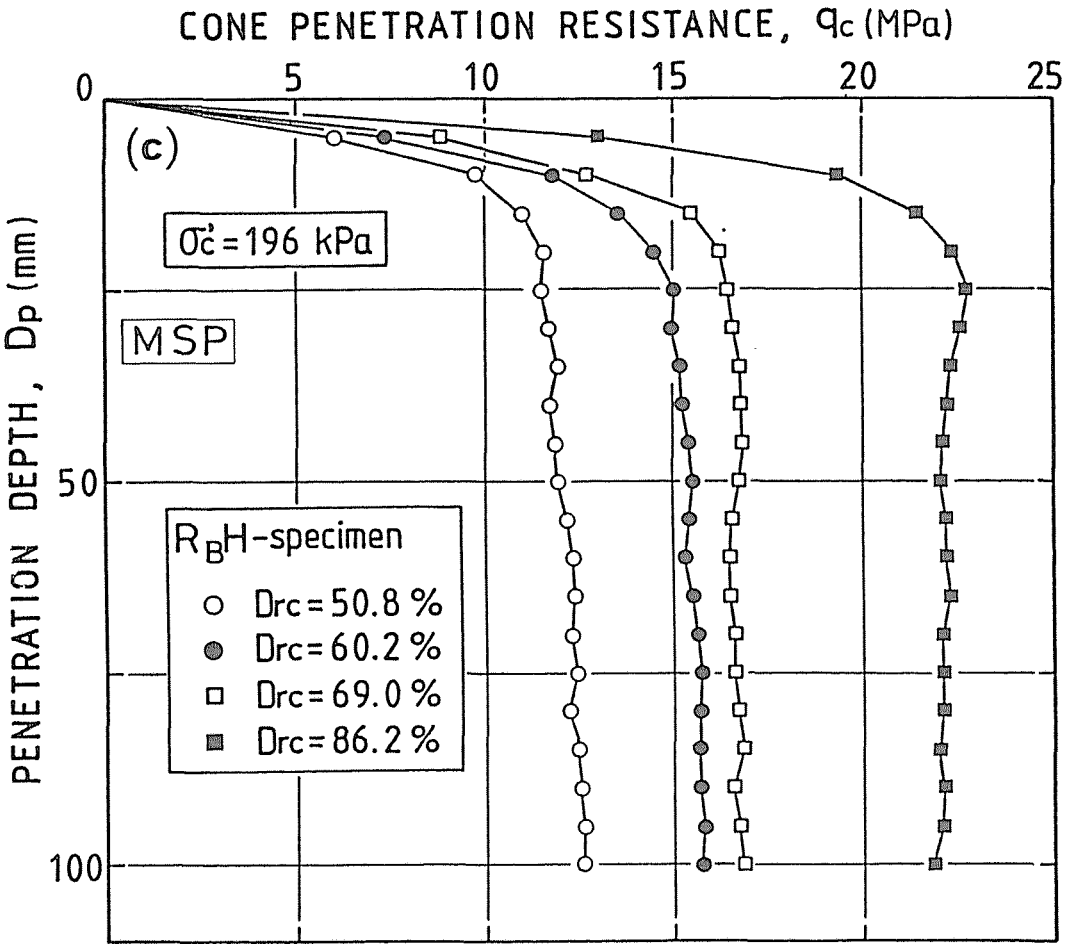

Fig.6-2(c) Typical test results of cone penetration resistance vs. penetration depth relationships for R_BH-specimens

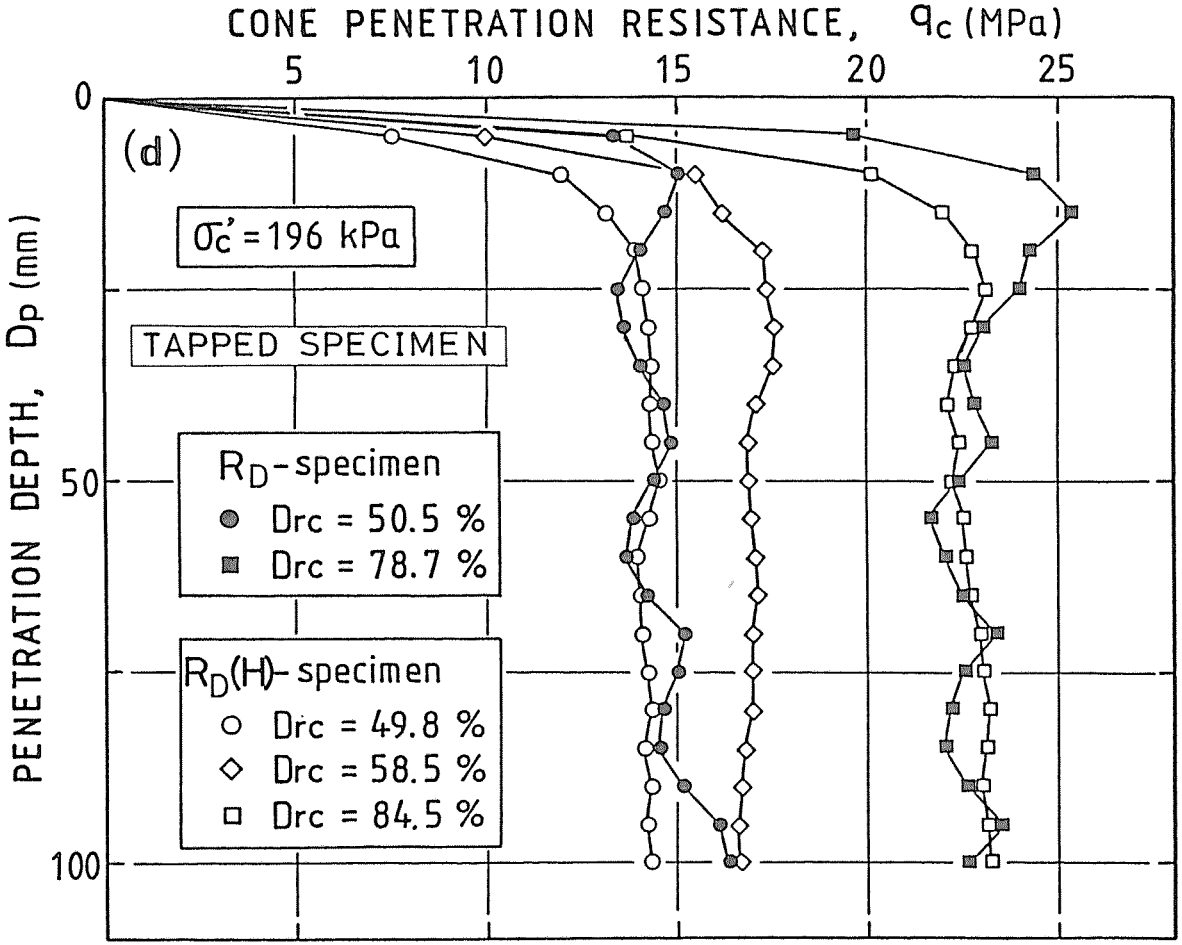

Fig.6-2(d) Typical test results of cone penetration resistance vs. penetration depth relationships for R_D- and R_D(H)-specimens

Test results indicate that the values of measured cone penetration resistance at $D_p \geqq 50$ mm all become the constant values excepting the tapped specimens, as shown in Figs.6-2(a) to (d). Accordingly, it would be reasonable that the mean value of the penetration resistances measured at the penetration depths over the range from 50 mm to 100 mm is considered as the cone penetration resistance for the sand specimens. This mean value will be denoted hereafter as $(q_c)_m$.

The variations in the cone penetration resistance values within the range of $D_p = 50$ mm to 100 mm are more significant in R_D-specimens formed by tapping method than in the specimens prepared by the pluviation through air method (MSP method), as shown in Fig.6-2(d). It can be considered that this is attributed to the non-uniformity introduced initially in R_D-specimens, irrespective of giving the extreme care in the sample preparations. This fact seems to exhibit that the cone employed in the present study can detect sensitively the non-uniformity with respect to the density existing in R_D-specimens and that the other specimens which are prepared by pluviating the sand particles possess the very homogeneous fabrics. All of the measured penetration resistances for R_D-specimens with non-uniformity will be, for comparison of test data with others, discussed based on $(q_c)_m$ as a temporary standard.

Shown in Fig.6-3 is the relationship between the mean cone penetration resistance $(q_c)_m$ and the relative density

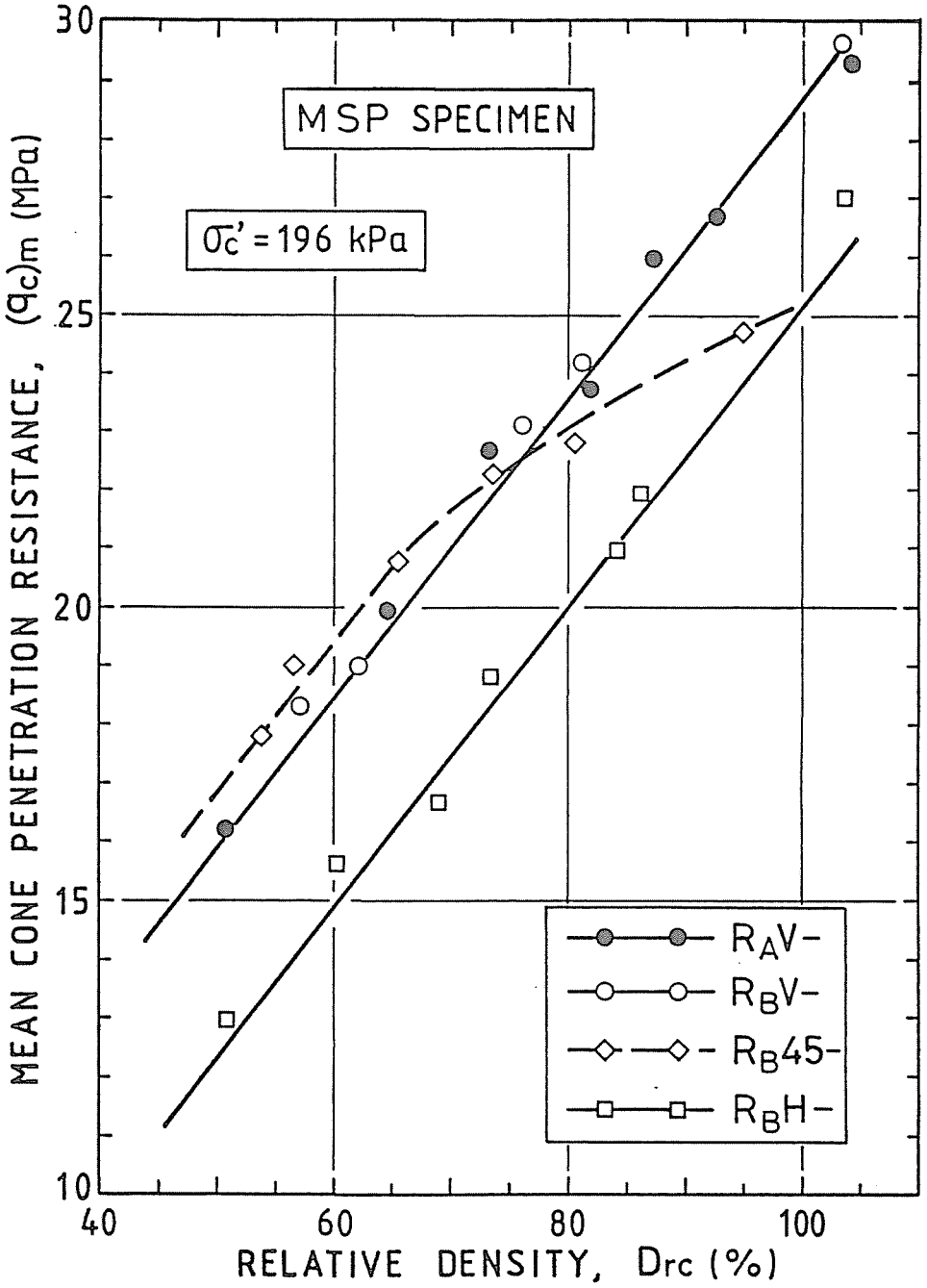

Fig.6-3 Effect of fabric anisotropy on the relationships between mean cone penetration resistance and relative density after consolidation for MSP specimens

after consolidation D_{rc} for four kinds of specimens prepared by pluviating the sand particles (MSP method). It can be seen in the figure that there is no differences in the values of $(q_c)_m$ at the same density between R_AV- and R_BV-specimens, and that $(q_c)_m$ vs. D_{rc} relationships for both specimens are represented by a straight line at least within D_{rc} of about 50 % to 100 %. This observation indicates that it is not necessary in the discussions on the cone penetration resistance to consider whether the specimens has been frozen during its preparation or not.

It should be noted in Fig.6-3 that $(q_c)_m$ vs. D_{rc} relationships which can be represented approximately by the parallel straight lines for all specimens excepting R_B45-specimens depend strongly on the fabric characteristics of the specimens. The marked differences in $(q_c)_m$ between R_AV- (or R_BV-) and R_BH-specimens could be observed, and the comparisons of test data of both specimens with the same relative densities show that $(q_c)_m$ of R_BH-specimens are remarkably lower values than those of R_BV- (or R_AV-) specimens. We should remember that pluviation of sand through air method such as MSP method induces the preferred alignment of long axes of particles nearly parallel to a bedding plane. As explained previously, there exists in both specimens the fabric characterized by the anisotropic property that the apparent long axis of the sand particles has strong preferred orientations in the vertical section for

R_BV- (or R_AV-) specimens and in the horizontal section for R_BH-specimens.

It can be considered from the above explanation that the differences in penetration resistance values are attributed to the anisotropic fabric of sands which is stiffer in the vertical direction than in the horizontal direction for R_BV- (or R_AV-) specimens and vice versa for R_BH-specimens. The anisotropic characteristics in the cone penetration mentioned above are almost identical to those observed in the conventional triaxial and cyclic undrained tests which were explained in the preceding chapters.

The cone penetration tests on R_B45-specimens show that the relationship between $(q_c)_m$ and D_{rc} cannot be expressed as the simple straight line as that for R_BV- and R_BH-specimens. As can be seen in Fig.6-3, $(q_c)_m$ of R_B45-specimens are equal to or some larger values than those of R_BV- (or R_AV-) specimens in $D_{rc} < 70$ %, but become gradually close on the values of R_BH-specimens according to the increase of the relative density. R_B45-specimens which should possess the intermediate property with respect to fabric characteristics between R_BV- and R_BH-specimens depict not necessarily the intermediate values of the cone penetration resistance between both specimens. It would be supposed that this is caused by the fact that the pattern of re-arrangement of sand particles due to cone penetration in R_B45-specimens does not occur as regularly as R_BV- (or

R_AV-) and R_BH-specimens do, but change according to the density.

Fig.6-4 shows $(q_c)_m$ vs. D_{rc} relationships for R_D- and R_D(H)-specimens prepared by tapping (R_D) method. The linear relationships between $(q_c)_m$ and D_{rc} for the tapped specimens are different from those for the pluviated specimens mentioned above, although it could be expected that the fabric characteristics of the tapped specimens are very similar to those of the pluviated specimens. The comparisons of the penetration resistances at the same relative densities indicate that $(q_c)_m$ of R_D-specimens are always lower values than those of R_BV- (or R_AV-) specimens and that $(q_c)_m$ are always higher values for R_D(H)-specimens than those for R_BH-specimens. That is, it can be seen in Fig.6-4 that the difference of $(q_c)_m$ between R_D- and R_D(H)-specimens at the same relative density is smaller than that between R_BV- (or R_AV-) and R_BH-specimens. These experimental facts infer that the fabric anisotropy of the pluviated specimens (MSP) is more intensive than that of the tapped specimens (R_D).

In summary, it can be pointed out that the cone penetration resistance is controlled not necessarily only by density, but also depends strongly on the fabric characteristics of sands.

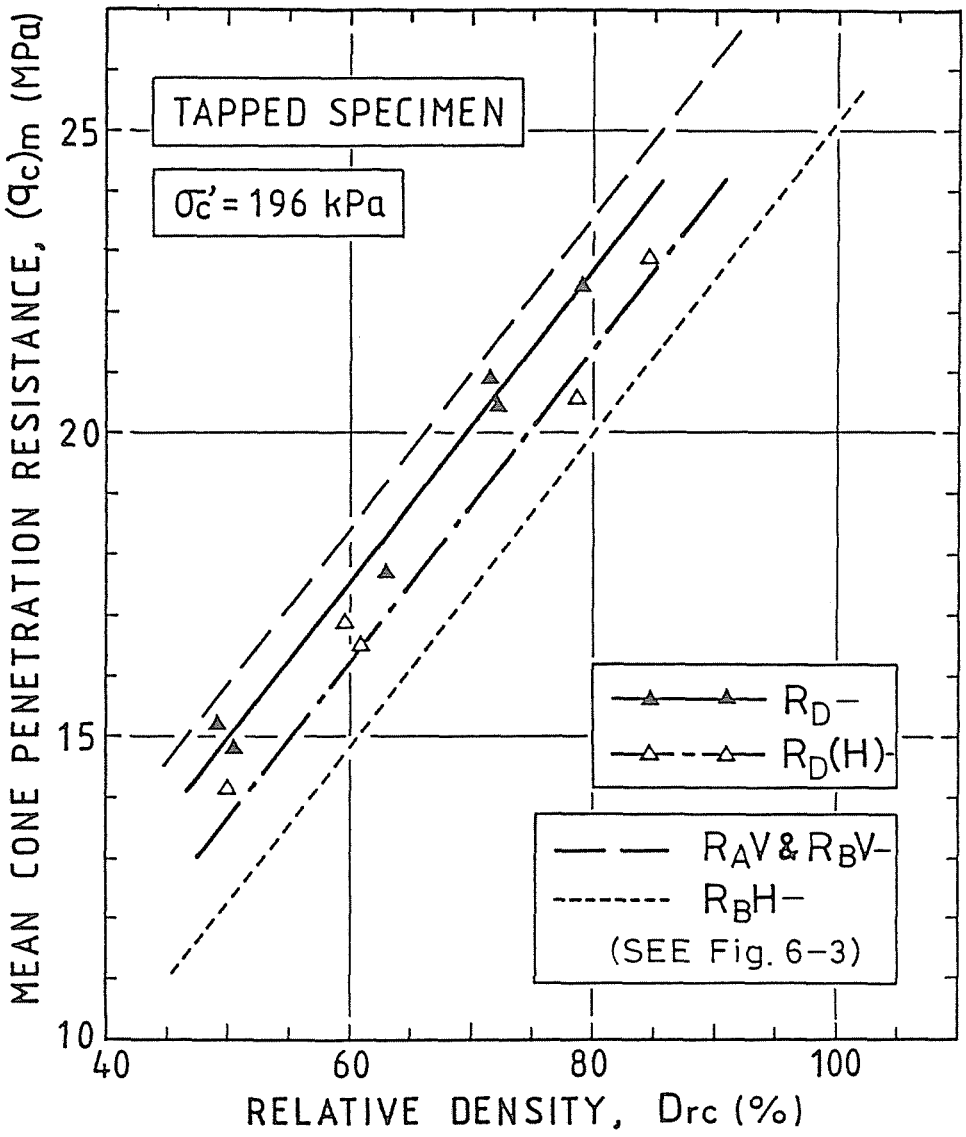

Fig.6-4 Relationships between mean cone penetration resistance and relative density after consolidation for tapped specimens and their comparison with MSP specimens

6.4 Correlation between Cone Penetration Resistance and Angle of Shearing Resistance

Shown in Figs.6-5(a) and (b) are the relationships between the angle of shearing resistance ϕ_d and the relative density after consolidation D_{rc} obtained from the drained triaxial compression tests on the specimens prepared by the various methods. Fig.6-5 indicates that the freeze-thaw sequence had no significant effects on ϕ_d and that ϕ_d may changes remarkably according to the difference in the fabric characteristics of sand specimens, as can be seen in the relationship between $(q_c)_m$ and D_{rc} (Figs.6-3 and 6-4). We can point out that the dependency of ϕ_d values on the relative density and the fabric anisotropy of sand specimens is all similar to that of $(q_c)_m$.

Fig.6-6 shows the ϕ_d vs. $(q_c)_m$ relationship for the above six kinds of sand specimens obtained from Figs.6-3 to 6-5. It should be noted that the relationship between ϕ_d and $(q_c)_m$ can be denoted by a unique straight line irrespective of the fabric characteristics of sand specimens. It is a fact of absorbing interest that ϕ_d vs. $(q_c)_m$ relationship of R_B45-specimens for which $(q_c)_m$ and ϕ_d values did not change linearly with D_{rc} can be also represented by this unique straight line. In the present state, the relative density or void ratio can never express the variation in mechanical properties due to the difference of fabric characteristics of sands. Accord-

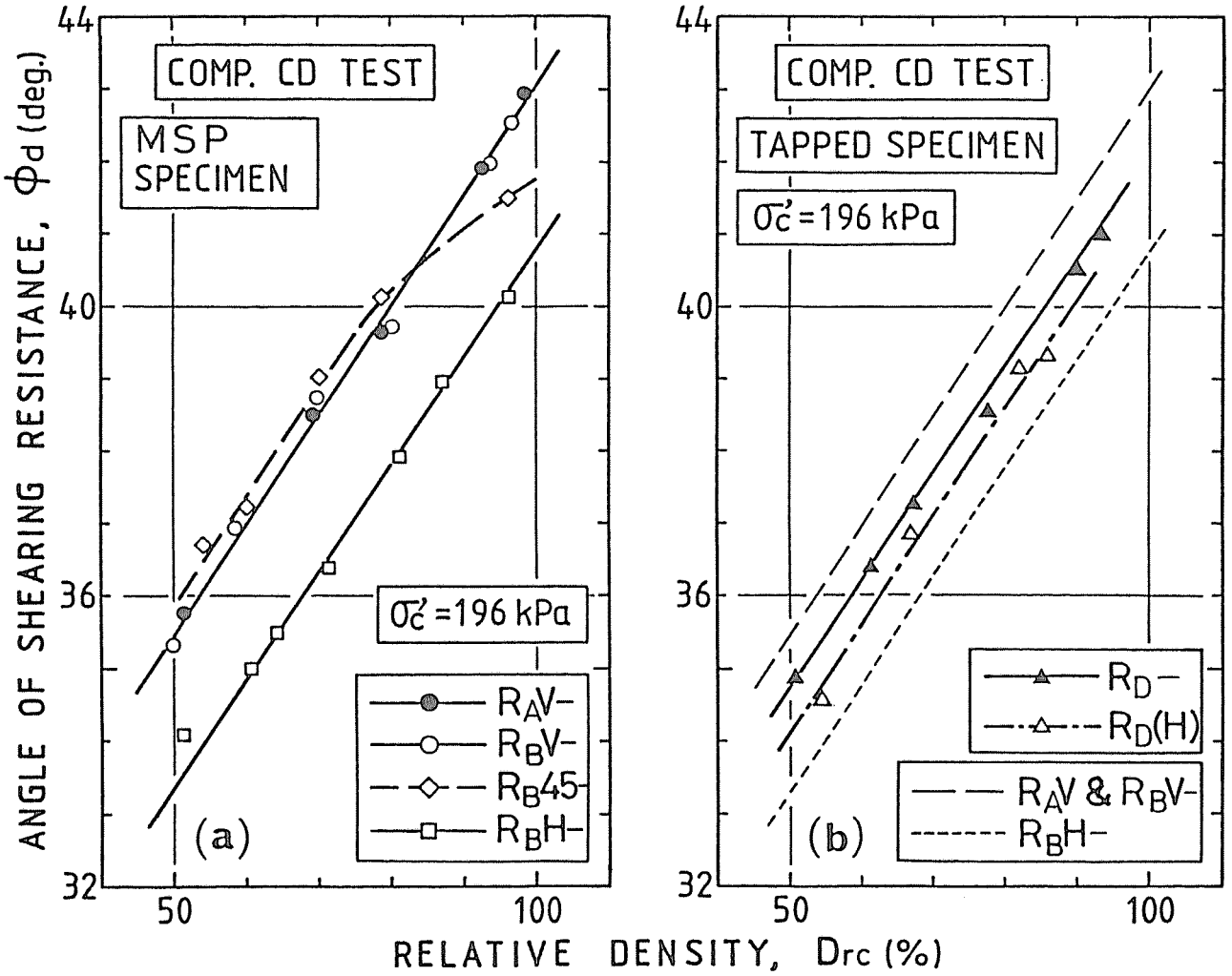

Fig.6-5 Effect of fabric characteristics on the relationships between angle of shearing resistance and relative density after consolidation obtained from drained triaxial compression tests; (a) MSP specimens, (b) tapped specimens

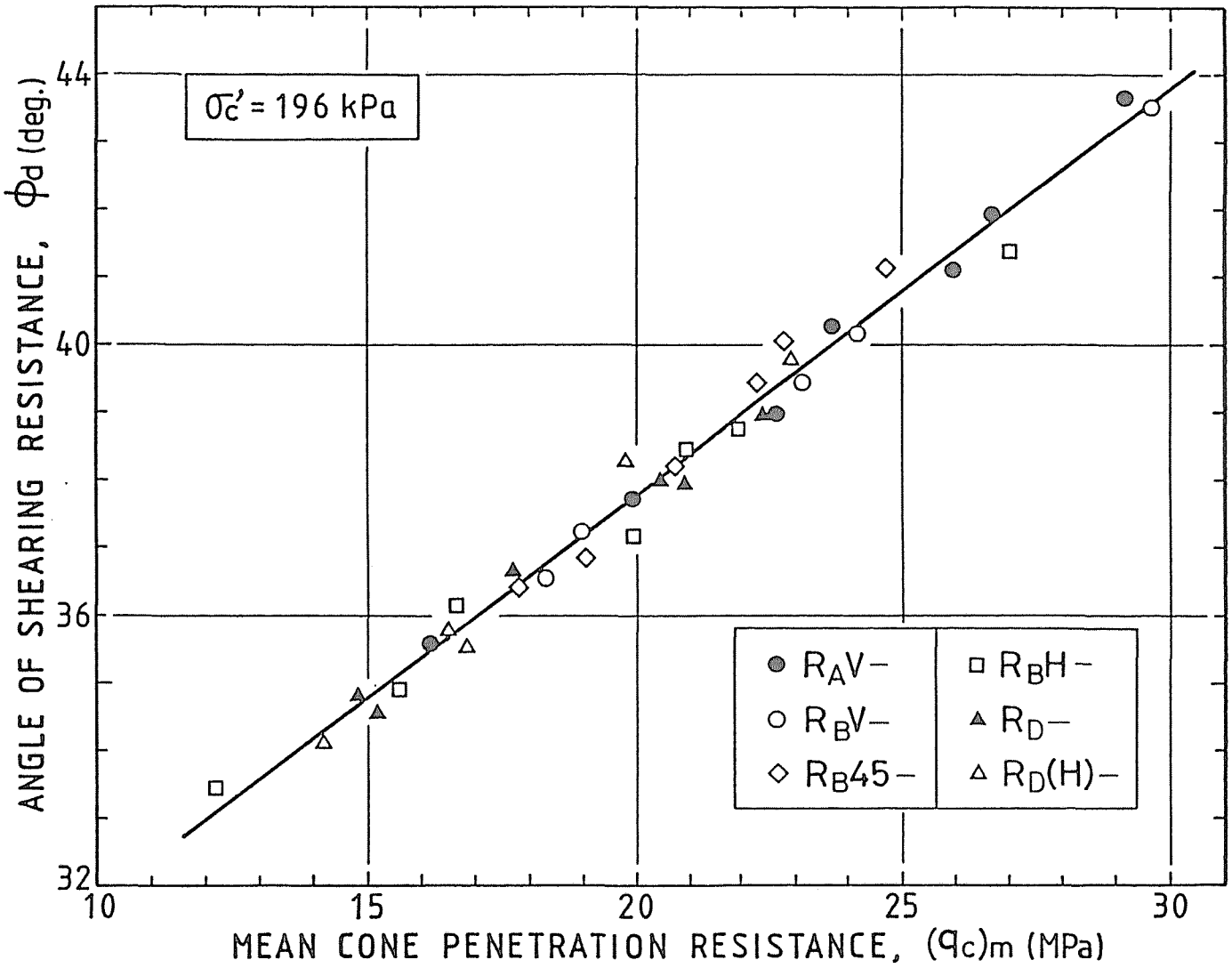

Fig.6-6 Relationship between angle of shearing resistance and mean cone penetration resistance for sands with various fabric characteristics

ingly, it is noteworthy to pursue the direct relationship between the cone penetration resistance and angle of shearing resistance.

The correlation between ϕ_d and $(q_c)_m$ obtained in this study indicates that it is possible to estimate directly the angle of shearing resistance of sand with any fabric characteristics from the value of cone penetration resistance.

6.5 Dilatancy Characteristics during Cone Penetration

The cone penetration tests in the present study were conducted under the perfectly drained condition. By measuring the volume changes in the specimens, consequently, the dilatancy phenomena due to the cone penetration can be examined in detail. Shown in Figs.6-7(a) and (b) are the typical behaviors of the volume change ΔV due to penetrating the cone into $R_A V$- and R_D-specimens with the relative densities over the range from about 50 % to 100 %. ΔV denotes the net amount of volume contraction or volume expansion of specimens which is calculated by subtracting the beforehand calibrated volume of the point of cone and penetration rod from the total volume change of specimens measured in the burette. ΔV presumes volume contraction as positive. It can be seen in the figures that the volume change due to cone penetration has a tendency to vary remarkably with the density of sand specimens, but is produced at a constant ratio in not less than a penetration depth. These experimental results seem to correspond with the fact that the cone penetration resistance values become constant in not less than a penetration depth as shown in Fig. 6-2.

The volume changes during the cone penetration could be assumed to be divided into the volume contractions due to increase of mean principal stress and the volume expansions due to

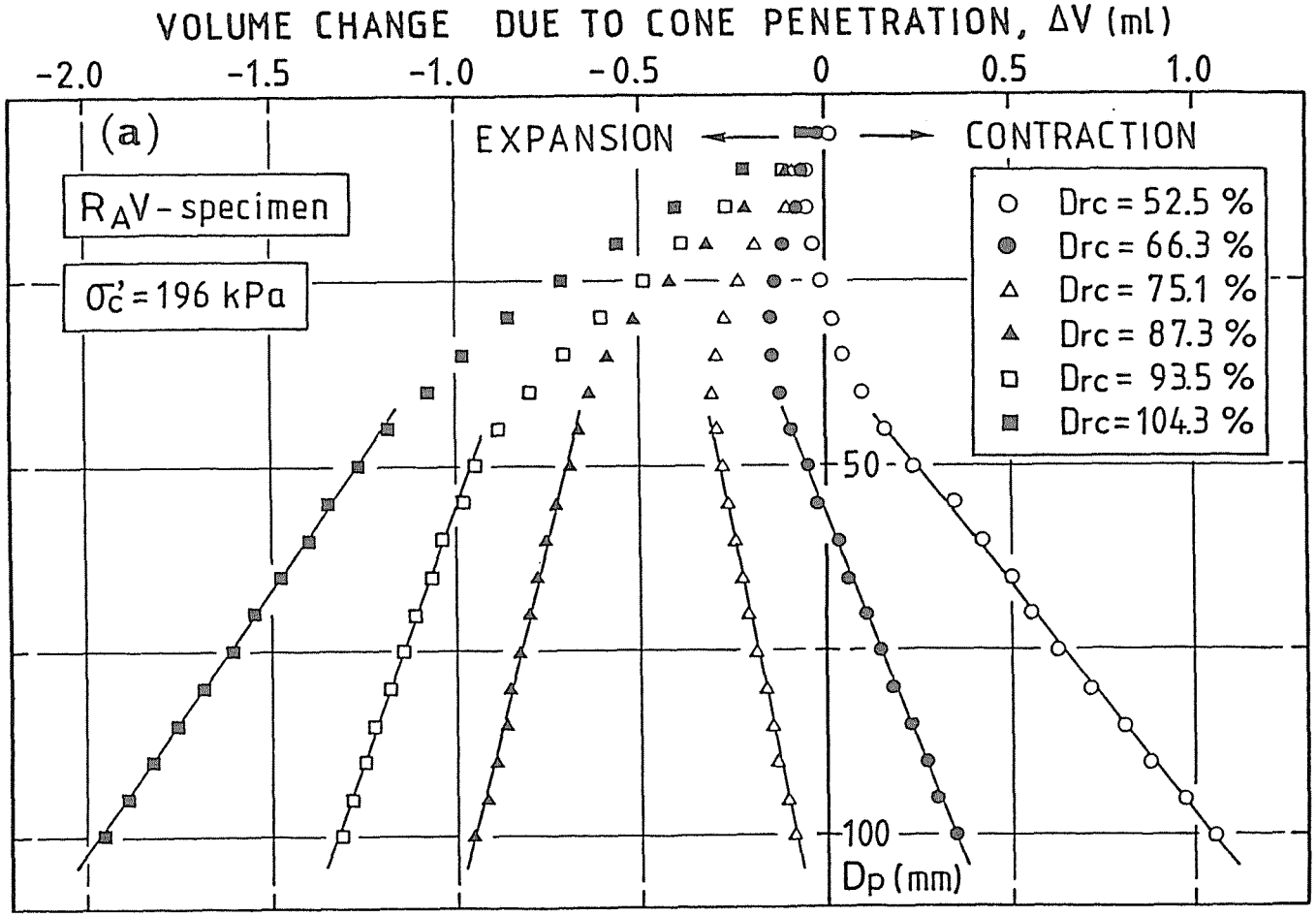

Fig.6-7(a) Characteristics of volume change due to cone penetration in R_AV-specimens

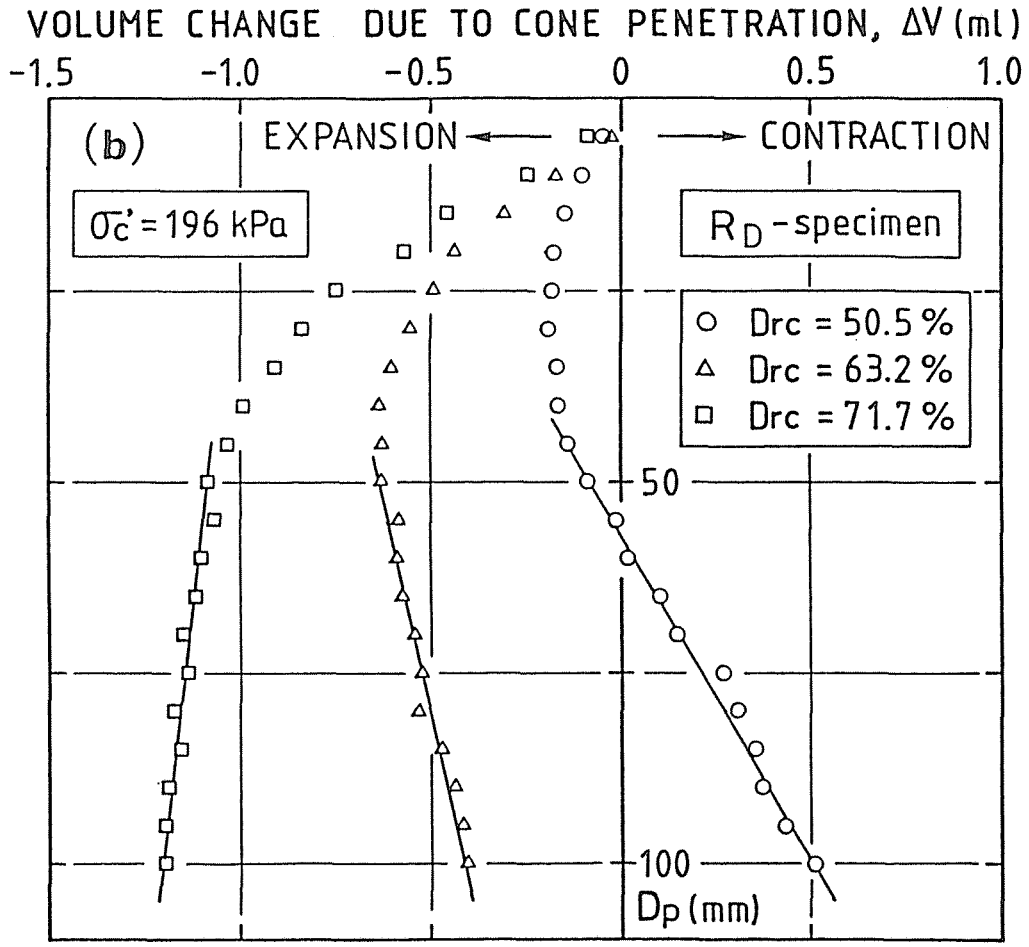

Fig.6-7(b) Characteristics of volume change due to cone penetration in R_D-specimens

dilatancy induced by shear in the plastic zone formed around the cone. As can be seen in Fig.6-7, the volume expansions occur in the dense sand specimens. This indicates that the volume changes due to cone penetration would be attributed mainly to the dilatancy induced by shear, although we cannot give in the present a clear distinction between them. What the dilatancy behaviors during cone penetration may change significantly with the differences of the relative density is the natural results in the same manner as the fact in which the dilatancy characteristics in the conventional shear tests depend strongly on the relative density.

Fig.6-8 shows the comparison of volume change ratio with respect to penetration depth $d(\Delta V)/dD_p$ at $D_p \geqq 50$ mm vs. D_{rc} for $R_A V$- and R_D-specimens. $d(\Delta V)/dD_p$ vs. D_{rc} relationships for both specimens can be denoted by the straight lines, but both straight lines do not coincide with each other. Fig.6-8 also indicates that the tendency of volume expansion due to cone penetration is more significant for R_D-specimens than for $R_A V$-specimens. On the other hand, $(q_c)_m$ and ϕ_d obtained from the triaxial compression tests for $R_A V$-specimens are higher values at the same relative densities than those for R_D-specimens, as can be seen in Figs.6-4 and 6-5. These results do not support an intuitive concept in which the sand specimens having more significant positive dilatancy at failure may possess larger values of $(q_c)_m$ and ϕ_d, because the dilatancy behaviors

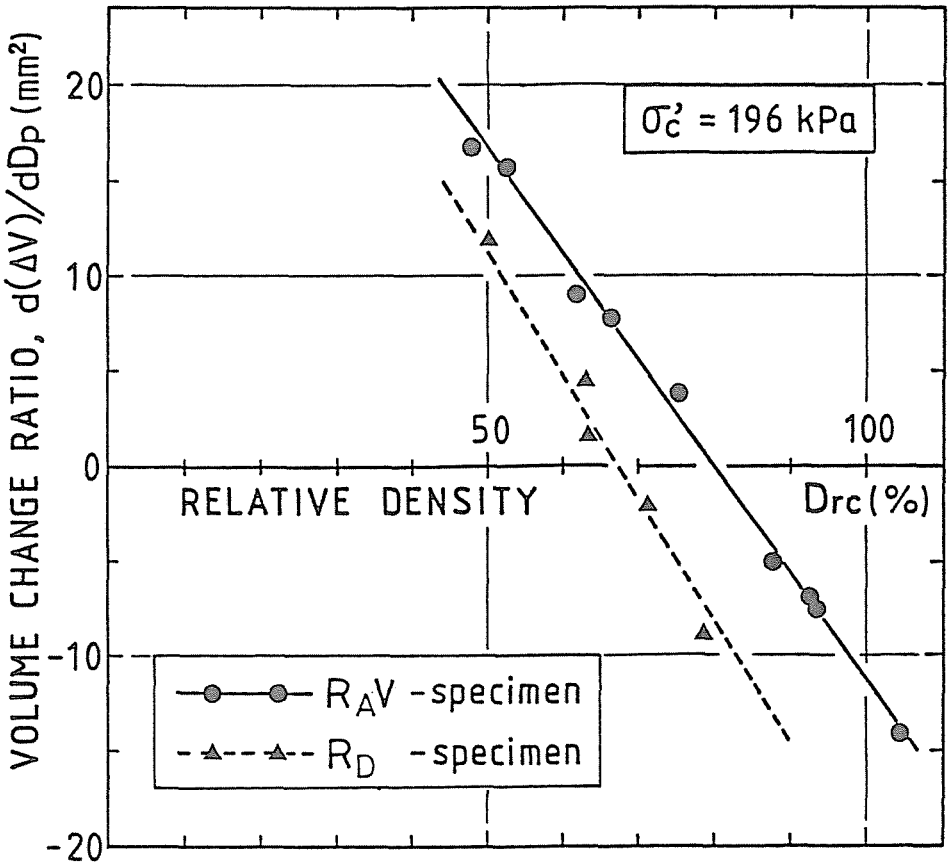

Fig.6-8 Dependency of relationship between volume change ratio and relative density after consolidation on fabric characteristics of sand specimens

during the cone penetration are intimately related to those of the triaxial extension tests as discussed in the following paragraph. Fig.6-8 means that the dilatancy behaviors during cone penetration may be affected appreciably by the fabric characteristics of sand specimens. Such effects of the fabric characteristics on the dilatancy due to penetrating the cone into the sands are very similar to those observed in the triaxial compression and extension tests as described previously.

It could be considered from these facts that the variations of the cone penetration resistance values clarified in the preceding paragraphs do not have nothing to do with those of dilatancy behaviors due to the differences of fabric characteristics.

6.6 Comparison of Dilatancy Characteristics between Cone Penetration and Triaxial Tests

A shear failure is considered to occur succesively in the zone of plastic flow near the cone which is formed by penetrating the cone into the sand. This idea permits that the volume changes measured in the cone penetration tests can be assumed as those induced in the zones of plastic flow of the sand specimens. Accordingly, it follows that the outer zones of plastic flow continue to retain the fabrics after completion of consolidation during the cone penetration tests. The zones of plastic flow are newly formed in the lower portion of sand specimen, as the cone penetration proceeds. It is assumed in the present study that the subsequent cone penetration does not vary the shape of the plastic zone which is formed at a penetration depth. Therefore, the increments of plastic zone due to an additional cone penetration dD_p could be denoted as the product of the sectional area surrounded by the plastic zone and dD_p. On the other hand, the increments of volume change induced in the plastic zone of sand specimen, when undergoing the penetration of cone (dD_p), are evaluated as $d(\Delta V)$. By using the volume change ratio $d(\Delta V)/dD_p$ defined in the preceding paragraphs, consequently, the volumetric strain $(\varepsilon_v)_c$ which is induced in the zones of plastic flow due to the penetration of cone can be expressed

as follows:

$$(\varepsilon_v)_c = \frac{d(\Delta V)}{dD_p} \cdot \frac{1}{A_{max}} \cdot 100 \quad (\%) \qquad (6\text{-}1)$$

where A_{max} denotes the maximum sectional area of the plastic zone as shown in Fig.6-9.

In order to determine the value of A_{max} concretely, the shape of two-dimensional plastic zone proposed by Meyerhof (1961) is adopted in the present study. That is, the sectional area A_{max} is calculated on the basis of the solid which is formed by a revolution of the two-dimensional plastic zone round the axis of cone penetration as shown in Fig.6-9. The values of A_{max} in Eq.(6-1) which vary depending on the roughness of the cone surface can be given by the following expressions.

$$A_{max} = \frac{\pi d^2}{4} \left[\frac{\exp\{(\frac{\pi}{4} + \frac{\phi}{2} + \alpha) \tan\phi\} \tan\phi}{2 \cdot \sin\alpha \cdot \cos(\frac{\pi}{4} + \frac{\phi}{2})} + 1 \right]^2 \quad (\text{for smooth surface}) \qquad (6\text{-}2)$$

$$A_{max} = \frac{\pi d^2}{4} \left[\frac{\exp\{(\frac{\pi}{2} + \phi + \alpha) \tan\phi\} \cos\phi}{\sin\alpha} + 1 \right]^2 \quad (\text{for rough surface}) \qquad (6\text{-}3)$$

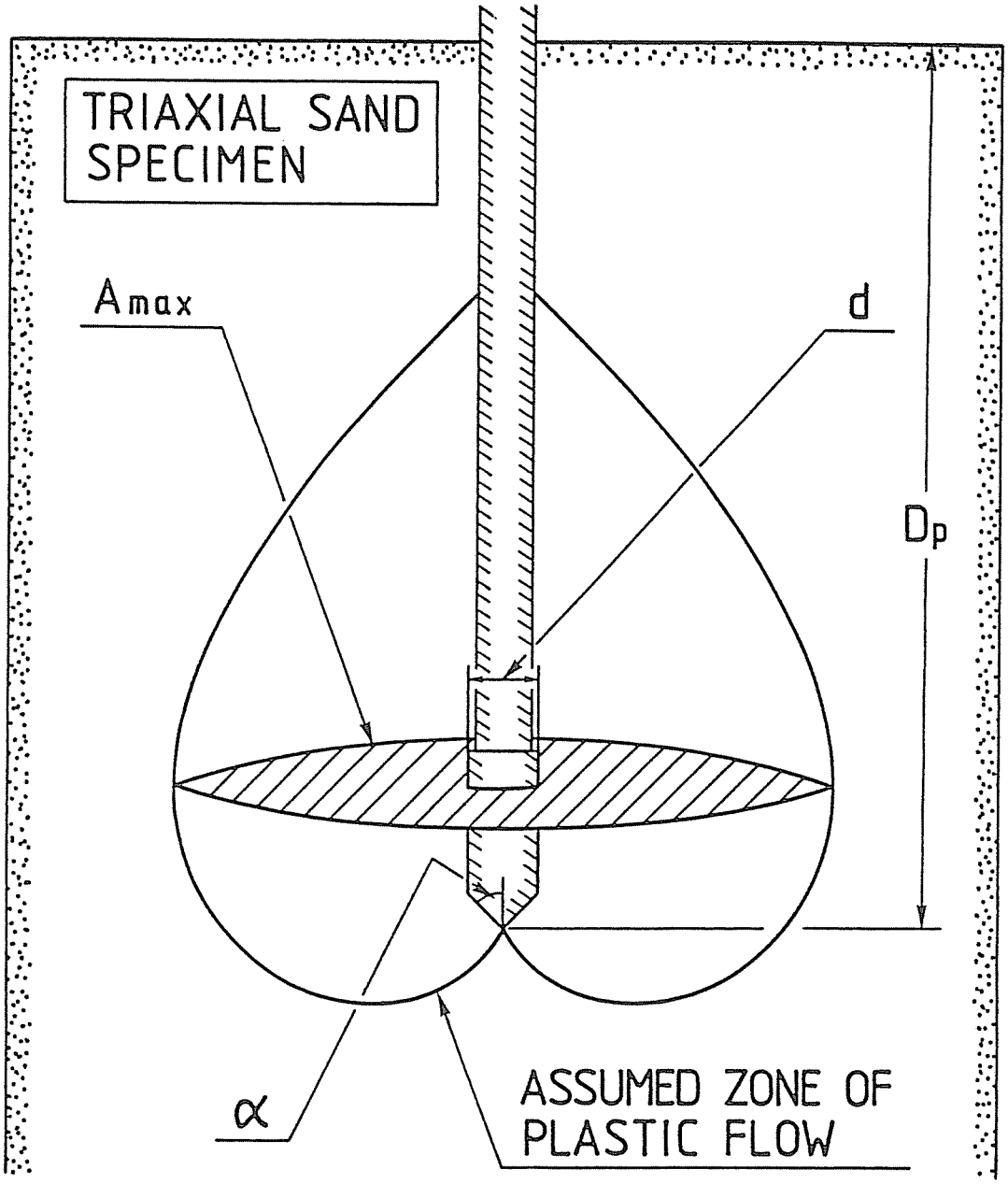

Fig.6-9 Shape of plastic zone around cone in sand specimen which is formed by a revolution of the two-dimensional plastic zone (Meyerhof, 1961) round the axis of cone penetration

in which d, α and ϕ denote the diameter of cone, semi-apex angle of cone tip and angle of shearing resistance, respectively. The values of d and α in the present study are 5 mm and 45°, respectively. Taking account of the fact that the cone penetration tests are performed under the drained conditions and that there exists the unique correlation between $(q_c)_m$ and ϕ_d, ϕ_d obtained from the drained triaxial tests is substituted for ϕ in Eqs.(6-2) and (6-3). $(\varepsilon_v)_c$ at any relative densities can be calculated through the relationships between $d(\Delta V)/dD_p$ and D_{rc} shown in Fig.6-8 and between ϕ_d and D_{rc} shown in Fig.6-5 based on Eqs.(6-1) and (6-2) (or (6-3)).

Shown in Figs.6-10(a) and (b) are the relationships between $(\varepsilon_v)_c$ and D_{rc} for R_AV- and R_D-specimens. The volumetric strain at failure $(\varepsilon_v)_f$ vs. D_{rc} relationships obtained from a series of triaxial compression and extension tests on R_AV- and R_D-specimens are also represented in both figures. It can be seen in the figures that, for D_{rc} over the range from about 50 % to 100 %, the volumetric strains due to cone penetration are closer to the volumetric strains at failure in the triaxial extension tests than those in the triaxial compression tests. It can be also recognized that the relative densities at which the volumetric strains transfer from positive to negative values almost coincide in both specimens.

These facts indicate that the dilatancy behaviors during the cone penetration are closely connected with those of the

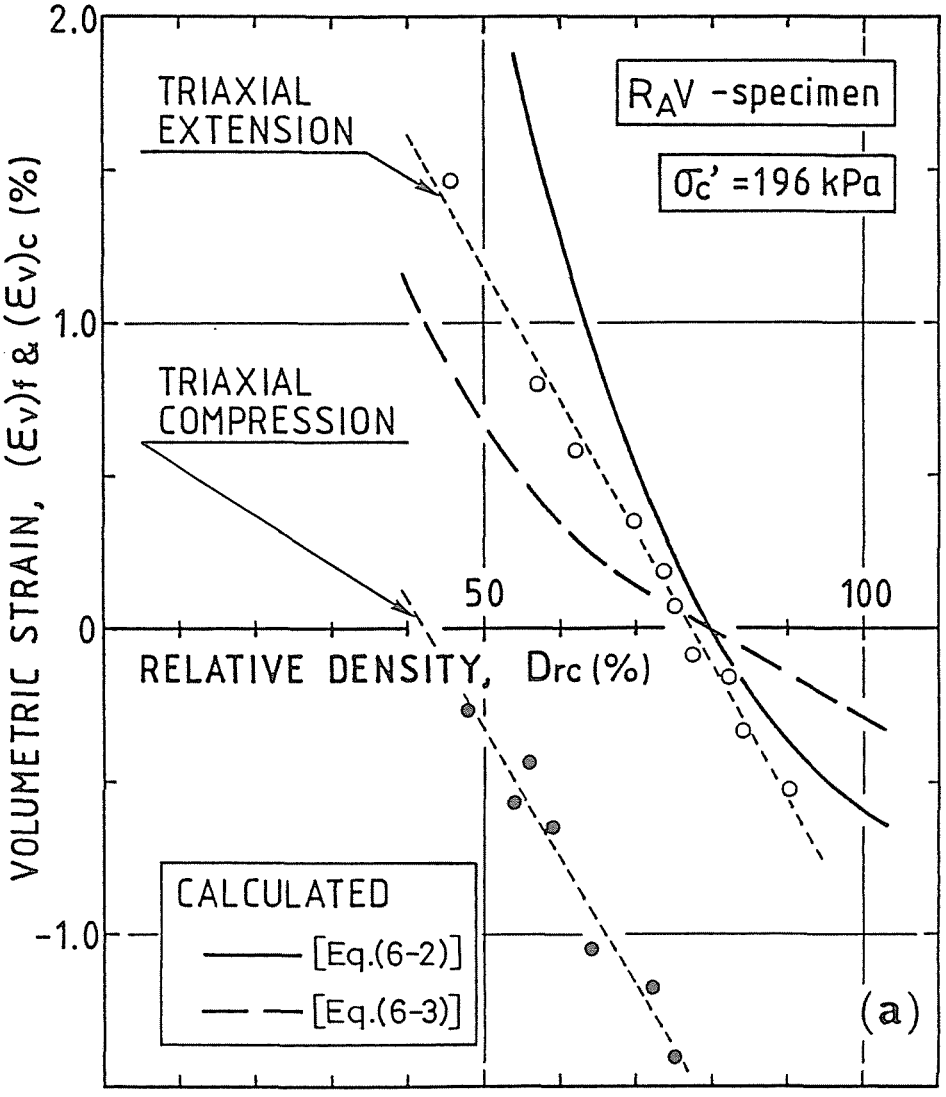

Fig.6-10(a) Comparison of the calculated and measured relationships for volumetric strain vs. relative density after consolidation in R_AV-specimens

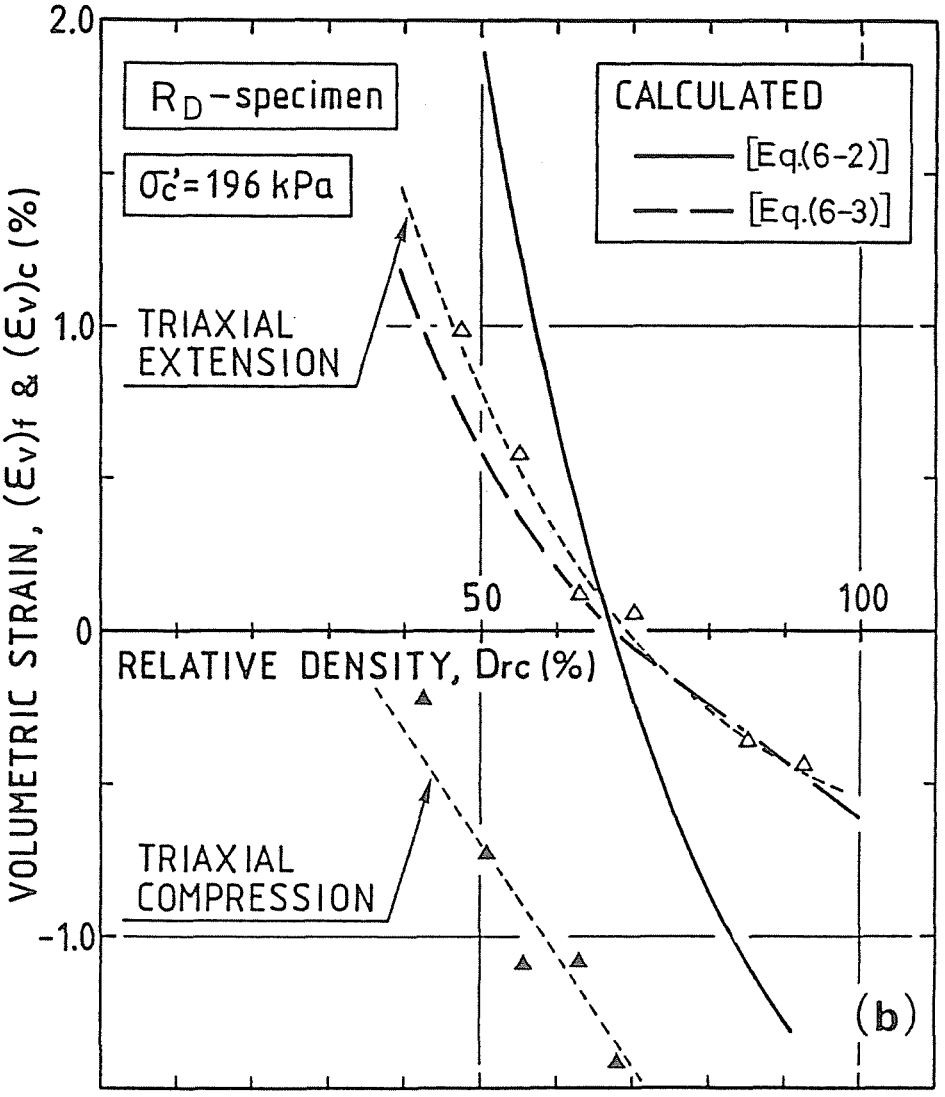

Fig.6-10(b) Comparison of the calculated and measured relationships for volumetric strain vs. relative density after consolidation in R_D-specimens

triaxial extension tests. However, the reason why there exists such correlations irrespective of the fabric characteristics of sand must be experimentally or theoretically investigated in future.

6.7 Correlation between Cone Penetration Resistance and Cyclic Undrained Strength

The correlation between the cone penetration resistance and the cyclic undrained triaxial strength for the specimens with the different fabrics is examined in this section.

Fig.6-11 shows a typical comparison of cyclic undrained strength values obtained from the cyclic triaxial tests on three kinds of specimens with D_{rc} of 55 % prepared by pluviating the sand particles (MSP method) for the failure defined as initial liquefaction. This figure makes clear that the cyclic undrained triaxial strength are significantly affected by the fabric characteristics of sand specimens as can be seen in CHAPTER 4. Although we can say that not only static cone penetration characteristics but also liquefaction behavior are extremely sensitive to the fabrics of sand, it should be noted that the magnitude relation of cyclic stress ratio ($\sigma_d/2\sigma_c'$) observed in these specimens differs from that of $(q_c)_m$ at the same relative density (See Fig.6-3). Furthermore, the previous considerations in the present paper (CHAPTER 4) have shown that the cyclic undrained triaxial strength of R_D-specimens which have lower $(q_c)_m$ than those of R_AV- (or R_BV-) specimens as shown in Fig.6-4 is higher than that of R_AV-specimens. From these facts, we cannot draw a unique relationship between the mean cone penetration resistance measured in the axial

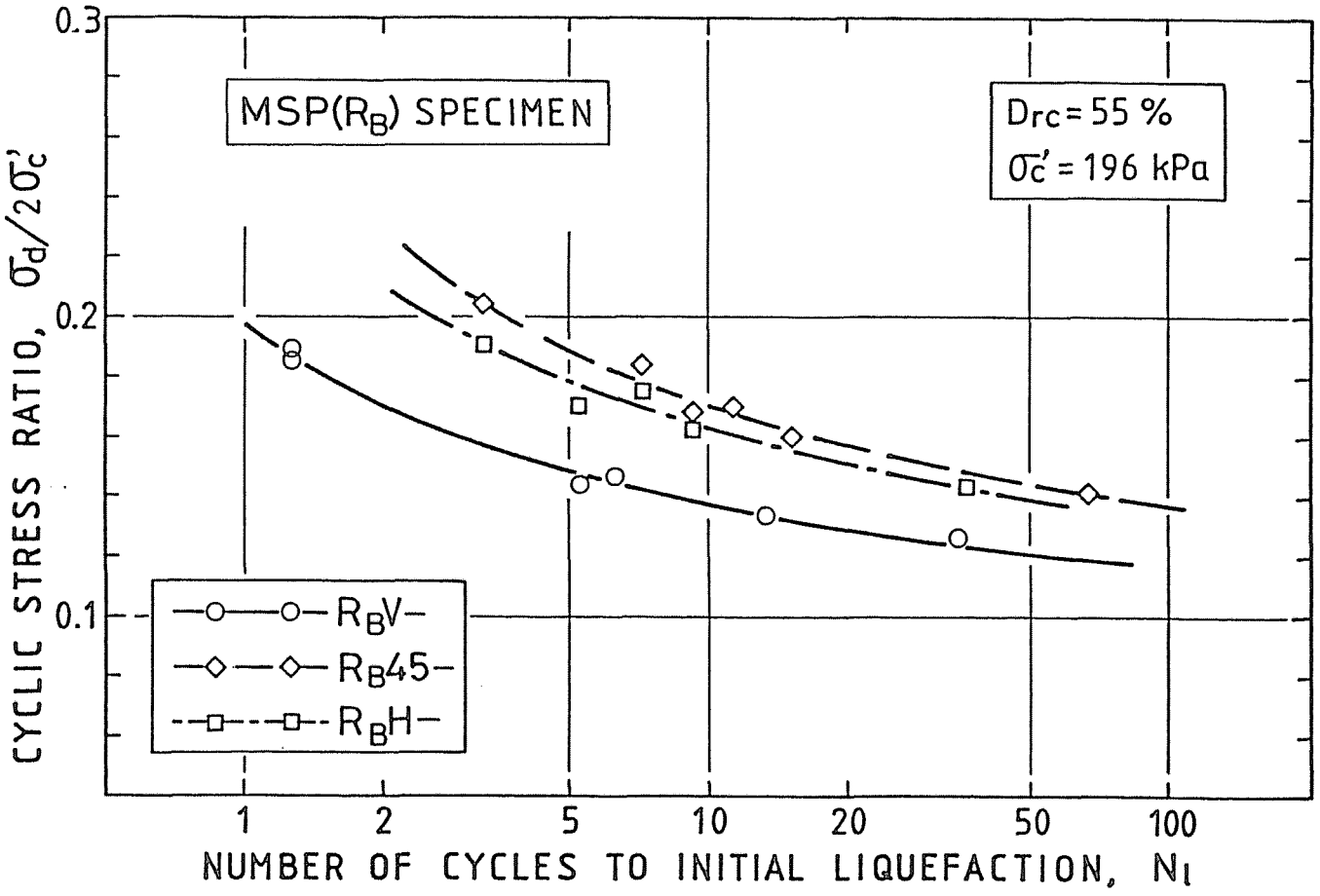

Fig.6-11 Comparison of cyclic stress ratio vs. number of loading cycles to initial liquefaction for R_BV-, R_B45- and R_BH-specimens

direction of the triaxial specimens and the cyclic undrained triaxial strength.

It has been also indicated in CHAPTER 4 that the variations of the cyclic undrained triaxial strength values due to the differences of the fabric characteristics are attributed to a considerable degree to those of the dilatancy properties of the extensional sides. Consequently, one may conceive to know about the horizontal cone penetration resistance whose direction coincide with that of the major principal stress in the triaxial extension test. For this purpose, a Cartesian coordinate system in which the z-axis is chosen to coincide with the vertical direction of sand specimens is employed for designating schematically the relation between the direction of cone penetration and the fabric characteristics of R_BV-, R_B45- and R_BH-specimens, as shown in Fig.6-12. The all values of cone penetration resistance obtained in the present experiments are measured as those in the z-direction of the specimens. However, it could be considered that the cone penetration resistances in the x- and y-directions are substituted by those in z-direction, because the cone penetration tests are performed under the isotropic stress conditions. By denoting $(q_c)_z$ (= $(q_c)_m$) in the z-directions of R_BV-, R_B45- and R_BH-specimens as $(q_c)_V$, $(q_c)_{45}$ and $(q_c)_H$, respectively, the values of $(q_c)_x$ and $(q_c)_y$ in the radial directions for each specimen can be represented as those shown in Figs.6-12(a), (b) and (c). R_B45- and

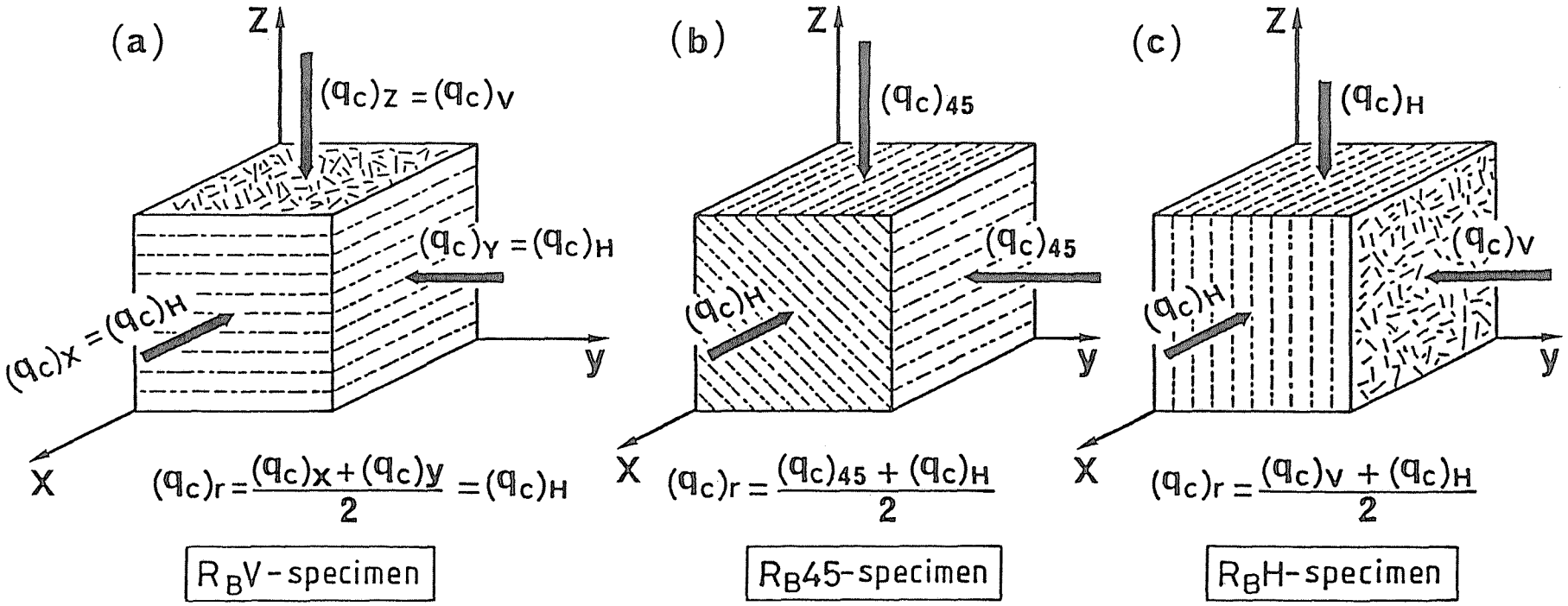

Fig.6-12 Schematic representation of relation between direction of cone penetration and and fabric characteristics; (a) R_BV-specimen, (b) R_B45-specimen, (c) R_BH-specimen

R_BH-specimens do not seem to be characterized by the orthotropic fabrics that the apparent long axis of the sand particles has preferred orientations in the horizontal section, but almost completely random orientations in the vertical section as can be seen in R_BV-specimens. In the present study, it is assumed that the cone penetration resistance in the radial direction $(q_c)_r$ can be denoted tentatively by the average values of $(q_c)_x$ and $(q_c)_y$. Consequently, $(q_c)_r$ for R_BV-, R_B45- and R_BH-specimens are $(q_c)_H$, $\{(q_c)_{45} + (q_c)_H\}/2$ and $\{(q_c)_V + (q_c)_H\}/2$, respectively.

Shown in Fig.6-13 is the relationship between the cone penetration resistance in the radial direction $(q_c)_r$ and the cyclic stress ratio required to the initial liquefaction at any number of cycles $(\sigma_d/2\sigma_c')_1$. $(q_c)_r$ of the sand specimens with D_{rc} of 55 % is given from the relationships between $(q_c)_m$ and D_{rc} shown in Fig.6-3. The values of $(\sigma_d/2\sigma_c')_1$ in the figure indicate the cyclic stress ratio causing the initial liquefaction at the number of cycles $N_1 = 5$, 10, 20, 30 and 50 and are calculated from Fig.6-11. As can be seen in the figure, there exists the unique relationship between $(q_c)_r$ and $(\sigma_d/2\sigma_c')_1$ regardless of the number of cycles. This shows that the cyclic undrained triaxial strength is estimated to a certain degree by the cone penetration resistance in the radial direction irrespective of the fabric characteristics of sand specimens. This unique correlation seems to be attributed

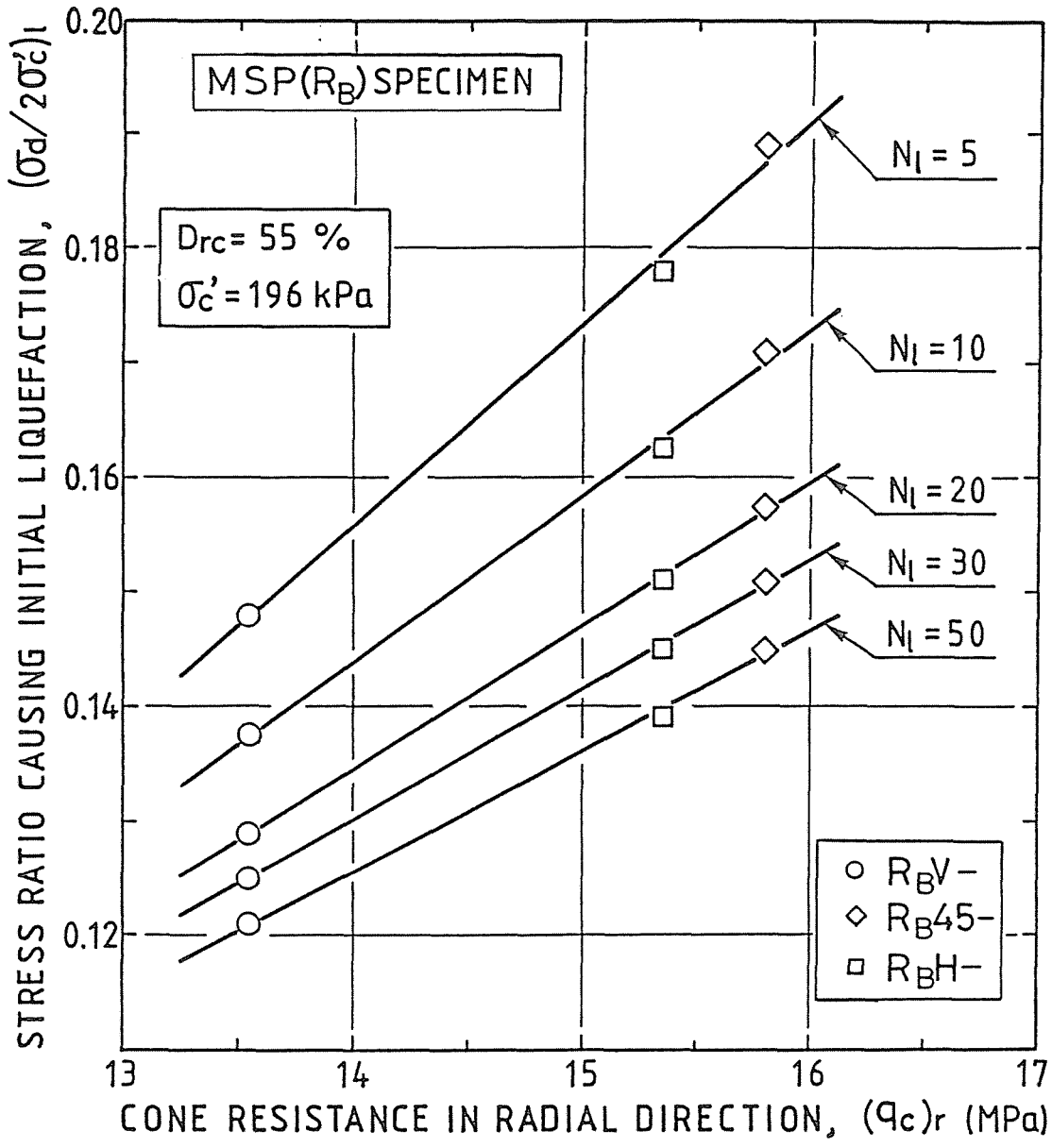

Fig.6-13 Relationship between cyclic stress ratio vs. cone penetration resistance in radial direction for sands with various fabric characteristics

to the fact that the liquefaction behavior is related intimately to the dilatancy characteristics of the triaxial extension tests in which the major principal stress is in the radial direction.

In summary, it can be said from the facts mentioned above that the relationship between the vertical cone penetration resistance values observed in the conventional cone penetration tests and the liquefaction strength is strongly dependent on the fabric characteristics of sand specimens and should not be given by taking no account of the fabric anisotropy of sand deposits.

6.8 Prediction of Anisotropic Cone Penetration Resistance by Cavity Expansion Theory

6.8.1 Cavity expansion theory

The static cone penetration resistance and the bearing capacity of foundations have been analyzed by considering the soils as the rigid-plastic material. As is commonly known, these analyses disregard the deformation of soils due to penetration of the cone, footing or pile. As mentioned in the preceding sections, however, the cone penetration resistance depends remarkably not only on the fabric characteristics but also on the dilatancy properties.

Vesic (1972) has developed a theory for bearing capacity which can take account of the deformability of sand within the plastic zone formed according to the expansion of cavity. In his theory, the ultimate cavity expansion pressure p_u at which the cavity expands until the state of limiting equilibrium is expressed as follows:

$$p_u = c F_c + \sigma_q F_q \qquad (6\text{-}4)$$

where F_c and F_q are the dimensionless cavity expansion factors and c and σ_q denote the cohesion and initial isotropic effective stress prior to cavity expansion in the entire soil mass.

The cavity expansion factors F_c and F_q depend not only on the angle of shearing resistance ϕ but also on the volumetric strain Δ within the plastic zone. The preliminary examinations on the factors influencing the shear strength of sand in CHAPTER 3 have shown that there is a remarkable reduction of the angle of shearing resistance ϕ_d with the increase of the effective confining pressure (See Fig.3-16). Accordingly, it is considered that this phenomenon should not be neglected in the analysis of the static cone penetration resistance.

Baligh (1976) has also evaluated the ultimate cavity pressure, taking the failure envelope curvature as well as the compressiblity of the sand into account. The development of his theory is based on the following equations for the curvature of the Mohr-Coulomb envelope.

$$\tau = \sigma \{ \tan \phi_0 + \tan \beta \, (\frac{1}{2.3} - \log \frac{\sigma}{\sigma_0}) \} \qquad (6\text{-}5)$$

in which ϕ_0 and β are the constant angles defining the failure envelope and σ_0 is an arbitrary reference stress. τ and σ are the shear and normal stresses on the failure plane at failure. If the cavity expands spherically in the sands, the cone penetration resistance can be expressed, taking account of the failure envelope curvature (Eq.(6-5)), as follows (Vesic,

1977):

$$q_c = \frac{p_u}{1 + \sin\phi} \tan^2\left(\frac{\pi}{4} + \frac{\phi}{2}\right) \exp\left\{\left(\frac{\pi}{2} - \phi\right) \tan\phi\right\} \qquad (6\text{-}6)$$

The derivation of Eq.(6-6) has been introduced in detail by Toki et al. (1982).

6.8.2 Predicted anisotropic cone penetration resistance

For the estimation of the cone penetration resistance based on Eq.(6-6), the volumetric strain Δ within the plastic zone must be evaluated. In order to calculate Δ, Vesic (1972) has proposed an experimental relationship which is formulated by a series of drained triaxial compression tests under the different effective confining stresses and the isotropic consolidation test. This relationship is expressed as follows:

$$\Delta = C_0 (f_m - 1) \left(\frac{\sigma_q}{\bar{p}} \right)^m + C_1 + C_2 f_n \left(\frac{\sigma_q}{\bar{p}} \right)^n \qquad (6\text{-}7)$$

where the parameters C_o and m are determined by the isotropic consolidation test and C_1, C_2 and n are the parameters obtained from the drained triaxial compression tests. The factors f_m and f_n are obtained concretely from the parameters ϕ, m and n. $\bar{p}$ denotes the unit mean principal stress which is needed to make the expression dimensionally correct. Substitution of F_c and F_q which can be determined from Δ estimated by Eq.(6-7) and ϕ into Eq.(6-4) gives the ultimate cavity expansion pressure p_u. Therefore, the cone penetration resistance q_c can be calculated by Eq.(6-6). It should be noted that the dependency of the angle of shearing resistance ϕ in Eqs.(6-4), (6-6)

and (6-7) on the effective confining pressure is evaluated according to Eq.(6-5).

Table 6-1 shows the parameters required to predict the cone penetration resistance value which are obtained by the tests on R_AV-specimens with D_{rc} of 55 %. The values of cone penetration resistances under the effective confining stresses of 49 kPa to 392 kPa predicted based on these parameters are compared with the measured ones of R_AV- and R_BH-specimens in Fig.6-14. V_1-line denotes the predicted values for R_AV-specimens. It can be seen in the figure that V_1-line gives the over-prediction of q_c (= $(q_c)_m$) irrespective of the magnitude of σ_c'. This is due to the fact that if we adopt the parameters C_1 and C_2 obtained from the drained triaxial compression tests, then the value of Δ always becomes negative. Vesic (1972) has recommended that the assumption of which $\Delta = 0$, i.e. the sands within the plastic zone are imcompressible is used for the case of $\Delta < 0$. As can be seen in Fig.6-8, however, the volume contraction during the cone penetration occurs in the R_AV-specimens with D_{rc} of 55 %. Consequently, it would be considered that the assumption of which $\Delta = 0$ cannot support the experimental facts of the looser sand specimens.

It should be remembered that the characteristics of volumetric strains due to cone penetration are closely connected with those at failure in the drained triaxial extension tests, as shown in Fig.6-10(a).

Table 6-1 Parameters used in the theory of cavity expansion for anisotropic sands with D_{rc} of 55 % (Values of C_1', C_2' and n' are determined from the drained triaxial extension test)

for σ_0 = 1 kPa		for $\bar{p}$ = 1 kPa							
ϕ_0 (deg)	β (deg)	C_0	m	C_1	C_2	n	C_1'	C_2'	n'
41.1	3.04	0.000125	0.670	-0.445	0.424	0.0067	-0.360	0.356	0.0067

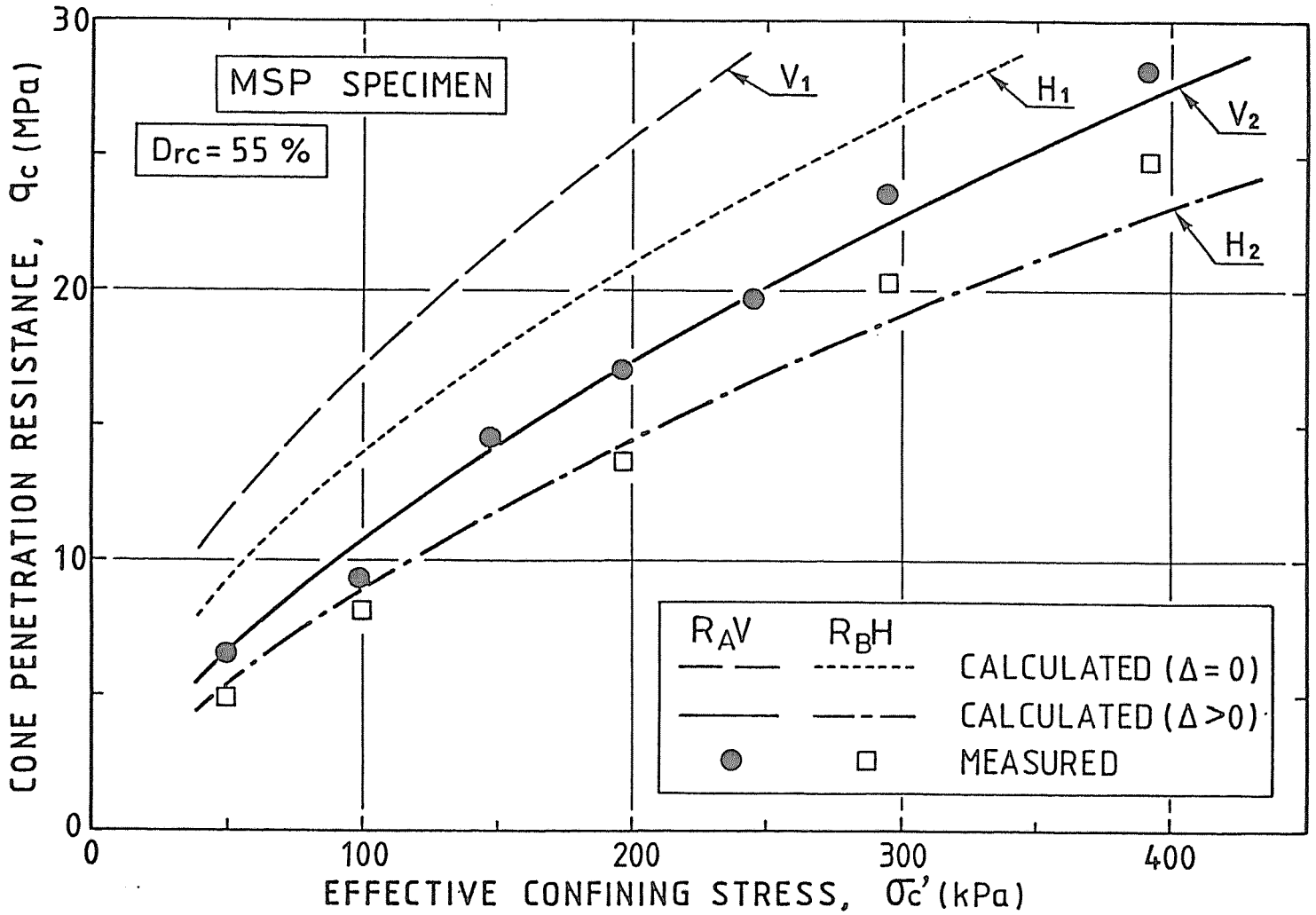

Fig.6-14 Comparison of the measured and calculated values of cone penetration resistance under any effective confining stresses for anisotropic sand

The cone penetration resistance values predicted by using the parameters C_1', C_2' and n' obtained from the drained triaxial extension tests on R_AV-specimens instead of the parameters C_1, C_2 and n are represented as V_2-line in Fig.6-14. It is noteworthy that V_2-line explains well the measured values of R_AV-specimens under the various effective confining stresses. This indicates that the dilatancy characteristics in the triaxial extension stress conditions must be introduced in the parameters for R_AV-specimens having the anisotropic properties characterized by which the deformability is extremely lower in the vertical direction than in the horizontal direction.

The difference in the fabric characteristics between R_AV- and R_BH-specimens seems to be that the preferred alignment of apparent long axes of sand particles is parallel either to the horizontal direction or to the vertical direction. Accordingly, it could be expected that the characteristics of volume changes within the plastic zone exhibit the same tendency in both specimens, if the cavity expands spherically in the sands. In order to calculate Δ for R_BH-specimens, consequently, it is admitted to use the parameters of R_AV-specimens given in Table 6-1. By assuming the variations in the angle of shearing resistance ϕ_d due to fabric anisotropy shown in Fig.6-5(a), the cone penetration resistance values of R_BH-specimens are predicted as shown in Fig.6-14. The predicted values of R_BH-specimens are represented as H_1-line obtained from the parameters C_1,

C_2 and n and H_2-line from the parameters C_1', C_2' and n'. As can be seen in Fig.6-14, the predicted values denoted by H_2-line agree well with measured ones irrespective of the magnitude of effective confining stress σ_c'. It can be also pointed out that the prediction in the present study explains well such observed characteristics as the cone penetration resistance values depend remarkably on the fabric anisotropy and on the effective confining stress.

The analysis of the static cone penetration resistance by the cavity expansion theory should take account of the compressibility and its dependency on the fabric anisotropy within the plastic zone in the sands.

CHAPTER 7 CONCLUSIONS

On the basis of the limited experimental data and theoretical considerations described so far, the following conclusions may be drawn.

The results of the study on sand sample preparation method for laboratory testing in CHAPTER 2 are summarized as follows:

(1) A sand sample preparation method using multiple sieve pluviation apparatus developed in the present study (MSP method) can give a wide range of specimen density by controlling the height of fall and the nozzle diameter. But the nozzle diameter is the primary variable controlling density. The reproducibility and uniformity of sample made by this simple preparation method was confirmed in several aspects.

(2) A very high density, higher than the maximum density determined by the proposed method of JSSMFE for uniformly graded sands, can be easily achieved by MSP method.

From the study for fabric characterization of undisturbed and reconstituted sand samples in CHAPTER 3, it may be concluded that;

(1) The variations in fabric characteristics due to the

differences of sand sample preparation method are clearly observed.

(2) The sand specimen made by MSP method has strongly preferred orientations of particles in the vertical section of specimen and almost random orientations in its horizontal section, i.e. the fabric of MSP (R_AV- or R_BV-) specimen is of the orthotropic type with a vertical axis of rotational symmetry and horizontal planes of isotropy.

(3) The fabric of undisturbed sands sampled from the natural in-situ deposits is significantly anisotropic, and its characteristic shows a very similar pattern to that of MSP specimen.

The results of the study on static and cyclic stress-strain-strength behaviors of reconstituted and undisturbed sands in CHAPTER 4 are summarized as follows:

(1) The anisotropic mechanical properties of MSP specimens are not altered by the height of fall and the rate of sand discharge as far as sand particles are pluviated freely through air.

(2) The static stress-strain-dilatancy characteristics of the undisturbed sand obtained by block sampling at natural sand deposits are remarkably anisotropic; the triaxial specimen whose axial direction is selected to be the vertical direction in in-situ sand deposits is less compressible and more extensible than that with the axial direction perpendicular to it.

(3) The results of a series of cyclic undrained triaxial tests

on two kinds of undisturbed sand also indicate that natural in-situ sand deposits display a significantly anisotropic time history pattern. These anisotropic cyclic deformation performance make a remarkable difference in the cyclic undrained triaxial strength value.

(4) It is considered that the remarkable anisotropy in mechanical properties of undisturbed sands is attributed mainly to the fabric anisotropy which existed in-situ. In particular, the feature of anisotropic mechanical properties of two naturally deposited sands observed in this study is very similar to that of artificial anisotropic sand specimen made by the method of pluviation of sand through air such as MSP method.

(5) The feature of anisotropic static and cyclic deformation-strength properties of relatively clean sand sampled from natural deposits could be reproduced by a suitable sample preparation method (R_B method) which may simulate the block sample procedure used in this study in the laboratory.

(6) It can be said that sand freezing technique used in the present block sampling is an available means to obtain the undisturbed sand samples which retain to a certain degree both the in-situ anisotropic fabric and sampled density. In order to assess the true static and cyclic deformation-strength properties of in-situ sand grounds, however, it seems necessary that a more detailed research is performed in this respect.

The results of the study for predicting three-dimensional stress-strain behavior of sand with inherently anisotropic fabric (orthotropic type) in CHAPTER 5 are summarized as follows:

(1) The relationship between stress ratio and plastic strain increment ratio depend only on the stress system, but are not affected by the inherent anisotropy of sands. Based on these facts, the stress system-dependent plastic potential function can be formulated for the general stress conditions.

(2) From the fact that the influence of the fabric anisotropy of sand specimens on the relationships between plastic work and hardening function under shear process is observed clearly, the hardening function which can explain the anisotropic occurrence of strain due to fabric anisotropy is derived for three-dimensional stress conditions based on the concept of compounded mobilized plane.

(3) Elastoplastic stress-strain relationship for sand with orthotropic fabric under three different principal stresses is derived by using the yield, plastic potential and hardening functions whose formulation are based on the experimental data. Parameters required to predict the three-dimensional stress-strain behaviors can be evaluated easily from the conventional triaxial compression and extension tests and isotropic consolidation-swelling test.

(4) Anisotropic stress-strain-dilatancy behaviors of two kinds of loose sands under the three-dimensional stress conditions can

be predicted well by the proposed elastoplastic work-hardening model.

The results of the study for cone penetration characteristics and its correlation to static and cyclic deformation-strength behaviors of anisotropic sand in CHAPTER 6 are summarized as follows:

(1) The cone penetration resistance value is controlled not necessarily only by density, but also depends remarkably on the fabric characteristics of sands. And also the non-uniformity with respect to the density existing in the sand specimens is reflected in the observed cone penetration resistance.

(2) The relationship between the angle of shearing resistance obtained from the triaxial compression test and the cone penetration resistance value can be denoted by a unique straight line which is not influenced by the fabric anisotropy and density of sand.

(3) The dilatancy characteristics due to cone penetration change significantly with the differences of relative density and fabric characteristics of sand specimens and are closely connected with those at failure of the triaxial extension test. The variations in the cone penetration resistance values do not have nothing to do with those in dilatancy behaviors due to the differences of fabric characteristics.

(4) The cyclic undrained triaxial strength cannot be estimated

directly from the vertical cone penetration resistance value measured in the conventional cone penetration tests. And yet there exists the unique relationship between the cone penetration resistance in the radial direction and the cyclic undrained triaxial strength irrespective of the number of cycles and the fabric anisotropy of sand specimens.

(5) Cone penetration resistance values under any effective confining stresses predicted by the cavity expansion theory agree well with measured ones of sand specimens with the fabric anisotropy. However, not only the compressibility but also its dependency on the fabric anisotropy of sands should be considered in the theoretical analysis.

ACKNOWLEDGEMENT

The author would like to express his sincere gratitude to Professor Shosuke Toki of Hokkaido University for his continual guidance and encouragement given throughout the present study and a critical reading of the manuscript. The author also wishes to acknowledge his indebtedness to Professor Shigeru Kitago and Associate Professor Toshiyuki Mitachi of Hokkaido University for their kind advice and valuable suggestion during the course of this work.

The author would like to emphasize that the present study has been supported by many colleagues in the Soil Mechanics and Foundation Engineering Laboratories of Hokkaido University. In this respect he wishes to extend his gratitude to Messrs. Akira Kamada, Hirokatsu Saga, Hideki Asami, Naomi Ine and Fusao Tanizawa for their discussion and support. The author is also grateful to Messrs. Hiroshi Shimokura, Akira Terayama, Muneo Sato, Yoshitaka Hachiya, Akira Sasaki, Fumiaki Sasaki, Minashi Narita, Nagamasa Nagata, Takeshi Nakagaki and Kinya Miura who conducted the major part of the experiments in the present study. He is indebted especially to Mr. Yutaka Kudo for his preparation of the figures.

The author is also indebted to Professor Kenji Ishihara and Assistant Professor Yasuo Yamada of Tokyo University for their kind discussion and the offer of their published experimental data.

REFERENCES

1) Arthur, J.R.F. (1971): " New techniques to measure new parameters," Proc., Roscoe Memorial Symposium, Cambridge University, pp.340-346.

2) Arthur, J.R.F. and Menzies, B.K. (1972): " Inherent anisotropy in a sand," Geotechnique, Vol.22, No.1, pp.115-128.

3) Baldi, G., Bellotti, R., Ghionna, V., Jamiolkowski, M. and Pasqualini, E. (1981): " Cone resistance of a dry medium sand," Proc., 10th ICSMFE, Vol.2, pp.427-432.

4) Baldi, G., Bellotti, R., Ghionna, V., Jamiolkowski, M. and Pasqualini, E. (1982): " Design parameters for sands from CPT," Proc., 2nd European Symp. on Penetration Testing, pp.425-432.

5) Baligh, M.M. (1976): " Cavity expansion in sands with curved envelopes," Proc., ASCE, Vol.102, No.GT11, pp.1131-1146.

6) Barden, L. and Khayatt, A.J. (1966): " Incremental strain rate ratios and strength of sand in the triaxial test," Geotechnique, Vol.16, No.4, pp.338-357.

7) Barden, L., Ismail, H. and Tong, P. (1969): " Plane strain deformation of granular material at low and high pressures," Geotechnique, Vol.19, No.4, pp.441-452.

8) Bishop, A.W. and Eldin, A.K. Gamal. (1953): " The effect of stress history on the relation between φ and porosity in sand," Proc., 3rd ICSMFE, Vol.1, pp.100-105.

9) Bishop, A.W. (1966): " The strength of soils as engineering materials," Geotechnique, Vol.16, No.2, pp.91-130.

10) Chan, C.K. and Mulilis, J.P. (1976): " Pneumatic sinusoidal loading system," Proc., ASCE, Vol.102, No.GT3, pp.277-282.

11) Chaney, R. and Mulilis, J.P. (1978): " Suggested method for soil specimen remolding by wet-raining," Geotechnical Testing

Journal, ASTM, Vol.1, No.2, pp.107-108.

12) Chapman, G.A. and Donald, I.B. (1981): "Interpretation of static penetration tests in sand," Proc., 10th ICSMFE, Vol.2, pp.455-458.

13) Cole, E.R.L. (1967): " The behaviour of soils in the simple shear apparatus," Ph. D. Thesis, University of Cambridge.

14) Committee of JSSMFE on the Test Method of Relative Density of Sand (1979): " Maximum-minimum density test method of sand," Procedures for Testing Soils, 2nd Revised Edition, JSSMFE, Part 2, Chapter 9, pp.172-188 (in Japanese).

15) Curray, J.R. (1956): " The analysis of two-dimensional orientation data," Journal of Geology, Vol.64, pp.117-131.

16) De Beer, E.E. (1965): " Influence of the mean normal stress on the shearing strength of sand," Proc., 6th ICSMFE, Vol.1, pp.165-169.

17) Drucker, D.C., Gibson, R.E. and Henkel, D.J. (1957): " Soil mechanics and work-hardening theories of plasticity," Transactions, ASCE, Vol.122, pp.338-346.

18) Durgunoglu, H.T. and Mitchell, J.K. (1975a): " Static penetration resistance of soils : 1-Analysis," Proc., ASCE Specialty Conf. on In Situ Measurement of Soil Properties, Vol.1, pp.151-171.

19) Durgunoglu, H.T. and Mitchell, J.K. (1975b): " Static penetration resistance of soils : 2-Evaluation of theory and implications for practice," Proc., ASCE Specialty Conf. on In Situ Measurement of Soil Properties, Vol.1, pp.172-189.

20) El-Sohby, M.A. (1969): " Deformation of sands under constant stress ratios," Proc., 7th ICSMFE, Vol.1, pp.111-119.

21) El-Sohby, M.A. and Andrawes, K.Z. (1972): " Deformation characteristics of granular materials under hydrostatic compression," Canadian Geotechnical Journal, Vol.9, No.4, pp.338-350.

22) Finn, W.D.L., Bransby, P.L. and Pickering, D.J. (1970): " Effect of strain history on liquefaction of sand," Proc., ASCE, Vol.96, No.SM6, pp.1917-1934.

23) Finn, W.D.L., Pickering, D.J. and Bransby, P.L. (1971): " Sand liquefaction in triaxial and simple shear tests," Proc., ASCE, Vol.97, No.SM4, pp.639-659.

24) Frydman, S. (1976): " The strain hardening behaviour of particulate media," Canadian Geotechnical Journal, Vol.13, No.3, pp.311-323.

25) Green, G.E. and Bishop, A.W. (1969): " A note on the drained strength of sand under generalized strain conditions," Geotechnique, Vol.19, No.1, pp.144-149.

26) Green, G.E. (1971): " Strength and deformation of sand measured in an independent stress controll cell," Proc., Roscoe Memorial Symposium, Cambridge University, pp.285-323.

27) Green, G.E. and Reades, D.W. (1975): " Boundary conditions, anisotropy and sample shape effects on the stress-strain behaviour of sand in triaxial compression and plane strain," Geotechnique, Vol.25, No.2, pp.333-356.

28) Haruyama, M. (1981): " Anisotropic deformation-strength characteristics of an assembly of spherical particles under three dimensional stresses," Soils and Foundations, Vol.21, No.4, pp.41-55.

29) Hill, R. (1950): " The mathematical theory of plasticity," Oxford Univ. Press, London.

30) Horn, H.M. and Deere, D.U. (1962): " Frictional characteristics of minerals," Geotechnique, Vol.12, No.3, pp.319-335.

31) Ichihara, M. and Matsuzawa, H. (1970): " Experiments on shearing characteristics of dry sand under plane strain condition and axial symmetric strain condition," Proc., JSCE, No.173, pp.47-59(in Japanese).

32) Ishibashi, I. and Scherif, M.A. (1974): " Soil liquefaction by torsional simple shear device," Proc., ASCE, Vol.100, No.GT8, pp.871-888.

33) Ishihara, K. and Li, S. (1972): " Liquefaction of saturated sand in triaxial torsion shear test," Soils and Foundations, Vol.12, No.2, pp.19-39.

34) Ishihara, K. and Okada, S. (1978): " Effects of stress history on cyclic behavior of sand," Soils and Foundations, Vol.18, No.4, pp.31-45.

35) Ishihara, K., Silver, M.L. and Kitagawa, H. (1978): " Cyclic strengths of undisturbed sands obtained by large diameter sampling," Soils and Foundations, Vol.18, No.4, pp.61-76.

36) Ishihara, K. and Takatsu, H. (1979): " Effects of overconsolidation and K_o conditions on the liquefaction characteristics of sands," Soils and Foundations, Vol.19, No.4, pp.59-68.

37) Kjellman, W. (1936): " Report on an apparatus for consummate investigation of the mechanical properties of soils," Proc., 1st ICSMFE, Vol.2, pp.16-20.

38) Ko, H.Y. and Scott, R.F. (1967): " A new soil testing apparatus," Geotechnique, Vol.17, No.1, pp.40-57.

39) Kokusho, T. (1980): " Cyclic triaxial test of dynamic soil properties for wide strain range," Soils and Foundations, Vol.20, No.2, pp.45-60.

40) Kolbuszewski, J.J. (1948): " An experimental study of the maximum and minimum porosities of sands," Proc., 2nd ICSMFE, Vol.1, pp.158-165.

41) Kovacs, W.D., Evans, J.C. and Griffith, A.H. (1977): " Towards a more standardized SPT," Proc., 9th ICSMFE, Vol.2, pp.269-276.

42) Ladd, R.S. (1974): " Specimen preparation and liquefaction of sands," Proc., ASCE, Vol.100, No.GT10, pp.1180-1184.

43) Ladd, R.S. (1978): " Preparing test specimens using under-compaction," Geotechnical Testing Journal, ASTM, Vol.1, No.1, pp.16-23.

44) Lade, P.V. and Duncan, J.M. (1973): " Cubical triaxial tests on cohesionless soil," Proc., ASCE, Vol.99, No.SM10, pp.793-812.

45) Lade, P.V. and Duncan, J.M. (1975): " Elastoplastic stress-strain theory for cohesionless soil," Proc., ASCE, Vol.101, No.GT10, pp.1037-1053.

46) Lambe, T.W. and Whitman, R.V. (1969): " Soil Mechanics," John Wiely & Sons, New York.

47) Lee, K.L. and Seed, H.B. (1967): " Drained strength characteristics of sands," Proc., ASCE, Vol.93, No.SM6, pp.117-141.

48) Marcuson, W.F.III, and Bieganousky, W.A. (1977): " Laboratory standard penetration tests on fine sands," Proc., ASCE, Vol.103, No.GT6, pp.565-588.

49) Marsal, R.J. (1967): " Large scale testing on rockfill materials," Proc., ASCE, Vol.93, No.SM2, pp.27-43.

50) Matsuoka, H. (1974): " Stress-strain relationships of sands based on the mobilized plane," Soils and Foundations, Vol.14, No.2, pp.47-61.

51) Matsuoka, H. and Nakai, T. (1977): " Stress-strain relationship of soil based on the "SMP"," Proc., Specialty Session 9, 9th ICSMFE, pp.153-162.

52) Matsuoka, H. and Nakai, T. and Ishizaki, H. (1980): " A stress-strain relationship for anisotropic soils based on compounded mobilized planes," Proc., JSCE, No.300, pp.57-67(in Japanese).

53) Meyerhof, G.G. (1961): " The ultimate bearing capacity of wedge-shaped foundations," Proc., 5th ICSMFE, Vol.2, pp.105-109.

54) Mikasa, M. (1964): " Classification table of the engineering property of soil and its significance," Tsuchi-to-Kiso, JSSMFE,

Vol.12, No.4, pp.17-24 (in Japanese).

55) Miura, S., Toki, S. and Narita, M. (1980): " Dependency of dilatancy characteristics of saturated sand on stress path," Proc., 35th Annual Meeting of JSCE, pp.29-30 (in Japanese).

56) Miura, S., Toki, S. and Miura, K. (1982a): " Change in deformation-strength characteristics of sand due to sampling and freezing," Proc., 17th Annual Meeting of JSSMFE, pp.325-328 (in Japanese).

57) Miura, S., Toki, S. and Ine, N. (1982b): " An elastoplastic stress-strain relationship for sand subjected to cyclic loading," Bulletin of the Faculty of Engineering, Hokkaido University, No.111, pp.13-23 (in Japanese).

58) Miura, S., Toki, S. and Miura, K. (1983a): " Modeling of drained shear characteristics of anisotropic sands under three-dimensional stress system," Proc., 18th Annual Meeting of JSSMFE, pp.343-346 (in Japanese).

59) Miura, S., Toki, S. and Miura, K. (1983b): " An elastoplastic model for anisotropic sands under different three principal stresses," Bulletin of the Faculty of Engineering, Hokkaido University, No.116, pp.1-13 (in Japanese).

60) Miura, S. (1983): " A procedure for reaching 100% saturation of triaxial specimen (CO_2 method)," Tsuchi-to-Kiso, JSSMFE, Vol.31, No.7, pp.59-60 (in Japanese).

61) Miyamori, T. (1976): " Deformation and strength of a sand in three-dimensional stress state," Proc., JSCE, No.255, pp.81-91 (in Japanese).

62) Mulilis, J.P., Chan, C.K. and Seed, H.B. (1975): " The effects of method of sample preparation on the cyclic stress-strain behavior of sands, " Report No.EERC 75-18, Univ. of California.

63) Nash, K.L. (1953): " The shearing resistance of a fine closely graded sand," Proc., 3rd ICSMFE, Vol.1, pp.160-164.

64) Nishi, K. and Esashi, Y. (1978): " Stress-strain relationships of sand based on elasto-plasticity theory," Proc., JSCE, No.280, pp.111-122.

65) Ochiai, H. and Lade, P.V. (1983): " Three-dimensional behavior of sand with anisotropic fabric," Proc., ASCE, Vol.109, No.GT10, pp.1313-1328.

66) Oda, M. (1972a): " Initial fabrics and their relations to mechanical properties of granular material," Soils and Foundations, Vol.12, No.1, pp.17-36.

67) Oda, M. (1972b): " The mechanism of fabric changes during compressional deformation of sand," Soils and Foundations, Vol.12, No.2, pp.1-18.

68) Oda, M. (1977): " Co-ordination number and its relation to shear strength of granular material," Soils and Foundations, Vol.17, No.2, pp.29-42.

69) Oda, M., Koishikawa, I. and Higuchi, T. (1978): " Experimental study of anisotropic shear strength of sand by plane strain test," Soils and Foundations, Vol.18, No.1, pp.25-38.

70) Oda, M. and Koishikawa, I. (1978): " Strength anisotropy of sand ground and its significance in soil engineering," Proc., JSCE, No.273, pp.111-120 (in Japanese).

71) Oda, M. (1978): " Fundamental properties of granular materials and their significance in soil engineering," Tsuchi-to-Kiso, JSSMFE, Vol.26, No.8, pp.63-70 (in Japanese).

72) Peacock, W.H. and Seed, H.B. (1968): " Sand liquefaction under cyclic loading simple shear conditions," Proc., ASCE, Vol.94, No.SM3, pp.689-708.

73) Poorooshasb, H.B., Holubec, I. and Scherbourne, A.N. (1966): " Yielding and flow of sand in triaxial compression, Part I," Canadian Geotechnical Journal, Vol.3, No.4, pp.179-190.

74) Poorooshasb, H.B. (1971): " Deformation of sand in triaxial

compression," Proc., 4th Asian Regional Conf. on SMFE, Vol.1, pp.63-66.

75) Raju, V.S. and Sadasivan, S.K. (1974): " Membrane penetration in triaxial tests on sands," Proc., ASCE, Vol.100, No.GT4, pp.482-489.

76) Roscoe, K.H., Schofield, A.N. and Thurairajah, A. (1963): " Yielding of clays in states wetter than critical," Geotechnique, Vol.13, No.3, pp.211-240.

77) Roscoe, K.H. and Burland, J.B. (1968): " On the generalized stress-strain behaviour of wet clay," Engineering Plasticity, Cambridge Univ. Press, pp.535-609.

78) Rowe, P.W. (1962): " The stress-dilatancy relation for static equilibrium of an assembly of particles in contact," Proc., Roy. Soc. A., Vol.269, pp.500-527.

79) Schmertmann, J.H. (1975): " Measurement of insitu shear strength," Proc., ASCE Specialty Conf. on In Situ Measurement of Soil Properties, Vol.II, pp.57-138.

80) Schofield, A.N. and Wroth, C.P. (1968): " Critical State Soil Mechanics," McGraw-Hill, London.

81) Seed, H.B. (1979): " Soil liquefaction and cyclic mobility evaluation for level ground during earthquakes," Proc., ASCE, Vol.105, No.GT2, pp.201-255.

82) Seed, H.B., Singh, S. and Chan, C.K. (1982): " Considerations in undisturbed sampling of sands," Proc., ASCE, Vol.108, No.GT2, pp.265-283.

83) Silver, M.L., Tatsuoka, F., Phukunhaphan, A. and Avramidis, A.S. (1980): " Cyclic undrained strength of sand by triaxial test and simple shear test," Proc., 7th World Conf. on Earthquake Engineering, Vol.3, pp.281-288.

84) Singh, S., Seed, H.B. and Chan, C.K. (1982): " Undisturbed sampling of saturated sands by freezing," Proc., ASCE, Vol.108,

No.GT2, pp.247-264.

85) Sture, S. and Desai, C.S. (1979): " Fluid cushion truly triaxial or multiaxial testing device," Geotechnical Testing Journal, Vol.2, No.1, pp.20.33.

86) Sutherland, H.B. and Mesdary, M.S. (1969): " The influence of the intermediate principal stress on the strength of sand," Proc., 7th ICSMFE, Vol.1, pp.391-399.

87) Tatsuoka, F. (1972): " A fundamental study on the deformation of a sand by triaxial tests," Dr. Thesis, University of Tokyo (in Japanese).

88) Tatsuoka, F. and Ishihara, K. (1974a): " Yielding of sand in triaxial compression," Soils and Foundations, Vol.14, No.2, pp.63-76.

89) Tatsuoka, F. and Ishihara,K. (1974b) : " Drained deformation of sand under cyclic stresses reversing direction," Soils and Foundations, Vol.14, No.3, pp.51-65.

90) Tatsuoka, F., Iwasaki, T., Tokida, K., Yasuda, S., Hirose, M., Imai, T. and Kon-no, M. (1978): " A method for estimating undrained cyclic strength of sandy soils using standard penetration resistances," Soils and Foundations, Vol.18, No.3, pp.43-58.

91) Tatsuoka, F. (1980): " Stress-strain behavior of an idealized anisotropic granular material," Soils and Foundations, Vol.20, No.3, pp.75-90.

92) Tatsuoka, F., Iwasaki, T., Tokida, K. and Kon-no, M. (1981): " Cyclic undrained triaxial strength of sampled sand affected by confining pressure," Soils and Foundations, Vol.21, No.2, pp.115-120.

93) Tatsuoka, F., Muramatsu, M. and Sasaki, T. (1982): " Cyclic undrained stress-strain behavior of dense sands by torsional simple shear test," Soils and Foundationd, Vol.22, No.2, pp.55-70.

94) Tohno, I. (1977): " Methods to evaluate quality of undisturbed samples of sands," Proc., Specialty Session 2 on Soil Sampling, 9th ICSMFE, pp.29-35.

95) Toki, S. and Kitago, S. (1974): " Effects of repeated loading on deformation behavior of dry sand," Jour. of JSSMFE, Vol.14, No.1, pp.95-103 (in Japanese).

96) Toki, S., Miura, S., Kamada, A., Shimokura, H. and Hachiya, Y. (1978): " Influence of stress history on liquefaction characteristics of saturated sand," Technical Report, JSSMFE, Hokkaido Branch, No.18, pp.151-160 (in Japanese).

97) Toki, S. and Miura, S. (1979): " Sand sample preparation method for laboratory test," Proc., 24th Symposium on Soil Mechanics, JSSMFE, pp.173-180 (in Japanese).

98) Toki, S., Miura, S. and Tanizawa, F. (1981): " A few consideration on relative density and mechanical properties of sand," Proc., Symposium on Relative Density and Engineering Property of Sand, JSSMFE, pp.79-86 (in Japanese).

99) Toki, S., Miura, S. and Tanizawa, F. (1982): " Laboratory study on the correlation between mechanical properties and static cone penetration characteristics of sand," Bulletin of the Faculty of Engineering, Hokkaido University, No.111, pp.1-12 (in Japanese).

100) Toki, S., Miura, S. and Nakagaki, T. (1983): " Cyclic undrained behavior of undisturbed sands," Technical Report, JSSMFE, Hokkaido Branch, No.23, pp.43-52 (in Japanese).

101) Tschebotarioff, G.P. and Welch, J.D. (1948): " Lateral earth pressures and friction between soil minerals," Proc., 2nd ICSMFE, Vol.7, pp.135-138.

102) Veismanis, A. (1974): " Laboratory investigation of electrical friction-cone penetrometers in sand," Proc., European Symp. on Penetration Testing, Vol.2:2, pp.407-419.

103) Vesic, A.S. and Clough, G.W. (1968): " Behavior of granular materials under high stresses," Proc., ASCE, Vol.94, No.SM3, pp.661-688.

104) Vesic, A.S. (1972): " Expansion of cavities in finite soil mass," Proc., ASCE, Vol.98, No.SM3, pp.265-290.

105) Vesic, A.S. (1977): " Design of pile foundations, " National Cooperative Highway Research Program. Report 42, Transportation Research Board, Washington.

106) Walberg, F.C. (1978): " Freezing and cyclic triaxial behavior of sands," Proc., ASCE, Vol.104, No.GT5, pp.667-671.

107) Yamada, Y. and Ishihara, K. (1979): " Anisotropic deformation characteristics of sand under three dimensional stress conditions," Soils and Foundations, Vol.19, No.2, pp.79-94.

108) Yamada, Y. and Ishihara, K. (1981): " Undrained deformation characteristics of loose sand under three-dimensional stress conditions," Soils and Foundations, Vol.21, No.1, pp.97-107.

109) Yoshimi, Y. and Oh-oka, H. (1973): " A ring torsion apparatus for simple shear tests," Proc., 8th ICSMFE, Vol.1, pp.501-506.

110) Yoshimi, Y., Hatanaka, M. and Oh-oka, H. (1978): " Undisturbed sampling of saturated sands by freezing," Soils and Foundations, Vol.18, No.3, pp.59-73.

111) Yoshimi, Y. and Tokimatsu, K. (1983): " SPT practice survey and comparative tests," Soils and Foundations, Vol.23, No.3, pp.105-111.